Synthesis and characterization of transition metal complexes: Kinetic investigation with biomolecules, DNA/BSA binding abilities and cytotoxic studies

Dissertation

Vorgelegt von

MILAN M. MILUTINOVIĆ

Fakultät für Naturwissenschaften

UNIVERSITÄT PADERBORN

Zur Erlangung der Würde eines

DOKTORS DER NATURWISSENSCHAFTEN (DR. RER. NAT.)

im Department Chemie

2018

Promotionskommission

Prof. Dr. Gerald Henkel	Vorsitz
Prof. Dr. René Wilhelm	Erstgutachter
Prof. Dr. Jovana Bogojeski	Zweitgutachter
PD Dr. Hans Egold	

DEDICATED TO MY PARENTS AND MY SISTER

The present is theirs; the future, for which I really worked, is mine.

Nikola Tesla
"The greatest mind in the world; Serbian-American inventor"

EIDESSTATTLICHE ERKLÄRUNG

Hiermit versichere ich, die vorliegende Arbeit selbständig angefertigt und keine anderen als die von mir angegebenen Hilfsmittel verwendet zu haben. Wörtliche und sinngemäße Zitate wurden als solche gekennzeichnet und die Genehmigungen zur Veröffentlichung der urheberrechtlich geschützten Publikationen wurden eingeholt.

_____

PADERBORN, 07. NOVEMBER 2018 MILAN M. MILUTINOVIĆ

ABSTRACT

Transition metals and their complexes have an important impact on chemistry and are found in many application in life in general. Ruthenium and rhodium are two members of noble metals and proved to be suitable for anticancer activity.

With the aim of changing the coordination environment in ruthenium and rhodium complexes, this thesis presents a series of ruthenium(II) polypyridyl and rhodium(III) pincer-type complexes. All new ruthenium(II) and rhodium(III) complexes were characterized by NMR spectroscopy, ESI-MS spectrometry and UV-Vis spectrophotometry . For some of the complexes a single crystal X-ray crystallography was performed.

The substitution reactions of ruthenium(II) and rhodium(III) complexes with mononucleotides, oligonucleotides and amino acids were studied quantitatively by UV-Vis spectroscopy. Measurements of the activation enthalpies and entropies for all synthesized complexes are supporting an associative mechanism for the substitution process. NMR spectroscopy studies were performed on some ruthenium(II) complexes where after the hydrolyses of the metal-Cl bond the complexes are capable to interact with guanine derivatives forming monofunctional adducts via N7 atom. The interactions of ruthenium(II) and rhodium(III) complexes with fully complementary 15-mer and 22-mer duplexes of DNA and fully complementary 13-mer duplexes of RNA were studied by UV-Vis spectroscopy. The interactions of ruthenium(II) and rhodium(III) complexes with calf thymus and herring testes DNA were examined by absorption using UV-Vis spectroscopy, fluorescence emission spectral studies by ethidium bromide displacement studies and viscosity measurements. For some of the complexes molecular docking studies were carried out. Cytotoxic studies, *in vitro* and *in vivo,* have been performed on selected cancer cell lines and on mice. Ruthenium and rhodium, as a newly synthesized complexes, represent the high potential as an appropriate anticancer agents.

KURZZUSAMMENFASSUNG

Übergangsmetalle und ihre Komplexe besitzen einen wichtigen Stellenwert in der Chemie und werden generell in vielen wichtigen biologischen Prozessen gefunden. Ruthenium und Rhodium sind zwei Vertreter von Edelmetallen und einige Komplexe dieser beiden Metalle haben eine biologische Aktivität gegen Krebs gezeigt.

Mit dem Ziel die koordinative Umgebung von Ruthenium- und Rhodiumkomplexen zu verändern wird in dieser Doktorarbeit eine Serie von Ruthenium(II)polypyridyl und Rhodium(III)-Pincer-Typ-Komplexen präsentiert. Alle neuen Ruthenium(II)- und Rhodium(III)-Komplexe wurden mittels NMR-Spektroskopie, ESI-MS Spektroskopie und UV-Vis Spektroskopie charakterisiert.

Die Substitutionsreaktion von Ruthenium(II)- und Rhodium(III)-Komplexen wurden mit Mononukleotiden, Oligonukleotiden und Aminosäuren mittels UV-Vis Spektroskopie quantitativ untersucht. Die Messungen der Aktivierungsenthalpien und -entropien für alle neuen synthetisierten Komplexe unterstützen einen assoziativen Mechanismus für den Substitutionsprozess. NMR-spektroskopische Untersuchungen wurden für einige Ruthenium(II)-Komplexe durchgeführt, wobei sich zeigte, dass nach der Hydrolyse der Metall-Chlorid Bindungen die Komplexe mit Guanin-Derivaten monofunktionale Addukte über das N7-Atom bilden. Die Wechselwirkungen der Ruthenium(II)- und Rhodium(III)-Komplexe mit komplett komplementären 15-mer und 22-mer Duplexes von DNA und komplett komplementären 13-mer Duplexes von RNA wurden mittels UV-Vis Spektroskopie untersucht. Die Interaktionen der Ruthenium(II)- und Rhodium(III)-Komplexe mit DNA aus der Thymusdrüse von Kälbern und Heringshoden wurden mittles UV-Vis Spektroskopie und Emissionsfluoreszenz Spektroskopie evaluiert. Im letzteren Fall wurden dabei die Studien mit Ehidiumbromid durchgeführt, wobei dieses durch die Komplexe in der DNA ausgetauscht wurde. Zusätzlich wurden auch Viskositätsmessungen durchgeführt. Für einige Komplexe konnten molekulare Docking Studien mittels DFT ausgeführt werden. Cytotoxische Untersuchungen, sowohl in vitro als auch in vivo, an ausgesuchten Zelllinien und an Mäusen zeigten das Potential der neuen Komplexe als Antikrebsmedikamente.

ACKNOWLEDGEMENT

Every person in the world has some goals in their life. One of my personal goals is to finish the doctorate studies. Today is the day: writing this note of thanks is the finishing touch on my dissertation of my doctorate studies. It has been a period of intense learning for me, not only in the scientific area, but also on a personal level. I have been living in three countries during my doctorate studies so it has been a long, tough and hard road but still also grateful, enjoyable and happy as well. Writing this dissertation has had a big impact on me. I would like to reflect on the people who have supported and helped me so much throughout this period.

First, I would like to thank my supervisor from Serbia at the University of Kragujevac, the late Prof. Dr. Živadin D. Bugarčić, who invited me to start my doctorate studies in his research group. I learned so much from him, not only from the scientific part, but as well on the personal level-how to be strong and independent. Many thanks goes to my colleagues from the Prof. Bugarčić's group: Prof. Dr. Biljana Petrović, Prof. Dr. Jovana V. Bogojeski, Dr. Snežana Jovanović, Dr. Mirjana D. Đurović and Dr. Ana Rilak Simović who were there for me at any time and situation. I have been listening to their advice and implementing them, not only in the research but as well on the personal level. Many thanks goes to my colleagues from the department of Chemistry at the Faculty of Science at the University of Kragujevac where I worked for two years.

I would like to thank Prof. Dr. Sofi K. C. Elmroth who hosted me as guest scientist at the Department of Biochemistry, Lund University in Sweden where I stayed for almost 3 months.

Special thanks go to my supervisor Prof. Dr. René Wilhelm who has accepted me in his research group and who believed in me. From the very first days at the University of Paderborn Prof. Dr. Wilhelm was there to help me in almost everything, in the laboratory whenever I had any kind of problem (sometimes extremely stupid ones), analyzing data for hours, preparing documents for the scholarships and so many more things. Many thanks goes to Dr. Maren Muntzeck, Dr. Eduard Rais, Dr. Marta Rosenthal and M. Sc. Xiao Fu from Prof. Dr. Wilhelm's group. Many thanks goes to all of my colleagues from the Department of Organic Chemistry at the Faculty of Science at the University of Paderborn.

I would like to thank all of my friends and family from Serbia and from all around the world for their support. Like I mentioned above, I have been living in 3 countries where I made friends from all around the world and I would need at least 10 pages to write the acknowledgment for each of them but I am positively sure all of them know how much they have influenced my personal and professional life.

At the end the greatest thanks go to my parents Miloš and Ružica, and to my sister Milica who have given me infinite love, strength and support during my whole life and I would not be the person I am today if it weren't for them.

LIST OF PUBLICATIONS

1. **M. M. Milutinović**, J. V. Bogojeski, O. Klisurić, A. Scheurer, S. K. C. Elmroth, Ž. D. Bugarčić:"Synthesis and structure of a pincer-type rhodium(III) complex: reactivity toward biomolecules", *Dalton Trans.*, **2016**, 45, 15481-15491.
2. **M. M. Milutinović**, A. Rilak, I. Bratsos, O. Klisurić, M. Vraneš, N. Gligorijević, S. Radulović, Ž. D. Bugarčić:"New 4´-(4-chlorophenyl)-2,2´:6´,2´´-terpyridine ruthenium(II) complexes: Synthesis, characterization, interaction with DNA/BSA and cytotoxicity studies", *J. Inorg. Biochem.*, **2017**, 169, 1-12.
3. **M. M. Milutinović**, S. K. C. Elmroth, G. Davidović, A. Rilak, O. Klisurić, I. Bratsos, Ž. D. Bugarčić:" Kinetic and mechanistic study on the reactions of ruthenium(II) chlorophenyl terpyridine complexes with nucleobases, oligonucleotides and DNA", *Dalton Trans.*, **2017**, 46, 2360-2369.
4. **M. M. Milutinović**, Ž. D. Bugarčić, R. Wilhelm:"A camphor based 1,3-diamine Ru(II) terpyridine complex: synthesis, characterization, kinetic investigation and DNA binding", *New J. Chem.*, **2018**, 42, 7607-7611.
5. **M. M. Milutinović**, P. Čanović, D. Stevanović, R. Masnikosa, M. Vraneš, A. Tot, M. Zarić, B. Simović Marković, M. Misirkić Marjanović, Lj. Vukičević, M. Savić, V. Jakovljević, V. S. Trajković, V. Volarević, T. Kanjevac, A. Rilak Simović:"Newly synthesized heteronuclear ruthenium(II)/ferrocene complexes suppress 4T1 mammary carcinoma growth in BALB/c mice by promoting activation of anti-tumor immunity", *Organometallics*, **2018**, 37, 4250-4266.
6. A. Petrović, **M. M. Milutinović**, M. Živanović, N. Milivojević, R. Puchta, A. Scheurer, J. Korzekwa, O. Klisurić, J. V. Bogojeski:" Synthesis of Camphor-Derived Bis(pyrazolylpyridine) Rhodium(III) Complexes: Structure−Reactivity Relationships and Biological Activity", *Inorg. Chem.*, **2019**, 58, 307-319.

TALKS

1. **M. M. Milutinović**, Ž. D. Bugarčić: "Synthesis, characterization and mechanistic investigation of the substitution reactions of ruthenium(II) complexes", 53rd Counseling of the Serbian Chemical Society, June **2016**, Kragujevac, Serbia.

POSTER PRESENTATIONS

1. **M. M. Milutinović**, A. Rilak, Ž. D. Bugarčić:" Synthesis, characterization and mechanistic investigation of the substitution reactions of ruthenium(II) complexes", 3rd Conference of the Young Chemist of Serbia, October **2015**, Belgrade, Serbia.
2. S. Radisavljević, **M. M. Milutinović**, A. Rilak, Ž. D. Bugarčić:"Synthesis and characterization of new ruthenium(II) polypyridyl complexes and their interactions with DNA", 4th Conference of the Young Chemist of Serbia, November **2016**, Belgrade, Serbia.
3. **M. M. Milutinović**, A. Rilak, I. Bratsos, O. Klisurić, Ž. D. Bugarčić," 24th Young Research Fellow Meeting (Journées des Jeunes Chercheurs, JJC), At Châtenay-Malabry, February **2017**, Paris, France.
4. **M. M. Milutinović**, Ž. D. Bugarčić, R. Wilhelm:" Synthesis and characterization of new Ru(II) terpyridine complexes with new camphor based diamine ligands: Kinetic investigation and DNA/BSA binding ability", International Symposium on Metal Complexes – ISMEC, June **2017**, Dijon, France - **1st prize award**.
5. A. Petrović, **M. M. Milutinović**, M. Živanović, A. Scheurer, R. Puchta, O. Klisurić, J. Bogojeski:"Structure-reactivity relationship and biological activity of the camphor-derived ot the bis-pyrazolylpyridine Rh(III) complexes", 55th Counseling of the Serbian Chemical Society", June **2018**, Novi Sad, Serbia.
6. **M. M. Milutinović**, J. Bogojeski, A. Petrović, R. Wilhelm:"ACS Publications Forum: Scientific Diversity in Inorganic/Organic Chemistry in Europe", October **2018**, Heidelberg, Germany.

TABLE OF CONTENTS

CHAPTER 1

INTRODUCTION

1.1. Outline

Transition metals and their complexes play a very important role in various biochemical and metabolic processes. In addition, non-essential metal ions are often applied in biological systems for therapeutic and diagnostic purposes. A wide range of available oxidation states, coordination numbers and geometry, as well as the thermodynamic and kinetic properties of metal ion, lead to compounds that offer the ability to design various therapeutic agents. Discoveries in inorganic and bioinorganic chemistry have an important influence on modern clinical medicine.[1] A mechanism of some complexes in biological systems is still not well known, so today a large number of researchers are engaged in research in this area. Due to the fact that a disease in the initial phase takes place at the cellular level it is necessary to seek answers and solutions whether the disease can be stopped at that certain level or not.[2-4] One of the leading causes of death worldwide is cancer. The growth of anomalous cells is called tumor in humans or animals.[5-7] Observing the reports in the last decades there is no current oncotherapy which is able to completely stop the growth or cure the unhealthy cells.[6] Taking this into consideration there is an urgent need for discovery of novel active chemotherapeutics. The most common used chemotherapeutic in the last decades is cisplatin or platinum based complexes known as carboplatin and oxaliplatin. However, the use of these complexes is limited by their toxicity and acquired drug resistance.[8-10]

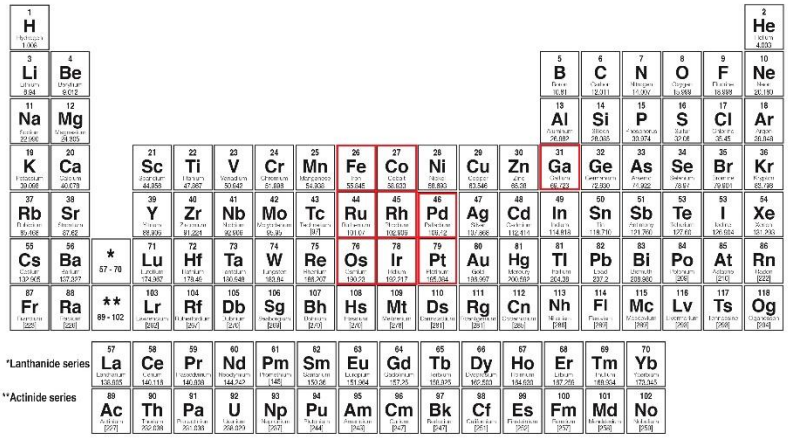

Scheme 1. Periodic system of elements where the elements are marked with color which exhibit antitumor activity.[11,12]

This conclusion has led to a growing interest in the antineoplastic and antimetastatic properties of complexes containing metals other than platin, that clearly cannot mimic cisplatin in their mode of action.[13-15] Owning to the similarity of their ligand exchange rates in aqueous solution[16] and their lower general toxicity, ruthenium (II/III) complexes have received considerable attention as possible alternatives to Pt(II) anticancer agents.[17,18-21] It is believed that this is due to the possibility of ruthenium to replace the iron in coordination with biomolecules. Two structurally related isoelectronic ruthenium(III) complexes, [HIm]*trans*-[$RuCl_4$(Im)(DMSO-S)] (NAMI-A) and [HInd]*trans*-[$RuCl_4(Ind)_2$] (KP1019) (Im = imidazole, Ind = indazole), have completed phase 1 clinical trials as, respectively, antineoplastic and antimetastatic drugs. There is an increased interest in the use of organometallic compounds, a complex with at least one metal-nonmetal bond, in biology and medicine. Organometallic arene ruthenium(II) complexes have attracted a lot of attention because it is known that arene ligands stabilize ruthenium in the +2 oxidation state. The ruthenium(III) complexes are more inert than the corresponding complexes of ruthenium(II).[22] The half-sandwich arene ruthenium(II) complexes, [Ru(η^6-arene)(X)(*N*-*N*)] (X = halogen, *N*-*N* = bidentate ligand), often possess good solubility in water, which is the advantage for clinical use, as well as the fact that arene ligands are relatively inert to changes in physiological conditions. The influence of structural variations on the anticancer activity of the arene ruthenium complexes is constantly investigated. It is believed that the main target of arene ruthenium complexes is DNA or RNA, as well as proteins.

In the last few decades numerous studies have focused on the synthesis of ruthenium(II) polypyridyl complexes. The subject of the studies was their ability to coordinate to DNA, whereby most of these complexes were found to bind covalently to the N7 atom of guanine forming the monofunctional products and some of them stop the replication of DNA. Most ruthenium(II) terpyridine complexes with the *N*-*N* bidentate ligand such as bipyridine (bpy) are resulting in a very low solubility in aqueous solution, and hence limiting their biologically relevant research.

In contrast, much fewer investigations on the biological effects of compounds of the neighboring group 9 metals, such as rhodium, in particular in the +3 oxidation state, have appeared.[15,23,24] It is only in the past 10 years that the structure-activity relationships (SARs) and cellular effects of cytotoxic rhodium(III) compounds have been systematically studied.[15] Rhodium(III) and rhodium(II) complexes have aroused more interest in this respect, in particular dirhodium(II) tetracarboxylate complexes $[Rh_2L_2(RCOO)_4]$ (L = H_2O or other solvent), following the discovery of their antitumor activity 40 years ago by Bear and co-workers.[23-26] Early work up to 2002 on rhodium anticancer complexes in the oxidation state +1 to +3 were summarized in a few articles.[23,24]

The subject of this doctoral dissertation is the synthesis and characterization of new ruthenium(II) complexes, such as the ruthenium(II) terpyridine and ruthenium(II) arene complexes, as well as the synthesis and characterization of new pincer-type rhodium(III) complexes. All new complexes were investigated in interaction with guanine derivatives, amino acids and heterocyclic compounds, as well as in interaction with DNA and RNA molecules, including also studies of newly synthesized complexes and monitoring their behavior with bovine serum albumin protein.

Due to this rather exceptional combination of metals and their application in anticancer treatment, this thesis is divided into two subdivisions: ruthenium complexes in anticancer treatment (**Chapter 2**) and rhodium complexes in anticancer treatment (**Chapter 3**). These studies can be overviewed in the following way:

Chapter 2:

- Synthesis and characterization of ruthenium(II) terpyridine complexes with the general formula $[Ru(L_3)(N\text{-}N)X][Y]_n$, where L_3 = 2,2':6',2"-terpyridine (tpy) or 4′-chloro-2,2′:6′,2″-terpyridine (Cl-Ph-tpy); *N-N* = 1,2-diaminoethane (en), 1,2-diaminocyclohexane (dach), 2,2'-bipyridine (bpy), (2-(methylthio)ethyl)ferrocene (mtefc), (3-(methylthio)propyl)feroccene (mtpfc) or κ^2(*1S,3R*)-$NH_2 \cap NH_2$; X = Cl; n = 1 or 2 which depend on nature of X). Stability investigation (hydrolysis reaction) of newly synthesized complexes in solutions, as well as the determination of the mechanism of substitution reactions of ruthenium(II) terpyridine complexes with biologically significant ligands. Some of the obtained results were confirmed using DFT calculations.
- Kinetic studies of substitution reactions of ruthenium(II) complexes with significant biomolecules, nitrogen- and sulfur-donor nucleophiles, using UV-Vis spectrophotometry and NMR spectroscopy.
- Investigation of ruthenium(II) complexes with DNA/RNA molecules and with proteins by UV-Vis and fluorescence spectroscopy and by viscosity measurements. For some complexes molecular docking studies with DNA were performed in order to achieve a deeper understanding of the interaction with DNA.
- Cytotoxic investigation of ruthenium(II) complexes on different cell lines, *in vitro* studies, as well as for some complexes *in vivo* studies on 4T1 tumor bearing mice.

Chapter 3:

- Synthesis and characterization of rhodium(III) complexes with the general formula $[Rh^{III}(X)Cl3]$, where X = 2,6-bis(5-*tert*-butyl-1*H*-pyrazol-3-yl)pyridine (H_2L^{tBu}), 2,6-*bis*((4*S*,7*R*)-7,8,8-trimethyl-4,5,6,7-tetrahydro-1*H*-4,7-methanoindazol-3-yl)pyridine (H_2L*) or 2,6-*bis*((4*S*,7*R*)-1,7,8,8-tetramethyl-4,5,6,7-tetrahydro-1*H*-4,7-methanoindazol-3-yl)pyridine (Me_2L*). Determination of the mechanism of the substitution reactions of ruthenium(II) terpyridine complexes with biologically significant ligands was carried out. Some of the obtained results were confirmed by DFT calculations.
- Kinetic studies of substitution reactions of rhodium(III) complexes with significant biomolecules, nitrogen- and sulfur-donor nucleophiles, using UV-Vis spectrophotometry and NMR spectroscopy.

- Investigation of rhodium(III) complexes with DNA/RNA molecules, as well as protein studies, by UV-Vis and fluorescence spectroscopy and by viscosity measurements.
- *In vitro* investigation of rhodium(III) complexes on human epithelial colorectal carcinoma HCT-116 cell line.

1.2. Ruthenium

Ruthenium is in group 8 of the transition metals and together with Os, Rh, Ir, Pd and Pt belongs to a noble group of metals. Ruthenium was named after the Latin name for Russia (*Ruthenia*) and it has the atomic number of 44 (Kr $5s^1 4d^7$) and atomic mass of 107.07. There are several isotopes of ruthenium (^{96}Ru, ^{98}Ru, ^{99}Ru, ^{100}Ru, ^{101}Ru, ^{102}Ru and ^{104}Ru), of which the ^{102}Ru isotope is the most present in nature with 31.6%. Ruthenium has a wide range of oxidation states from −1 to +8. Therefore, ruthenium complexes are reductively active and their application as reduction agents are of great importance in various chemical reactions. In physiological conditions, it can exists in three oxidation states: ruthenium(II), ruthenium(III) and ruthenium(IV). Ruthenium(III) is the dominant oxidation state in physiological conditions whereas ruthenium(II) and ruthenium(IV) oxidation states are easily achieved in the presence of biological reductants (ascorbic acid and glutathione) or in the presence of oxidation agents (O_2 or H_2O_2). All three oxidation states form coordination compounds with octahedral geometry, while ruthenium(II) can form compounds of *pseudo*-octahedral geometry, the so-called "piano stool" complexes.[1]

1.2.1. Anticancer ruthenium complexes

Cisplatin, which is used in most chemotherapies, has a structure which contains two labile chlorides in *cis* position and two amine groups, and has led Clarke and co-workers to synthesize ruthenium(III) complexes containing the above mentioned ligands, *fac*-$[Ru^{III}Cl_3(NH_3)_3]$,[27] and *cis*-$[Ru^{III}Cl_2(NH_3)_4]^+$.[28,29] In contrast to cisplatin, which predominantly binds to the residues of guanine within a single DNA chain, ruthenium(III) complexes interact with DNA by binding between the two chains probably due to the octahedral geometry of the complex.[30] Although this kind of ruthenium(III) complexes have shown very good antitumor activity, low solubility has limited their further studies.[31-33]

Mestroni and co-workers have examined the antitumor activity of ruthenium(II) complexes, *cis*-$[RuCl_2(DMSO)_4]$ (DMSO = dimethyl sulfoxide) where their results showed that this complex was not cytotoxic *in vitro*, but *in vivo* it showed a toxicity three times smaller compared

to cisplatin.[34] However, at maximum tolerated dose this complex showed a high activity for primary tumor and for the metastases in the case of a mouse with a solid metastatic tumor.[35] The cytotoxicity of the *trans* isomer is about 20 times higher compared to the *cis* isomer of this complex. Complex *trans*-[$RuCl_2(DMSO)_4$] is more effective compared to the cisplatin in terms of postoperative prolongation of the life span, *i.e.* this complex showed lower activity towards primary tumors but greater selectivity and efficiency towards metastases.[34]

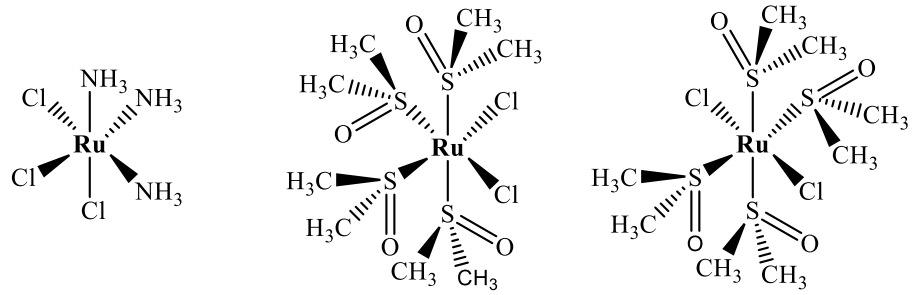

Scheme 2. Structural formulas of some ruthenium complexes that demonstrate antitumor activity.

In the last 10 to 15 years, the research has focused on two types of ruthenium complexes, NAMI-A[36-38] and KP1019,[39-41] and a group of complexes with similar ligands, such as amines, polypyridyl,[42-44] polyamine carboxylates,[45] or arenes,[46-50] as well as on various types of studies in the biological environment. Based on the reports it has been concluded that the antimethastatic activity of the ruthenium(II) arene complex is related to the interaction with the extracellular matrix and the cell surface rather than with the DNA in the cell nucleus.[51] In the past, many studies have focused on the binding of the ruthenium complex with DNA and its components,[32,42,43,52,53] while lately the main focus has been on interactions with the proteins from blood plasma.[41,54] In the proposed mechanism after intravenous administration, the ruthenium complex may be subjected to greater or lesser hydrolysis in the blood plasma and then binding to the serum of proteins such as albumin or transferrin. The proposed mechanism is to release ruthenium(II) complex from the ruthenium(III)-transferrin complex within the cell after reduction by glutathione or ascorbic acid.[39] However, if the ruthenium(III) complex reaches the cell in the form of a stable complex with a transferrin, it will follow the metabolic pathway of the iron(III)-transferrin complex within the binding to transferrin receptors on the surface of the cell. After the encapsulation in the endosome it is released as a complex of ruthenium(II) by a combination of enzymatic reduction due to the reduced pH value in the endosome.[55] If the ruthenium complex does not bind to proteins in the blood plasma it can

diffuse into the extracellular matrix and form adducts with collagen or proteins on the surface of the cell, such as actin, that may be responsible for the antimetastatic activity of NAMI-A[56-58] and ruthenium(II) arene complexes.[51] The unreacted complex can further diffuse through the cell membrane into the cytoplasm and bind to active centers of various enzymes, covalently[59-61] or non-covalently.[62,63] Finally, species that reach the cell nucleus *via* diffusion or transport mechanism, can form DNA adducts.[40,53,64] The ability to monitor the pathway of the ruthenium complex from the blood plasma to the cell, as well as the chemical transformation of ruthenium, are extremely important for understanding the mechanism of antitumor activity of the ruthenium complex.

1.2.2. NAMI-A and KP1019

Complex [Na]*trans*-[$RuCl_4$(Im)(DMSO-S)], NAMI, has been synthesized at the beginning of 1990s, and it is active against solid metastatic tumors.[37,65,66] In preclinical research, NAMI was replaced by its analogue, [Him]*trans*-[$RuCl_4$(Im)(DMSO-S)], NAMI-A. This is the first ruthenium complex which entered in the Phase 1 of clinical trials in 1999 at the Dutch Cancer Institute in Amsterdam. NAMI-A possesses favorable biological and chemical characteristics such as good antimetastatic activity, low toxicity, reproductive preparation and good stability. These properties initiate its further development. Successful completion of the Phase 1 was done on 24 patients demonstrating good tolerance without unexpected toxicity.

Simultaneously with the development of the NAMI-A, the ruthenium(III) complex KP1019 was synthesized by Alessio and co-workers in cooperation with Keppler and co-workers, [HInd]*trans*-[$RuCl_4(Ind)_2$] (Ind = indazol). KP1019 exhibits a high activity against primary cisplatin-resistant colorectal tumors, but does not exhibit significant antimetastatic activity. KP1019 has entered the Phase 1 of clinical trials in 2004, giving promising results, such as that five out of six patients experienced disease stabilization and the treatment was followed by moderate toxicity which can be caused by high binding ability to proteins, as well as by selective activation in the tissue of the tumor.[39,40] However, this complex was replaced by its analogue due to relatively poor solubility labeled as sodium salt KP1339. KP1339 is quite stable in saline solution, which is of great importance for the storage and transport of the complex as well as for clinical use. The speed of hydrolysis depends on the temperature and pH of the solution. In water at room temperature a small amount of the complex, about 2%, is hydrolyzed for 1h at pH 6.00 and 7.40, where the half time reaction is 5.4 and 0.5 h at 37 °C.

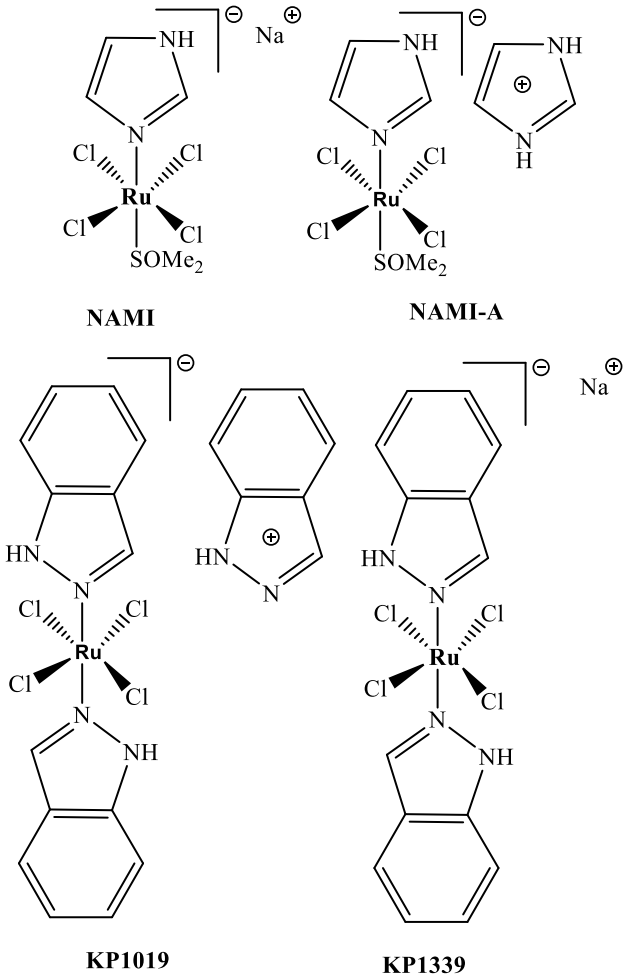

Scheme 3. Structural formulas of selected ruthenium(III) complexes who are in Phase 1 clinical trial.

The mechanism of NAMI-A complex is still unknown. *In vitro* and *in vivo* tests show that NAMI-A strongly binds to plasma proteins, such as albumin and transferrin.[67,68] NAMI-A complex has the ability to interact with DNA, but it is not considered to be the primary target. Interaction with actin within the cell,[56,57] or with collagen, leads to a reduced mobility of invasive cancer cells, and it was proposed as the possible mechanism of NAMI-A. It shows the ability not only to prevent the formation of metastases but also to inhibit the growth of cancer cells.[69]

The suggested mechanism of NAMI-A includes:[70] a) interaction within the cell cycle that results in a transient accumulation of cells in the G2/M phase, b) inhibition of metalloproteinases and activation of adhesion molecules, c) increase of the thickness of the capsule around the primary tumor and extracellular surrounding tissue and blood vessels, d) binding to nucleic acids, showing a direct effect on the DNA of the cancer cells.

The suggested mechanism of KP1019 complex includes: a) hydrolysis of the complex in blood followed by interaction with proteins such as albumin and transferrin, b) transportation of the complex into the cell through the transferrin cycle, c) release of the complex caused by pH value, d) reduction in the hypoxic tumor cell, e) binding to nucleic acids and induction of apoptosis *via* the mitochondrial pathway.

1.2.3. Organometallic ruthenium(II) arene complexes

In the last two decades numerous studies have been focused on organometallic "half-sandwich" ruthenium(II) complexes, which possess an antitumor activity *in vitro* and in some cases *in vivo*. Organometallic ruthenium(II) complexes, with the general formula [(η^6-arene)Ru(XY)Z], arene = benzene or derivatives of benzene, XY = *N*,*N*-, *N*,*O*- or *O*,*O*-chelate ligand, Z = halogen, have been extensively studied by Sadler and co-workers.[47,49,71] These types of complexes have a *pseudo*-octahedral "piano-stool" structure with a neutral arene ligand that occupies three coordination positions making the "piano stool", and a chelating ligand together with a halogen making "the legs of the chair". Similar diamino ligands have been prepared by Wilhelm's group.[47]

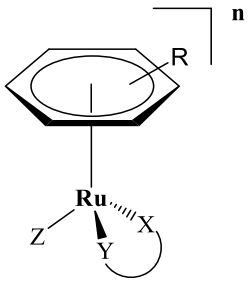

Scheme 4. General structure of ruthenium(II) arene complexes.

The structure of ruthenium(II) arene complexes allows a fine adjustment *via* synthesis for the pharmacological properties.[50] The presence of a coordinated arene ligand provides hydrophobic properties to the complex and stabilizes the ruthenium in the +2 oxidation state making the oxidation to ruthenium(III) very difficult. The nature of the arene ligand can facilitate the acquisition of complexes and interactions with potential biological targets. The leaving group, which is usually chloride, is on active position for the binding of biomolecules with the metal center and may be important for the control of activation for the kinetic reaction of the complex. Substitution of chloride by another halogen (bromide or iodide) has very little effect on the cytotoxicity of the complex. Chelate ligands can determine the stability and

kinetics of the ligand substitution in the complex. Complexes containing bidentate chelate ligand show greater activity compared to complexes with monodentate ligands.[72]

Relationship between the structure and the activity of the corresponding complexes has been studied intensively and has shown that the most active complexes are those with the chelating ligand XY = 1,2-diaminoethane (en) and the leaving group Z = Cl. The complexes of [Ru(η^6-arene)(en)Cl][PF_6] showed promising anticancer results *in vitro*, including against cisplatin resistant carcinogenic cell AR2780*cis*, and *in vivo*, showed a significant growth prevention of A2780 and A2780*cis* cells.[49,73]

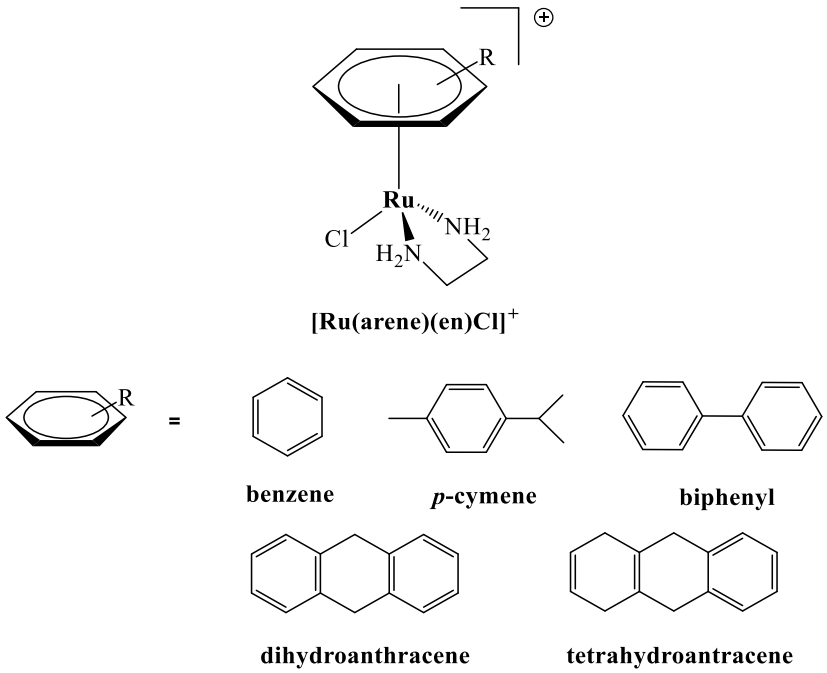

Scheme 5. Ruthenium(II) arene complexes with different arene ligands.

The cytotoxicity increases with an increasing size of the coordinate arene ligand: benzene < *p*-cymene < biphenyl < dihydroanthracene (DHA) < tetrahydroanthracene (THA). Complexes with biphenyl have similar cytotoxicity as carboplatin (IC_{50} = 6 μM) where the complex with THA has a cytotoxicity similar to cisplatin (IC_{50} = 0.6 μM), *Table 1*.

Complexes	IC_{50}/μM
$[Ru(\eta^6\text{-}C_6H_6)(en)Cl]^+$	17
$[Ru(\eta^6\text{-}p\text{-cymene})(en)Cl]^+$	10
$[Ru(\eta^6\text{-}C_6H_5C_6H_5)(en)Cl]^+$	5
$[Ru(\eta^6\text{-DHA})(en)Cl]^+$	2
$[Ru(\eta^6\text{-THA})(en)Cl]^+$	0,5
Carboplatin	6
Cisplatin	0,5

Table 1. Selected IC_{50} values of some ruthenium(II) arene complexes studied on an A2280 cell line after 24h.[72]

Hydrolysis of ruthenium(II) complexes plays an important role in determining the mechanism of cytotoxic activity.[21,74,75] Complexes with the general formula $[Ru(\eta^6\text{-arene})(L)Cl]^+$ are subjected to hydrolysis by making corresponding aqua complexes $[Ru(\eta^6\text{-arene})(L)H_2O]^{2+}$, *Scheme 6*. By a dissociative mechanism of the substitution reaction, a chloride is exchanged with the solvent molecule, and the generated complexes under physiological conditions react very quickly with biomolecules, which are significantly affective in pharmacokinetic and pharmacodynamic parameters.[54,76]

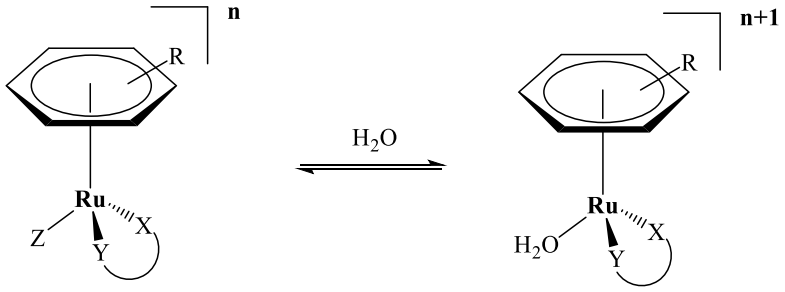

Scheme 6. Hydrolysis of ruthenium(II) arene complexes in water and formation of an aqua adduct.

The reaction of hydrolysis of the $[Ru(\eta^6\text{-arene})(en)Cl][PF_6]$ (arene = biphenyl, DHA or THA) at 37 °C, in a 0.1 M $NaClO_4$ solution (k_{H2O} = 3.95 – 6.84 x 10^{-3} s^{-1}) is one order of magnitude faster than the cisplatin hydrolysis reaction.[77] Anation reactions in the presence of 100 mM NaCl (similar to blood plasma concentrations) are very fast (k_{Cl} = 0.435 – 0.722 $M^{-1}s^{-1}$). The rate constant of hydrolysis and anation depends on the steric and electronic effect of the arene ligands. Complexes with DHA and THA ligands are subjected to hydrolysis and anation reactions twice as fast compared to a complex with a biphenyl ligand. It was found also that the rate constant of hydrolysis highly depends on the nature of the bidentate ligand and also on the pKa value of an aqua adduct.

Dyson's group and co-workers have synthesized ruthenium(II) arene complexes with the general formula [Ru(η^6-arene)$(X)_2$(pta)] (pta = 1,3,5-triaza-7-phosphatetricyclo-[3.3.1.1]decane), X = Cl or dicarboxylate), *Scheme 7*, and called them RAPTA complexes.[78] This kind of complexes are specific because of the presence of the pta ligand at the position of 1,2-diaminoethane (en). Complexes [Ru(η^6-*p*-cymene)Cl_2(pta)] (RAPTA-C) and [Ru(η^6-toluene)Cl_2(pta)] (RAPTA-T) were examined *in vitro* and *in vivo*.[51,79] *In vitro* results have shown that RAPTA-T does not have any cytotoxic effects but interacts with the components of the extracellular matrix and inhibits some of the phases of the metastatic processes, such as the separation of cells from primary tumors.[51] The most interesting fact is that the effects are higher on more invasive cancer cells than on less invasive cells. *In vivo* tests showed similar results as with the NAMI-A complex, which is surprising, taking their structural differences into consideration.

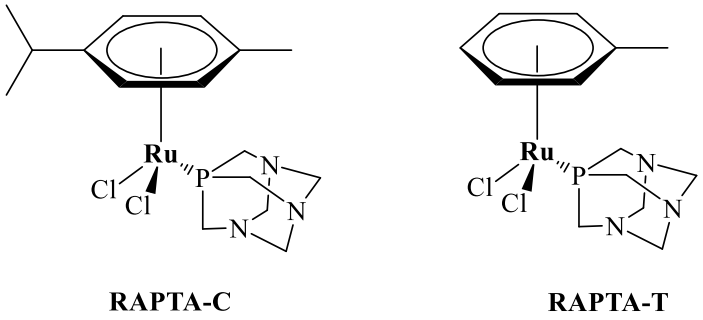

Scheme 7. Structural formulas of RAPTA complexes.

The design concept of coordinating bioactive ligands to metal centers is of great importance where such complexes can have an interesting biological activity. Hartinger's group has prepared [Ru(η^6-*p*-cymene)(flavonolato)Cl] compounds[82-85] that are able to form covalent bonds with DNA, while the complex inhibits topoisomerase IIa. The potent antiproliferative activity of organoruthenium compounds has driven by the cytotoxicity of the flavonol ligands, and the complexes were more potent topoisomerase inhibitors than the flavonols which was also dependent on the substituents found at their phenyl ring. However, the aqueous solubility of flavonols and their ruthenium(II) arene complexes was limited. They have overcome this issue by replacing the apolar arene with a L-phenylalanine (L-Phe)-derived arene ligand.[85] Phenylalanine is bioactive and inhibits alkaline phosphatase, an enzyme which is overexpressed in many tumors.[85,86]

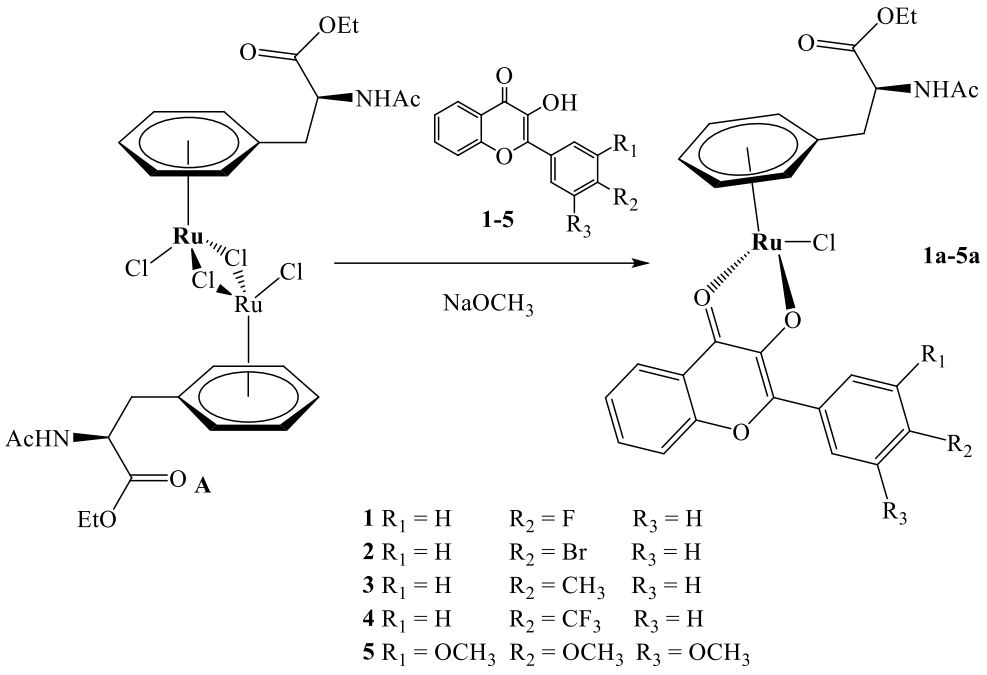

Scheme 8. Preparation of bioactive ruthenium(II) phenylalanine-derived arene complexes.

The obtained complexes have high stability in aqueous solution after dissolution in DMSO and rapidly forming adducts. The reactions with amino acids L-His, L-Met and L-Cys showed quick cleavage of the flavonolato ligand from the ruthenium center, while incubation with 9-ethylguanine (9EtG) resulted in the substitution of the chlorido ligand with the DNA model compound. From the obtained MTT assay results on NCI-H460 non-small lung cancer cells, the IC_{50} values did not follow the same trends as observed for their *p*-cymene analogues, but the values were in a similar range. This was surprising given the fact that the cellular accumulation of a representative L-Phe-derived complex was found to be much higher than its *p*-cymene analogue, independent of the concentration used and the incubation times. The compounds were synthesized to be able to coordinate to DNA, which was confirmed in the reactivity with 9EtG. It is important to note that they damage DNA, which may contribute to their cytotoxic activity. The DNA damage profile was similar to cisplatin, however, the amount of DNA damage detected was lower for the tested compounds than for cisplatin.[85]

1.2.4. Interactions of ruthenium(II) arene complexes with biomolecules

Interactions or ruthenium(II) arene complexes with biomolecules are of great importance due the fact that the DNA is the primary target of antitumor complexes such as cisplatin. Therefore, Sadler's group has studied the reactions of the complexes $[Ru(\eta^6\text{-arene})(en)X]^{n+}$, where η^6-arene = biphenyl, THA, DHA, *p*-cymene and benzene,

X = Cl^- or H_2O, with derivatives of nucleic acids which represent a DNA model.[87] Predominantly, results have shown the formation of a monofunctional product where the ruthenium complexes have interacted with the N7 nitrogen atom of guanine, *Scheme 9*. The reactivity of complexes with different positions of interaction at a neutral pH decreases in the following sequence: guanosine (N7) > cytidine (N3) > adenosine (N7) > adenosine (N1). With the interaction of 9-ethylguanine (9EtG) a new product has been synthesized and characterized with X-Ray structural analysis where a selective Ru-N7 (guanine) coordination was detected and concluded that the Ru-N7 bond was further stabilized by a stereospecific hydrogen bond between C6=O guanine and NH group from 1,2-diaminoethane (en), as well as by π-π interactions between the aromatic ligand and nucleobases.[71] Similar results were obtained with mononucleotides (5'-GMP, 5'-AMP, 5'-CMP and 5'-TMP) with the above mentioned ruthenium(II) arene complexes. The pathway of the reaction happens with hydrolysis of the complex and the formation of the active aqua adduct. The latter first coordinates with the nucleotide over the oxygen from the phosphate group and then continues to the formation of the N7 adduct as the main product.[87]

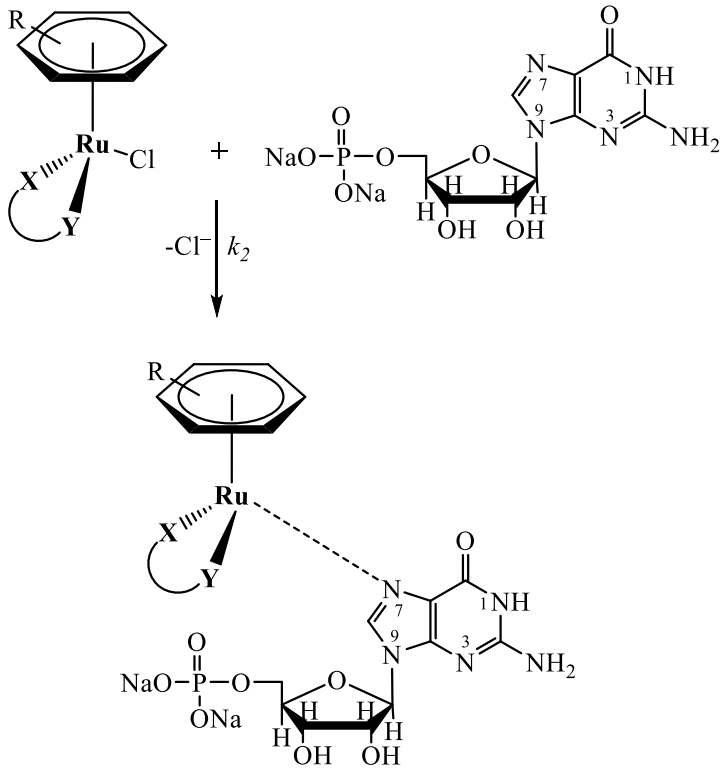

Scheme 9. Pathway of interaction of the ruthenium(II) arene complexes with guanosine-5'-monophosphate.

Taking into consideration the interactions with the oligonucleotides, the complex [Ru(η^6-*p*-cymene)(en)Cl][PF_6] is selectively binding to guanine (G) in oligonucleotides, forming the monofunctional Ru-G7 and Ru-G8 adducts, as well as the bifunctional adduct G7(Ru)-G8(Ru).[88] Interactions of the complex [Ru(η^6-biphenyl)(en)Cl][PF_6] with duplex d(ATACATGGTACATA) or d(TAT^{17}G^{18}TACCATGTAT) was studied using the HPLC-ESI-MS method, as well as using 2D NOESY NMR spectroscopy. It was found that the ruthenium is coordinated *via* N7 atoms from G and binding mono- and bifunctional to the oligonucleotide. On one conformer, an intercalation of a biphenyl arene part between the G18 and T17 has been noticed, while the second conformer has no intercalation, but the arene ligand leans on a T17.[88]

The reactions of ruthenium(II) arene complexes with the amino acids containing sulfur, such as L-cysteine (L-Cys) and L-methionine (L-Met) are of great interest in sense of the strong impact on intracellular chemistry of ruthenium antitumor complexes and especially their detoxification and resistance mechanism.[89] Proteins can also play an important role in the mechanism of action of the ruthenium(II) arene complexes, including the possibility that ruthenium can replace iron in proteins. According to the results for complex [Ru(η^6-biphenyl)(en)Cl]$^+$, it was found that it reacts slowly with the thiol group from the L-Cys amino acid in a ratio of 1:2 in an aqueous solution at 37 °C. Monitoring the experimental results, at the start of the reaction three mononuclear adducts were formed where L-Cys is coordinated for ruthenium *via* sulfur or oxygen. After 24 hours, two dinuclear adducts were formed, which contain one or two bridged ligands from cysteine as a ligand. The unusual cluster {Ru(η^6-biphenyl)}$_8$ was also formed at higher concentrations of L-Cys. Regarding the reactions with L-Met it was found that the interactions were also poor and only 28% of the [Ru(η^6-biphenyl)(en)Cl]$^+$ complex reacted and gave one final product of [Ru(η^6-biphenyl)(en)(L-Met-S)]$^{2+}$. Analyzing the results it can be concluded that the investigated arene complexes have an affinity to react with nitrogen donors from guanine which indicates that adducts with DNA can be formed even in the presence of amino acids, peptides and proteins. In contrast, ruthenium(III) complexes bound more firmly to proteins such as albumin or transferrin, compared to interaction with DNA, where proteins can be used as a transporter of the complexes to the cancer cells.[90,91] This indicates the differences between the mechanism of actions of ruthenium(II) arene complexes and ruthenium(III) complexes.

The obtained results from observing the interactions of two ruthenium arene complexes [Ru(η^6-*p*-cymene)(en)Cl][PF_6] and [Ru(η^6-biphenyl)(en)Cl][PF_6] with human serum albumin using mass spectrometry (MS) show that both complexes coordinate with histidine (His128,

His247, His510) and methionine (Met268) on the surface of the albumin.[92] In addition, the complex [Ru(η^6-*p*-cymene)(en)Cl][PF_6] can enter inside of the structure of the protein where it binds to Cys34. There it can induce the oxidation of the thiolate to a sulfonate. Since Cys34 is inside of the protein structure, the complex [Ru(η^6-biphenyl)(en)Cl][PF_6] cannot coordinate to Cys34 due to the fact that a phenyl ring makes it difficult. It was concluded that the arene ligand plays a key role in protein interactions. Therefore, such oxidation reactions of thiols caused by the coordination of ruthenium can be very significant in the pharmacological activity of these ruthenium(II) complexes.

1.2.5. Ruthenium(II) polypyridyl complexes

In the last few decades ruthenium polypyridyl has been most attractive in senses of an alternative for the use in classical chemotherapy and some of them have been found to have a promising antitumor activity.[89,93] The direct relationship between cytotoxicity and the coordination of the ruthenium polypyridyl complexes to DNA was initiated by Brabec and co-workers.[93] Cytotoxicity of the three ruthenium(II) polypyridyl complexes [Ru(tpy)(bpy)Cl][Cl], *cis*-[Ru(bpy)$_2$Cl$_2$] and *mer*-[Ru(tpy)Cl$_3$] (tpy = 2,2',6',2''- terpyridine, bpy = 2,2'=bipyridine) was tested for various tumor cell lines.[53,93] The complex *mer*-[Ru(tpy)Cl$_3$] showed significantly higher cytotoxicity compared to the other two complexes. The high activity of this complex is due its ability to bind to DNA through two guanine derivatives in the *trans* position.[94] Reedijk and co-workers have shown that *cis*-[Ru(bpy)$_2$Cl$_2$] forms a monoadduct with 9-ethylguanine (9EtG) and a crystal structure of the complex revealed the coordination of 9EtG through the N7 position of the nitrogen atom.[95] Alberto and co-workers, on the other hand have shown that under the same conditions the quantitative coordination of the two guanine derivatives from 9-methylguanine (9MeG) in the *cis* position through N7 of the nitrogen atom.[96] During the last years numerous ruthenium(II) complexes containing terpyridine have been synthesized with the general formula *mer*-[Ru(tpy)(*N*-*N*)Cl]$^+$ where *N*-*N* = bidentate nitrogen-donor ligand.[44,97-100] Their DNA binding ability was studied and it was found that most of these complexes bind covalently through N7 of the nitrogen atom in guanine and some of them stop DNA replication.[93,97] Three isomeric ruthenium(II) polypyridyl complexes α-, β- and γ-[RuCl$_2$(azpy)$_2$] where azpy = phenylazopyridine were tested on the cancer cell lines: MCF-7, EVSA-T, WIDR, IGROV, M19, A498, H266 and A2780.[101-103] Complex α-[RuCl$_2$(azpy)$_2$] showed the highest activity with IC_{50}'s value of 0.86 and 0.98 μM for the A2780 and A2780*cis*R cell lines which is in the same range as the cytotoxicity of the ruthenium(II) arene complexes at the same cell lines.[104]

Complexes with general formula trans-$[RuL_3][PF_6]_2$ (L = 2-phenylazopyridine or *o*-tolylazopyridine) and complexes with the general formula $[RuL_2'L''][PF_6]2$ (L = 2-phenylazopyridine or bipyridine) were studied for cytotoxic activity as well.[105] These complexes were designed to examine the hypothesis that the complex α-$[RuCl_2(azpy)_2]$ possesses high cytotoxic activity due to two *cis* chloride ligands, which can be preplaced by interaction with DNA, as in the case with cisplatin. Complexes *mer*-$[Ru(azpy)_3]$ and *mer*-$[Ru(tazpy)_3]$ showed cytotoxic activity for a series of cancer cell lines: MCF-7, EVSA-T, WIDR, M19, A498, H266. The conclusion is that even in the absence of a chloride ligand a cytotoxic activity is detected. This would mean that 2-phenylazopyridine ruthenium(II) complexes act with a completely different mechanism compared to cisplatin.

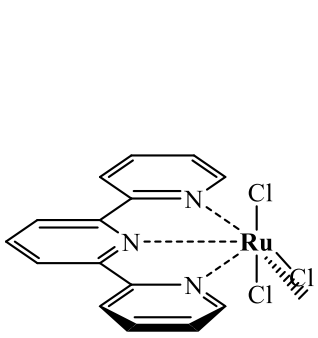

***mer*-[Ru(tpy)Cl$_3$]**

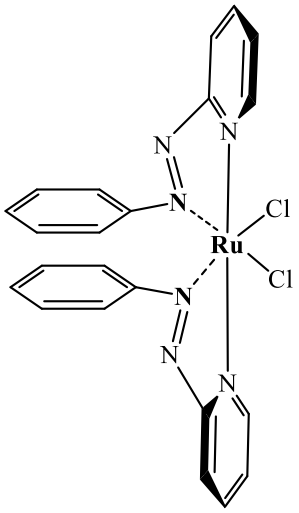

***cis*-[RuCl$_2$(aypy)$_2$]**

Scheme 10. Structures of some ruthenium(II/III) polypyridyl complexes.

Recently, Bugarčić and co-workers have developed new ruthenium(II) polypyridyl complexes of the general formula *mer*-$[Ru(L_3)(N\text{-}N)X][Y]n$ in which L_3 = terpyridine or chloride-terpyridine, X = Cl or dmso-S, *N-N* = 1,2-diaminoethane (en), 1,2-diaminocyclohexane (dach) and bipyridine (bpy), Y = Cl, PF_6 or CF_3SO_3 and n = 1 or 2, depending on the nature of X.[106] Studies of three ruthenium polypyridyl complexes, *i.e.* [Ru(Cl-tpy)(en)Cl][Cl], [Ru(Cl-tpy)(dach)Cl][Cl] and [Ru(Cl-tpy)(bpy)Cl][Cl], *Scheme 11*, showed that they are capable to bind on guanine derivatives after the dissociation of the monodentate ligand, *i.e.* Cl, forming monofunctional adducts. They bind strongly to CT-DNA ($K_b = 10^4 – 10^5$ M^{-1}), both covalently and non-covalently, intercalating between base pairs,[107] which means they can be referred to as classical compounds. Knowing that proteins play a crucial role in the transport and deactivation of ruthenium drugs, detailed studies have been

conducted in interaction with human serum albumin (HSA) and transferrin (Tf).[108] Compared to Tf, HSA appears to be a more favorable binding partner for the studied ruthenium compounds. Moderate to strong binding to HSA was found, whereas their affinity for Tf was much lower. Complexes containing en and dach were more reactive with HSA and Tf than to the complex containing bpy, possibly due to the easier release of chloride. The binding of the compounds to HSA and Tf did not affect secondary structures of the proteins much, whilst their tertiary structures showed some alternatives.[108] This is important knowing that the native conformation of a transport protein should not be markedly altered upon binding a drug. Such occurrence may prevent the protein from performing its normal actions, *i.e.* binding cellular receptors and delivering the drug, or it may even be sent down a degradation pathway. Overall, the study implies that proteins are biological targets of the ruthenium(II) terpyridine compounds. The cytotoxicity of this kind of complexes was studied by MTT assay using human lung carcinoma (A549), human colon carcinoma (HCT116) and mouse colon carcinoma (CT26) cell lines. It was found that [Ru(Cl-tpy)(en)Cl][Cl] and [Ru(Cl-tpy)(dach)Cl][Cl] showed high to moderate *in vitro* cytotoxicity, with IC_{50}'s of 32.80 – 66.30 μM.[107,109]

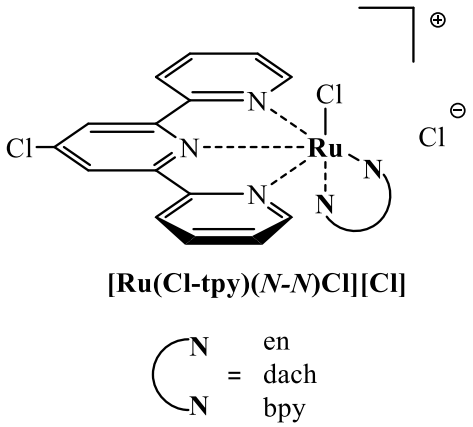

Scheme 11. General formula of ruthenium(II) terpyridine complexes.

1.3. Rhodium

Rhodium belongs to the IX group of transition metals and the name was introduced from the Greek name for a rose (*rhodon*). Rhodium has a atomic number 45 (Kr $5s^1 4d^8$) and atomic mass of 102.90. There are several isotopes of rhodium (more than 20 isotopes starting from ^{93}Rh to ^{117}Rh), but naturally occurring rhodium is composed of only one isotope ^{103}Rh and the most stabile radioisotopes are ^{101}Rh, ^{102}Rh, ^{102m}Rh and ^{99}Rh. Rhodium has a wide spectra of applications but the major one is as a catalytic converter, changing harmful unburned hydrocarbons, carbon monoxide and nitrogen oxide exhaust emissions into less noxious

gasses.[110] Rhodium is a non-biological precious metal and has been relatively little used in biological or medicinal contexts. However, rhodium complexes have desirable attributes for use in a complex biological milieu where rhodium complexes occur in oxidation states 0, +1, +2, +3 and display low oxophilicity, *i.e.* broad functional group tolerance and aqueous stability.[111-114]

1.3.1. Anticancer rhodium complexes

The first mention of anticancer properties of a rhodium complex, $RhCl_3 \cdot 3H_2O$, appeared in 1953, preceding Rosenberg's accidental discovery of cisplatin activity by more than a decade.[13,14] There were some reports of antitumor activity of some complexes such as *mer*-[$RhCl_3(NH_3)_3$] and *mer,cis*-[$RhCl_3(DMSO)_2(NH_3)$],[15,115,116] but the most recent research of biological interest happened in the last 10 years, and the structure-activity relationship and cellular effects of cytotoxic rhodium(III) compounds have been systematically studied.

Two complementary rational approaches for designing rhodium(III) complexes with increased activity involved: a) introduction of one or more ligands with a stronger *trans* effect to significantly improve the rate of substitution of the opposite halide ligands and b) the coordination of ligands that themselves are cytotoxic and that can potentially participate in specific interactions with some biological targets.[15] Among the most-well known ruthenium complexes mentioned above are NAMI-A and KP1019. Making the analogues of this kind of complexes where rhodium was used as a metal center instead of ruthenium, the complex [ImH][*trans*-[$RhCl_4(Im)_2$] where Im = imidazole, was synthesized. The results showed that ligand exchange reactions proceed significantly more slowly than for the structurally related ruthenium(III) anticancer agent KP1019, and the rhodium(III) complex is biologically inactive.[15,116]

1.3.2. Trichlorido- and dichloridorhodium(III) complexes

The biological properties of trichloridorhodium(III) complexes should be significantly modified due to higher rates of DMSO and/or chloride exchange. Meridional complexes *mer*-[$RhCl_3$(DMSO)(pp)], *Scheme 12*, have been prepared by treatment in the dark of *mer,cis*-[$RhCl_3$(DMSO-κ*S*)$_2$(DMSO-κ*O*)] with the appropriate pp ligand in CH_3OH/H_2O where pp = bpy (bipyridine), phen (phenanthroline), dpq (dipyrido[3,2-*d*:2',3'-*f*]quinoxaline), dppn (benzo[*i*]dipyrido[3,2-*a*:2',3'-*c*]phenazine), dppy (dipyrido[3,2-*a*:2',3'-*c*]phenazine),[15,117] or due to lower solubility of substituted phen ligands in non-polar solvent $CHCl_3$ for pp = 5-Clphen, 5-NO_2phen.[118] Complexes *mer*-[$RhCl_3$(DMSO)(pp)] were stable in $CHCl_3$

solution on roomlight irradiation for 24h but slowly isomerized to *mer/fac* mixtures in polar DMSO solutions under similar conditions.[15,117]

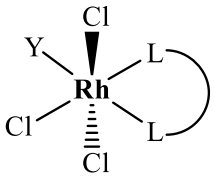

Y = DMSO; LL = bpy, phen, dpq, dppn, dppy, dab and [6]aneS$_2$

Scheme 12. Structures of *mer*-[RhCl$_3$(DMSO)(pp)] complexes that showed cytotoxic activity on cancer cells.

All of the complexes showed the activities on cancer cell lines MCF-7, HT-29 and HEK-293. The following SARs could be established for their IC$_{50}$ values: a) bpy > phen > dpq, dppz, dppn where Y = DMSO; b) phen > 4,7-Me$_2$phen > 5,6-Me$_2$phen, 5-Clphen, 5-NO$_2$phen where Y = DMSO; c) LL = en > dab (1,2-diaminobenzene), [6]aneS$_2$ > bpy where Y = DMSO; d) Y = CH$_3$CN > TMTU > DMSO for LL = phen where TMTU = tetramethylthiourea. High IC$_{50}$ values for the κ^2*N*(diamino) LL ligands en and dab in the series en > dab > [6]aneS$_2$ > bpy underlined the importance of the popypyridyl ligands for understanding cytotoxicity. However, the IC$_{50}$ value for the κ^2*S* [6]aneS$_2$ complex towards MCF-7 cells was only 2.2 times higher than that of the bpy complex, suggesting that alone the presence of soft donor atoms in the chelating ligand may be crucial.[15]

As for the *facial* trichloridorhodium(III) complexes, UV-Vis and CD studies were in accordance with the absence of significant DNA intercalation by the complexes *mer*-[RhCl$_3$(DMSO)(pp)].[15,117-119] Gel retardation assays with plasmid pBr322 revealed no significant DNA cleavage of the dpq and dppz complexes either in the dark or following 30 min irradiation at selected wavelengths.[120] Time dependent ^{1}H NMR investigations of 1:2 M aqueous solutions of the dpq and dppz complexes with 5'-GMP and Ac-Met-OH at 40 °C also provided no evidence for the coordination of either the guanine N7 atoms or the thiaether *S*- atoms of the latter biomolecules over a 72 h period.[15]

Morrison and co-workers have studied in detail the complexes bis(bipyridyl)rhodium(III), *Scheme 13*, such as *cis*-[RhCl$_2$(dppz)(phen)]Cl and *cis*-[RhCl$_2$(3,4,7,8-Me$_4$phen)$_2$]Cl complexes as potential phototoxic agents for the destruction of cancer cells.[15, 121-123]

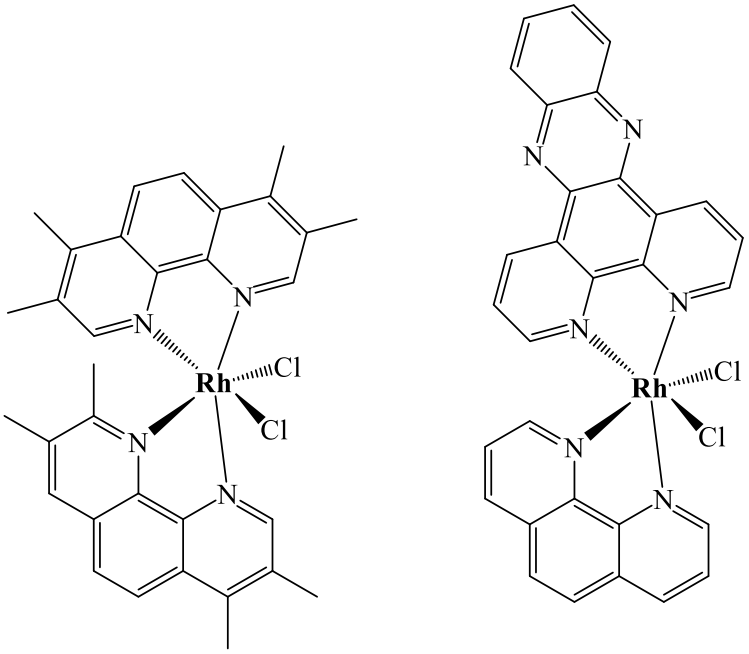

Scheme 13. Structures of the dichloridorhodium(III) complex cations a) *cis*-$[RhCl_2(3,4,7,8\text{-}Me_4phen)_2]^+$ and b) *cis*-$[RhCl_2(dppz)(phen)]^+$.

Light-activated drugs offer an attractive therapeutic strategy that minimizes damage to normal surrounding tissues by enabling both temporal and spatial control over toxicity.[15] After the titration of CT-DNA and observation of hypochromic and bathochromic shifts for dppz MLCT bands, it is confirmed that a relatively strong intercalation is present. In contrast, after the irradiation at 330 nm there was a rapid photo induced Cl^-/H_2O exchange and a formation of the dicationic aqua species *cis*-$[RhCl(H_2O)(dppz)(phen)]^{2+}$. Dose dependent nicking of supercoiled plasmid DNA was observed in the presence of *cis*-$[RhCl_2(dppz)(phen)]Cl$ upon irradiation at 311 nm. The dppz compound was an effective phototoxic agent at 311 nm against the cancer cell lines KB (human nasopharyngeal carcinoma), GN4 (canine prostate carcinoma) and M109 (human lung carcinoma) but exhibited no cytotoxicity in the dark.[15]

An analogous application of *cis*-$[RhCl_2(dppz)(phen)]$ in photochemotherapy was restricted by its modest hydrophobicity, which prevented its passing through the cell membranes of HeLa and KB cells.[122] In contrast, the complex *cis*-$[RhCl_2(3,4,7,8\text{-}Me_4phen)_2]Cl$ was synthesized which successfully increased the hydrophobicity to enable significant uptake by KB cells. After 3h of incubation period of the KB cells with 55 μM solution of *cis*-$[RhCl_2(3,4,7,8\text{-}Me_4phen)_2]Cl$ complex and irradiation at 311 nm about 55% cell death occurred in 40 min. As the exposure to UV light led to rapid formation of *cis*-$[RhCl(H_2O)(3,4,7,8\text{-}Me_4phen)_2]Cl_2$, it is believed that this is the major photoactive agent.

The photoactivated *cis*-[$RhCl_2$(3,4,7,8-Me_4phen)$_2$]Cl complex restricted *in vitro* malignant melanoma cell growth by about 40% at 100 µM and inhibited cancer growth in a xenograft melanoma model by about 50% after 60 days.[15,123]

1.3.3. Cyclopentadienyl complexes

Replacement of three water molecules in the hexaaqua cation $[Rh(H_2O)_6]^{3+}$ by *facial* cyclopentadienyl ligand leads to a dramatic increase in the liability of the remaining aqua ligands. The rate constant, k_{ex}, for H_2O exchange increases for $[Rh(\eta^5\text{-Cp*})(H_2O)_3]^{2+}$ up to 1.6 x 10^5 s^{-1}.[124] Introduction of the bpy ligand in the complex reduces the liability of the remaining aqua ligand by about two orders of magnitude down to 1.59 x 10^3 s^{-1}. Polypyridyl complexes of the type $[Rh(\eta^5\text{-Cp*})(pp)]^+$ also undergo rapid aquation due to the strong *trans* effect of the anionic $[Cp^*]^-$ ligand.[15,125]

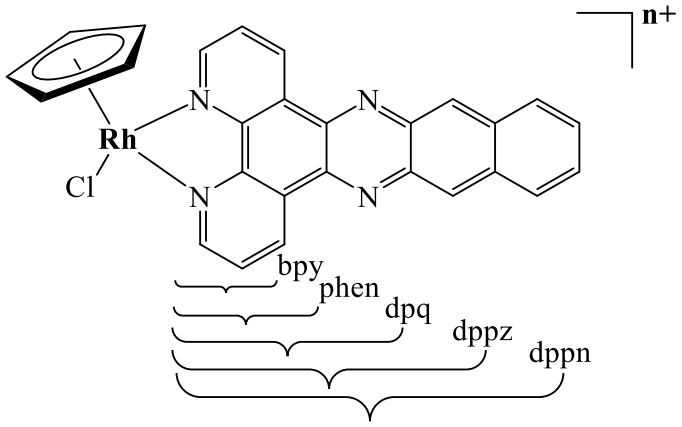

Scheme 14. Structures of cytotoxic half-sandwich Rh^{III} complexes with pp ligands.

The IC_{50} values of complexes $[Rh(\eta^5\text{-Cp*})(pp)](CF_3SO_3)$ towards MCF-7, HT-29 and HEK-293 cancer cell lines have been done, *Table 2*. The complexes with the large dppz ligand exhibited closely similar IC_{50} values of 1.5/4.3 µM for the MCF-7/HT-29 cells, which were a bit higher than those of 0.8/1.8 µM for the free ligand. Replacement of dppz by the smaller phen and phen* ligands had little effect on the activity of the rhodium(III) complexes, which all lay within the narrow IC_{50} range of 2.27/8.21 µM.[15]

Ligand pp	IC_{50}/μM MCF-7	IC_{50}/μM HT-29	IC_{50}/μM HEK-293
en	100	100	n.d.
bpy	100	100	n.d.
phen	4.7	8.0	0.7
5-Clphen	3.5	8.2	8.3
5-NO_2phen	4.3	4.6	3.9
4,7-Me_2phen	2.5	2.2	0.4
5,6-Me_2phen	3.9	n.d.	0.8
4,7-$(MeO)_2$phen	3.6	3.5	n.d.
dpq	5.1	8.5	n.d.
dppz	1.5	4.3	n.d.
12,13-Me_2dppz	0.9	0.9	2.4
dppn	0.8	3.2	n.d.

Table 2. Selected IC_{50} values for half-sandwich rhodium complexes of type [Rh(η^5-Cp*)(pp)](CF_3SO_3) towards MCF-7, HT-29 and HEK-293 cell lines after incubation period of 72 and 96h.

DNA is considered to be a potential intracellular target for ruthenium(II) arene complexes and both intercalative and covalent Ru-*N* binding modes have been established in model studies. The binding preference of the cyclopentadienyl rhodium(III) complexes is dependent on both the aromatic surface area of chelating ligands and the HSAB properties of the metal center. UV-Vis and CD spectroscopic studies indicated stable intercalative binding by the analogous cyclopentadienyl rhodium(III) dpq and dppz complexes, as confirmed by viscosity increases due to marked DNA lengthening.[126] On the other hand, ^{1}H NMR spectra documented rapid reaction of these rhodium(III) complexes with 5'-GMP in aqueous solution at 30 °C leading to effectively quantitative guanine N7 coordination within 5 min.[15, 126]

Cyclopentadienyl rhodium(III) complexes containing κ^2*N,O* ligand $qnol^-$ and $npox^-$ have also been investigated as potential anticancer agents, *Scheme 15*.[127,128] Respective IC_{50} values of 0.8, 0.9 and 5.9 μM were established on the basis of a WST-1 cell assay for [Rh(η^5-Cp*)(qnol)] towards the human melanoma SK-Mel and C-32 cells and human glioblastoma SNB-19 cells after a 72 h incubation.[128] The IC_{50} values were obtained, 4.9 and 9.8 μM. Both complexes had no activity on human melanoma SH-4 cells. During the treatments lasting 24 or 48 h complex [Rh(η^5-Cp*)(npox)] inhibited growth of HeLa and promyelocytic leukemia (HL60) cells and the obtained IC_{50} values were 2.2 and 2.0 μM.[15,127]

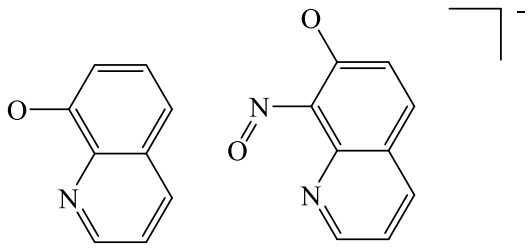

qnol$^-$ **npox$^-$**

Scheme 15. Selected ligands in coordination with cyclopentadienyl rhodium(III) complex with cytotoxic activity.

The IC_{50} values for complexes containing pp ligands (5,6-Me_2phen, 5-Clphen, 5-NO_2phen, dppz) towards HEK-293 cells were closely similar to the values recorded for HT-29 cells.[15]

1.3.4. Dirhodium(II) complexes

The exploration of dirhodium(II,II) complexes as anticancer agents dates back to the 1970s, with the rhodium carboxylate [$Rh(CH_2COO)_4$] being found to show carcinostatic activity, although with a lower potency compared to cisplatin. Later studies suggested that the dirhodium(II,II) complexes exert antiproliferative activity by binding covalently to the purine bases of DNA, generating DNA intrastrand and interstrand crosslinking. Recent reports have indicated that dirhodium(II,II) complexes might also target proteins. Che and co-workers reported that dirhodium(II,II) complex A, *Scheme 16*, inhibited the UPS (ubiquitin-proteasome system) at sub-micromolar concentrations, which was attributed to its ability to inhibit proteolysis.[129,130] The dirhodium(II,II) carboxylates inhibited UPS at concentrations that were at least 10-fold lower than that required for inducing DNA damage, suggesting that cytotoxic activities were linked to their actions on the UPS. Besides anticancer activity, dirhodium(II,II) complexes have also been tested for anti-inflammatory applications. Martinez-Manez and co-workers have reported non-toxic CO-releasing dirhodium complex B, *Scheme 16*, that inhibit NO production in stimulated macrophage cells. At low concentrations, CO can reduce NO production and thus such CO-releasing molecules might find potential use for the treatment of inflammatory diseases such as arthritis.[130,131]

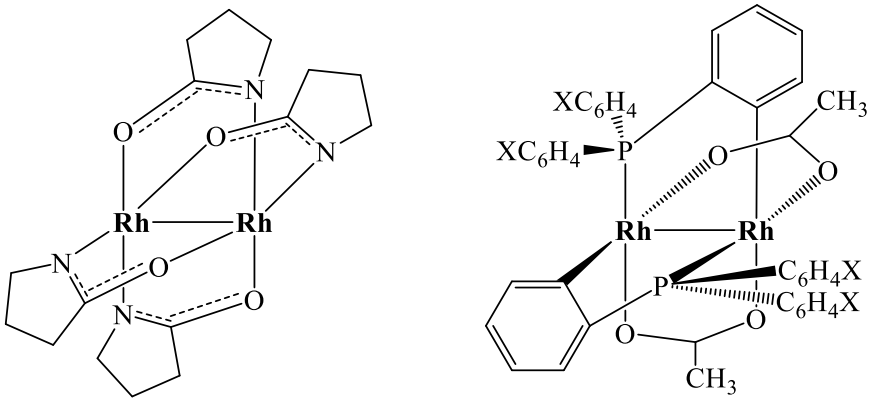

Scheme 16. Structures of dirhodium(II,II) complexes A and B.

Studies over many years established that dirhodium(II,II) complexes bind directly to Lewis bases on DNA *via* initial axial coordination and eventual displacement of equatorial ligands, such as acetate, to form bridging DNA complexes.[114,132-134] Ligands with extended π conjugation, such as 1,10-phenantroline derivatives, exhibit generally enhanced DNA affinity and cell-killing activity.[114,135]

1.4. Osmium

Osmium belongs to the VIII group of transition metals and the name was introduced from the Greek name for a "smell" (*osme*). Osmium has the atomic number 76 (Xe $6s^2 5d^6 4f^{14}$) and atomic mass of 190.23. Osmium has seven isotopes in nature where six of them are stable: ^{184}Os, ^{187}Os, ^{188}Os, ^{189}Os, ^{190}Os and ^{192}Os. Osmium has a wide range of use, but due to his toxicity osmium is rarely applied in its pure state, so instead was often used as alloy with other metals. Osmium derivatives are important oxidants in organic synthesis and in catalytic reactions.[153] Osmium compounds are rarely used, but it is used as an addition to alloys which increases hardness. Also it plays the role of an efficient catalyst in several chemical reactions.

1.4.1. Anticancer osmium complexes

Osmium complexes have received far less attention than ruthenium complexes in sense of implementation in medicinal chemistry. The general reason is partially motivated by the well-known toxicity of OsO_4.[154,155] However, in different forms osmium may possess properties useful for anticancer activity. The implementation of novel ligands and the diverse coordination geometries and oxidation states of osmium has led to the development of a limited range of osmium complexes as potential anticancer agents in the last six years.[155]

A precursor of the osmium analogue KP1019 was reported corresponding to *trans*-[$Os^{IV}Cl_4(HInd)_2$], where HInd is indazole. The coordination mode of indazol to osmium involves the unprecedented stabilization of the 2*H*-indazol tautomer. Compared to KP1019, *trans*-[$Os^{IV}Cl_4(HInd)_2$] showed suppressed hydrolysis in aqueous solution and similar antiproliferative activity in an ovarian cancer cell line.

The osmium analogue of NAMI-A is more inert and stable towards hydrolysis in aqueous and physiological media and, in contrast to NAMI-A derivatives, does not interact with 9-methyladenine.[156,158] *In vitro* cytotoxic studies of Os-NAMI-A showed a three-fold higher activity in colon carcinoma (HT-29) and a two-fold decrease in mammary carcinoma (SK-BR-3) cell lines compared to NAMI-A.[156,159]

The reactivity of the osmium analogue of RAPTA-C was studied towards a single-stranded 14-*mer* DNA fragment. While RAPTA-C formed mainly mono-adducts accompanied by arene retention owing to the increased inertness of osmium(II) towards ligand substitution.[156,160] Furthermore, the osmium analogue did not undergo excessive aquation and was inactive up to the maximum solubility in colon (HT-29), non-small cell lung (A549) and breast (T47D) carcinoma cell lines.[156,161]

Although the aqueous chemistry of osmium complexes is not completely understood,[162,163] some trends on physicochemical properties have emerged in comparison to isostructural ruthenium analogues.[156] A typical feature of osmium compounds is the increased inertness towards ligand substitution compared to ruthenium and therefore often results in a reduced or even suppressed hydrolysis of the metal-halido bonds.[156] Moreover, upon hydrolysis, the formed aqua adduct of the osmium complex tend to be more acidic than ruthenium aqua adducts, *i.e.* a pK_a drop of 1.5 pH units is often observed for the osmium(II) compounds compared to ruthenium(II) analogues.[156,164] Osmium(II) compounds may be found as unreactive hydroxido species under physiological conditions. According to the HSAB principle, osmium is slightly softer than ruthenium, which is expected to result in slightly different coordination preferences to biomolecules.[156]

1.5. Kinetic reactions of transition metal complexes

The study of the kinetics of a chemical reaction aims at determining the speed of the reaction, as well as determining the influence of different parameters (change of reactant concentration, pH, temperature and pressure change, catalyst, etc.) at the reaction rate. One of the objectives of studying the chemical reaction is determining the reaction mechanism,

i.e. determination of the elementary reaction steps which lead to the formation of the reaction product. Determining the reaction mechanism is implicative of the way in which a chemical bond breaks down and then the way in which a new chemical bond is formed. It must be taken into account that every elementary reaction step has its own mechanism where a complete explanation of the reaction mechanism is difficult to explain.

From *Scheme 17.* certain phases can be seen which must be taken into account when determing the chemical reaction mechanism.[136]

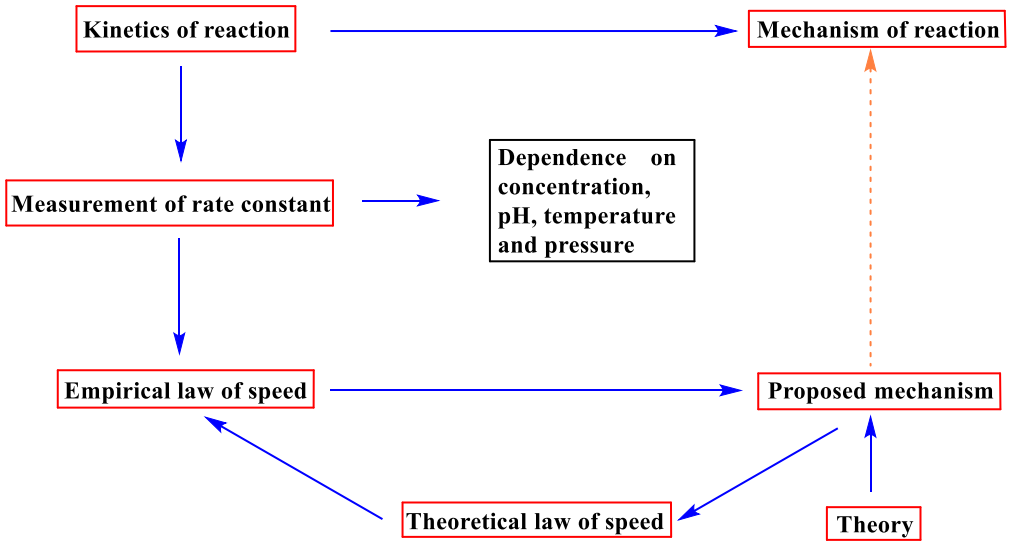

Scheme 17. Steps in determing a chemical reaction mechanism.[136]

The study of a mechanism of inorganic reactions has expanded with the development of organometallic and bioinorganic chemistry as well as with the expansion of the new techniques such as UV-Vis spectrophotometry, NMR spectroscopy, „stop-flow“ spectrophotometry, HPLC etc.

1.5.1. Substitution reactions of complexes

Substitution reactions of complexes can be electrophilic (S_E) and nucleophilic (S_N), depending on whether the substitution occurs in the substitution process of the central metal ions or ligands. If a metal ion is substituted during the reaction, *i.e.* electrophile, this is the reaction of an electrophilic substitution, equation 1.5.1, and if a ligand replacement is performed then the nucleophilic substitution reaction is happening, equation 1.5.2.

$$[ML_n] + M' \rightleftharpoons [M'L_n] + M \qquad S_E \qquad 1.5.1$$

$$[ML_n] + X \rightleftharpoons [ML_{n-1}X] + L \qquad S_N \qquad 1.5.2$$

Nucleophilic substitution reactions, according to *Langford* and *Gray*[137] take place by three different mechanisms:

- Dissociative mechanism (D)
- Associative mechanism (A)
- Mechanism of interchange (I)

With the dissociative mechanism (D), in the first stage of the reaction comes to dissociation of one ligand L from the coordinate sphere of the complex, whereby an intermediate with reduced coordination number is formed. In the next step, the input ligand K is bonded to the central metal ion. Since the first stage of the reaction is slower, it determines the overall rate of the substitution reaction.

With the associative mechanism (A), in the first stage the input ligand X is bound to a central metal ion generating the intermediate with an increased coordination number, and then in the second phase, the leaving ligand L leaves the coordination sphere of the complex.

The building reaction of an intermediate with an increased coordination number is slower and it determines the speed of the substitution process.

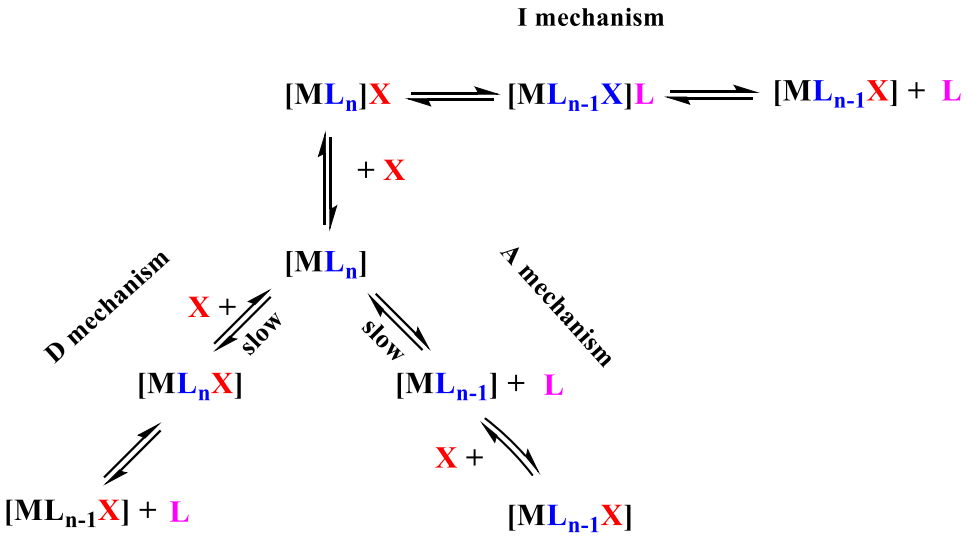

Scheme 18. Mechanisms of nucleophilic substitution of complexes.

The mechanism of interchange (I) is the process in which, in the first phase, the input ligand X binds to electrostatic forces for the external coordination sphere of the complex. Thereafter, the incoming ligand migrates from the external to the internal coordination sphere while simultaneously migrating to the outgoing ligand L from the inner into the outer coordination sphere. The ultimate process is to break the connection between the complex and the outgoing ligand. This mechanism, unlike the previous two, does not have an intermediate, but there is a transient state, *i.e.* the process has its own activation energy. The change mechanism can be divided into Ia, associative interchange, and Id, dissociative interchange, mechanisms. If the process of breaking the link between the central metal ion and the outgoing ligand L has a greater impact on the reaction rate of the chemical reaction, the mechanism is labeled with Id, and if the process of forming a new connection between the central metal ion and the input X has a greater impact on the rate of the chemical reaction, the mechanism is marked with Ia.[137,138]

1.5.2. Activation parameters

The determination of mechanism of the chemical reaction is based on the analysis of the obtained values of the thermodynamic parameters ($\Delta H^{\neq}$, $\Delta S^{\neq}$, $\Delta V^{\neq}$), which characterize a particular process. It is necessary to first define the value of the constant of the reaction rate *k*, for which there is a large number of experimental methods. The choice of the appropriate method depends on both the speed of the process being studied and the characteristics of the participants in the chemical reaction.[139]

Knowing the value of the constant of the reaction rate at different temperature allows the determination of their thermodynamic parameters. The value of the activation energy *Ea* is determined using the *Arrhenius* equation 1.5.3.[139-141]

$$k = k_0 \exp(-E_a/RT) \qquad 1.5.3$$

in which the rate of the reaction is constant, k_0 is the frequency factor, *R* is the gas constant and *T* is the temperature at which the value of the rate constant is determined. Logarithm of the equation 1.5.3 the term is given:

$$\ln k = \ln k_0 - E_a/RT \qquad 1.5.4$$

in which there is a linear dependence of *lnk* of *1/T*. This dependence is linear at a narrow temperature range of 30 – 40 °C. This means that by knowing the value of the chemical reaction

rate constant for at least three temperatures, the value of the $-E_a/R$ member, *i.e.* the activation energy for the studied reaction can be determined graphically.[139,140]

The enthalpy of the activation $\Delta H^{\neq}$ is determined from the equation 1.5.5.

$$\Delta H^{\neq} = E_a - RT \qquad 1.5.5$$

The entropy of activation $\Delta S^{\neq}$ is the value which represents the measurement of the *Gibbs* energy with the change of temperature *T* and can be expressed by equation 1.5.6,

$$\left(\frac{d\left(\Delta G^{\neq}\right)}{dT}\right) = -\Delta S^{\neq} \qquad 1.5.6$$

The value of $\Delta S^{\neq}$ is determined from the *Eyring* equation 1.5.7:

$$k = \frac{RT}{Nh}\exp\left(-\frac{\Delta G^{\neq}}{RT}\right) \qquad 1.5.7$$

Since the *Gibbs* energy can be expressed by changing the enthalpy of activation and entropy of activation, the equation 1.5.8:

$$\Delta G^{\neq} = \Delta H^{\neq} + T\Delta S^{\neq} \qquad 1.5.8$$

substituting in equation 1.5.7 gives the equation 1.5.9:

$$k = \frac{RT}{Nh}\exp\left(\frac{\Delta S^{\neq}}{R}\right)\exp\left(-\frac{\Delta H^{\neq}}{RT}\right) \qquad 1.5.9$$

Logarithm of the equation 1.5.9 gets:

$$\ln\left(\frac{k}{T}\right) = \ln\left(\frac{R}{Nh}\right) + \frac{\Delta S^{\neq}}{R} - \frac{\Delta H^{\neq}}{RT} \qquad 1.5.10$$

From the equation 1.3.8 it can be seen that there exists a linear dependence of *ln(k/T)* against *1/T* (*Eyring* plot), *i.e.* graphically based on this equation obtained from the slope value of the enthalpy of activation, $\Delta H^{\neq}$, and the value of entropy of activation, $\Delta S^{\neq}$, is determined, *Scheme 19*. The expression, *ln(R/Nh)* is a constant and amounts 23.8 at 25 °C.

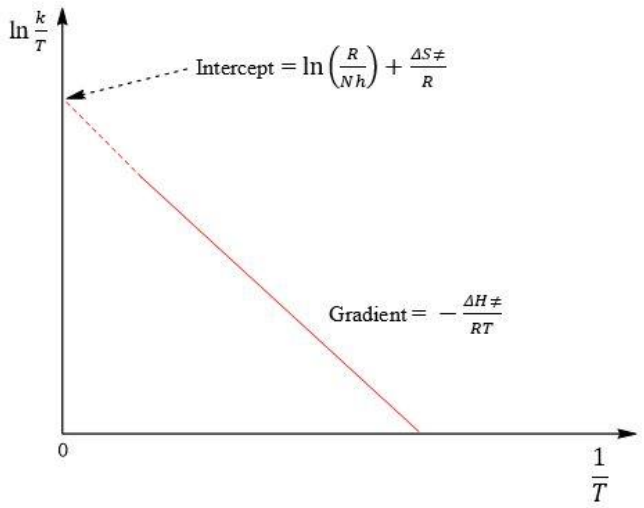

Scheme 19. An *Eyring* plot allows the activation parameters $\Delta H^{\neq}$ and $\Delta S^{\neq}$ to be determined from the temperature dependence of the rate constant; the dotted part of the line represents an extrapolation.

The volume of activation, $\Delta V^{\neq}$, is given by the *Van't Hoff* equation 1.5.11:

$$\left(\frac{d(\ln k)}{dP}\right)_T = -\frac{\Delta V^{\neq}}{RT} \qquad 1.5.11$$

The value of $\Delta V^{\neq}$ is obtained by monitoring the change of rate constant in pressure dependence and it is based on the equation 1.5.12:

$$\Delta V^{\neq} = -bRT \qquad 1.5.12$$

in which *b* represents the slope from *lnk = f(P)*. The volume of activation, $\Delta V^{\neq}$, consists of two members, equation 1.5.13:

$$\Delta V^{\neq} = \Delta V^{\neq}_{int} + \Delta V^{\neq}_{sol} \qquad 1.5.13$$

The first member $\Delta V^{\neq}_{int}$ refers to changes in the internuclear distances and correlation angles in the formation of the activated complex, while the other member $\Delta V^{\neq}_{sol}$ describes the changes in the charge, as well as the dipole interactions in the activated complex. Therefore, if the charged ions react in the substitution process the contribution of the second member can be greater than the first one, so the value of volume activation is not a reliable criterion for determining the mechanism. However, when there is no change in the charge during the substitution process, the second term in equation 1.5.13 can be neglected, *i.e.* the value of activation, $\Delta V^{\neq}$, depends only on $\Delta V^{\neq}_{int}$. In this case, the value of activation, $\Delta V^{\neq}$, is the most reliable criterion for determining the substitution mechanism.[141,142]

1.5.3. Determination of the mechanism of nucleophilic substitution reactions

The determination of the mechanism of the nucleophilic substitution reaction is performed on the basis of the values of the thermodynamic parameters,[140-144] which characterize the studied process. One of the parameters by which the substitution mechanism can be preliminarily determined in a very simple way is the rate of the constant. Based on the equations which represent the dissociative or associative mechanism and mechanism of interchange, it can be seen that the substitution process by the dissociative mechanism is a first order reaction, and by the associative mechanism a second order reaction. In this regard, when studying a reaction and if it is found that the nature of the input ligand does not affect the rate of reaction, then it is a dissociative or Id mechanism of substitution. On the opposite, if the rate of reaction depends on the nature of the input ligand then the reaction occurs by the associative or Ia substitution mechanism.[140-143]

A more reliable criterion for determining the mechanism is knowing the value of the entropy of activation, $\Delta S^{\neq}$. Since the entropy of activation is the measure of the system disorder, as well as the fact an intermediate is formed with higher or with lesser disorder with different mechanisms, this parameter makes it possible to determine the substitution mechanism. In case of a dissociative mechanism an intermediate with a reduced coordination number is generated, *i.e.* the system disorder is increased and the value of entropy of activation, $\Delta S^{\neq}$, has a positive value. With the associative mechanism an intermediate with an increased coordination number is generated and the system disorder is reduced, *i.e.* the value of entropy of activation, $\Delta S^{\neq}$, has a negative value. In the case of mechanism of interchange, I, the value of entropy of activation, $\Delta S^{\neq}$, is approximately equal to zero.

The most reliable criterion for determining the mechanism is the value of the volume of activation, $\Delta V^{\neq}$.[142,143] Taking into account the type of intermediate in different mechanisms, the increase in pressure will accelerate the associative mechanism reactions and slow down the reactions of the dissociative mechanism, D. Therefore, the negative value of volume of activation, $\Delta V^{\neq}$, indicates the D or Id substitution mechanism. In the case of the mechanism of interchange, the pressure does not significantly affect the rate of substitution.

1.5.4. Substitution reactions of octahedral complexes

Complexes with coordination number 6 most often have octahedral geometry. These complexes have an O_h symmetry group. A large number of elements with different electronic configurations have the ability to build octahedral complexes.

Thus, the ions Na and Mg, which belong to the group of *s*-elements form octahedral complexes, as well as some *p*-elements such as sulfur and silicon (SF_6 and $[SiF_6]^{2-}$) are forming the complexes.[137,138,140] However, most octahedral complexes are formed from transitional *d*-elements.

The process of ligand substitution in octahedral complexes differs from the substitution process for square-planar complexes. The p_z orbital from metal ions in square-planar complexes tends to receive an electronic pair from the input ligand in the process of substitution by A mechanism. In octahedral complexes the p_z orbital is already filled out from the metal ions. Moreover, the volatility of octahedral complexes is higher than in square-planar complexes, so the approach of the input ligand is difficult.[138]

The reaction of the substitution of octahedral complexes can also be performed by a D, A or I mechanism, as described in section 1.5.1. The inner-orbital octahedral complexes (d^2sp^3 hybridization) whose metal ions have the electronic configuration d^0, d^1, d^2 as well as the d^4 electronic configuration are coordinated unsaturated, *i.e.* they have empty internal *d*-orbitals. Therefore, these metal ions have the ability to receive an electronic pair of input ligands, which according to the A mechanism, will generate an intermediate with the coordinate number 7. However, for the outer-orbital octahedral complexes (sp^3d^2 hybridization) the D mechanism is expected. The largest number of substitution reactions of octahedral complexes occurs in the D or Id mechanism, while the nature of the outgoing ligand and the nature of the inert ligand have a great influence on the rate of the constant. In the case of these complexes steric disturbances are less significant.

1.5.5. Influence of the outgoing ligand

The influence of the outgoing ligand on the rate constant of the substitution reaction of octahedral complexes can be explained in the case of acid hydrolysis of the complex type $[Co(NH_3)_5X]^{2+}$:

$$[Co(NH_3)_5X]^{2+} + H_2O \rightarrow [Co(NH_3)_5(H_2O)]^{3+} + X^-$$

The speed at which the leaving ligand X leaves the coordination sphere depends on the strength of the chemical bond between the metal ion and the observed ligand. In the case of ligands of the same charge, the rate of the substitution reaction increases with the increase in the size of the ligand. However, if we observe ligands of different charge, the rate of the substitution reaction decreases with the increase in the charge of the outgoing ligand.

1.5.6. Influence of the inert ligand

The nature of the ligand has a significant influence on the octahedral complexes located in the *cis* or *trans* position relative to the outgoing ligand. This effect can be explained in the case of the complex $[Co(en)_2XCl]^+$, where X is an inert anionic ligand. Namely, the ligand X can influence the liability of the outgoing Cl^- ligand in the following order:

If X is in the *trans* position relative to Cl^- the lability drops in the series:

$$OH^- > NO^{2-} > N^{3-} > CN^- > Br^- > Cl^- > SO_4^{2-} > NCS^-$$

If X is in the *cis* position relative to Cl^- the lability drops in a series:

$$OH^- > Cl^- > Br^- > NO_2^- > SO_4^{2-} > NCS^-$$

Complexes with *cis* geometry mostly react faster than the corresponding *trans* complexes, except when $X = NO^{2-}$ or N^{3-}.[145]

1.5.7. Steric influence

If there are steric disturbances around the central ions of the metal, the substitution reaction of octahedral complexes takes place along the D mechanism, while the A mechanism implies sterically unprotected complexes. For example, the reaction of hydrolysis for the *meso* form of the complex $[Co(bn)_2Cl_2]^+$ (bn is butylenediamine) is approximately 30 times faster than the mixture of the *d* and *l* form due to the fact that the *meso* form is more sterically protected.[145]

1.6. Hydrolysis and hydration of metal ions

All ions, regardless of whether they are positively or negatively charged, are dissolved in water. The hydration energy, in case of a metal ion, can be defined as the amount of energy released when the free metal ion passes from the gas phase to the aqueous solution and is hydrated,[146] equation 1.6.1.

$$M^{n+}_{(g)} + n\,H_2O \longrightarrow M^{n+}_{(aq)} \qquad 1.6.1$$

The hydration energy is the result of the interaction between the metal ion and the water molecule. When the ionic ion is found in aqueous solution, it is surrounded by molecules of water whereby three hydratic spheres are formed.

Metal ions of large radius and a small charge, are subjected to hydration. The metal hydrate group includes ions from the first and second group of the periodic table (excluding beryllium). However, ions of a small metal radius and a large charge are subjected to hydrolysis (Al^{3+}, Fe^{3+}, etc.)

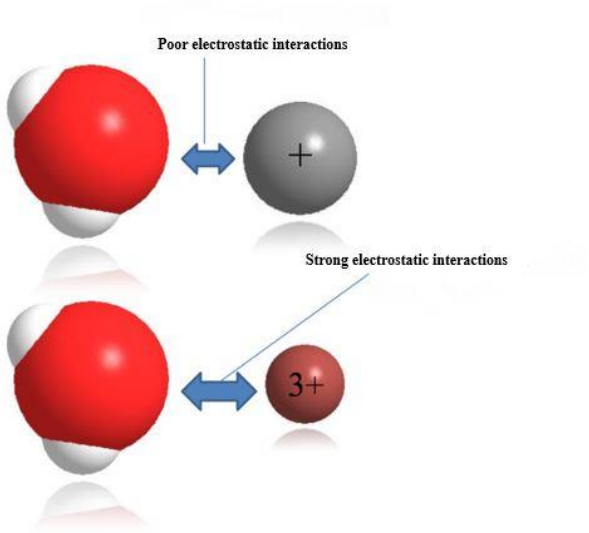

Scheme 20. An overview of electrostatic interactions between water molecules and metal ions.[11,12]

The electrostatic interactions between the large metal ions and water are sufficiently strong to lead to the release of H^+ ions from the water molecule, *Scheme 20*, which can be represented by the equation[144] 1.6.2.

$$p[M(H_2O)_n]^{z+} \rightleftharpoons [M_p(OH)_q(H_2O)_{n-q}]^{(zp-q)+} + q\ H \qquad 1.6.2$$

Based on the equation 1.6.2 it can be seen that these metal ions act as acids.[146,147] Recent studies have shown that if the angle between the axis passing through the metal oxygen bond and the oxygen-hydrogen bond is greater than 50°, metal complex hydrolyses, and if the angle is less than 50° metal complex hydrates.

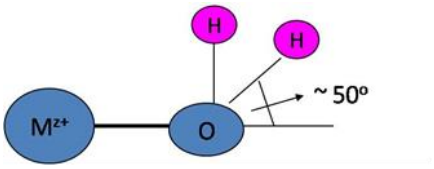

Scheme 21. Schematic representation of metal ion hydrolysis.

In the process of hydrolyzing metal ions, initially mononuclear hydrolytic complexes of type $[M(H_2O)_{(n-1)}(OH)]^{z-1}$ are formed which are then polymerized in the further course of the reaction giving polynuclear complexes of the type $[M_p(OH)_q]^{(zp-q)+}$. Hydroxide ions are most commonly bridged ligands due to a great ability to bond more than one metal ion. Therefore, they are responsible for the formation of polynuclear hydrolytic complexes.

Hydrolysis of metal complexes depends on the nature and concentration of the metal ion. In addition, it depends on the temperature, the ionic strength of the solution, the nature of the solvent and the presence of certain substances that can build complex compounds with metal ions.

1.7. DNA binding studies

1.7.1. Calculation of DNA binding constants

In order to compare quantitatively the binding strength of the complexes, the intrinsic binding constants K_b can be determined by monitoring the changes in absorption at the MLCT band with increasing concentration of CT-DNA using the following equation 1.7.1.[148]

$$[DNA]/(\varepsilon_A - \varepsilon_f) = [DNA]/(\varepsilon_b - \varepsilon_f) + 1/[K_b(\varepsilon_b - \varepsilon_f)] \quad 1.7.1$$

K_b is given by the ratio of slope to the *y* intercept in plots $[DNA]/(\varepsilon_A - \varepsilon_f)$ *versus* [DNA] , where [DNA] is the concentration of DNA in base pairs, $\varepsilon_A = A_{obs}/[complex]$, ε_f is the extinction coefficient for the unbound complex and ε_b is the extinction coefficient for the complex in the fully bound form.

1.7.2. Stern-Volmer equation for EB competitive studies

The relative binding of complexes to CT-DNA can be described by the *Stern-Volmer* equation 1.7.2 [149]

$$I_0/I = 1 + K_{sv}[Q] \quad 1.7.2$$

where I_0 and I are the emission intensities in the absence and the presence of the quencher, [Q] is the total concentration of quencher, K_{sv} is the *Stern-Volmer* quenching constant, which can be obtained from the slope of the plot of I_0/I *versus* [Q].

1.7.3. Stern-Volmer equation for BSA quenching studies

Fluorescence quenching can be described by the *Stern–Volmer* equation:

$$I_0/I = 1 + k_q\tau_0[Q] = 1 + K_{sv}[Q] \quad 1.7.3$$

where I_0 = the initial tryptophan fluorescence intensity of BSA, I = the tryptophan fluorescence intensity of BSA after the addition of the quencher, k_q = the quenching rate constant of BSA, K_{sv} = the dynamic quenching constant, τ_0 = the average lifetime of BSA without the quencher, [Q] = the concentration of the quencher respectively.

$$K_{sv} = k_q\tau_0 \quad 1.7.4$$

and, taking as fluorescence lifetime (τ_0) of tryptophan in BSA at around 10^{-8} s, K_{sv} (M^{-1}) can be obtained by the slope of the diagram I_0/I *vs* [Q] (*Stern-Volmer* plots), and subsequently the approximate k_q (M^{-1} s^{-1}) may be calculated.[149]

A factor, $\exp^{(V[Q])}$, where *V* is the static quenching constant, can be introduced into *Stern–Volmer*, equation 1.7.4, in order to describe both quenching modes[150,151]:

$$I_0/I = (1 + K_{sv}[Q])e^{V[Q]} \quad 1.7.5$$

The static quenching constant, *V* can be obtained from the equation 1.7.6 by plotting $I_0/Ie^{V[Q]}$ *versus* [Q] by varying *V* until a linear plot is obtained. The highest value of correlation coefficient can be used as criterion for linearity of the plot to obtain a precise value of *V*. The (dynamic) collisional quenching constant, K_{sv} can be then obtained from the slope of linear plots.

1.7.4. Scatchard equation for BSA quenching studies

From *Scatchard* equation:

$$r/D_f = nK - rK \quad 1.7.6$$

where *r* ($r = \Delta I/I_0$) is the moles of drug bound per mole of protein and D_f is the molar concentration of free metal complex. The association binding constant *K* (M^{-1}) may be

calculated from the slope in the *Scatchard* plots r/D_f *vs r* and the number of binding sites per albumin (n) is given by the ratio of *y* intercept to the slope (*Scatchard* plots).[152]

CHAPTER 2

RUTHENIUM AS POTENTIAL ANTICANCER DRUG

2.1. New 4'-(4-chlorophenyl)-2.2':6',2"-terpyridine ruthenium(II) complexes: Synthesis, characterization, interaction with DNA/BSA and cytotoxicity studies

Within the paper a series of new monofunctional ruthenium(II) complexes were made. All complexes were fully characterized by elemental analysis and spectroscopic techniques (IR, UV-Vis, 1D and 2D NMR). Their chemical behavior in aqueous solution was studied by UV-Vis spectroscopy, fluorescence quenching measurements and viscosity measurements. Competitive studies with ethidium bromide was studied, as well as the interaction with protein bovine serum albumin. *In vitro* studies were performed on HeLa and A549 carcinoma cell lines, as well as the cell cycle analysis by flow cytometry of HeLa and A549 cells was treated with complexes.

Participations in the publication:

M. M. Milutinović, A. Rilak, Ž. D. Bugarčić – Synthesis, UV-Vis spectroscopy, DNA/BSA interactions, implementation of all results and writing a paper;

I. Bratsos – NMR measurements;

O. Klisurić – X-ray measurements;

M. Vraneš – Viscosity measurements;

N. Gligorijević, S. Radulović – Cytotoxic investigation.

DOI: https://doi.org/10.1016/j.jinorgbio.2016.10.001

Journal of Inorganic Biochemistry 169 (2017) 1–12

Contents lists available at ScienceDirect

Journal of Inorganic Biochemistry

journal homepage: www.elsevier.com/locate/jinorgbio

New 4′-(4-chlorophenyl)-2,2′:6′,2″-terpyridine ruthenium(II) complexes: Synthesis, characterization, interaction with DNA/BSA and cytotoxicity studies

Milan M. Milutinović [a], Ana Rilak [a,*], Ioannis Bratsos [b], Olivera Klisurić [c], Milan Vraneš [d], Nevenka Gligorijević [e], Siniša Radulović [e], Živadin D. Bugarčić [a,*]

[a] Faculty of Science, University of Kragujevac, R. Domanovića 12, P. O. Box 60, 34000 Kragujevac, Serbia
[b] I.N.N., Dept. of Physical Chemistry, NCSR "Demokritos", 15310, Ag. Paraskevi, Athens, Greece
[c] Department of Physics, Faculty of Sciences, University of Novi Sad, Trg Dositeja Obradovića 4, 21000 Novi Sad, Serbia
[d] University of Novi Sad, Faculty of Sciences, Department of Chemistry, Biochemistry and Environmental Protection, Trg Dositeja Obradovića 3, 21000 Novi Sad, Serbia
[e] Institute for Oncology and Radiology of Serbia, Pasterova 14, 11000 Belgrade, Serbia

ARTICLE INFO

Article history:
Received 8 June 2016
Received in revised form 6 October 2016
Accepted 13 October 2016
Available online 14 October 2016

Keywords:
Ru(II) complexes
Meridional
Substituted terpyridine
DNA
Albumin
Cytotoxicity

ABSTRACT

In this study, we have developed a series of new monofunctional Ru(II) complexes of the general formula *mer*-[Ru(Cl-Ph-tpy)(*N-N*)Cl]Cl in which Cl-Ph-tpy is 4′-(4-chlorophenyl)-2,2′:6′,2″-terpyridine, *N-N* is a bidentate chelating ligand (1,2-diaminoethane (en, **1**), 1,2-diaminocyclohexane (dach, **2**) or 2,2′-bipyridine (bpy, **3**)). All complexes were fully characterized by elemental analysis and spectroscopic techniques (IR, UV–Vis, 1D and 2D NMR). Their chemical behavior in aqueous solution was studied by UV–Vis and NMR spectroscopy showing that all compounds are relatively labile leading to the formation of the corresponding aqua species **1aq**–**3aq**. Their DNA binding ability was evaluated by UV–Vis spectroscopy, fluorescence quenching measurements and viscosity measurements. Competitive studies with ethidium bromide (EB) showed that the complexes can displace DNA-bound EB, suggesting strong competition with EB ($K_{sv} = 1.1–2.7 \times 10^4\ M^{-1}$). These experiments show that the ruthenium complexes interact with DNA *via* intercalation. The complexes bind to serum protein albumin displaying relatively high binding constants ($K_{sv} = 10^4–10^5\ M^{-1}$). Compound **3** displayed from high to moderate cytotoxicity against two cancer cell lines HeLa and A549 (with IC_{50} *ca.* 12.7 μM and 53.8 μM, respectively), while complexes **1** and **2** showed only moderate cytotoxicity (with IC_{50} *ca.* 84.8 μM and 96.3 μM, respectively) against HeLa cells. The cell cycle analysis (by flow cytometry) of HeLa and A549 cells treated with complex **3** shows minor changes on the cell cycle phase distribution.

1. Introduction

In the past two decades ruthenium coordination compounds have attracted considerable interest as potential anticancer agents because of their low toxicity and their efficacy against platinum drug-resistant tumors, reflected in promising results in various stages of preclinical to early clinical studies [1–5].

Recently, we developed a series of new polypyridyl complexes of the general formula *mer*-[Ru(L_3)(*N-N*)(X)][*Y*]*n* where L_3 is either tpy (2,2′:6′,2″-terpyridine) or Cl-tpy (4′-chloro-2,2′:6′,2″-terpyridine), *N-N* is a bidentate chelating ligand (1,2-diaminoethane (en), 1,2-diaminocyclohexane (dach), 2,2′-bipyridine (bpy)), X is a monodentate ligand (Cl or dmso-*S*), Y is the counter anion (Cl, PF_6 or CF_3SO_3), and *n* depends on the nature of chel and X [6,7]. It was evidenced that ruthenium complexes strongly bind DNA by a dual function: by intercalation, interacting with the DNA helix through the insertion of the planar terpyridine ring between the DNA base pairs, and by covalent binding to guanine *N*7 [7]. In addition, it was proved that these complexes can covalently bind to bovine serum albumin (BSA) through the imidazole ring of histidine [8]. The cytotoxicity of these Ru(II)-tpy complexes was studied by MTT assay using human lung carcinoma (A549), human colon carcinoma (HCT116) and mouse colon carcinoma (CT26) cell lines. It was found that only [Ru(Cl-tpy)(en)Cl]Cl and [Ru(Cl-tpy)(dach)Cl]Cl showed from high to moderate in vitro cytotoxicity, with IC_{50}'s of 32.80–66.30 μM and 72.80–110.80 μM, respectively [7]. It is worth noting that both Ru(II)-tpy complexes hydrolyze the chloride ligand at a reasonable rate (i.e. within minutes) and they are capable to act as hydrogen bond donors through the chelating ligand. These two features seem to be a prerequisite for antiproliferative activity [7,8].

* Corresponding authors.
E-mail addresses: anarilak@kg.ac.rs (A. Rilak), bugarcic@kg.ac.rs (Ž.D. Bugarčić).

http://dx.doi.org/10.1016/j.jinorgbio.2016.10.001
0162-0134/

Varying substitutive group or substituent position in the intercalative ligand can create some interesting differences in the space configuration and the electron density distribution of Ru(II) polypyridyl complexes, which results in some differences in the behavior of the complexes in the interactions with DNA and proteins, and will be helpful to more clearly understand the binding mechanism of Ru(II) polypyridyl complexes to DNA and BSA [9–11]. The presence of electron donating substituents on the tpy fragment decreases the reactivity of the metal centre, whereas the addition of an electron withdrawing entity has the opposite effect [12–15]. Furthermore, additional functional groups, like halogens, on the tpy fragment might enhance the binding ability of the complexes on the biomolecules [6].

In this work, with the aim of further extending the structure-activity relationship of polypyridyl ruthenium compounds we have used a 4′-chlorophenyl-substituted tpy ligand, i.e. 4′-(4-chlorophenyl)-2,2′:6′,2″-terpyridine (Cl-Ph-tpy), to prepare three new complexes of the general formula [Ru(Cl-Ph-tpy)(*N-N*)Cl]Cl (where *N-N* = en (**1**), dach (**2**) or bpy (**3**); Fig. 1). All new complexes were fully characterized by elemental analysis and various spectroscopies, such as IR, UV–Vis, 1D and 2D NMR. Considering the importance of the hydrolysis in the mechanism of action of anticancer metal compounds, we investigated the kinetics of aquation of selected phenyl-substituted Ru(II)-tpy complexes by UV–Vis spectrophotometry, as well as the chemical behavior of all complexes in aqueous solution by ^{1}H NMR spectroscopy. The interaction of complexes **1**–**3** with calf thymus DNA (CT DNA) was studied, and a competitive study of the intercalative agent ethidium bromide (EB) was performed. Furthermore, the affinity of **1**–**3** towards bovine serum albumin was investigated, and their binding constants were determined. We report also the results of in vitro cytotoxicity tests performed on complexes **1**–**3** against two human cancer cell lines (human cervix carcinoma cell line (HeLa) and human lung carcinoma cells (A549)), and one normal cell line (human fetal lung fibroblast cells (MRC-5)) in comparison with their Cl-tpy analogues [Ru(Cl-tpy)(en)Cl]Cl (**4**), [Ru(Cl-tpy)(dach)Cl]Cl (**5**) and [Ru(Cl-tpy)(bpy)Cl]Cl (**6**), the respective precursor [Ru(Cl-Ph-tpy)Cl$_3$] (**P1**), and cisplatin. The lipophilic properties and cytotoxic effects of the complexes are assayed in order to elucidate the relationship between structure and activity.

2. Materials and methods

1,2-diaminoethane (en), (±)-trans-1,2-diamminocyclohexane (dach), 2,2′-bipyridine (bpy), 4′-chloro-2,2′:6′,2″-terpyridine (Cl-tpy), 4′-(4-chlorophenyl)-2,2′:6′,2″-terpyridine (Cl-Ph-tpy) and bovine serum albumin (BSA) are commercially available and were used as received. The complexes [Ru(Cl-tpy)(en)Cl]Cl (**4**), [Ru(Cl-tpy)(dach)Cl]Cl (**5**) and [Ru(Cl-tpy)(bpy)Cl]Cl (**6**) were synthesized as reported previously [6]. Microanalysis, UV–Vis spectra and ^{1}H NMR spectra were used to check the purity of these complexes and the spectra agreed well with the data already reported [6]. All other chemicals were used as purchased without further purification. Doubly distilled water was used as the solvent throughout the experiments. The stock solution of CT-DNA was prepared in 5 mM Tris-HCl/50 mM NaCl buffer at pH = 7.4, which gave a ratio of UV absorbances at 260 nm and 280 nm (A_{260}/A_{280}) of *ca.* 1.8–1.9, indicating that the DNA was sufficiently free of protein and the concentration was determined by UV absorbance at 260 nm ($\varepsilon = 6600\ M^{-1}\ cm^{-1}$) [16]. The stock solution of BSA was prepared by dissolving the solid BSA in 5 mM Tris-HCl/50 mM NaCl buffer at pH = 7.4, and the concentration was kept fixed at 2 μM. All stock solutions were stored at 4 °C and used within 5 days.

Mono- (^{1}H; 500 MHz) and bi-dimensional (^{1}H-^{1}H COSY) NMR spectra were recorded on a Bruker Avance 500 MHz spectrometer. ^{1}H chemical shifts in D_2O were referenced to the internal standard 2,2-dimethyl-2,2-silapentane-5-sulfonate (DSS) at $\delta = 0.00$ or to external 1,4-dioxane ($\delta = 3.75$), whereas in CD_3CN were referenced to the peak of residual non-deuterated solvent ($\delta = 1.94$). All NMR spectra were run at 298 K. The UV–Vis spectra were obtained on a Perkin-Elmer Lambda 35 double beam spectrophotometer, using 1.0 cm path-length quartz cuvettes (3.0 mL). Infrared spectra were recorded on a Perkin-Elmer 983G spectrometer. Fluorescence measurements were carried out on a RF-1501 PC spectrofluorometer (Shimadzu, Japan). The excitation and emission bandwidths were both 10 nm.

2.1. Synthesis

The aqua species that are obtained in aqueous solution from some complexes upon hydrolysis of Cl^- are labelled with the same number of the parent compound followed by "aq". The NMR assignments of these species are reported in the Supporting Information (Table S1).

2.1.1. Synthesis of [Ru(Cl-Ph-tpy)Cl$_3$] (*P1*)

A 262 mg amount of $RuCl_3 \cdot 3H_2O$ (1 mmol) was dissolved in 130.0 mL of ethanol and the solution was refluxed until the color of the solution changed from brown to green (*ca.* 2 h). Then a 344.5 mg amount of Cl-Ph-tpy (1 mmol) was added and reflux continued for 5 h. During this time the color of the solution turned again to brown reddish with the simultaneous formation of the product as a brown solid. The precipitation of the product was accomplished by cooling the solution to room temperature. The solid was collected by filtration, washed with ethanol and diethyl ether and dried under vacuum. Yield: 450.6 mg (82%). Anal Calcd for $C_{21}H_{14}Cl_4N_3Ru$ (551.24) requires: C, 45.76; H, 2.56; N, 7.62. Found: C, 45.76; H, 2.59; N, 7.65. Complex [Ru(Cl-Ph-tpy)Cl$_3$] is soluble in DMSO and acetonitrile, slightly soluble

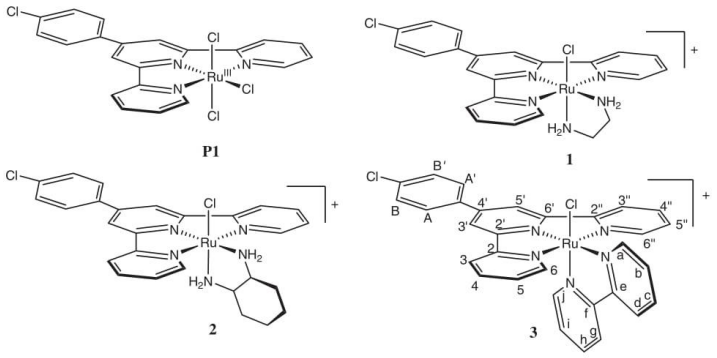

Fig. 1. Proposed structures of the precursor **P1** and complexes **1**–**3** with the numbering scheme of the Cl-Ph-tpy and bpy ligands used for the NMR characterization.

in water, methanol, ethanol, acetone, chloroform and dichloromethane. Selected IR (KBr, cm^{-1}): ν_{tpy} 3075 (m), 2924 (w), 1600 (vs), 1467 (vs), 1426 (s), 1243 (s), 1090 (s), 789 (vs), 654 (w). UV/visible spectrum (DMSO; λ_{max}, nm (ε, M^{-1} cm^{-1})): 283 (29196), 310 (22920), 414 (6820). The product was used without further purification.

*2.1.2. General synthetic procedure for [Ru(Cl-Ph-tpy)(N-N)Cl]Cl (**1**–**3**)*

A weighed amount of [Ru(Cl-Ph-tpy)Cl_3] (**P1**) was suspended in an ethanol/H_2O (3:1) mixture containing 10 eq. of LiCl and 3 eq. of triethylamine (Et_3N). The chelating ligand *N-N* (1.2 eq.; *N-N* = en, dach, bpy) was then added and the mixture was refluxed under argon for *ca.* 5 h with vigorous stirring. The violet to purple solution was filtered while hot to remove any undissolved material. Rotary concentration under reduced pressure to *ca.* ¼ of the initial volume and storage at 4.0 °C for 24 h induced the formation of the product as a dark solid. It was collected by filtration, washed with ice-cold H_2O, cold acetone and diethyl ether, vacuum dried and purified via column chromatography.

*2.1.3. [Ru(Cl-Ph-tpy)(en)Cl]Cl (**1**)*

100.0 mg (0.181 mmol) of **P1**, 13.9 μL (0.218 mmol) of en, 76.9 mg (1.814 mmol) of LiCl and 75.9 μL (0.544 mmol) of Et_3N in 20 mL of ethanol/H_2O afforded **1** as a dark purple solid. The product was purified via column chromatography on alumina using dichloromethane/methanol (95: 5, v/v) as eluent. The purple fraction was collected and the solvent removed to give a purple solid. Yield: 46.7 mg (44.7%). Anal Calcd for $C_{23}H_{22}Cl_3N_5Ru$ (575.88): C, 47.97; H, 3.85; N, 12.16. Found: C, 47.89; H, 3.93; N, 12.07. Complex **1** is soluble in water, methanol and ethanol, slightly soluble in acetonitrile, whereas it is insoluble in acetone, chloroform and dichloromethane. ^1H NMR (CD_3CN): 8.88 (d, 2H, J = 5.6 Hz, C6*H*/C6″*H*), 8.57 (s, 2H, C3′*H*/C5′*H*), 8.51 (d, 2H, J = 8.1 Hz, C3*H*/C3″*H*), 8.04 (d, 2H, J = 8.5 Hz, $C_AH/C_{A'}H$), 8.00 (t, 2H, C4*H*/C4″*H*), 7.65 (m, 4H, C5*H*/C5″*H*, $C_BH/C_{B'}H$), 5.37 (m br, 2H, NH_2 en), 3.26 (m, 2H, CH_2 en), the other two (i.e. CH_2 and NH_2) peaks of en resonate at *ca.* 2.38 and *ca.* 2.01, and are overlapped with the HOD and CH_3CN resonances. Selected IR (KBr, cm^{-1}): ν_{CH2} 2923 (m), 2850 (m); ν_{tpy} 1578 (vs), 1472 (m), 1408 (s), 1089 (vs), 785 (s), 651 (w). UV/visible spectrum (H_2O; λ_{max}, nm (ε, M^{-1} cm^{-1})): 285 (37196), 319 (28920), 485 (6826).

*2.1.4. [Ru(Cl-Ph-tpy)(dach)Cl]Cl (**2**)*

100.0 mg (0.181 mmol) of **P1**, 26.1 μL (0.218 mmol) of dach, 76.9 mg (1.814 mmol) of LiCl and 75.9 μL (0.544 mmol) of Et_3N in 20 mL of ethanol/H_2O (3:1) afforded **2** as a dark purple solid. The product was purified via column chromatography on silica gel using dichloromethane/methanol (85: 15, v/v) as eluent. The purple fraction was collected and the solvent removed to give a purple solid. Yield: 72.4 mg (63.4%). Anal Calcd for $C_{27}H_{28}Cl_3N_5Ru$ (629.97): C, 51.5; H, 4.48; N, 11.12. Found: C, 51.4; H, 4.42; N, 11.20. Complex **2** is soluble in water, methanol, ethanol and acetone, partially soluble in acetonitrile, whereas it is insoluble in chloroform and dichloromethane. ^1H NMR (CD_3CN): 9.04 (d, 1H, J = 5.4 Hz, C6*H*), 8.96 (d, 1H, J = 5.4 Hz, C6″*H*), 8.45 (s,1H, C3′*H*), 8.43 (s, 1H, C5′*H*), 8.37 (t br, 2H, C3*H*/C3″*H*), 7.98 (d, 2H, J = 8.5 Hz, $C_AH/C_{A'}H$), 7.87 (t, 2H, J = 7.6 Hz, C4*H*/C4″*H*), 7.62 (m br, 2H, C5*H*/C5″*H*), 7.49 (d, 2H, J = 8.5 Hz, $C_BH/C_{B'}H$), 5.86 (d, 1H, J = 12.0 Hz, N*H* dach), 5.06 (t, 1H, J = 11.9 Hz, N*H* dach), 2.71–2.62 (m, 1H, N*H* dach), 2.62–2.55 (m, 1H, C*H* dach), 2.12–1.88 (m, 2H, N*H* + C*H* dach), 1.87–1.71 (m, 2H, C*H* dach), 1.51 (t, 2H, J = 12.6 Hz, C*H* dach), 1.23 (m, 2H, C*H* dach), 1.11 (m, 1H, C*H* dach), 0.88 (m, 1H, C*H* dach). Selected IR (KBr, cm^{-1}): ν_{NH} 3133 (m); ν_{tpy} 1600 (s), 1473 (s), 1430 (s), 1088 (vs), 786 (vs), 652 (w). UV/visible spectrum (H_2O; λ_{max}, nm (ε, M^{-1} cm^{-1})): 285 (48050), 319 (38043), 492 (13932).

*2.1.5. [Ru(Cl-Ph-tpy)(bpy)Cl]Cl (**3**)*

100.0 mg (0.181 mmol) of **P1**, 34.0 mg, (0.218 mmol) of bpy, 76.9 mg (1.814 mmol) of LiCl and 75.9 μL (0.544 mmol) of Et_3N in 20 mL of ethanol/H_2O afforded **3** as a dark red crystalline solid. Yield: 106.5 mg (87.4%). Anal Calcd for $C_{31}H_{22}Cl_3N_5Ru$ (671.97): C, 55.41; H, 3.30; N, 10.42. Found: C, 55.40; H, 3.38; N, 10.40. Complex **3** is soluble in water, methanol, ethanol, acetone and acetonitrile, and partially soluble in chloroform and dichloromethane. ^1H NMR (D_2O): 9.55 (d, 1H, J = 5.6 Hz, Ca*H*), 8.82 (s, 2H, C3′*H*/C5′*H*), 8.67 (d, 1H, J = 8.2 Hz, Cd*H*), 8.52 (d, 2H, J = 8.1 Hz, C3*H*/C3″*H*), 8.36–8.26 (m, 2H, Cg*H*/Cc*H*), 8.03 (m, 3H, Cb*H*/$C_AH/C_{A'}H$), 7.97 (t, 2H, J = 7.9 Hz, C4*H*/C4″*H*), 7.81 (d, 2H, J = 5.6 Hz, C6*H*/C6″*H*), 7.72 (d, 2H, J = 8.1 Hz, $C_BH/C_{B'}H$), 7.67 (t, 1H, J = 7.8 Hz, Ch*H*), 7.38–7.28 (m, 3H, Cj*H*/C5*H*/C5″*H*), 6.92 (t, 1H, J = 6.7 Hz, Ci*H*). ^1H NMR (CD_3CN): 10.23 (d, 1H, J = 5.4 Hz, Ca*H*), 8.73 (s, 2H, C3′*H*/C5′*H*), 8.62 (d, 1H, J = 7.9 Hz, Cd*H*), 8.51 (d, 2H, J = 7.30 Hz, C3*H*/C3″*H*), 8.33 (d, 1H, J = 7.9 Hz, Cg*H*), 8.27 (m, 2H, Cc*H*), 8.10 (d, 2H, J = 8.3 Hz, $C_AH/C_{A'}H$), 7.98 (m, 1H, Cb*H*), 7.87 (t, 2H, J = 7.7 Hz, C4*H*/C4″*H*), 7.69–7.64 (m, 5H, Ch*H*/C6*H*/C6″*H*/$C_BH/C_{B'}H$), 7.31 (d, 1H, J = 5.7 Hz, Cj*H*) 7.27 (m, 2H, C5*H*/C5″*H*), 6.94 (t, 1H, J = 6.6 Hz, Ci*H*). Selected IR (KBr, cm^{-1}): ν_{tpy} 3058 (m), 1599 (s), 1455 (s), 1429 (s), 1091 (s), 790 (vs), 653 (m). UV/visible spectrum (H_2O; λ_{max}, nm (ε, M^{-1} cm^{-1})): 286 (57473), 315 (35855), 489 (12794).

2.2. Kinetic analysis

The hydrolysis kinetics of the complexes **1** and **2** were studied by stop-flow UV–Vis spectrophotometry by following the change in absorbance at specific wavelengths as a function of time. The working wavelength of each reaction corresponded to that of a maximum change in absorption derived from the difference spectra. The samples (0.1 mM) for the aquation studies, performed at 298 K, were prepared in distilled H_2O. The absorption/time data for each complex were computer-fitted to the *pseudo*-first-order rate equation (Eq. (1)), which gave the k_{obs} value (k) for each aquation process:

$$A = C_0 + C_1 e^{-kt} \quad (1)$$

C_0 and C_1 are computer-fitted constants, and A is the absorbance at time t.

All kinetic data were computer-fitted using the programs Microsoft Excel 2007 and Origin 8.

2.3. DNA-binding studies

2.3.1. Absorption spectroscopic studies

The interaction of complexes **1**–**3** with CT DNA was studied, using UV–Vis spectroscopy, in order to investigate the possible binding modes to CT DNA and to calculate the binding constants (K_b). The DNA-binding experiments were performed at 37 °C. Buffered solution (5 mM tris(hydroxymethyl)aminomethane (Tris)-HCl, 50 mM NaCl, pH = 7.4) was used for the absorption measurements. A series of complex–DNA solutions were prepared by mixing complex solutions of fixed concentration (12.5 μM) with increments of the DNA stock solution (2.0 mM).

2.3.2. Fluorescence quenching measurements

The binding interaction of the complexes with DNA was also studied by fluorescence spectroscopy. The fluorescence intensities were measured with the excitation wavelength set at 527 nm and the fluorescence emission at 612 nm. The excitation and emission slit widths (each 10 nm) and scan rate were maintained constant for all the experiments. Stock solutions of DNA (2.0 mM) and complexes (0.1 mM) were prepared in 5 mM Tris-HCl buffer (pH = 7.4, 50 mM NaCl). A series of complex-DNA solutions were prepared by mixing DNA solutions with different concentration of complexes. For fluorescence determination, the final DNA concentration was 80.0 μM, and the complex concentrations varied from 8.0 μM to 80.0 μM. Before measurements, the system was shook and incubated at room temperature for 5 min. The emission was recorded at 550–750 nm.

2.3.3. Viscosity measurements

The viscosity of a DNA solution was measured in the presence of increasing amounts of complexes **1**–**3**. The flow time was measured with a digital stopwatch, each sample was measured three times, and then the average flow time was calculated. The data were presented as $(\eta/\eta_0)^{1/3}$ against *r*, where η is the viscosity of DNA in the presence of complex and η_0 is the viscosity of DNA alone in the buffered solution. The viscosity values were calculated from the observed flow time of the DNA-containing solutions (t) corrected for the flow time of the buffer alone (t_0), $\eta = (t - t_0) / t_0$.

2.4. Albumin-binding studies

The protein binding study was performed by tryptophan fluorescence quenching experiments using bovine serum albumin (BSA, 2 μM) in buffered solutions (containing 5 mM Tris and 50 mM NaCl at pH 7.4). Quenching of the emission intensity of tryptophan residues of BSA at 352 nm was monitored using the complexes **1**–**3** as quenchers with increasing concentration (up to 3.0×10^{-5} M) [17]. Fluorescence spectra were recorded in the range 300–500 nm at an excitation wavelength of 295 nm. The fluorescence spectra of the compounds in buffered solutions were recorded under the same experimental conditions, and no fluorescence emission was detected. The Stern − Volmer and Scatchard equations (Supporting Information, Eqs. (S3)–(S6)) and graphs have been used to study the interaction of the complexes with serum albumin and to calculate the corresponding constants [17].

2.5. Lipophilicity assay

Log $P_{o/w}$ is the partition coefficient between octanol and water which is determined using the flask-shaking method [18]. An aliquot of a stock solution of complexes **1**–**3** in 100 mM aqueous NaCl (0.9% w/v to prevent aqueous interaction and remain saturated with octanol) was added to an equal volume of octanol (saturated with 0.9% NaCl w/v). The mixture was shaken overnight at 60 rpm at 298 K to allow partitioning. After standing, the aqueous layer was carefully separated from the octanol layer for ruthenium analysis. The ruthenium concentration in the aqueous phase was determined using UV–Vis spectrophotometry and used to calculate the $[Ru]_o/[Ru]_w$ ratio.

2.6. Cell culture

Human cervix carcinoma cells (HeLa), human lung carcinoma cells (A549), and human fetal lung fibroblast cells (MRC-5) were maintained as monolayer culture in the Roswell Park Memorial Institute (RPMI) 1640 nutrient medium (Sigma Chemicals Co, USA). RPMI 1640 nutrient medium was prepared in sterile ionized water, supplemented with penicillin (192 IU/mL), streptomycin (200 mg/mL), 4-(2-hydroxyethyl)piperazine-1-ethanesulfonic acid (HEPES) (25 mM), L-glutamine (3 mM) and 10% of heat-inactivated fetal calf serum (FCS) (pH 7.2). The cells were grown at 37 °C in a humidified atmosphere of 95% air and 5% CO_2.

2.7. Cytotoxicity assay (MTT test)

The cytotoxicity of complexes **1**–**6**, and precursor **P1** was determined using 3-(4,5-dymethylthiazol-yl)-2,5-diphenyltetrazolium bromide (MTT, Sigma) assay as described previously. Briefly, cells were seeded into 96-well cell culture plates (Thermo Scientific Nunc™), at an appropriate cell density for each cell line. After 24 h of growth, cells were exposed to the investigated ruthenium complexes. The investigated complexes were dissolved in DMSO at concentration of 10 mM and sequential dilutions were made in culture medium until to reach the desired concentrations. Final concentration of DMSO never exceeded 1% (v/v). After incubation periods of 72 h, 20 μL of MTT solution (5 mg/mL in phosphate buffer, pH 7.2) was added to each well. Samples were incubated for 4 h at 37 °C in humidified atmosphere of 5% CO_2, and then 100 μL of 10% sodium dodecyl sulfate (SDS) was added. Absorbance was recorded after 24 h, on an enzyme linked immunosorbent assay (ELISA) reader (Thermo Labsystems Multiskan EX 200–240 V), at the wavelength of 570 nm. The IC_{50} value, defined as the concentration of the compound causing 50% cell growth inhibition, was determined from the cell survival diagram.

2.8. Cell cycle analysis

Quantitative analysis of cell cycle phase distribution was performed by flow cytometric analysis of the DNA content in fixed HeLa and A549 cells, after staining with propidium iodide (PI) [19]. Cells were seeded at density of 2×10^5 cells/well at 6-well plate and growth in nutrition medium. After 24 h, cells were continually exposed to complex **3** or cisplatin. Control cells were incubated only in nutrient medium. After continual treatment, cells were collected by trypsinization, washed twice with ice-cold PBS, and fixed for 30 min in 70% EtOH. After fixation, cells were washed again with PBS and incubated with RNaseA (1 mg/mL) for 30 min at 37 °C. Cells were than stained with PI (at concentration of 400 μg/mL) for 15 min before flow cytometric analysis. Cell cycle phase distribution was analyzed using a fluorescence activated sorting cells (FASC) Calibur Becton Dickinson flow cytometer and Cell Quest computer software.

3. Results and discussion

3.1. Synthesis and characterization

Treatment of the neutral Ru(III) precursor *mer*-[Ru(Cl-Ph-tpy)Cl_3] (**P1**) with a neutral *N-N* chelating ligand, such as en, dach or bpy, in the presence of triethylamine (Et_3N) and excess of LiCl afforded the cationic Ru(II) complexes [Ru(Cl-Ph-tpy)(*N-N*)Cl]Cl (*N-N* = en (**1**), dach (**2**) and bpy (**3**)) in good yields. All new complexes were characterized by NMR, IR and UV–Vis spectroscopy, and elemental analysis. Crystals of [Ru(Cl-Ph-tpy)(en)Cl]Cl (**1**) were obtained, and the structure was partially solved by X-ray crystallography which confirmed the proposed structure (Fig. S1 in the SI). However, it could not be adequately refined because of the low crystal quality, and thus no crystal data are reported for the analysis. In the obtained structure of the complex cation, the Ru ion displays the typical octahedral geometry with the tridentate Cl-Ph-tpy ligand coordinated with the expected meridional geometry, the en acting as chelating ligand, whereas the sixth coordination site is occupied by a chloride ion.

The ^{1}H spectrum of **1** in CD_3CN is consistent with a *Cs* symmetry in solution due to the conformational mobility of the en backbone that averages it to a planar ligand. In the ^{1}H spectrum there are seven aromatic resonances assigned to the two equal halves of the Cl-Ph-tpy and two upfield peaks attributed to the equatorial half fragment (CH_2 and NH_2) of the en ligand (Fig. S2). The two en resonances of the axial fragment, which fall into the shielding cone of the adjacent Cl-Ph-tpy ligand and thus they are remarkably shifted upfield, are overlapped with the intense broad CD_3CN peaks.

Conversely, the ^{1}H NMR spectrum of **2** in CD_3CN is more complicated due to the conformational rigidity of coordinated dach [20,21] that removes the mirror plane bisecting the Cl-Ph-tpy ligand in **1**. Thus, in the ^{1}H NMR spectrum the resonances of the corresponding protons of the two halves of Cl-Ph-tpy are partially overlapped except for H6/H6″ (two doublets at $\delta = 9.04$ and 8.96) and *H*3′/H5′ (two singlets at $\delta =$ 8.45 and 8.37), which are well resolved (Fig. S3).

The ^{1}H NMR spectrum of **3** in CD_3CN is consistent with the symmetry of the complex: seven resonances attributed to the symmetric Cl-Ph-tpy ligand and eight multiplets assigned to the two inequivalent halves of bpy (Fig. 2). It is worth noting that each peak of the axial bpy ring is remarkably shifted upfield compared to that of the corresponding

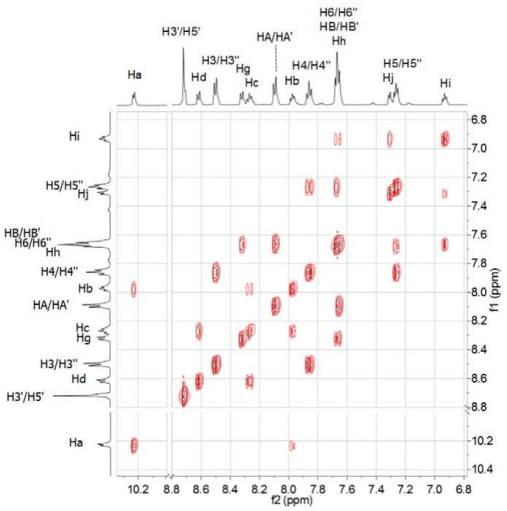

Fig. 2. The 2D homonuclear ^{1}H-^{1}H COSY NMR spectrum of [Ru(Cl-Ph-tpy)(bpy)Cl]Cl (**3**) in CD_3CN at 298 K.

proton on the other ring (e.g. δ Hi = 6.94 vs. δ Hb = 7.98) due to the shielding effect of Cl-Ph-tpy. Correspondingly, the protons of the terminal aromatic rings of Cl-Ph-tpy are affected by the shielding cone of bpy and thus their resonances are also remarkably upfield shifted; in particular the H6/H6″ protons resonate at 7.67 ppm, that is *ca.* 1.00 ppm more upfield compared to those of **1** and **2**.

The solid state IR spectra of complexes **1**–**3** show the typical bands of the terpyridine ligands: the aromatic C—H stretching in the region 3060–2850 cm^{-1}, and the most characteristic strong band in the region 1395–1616 cm^{-1} assigned to ν(C = N) and ν(C = C) stretching [22,23]. The band at 1011 cm^{-1}, present in the spectra of all complexes, results from the ring breathing modes of the individual pyridine rings [11,24].

The solution electronic absorption spectra of complexes **1**–**3** exhibited several intense bands in the UV region (200 < λ < 330 nm), attributed to intra-ligand ($\pi \rightarrow \pi^*$) charge transfer transitions, and a broad intense band (with an unresolved shoulder) in the visible region attributed to metal to ligand $d\pi(Ru) \rightarrow \pi^*$(polypyridyl) charge transfer (MLCT) transitions [11,22,25–28].

3.2. Chemical behavior in aqueous solution

The chemical behavior of the new complexes in aqueous solution was first investigated qualitatively by NMR spectroscopy in view of their potential reactivity towards biological (macro)molecules, such as proteins, DNA etc. The chloride ligand in the cationic complexes **1** and **2** turned out to be very labile in aqueous solution. After dissolution in D_2O, a new set of resonances was observed to grow both in the aromatic (Cl-Ph-tpy resonances) and in the upfield (en or dach resonances) regions of the ^{1}H NMR spectra. These new resonances, which grew at the expense of those of the parent compound, were attributed to the aqua species $[Ru(Cl\text{-}Ph\text{-}tpy)(en)(H_2O)]^{2+}$ (**1aq**) and $[Ru(Cl\text{-}Ph\text{-}tpy)(dach)(H_2O)]^{2+}$ (**2aq**), respectively (Scheme 1). According to integration, *ca.* 50% of complex **1** is already aquated 10 min after dissolution, and the system reached equilibrium within *ca.* 1 h with 1:9 ratio between **1** and **1aq** (Fig. S4). The chemical behavior in aqueous solution of the dach derivative **2** is very similar to that described for **1** (Fig. S5). Contrary to **1** and **2**, the bpy complex **3** release the Cl$^-$ ligand, yielding the aqua species $[Ru(Cl\text{-}Ph\text{-}tpy)(bpy)(H_2O)]^{2+}$ (**3aq**) at a much slower rate, but to a comparable extent (Fig. S6). The equilibrium was reached *ca.* 24 h after dissolution. The greater lability of the Cl$^-$ ligand in compounds **1** and **2** is attributed to the stronger *trans* influence of the pure σ-donor ligands en and dach, respectively, compared to the (also) π-acceptor bpy in compound **3**. Interestingly, no release of the *N-N* ligand was detected from all complexes during the observation times. Addition of a large excess of NaCl (*ca.* 1.00 M) into the equilibrated solution of **1aq**–**3aq** induced rapid precipitation of the chlorido derivatives **1**–**3**.

3.3. UV–Vis kinetics of aquation

The kinetics of aquation of complexes **1** and **2** were quantitatively studied by UV–Vis spectroscopy at 298 K on 0.1 mM solutions. Complex **3** was excluded from these studies because, according to the NMR evidences, it hydrolyzes the Cl ligand at a very slow rate. The rapid reversion of the equilibrium and the precipitation of the complexes upon addition of NaCl prohibited anation kinetics studies and, therefore, the calculation of the equilibrium constants K_{aq}.

The UV–Vis spectra of complexes **1** and **2** show significant time-dependent changes in the region 200–800 nm (Fig. S7) with clean isosbestic points that, consistent with the NMR observation, suggest the occurrence of a single hydrolytic process (i.e. conversion of the initial chlorido complex into the corresponding aqua species **1aq** and **2aq**, respectively). The wavelength corresponding to the maximum change in absorption (Fig. S7, difference spectra) was selected for the kinetic studies (470 nm for **1** and 471 nm for **2**). In each case the time course of the absorbance followed *pseudo*-first-order kinetics (Fig. 3) that afforded the rate constants k_{obs} listed in Table 1. It can be seen that both complexes hydrolyze at a similar rate, k_{obs} = 6.10×10^{-3} s^{-1} for **1** and 4.90×10^{-3} s^{-1} for **2**, respectively. Complexes **1** and **2** hydrolyze slightly faster than their Ru-tpy analogues [Ru(Cl-tpy)(en)Cl]Cl (**4**) and [Ru(Cl-tpy)(dach)Cl]Cl (**5**) (2.52–3.94×10^{-3} s^{-1}) [6], and *ca.* two orders of magnitude higher than those of the established anticancer drug cisplatin (6.32×10^{-5} and 2.5×10^{-5} s^{-1} for the first and second aquation process, respectively) [29]. These results imply that our coordination compounds evolve to the active aqua species much faster than cisplatin in low chloride concentration environments corresponding to intracellular conditions. However, it has been proved that fast aquation of complexes might lead to reduced activity and/or to increased toxicity due to their fast

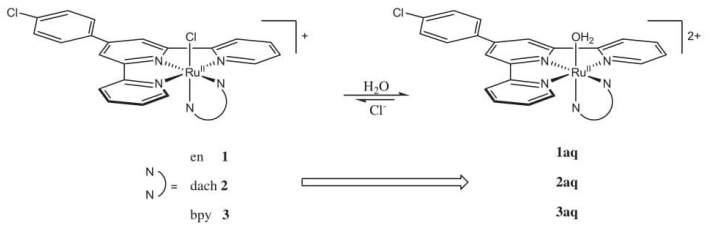

Scheme 1. Chemical behavior of complexes **1**–**3** in aqueous solution.

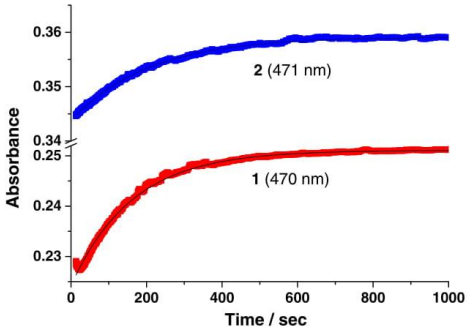

Fig. 3. Time-dependence of the absorbance during the aquation of **1** (at 470 nm, 0.05 mM, red squares) and of **2** (at 471 nm, 0.05 mM, blue squares) in H_2O at 298 K. The full lines represent computer fits giving the first order rate constants for the aquation of **1** and of **2**.

binding to biomolecules other than those responsible for tumor proliferation such as DNA.

3.4. DNA-binding studies

DNA is a critical therapeutic target that is responsible for, and the focus of, a wide variety of intracellular interactions [30–34]. Many ruthenium(II) polypyridyl complexes are well-established DNA intercalators with useful spectroscopic properties and relatively low toxicity [35] which makes them ideal diagnostic agents [36]. On the other hand, the most of ruthenium(II) complexes that contain a labile ligand (such as Cl^-), can bind covalently, after hydrolysis, to DNA through guanine *N*7 [37]. In our previous work, we revealed that the Ru(II)-tpy complexes **4**–**6** both intercalate and covalently bind to CT DNA [7]. The combination of these modes of interaction can be utilized to improve the binding affinity and selectivity of ruthenium complexes. The aim of this study was to investigate the effect of the phenyl-substituent on the terpyridyl ligand and of the nature of the inert chelating ligands on the binding mode of Ru(II)-polypyridyl complexes to DNA and to relate this to the differences in their anticancer activity.

3.4.1. Absorption spectroscopic studies

The application of electronic absorption spectroscopy is one of the most universally employed methods for the determination of the binding modes and binding extent of metal complexes with DNA. The absorption intensity of the complexes may decrease (hypochromism) or increase (hyperchromism) with a slight increase in the absorption wavelength (bathochromism) upon addition of DNA.

The UV–Vis spectra were recorded for a constant concentration of the complexes at different [complex]:[DNA] mixing ratios (r). The UV–Vis spectra of complexes **1**–**3** in the absence and presence of CT DNA are given in Fig. S8. The increase in the intensity at the MLCT band for all three complexes indicated that the interaction with CT DNA resulted in the direct formation of a new complex with double-helical CT DNA. In the UV–Vis spectrum of complex **1**, the two bands at 422 and 488 nm, present a hyperchromism upon addition of increasing amounts of CT DNA (Fig. S8), suggesting the tight binding to CT DNA. Additionally, the band at 422 nm presents a red shift (bathochromism) of 6 nm (up to 428 nm), suggesting the stabilization of the CT DNA duplex [17,38]. The behavior of complex **2** was quite similar (the band centered at 496 nm presents a hyperchromism) upon addition of increasing amounts of CT DNA (Fig. S8). The band at 424 nm exhibits a hyperchromism accompanied by a 4 nm red shift (to 428 nm). Similarly, in the UV–Vis spectrum of complex **3**, the two bands at 315 and 490 nm exhibit a hyperchromism upon addition of CT DNA (Fig. S8).

The above results suggest that all complexes can bind to CT DNA and stabilize the CT DNA duplex, although the exact mode of binding cannot be reliably proposed on the basis of UV–Vis spectroscopic studies [17,38]. It is important to emphasize that the studied complexes contain both a leaving group and a DNA intercalating ligand, and hence, they could interact with DNA in a bifunctional mode, including covalent binding to the nucleobases and non-covalent intercalation.

The intrinsic binding constants K_b of complexes **1**–**3**, calculated by the equation (S1) and the plots (Fig. S9), were $(1.0 \pm 0.2) \times 10^6\ M^{-1}$, $(2.8 \pm 0.1) \times 10^6\ M^{-1}$ and $(9.0 \pm 0.2) \times 10^6\ M^{-1}$, respectively (Table 2). The K_b values suggest a strong binding of the complexes to CT DNA, with complex **3** exhibiting higher K_b values compared to complexes **1** and **2**. For comparison, the polypyridyl compounds **4**–**6** that are believed to bind to DNA in a bifunctional manner (covalently and non-covalently), have K_b values $(2.1–10.0 \times 10^4\ M^{-1})$ [7] that are *ca.* from one to two orders of magnitude lower than those of complexes **1**–**3**, respectively, implying that the introduction of the chlorophenyl fragment in the tpy ligand has a significant effect on the DNA binding activity. Changing the overall nature (electron-donating or -withdrawing) of the substituents on the tpy moiety affects the π-back-donation ability of the ligand and hence the electrophilicity of the metal centre. The chlorophenyl-substitution on the 4′-position of tpy has a strong electron-withdrawing effect on the tpy ligand and, consequently, on the metal center. This results in an increase of the reactivity of the ruthenium complexes **1**–**3**. Furthermore, the K_b values of **1**–**3** are higher than that of the classical intercalator EB, which has a binding affinity for CT DNA of $1.23\ (\pm 0.07) \times 10^5\ M^{-1}$ [17,38,39].

3.4.2. Fluorescence quenching studies

Ethidium bromide (EB) is a classical intercalator that gives significant fluorescence emission intensity when it intercalates into the base pairs of DNA. When it is replaced or excluded from the internal hydrophobic environment of the DNA double helix by other small molecules, its fluorescence emission is effectively quenched by external polar solvent molecules such as H_2O [40]. Compounds **1**–**3** do not show any significant fluorescence at room temperature in solution or in the presence of CT DNA, when excited at 527 nm. Furthermore, the addition of complexes **1**–**3** to a solution containing EB does not provoke quenching of free EB fluorescence, and no new peaks appear in the spectra. The changes observed in the spectra of EB on its binding to CT DNA are often used for studying the DNA binding activity of metal complexes, since the addition of a compound, capable of intercalating DNA equally or more strongly than EB, could result in a quenching of the EB-DNA florescence emission.

The fluorescence quenching curves of EB bound to DNA in the absence and presence of the complexes are shown in Fig. 4. The addition of increasing amounts (up to $r = 1.0$) of complexes **1**–**3** resulted in significant decrease of the intensity of the emission band at 612 nm, indicating competition of the compounds with EB in binding to DNA (Fig. 4).

Table 1
Rate constants for the aquation and half-lives at 298 K in H_2O for compounds **1** and **2**.

Compound	λ_{max} [nm]	λ_{min} [nm]	Isosbestic points [nm]	k_{obs} [$10^{-3}\ s^{-1}$]	$(t_{1/2})_{H2O}$ [min]
1	470, 535	394, 579	362, 430, 552	6.10 ± 0.01	2.00 ± 0.03
2	393, 510, 581	471	347, 429, 494	4.90 ± 0.02	2.40 ± 0.02

Table 2
The DNA-binding constants (K_b) and Stern–Volmer constants (V, K_{sv}) from EB–DNA fluorescence for **1**–**3**.

Complex	K_b [M^{-1}]	K_{sv} [M^{-1}]	V (M^{-1})
1	1.0 (±0.2) × 10^6	1.9 (±0.1) × 10^4	1.1 (±0.3) × 10^4
2	2.8 (±0.1) × 10^6	2.7 (±0.1) × 10^4	1.2 (±0.3) × 10^4
3	9.0 (±0.2) × 10^6	1.1 (±0.1) × 10^4	8.9 (±0.3) × 10^3

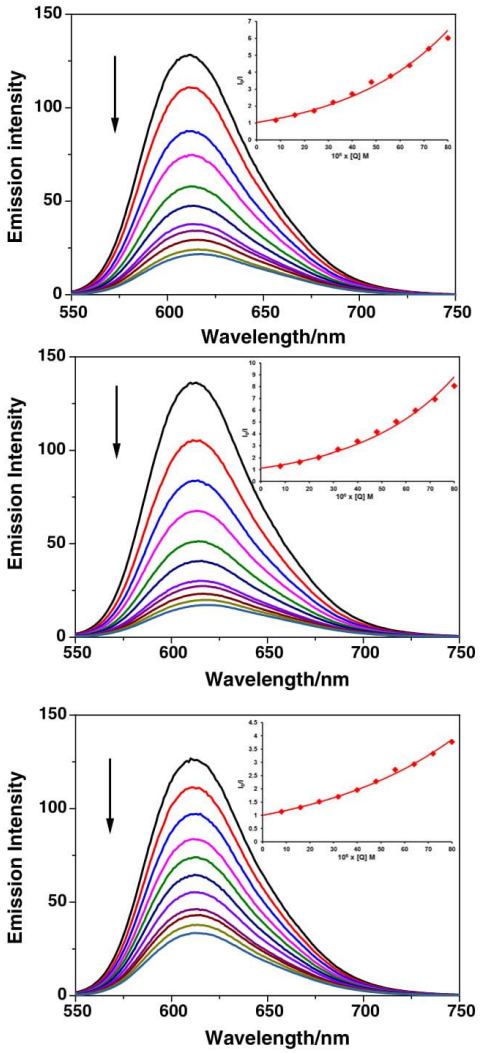

Fig. 4. Emission spectra of EB bound to DNA in the presence of complexes **1** (top), **2** (middle) and **3** (bottom). [EB] = 80 μM, [DNA] = 80 μM; [Ru] = 0–80 μM; λ_{ex} = 527 nm. The arrows show the intensity changes upon increased concentrations of the complexes. Insets: plots of I_0/I versus [Q]; with (■) are shown the experimental data points and the full line represents the exponential fitting of the data.

The observed quenching of DNA–EB fluorescence suggests that they can displace EB from the DNA–EB complex and that they can probably interact with CT DNA by the intercalative mode [38,41,42].

Quenching mechanism can be predicted from Stern-Volmer plots. In the case of all three complexes **1**–**3**, the simple Stern–Volmer plots (I_0/I versus [Q]) showed an upward curvature (Eq. (S2) and Fig. 4) which is obtained when both static and dynamic quenching occur. The static quenching constant V was obtained from the modified form of the Stern-Volmer equation (Eq. S3) by plotting $I_0/Ie^{V[Q]}$ versus [Q] by varying V until a linear plot was obtained. The highest value of correlation coefficient was used as criterion for linearity of the plot to obtain a precise value of V. The (dynamic) collisional quenching constant, K_{sv} was then obtained from the slope of the linear plots (Fig. S10). The V and K_{sv} values so obtained are given in Table 2. All three complexes showed high values of the quenching constant indicating their great efficiency to replace EB and bind strongly to DNA, which is in agreement with the high values of their DNA binding constant (K_b). These additional interactions could contribute to the unique binding modes to duplex DNA and induce different structural distortions in DNA compared to cisplatin. Similar observations were reported by Sadler and coworkers for the promising antitumor group of organoruthenium(II) complexes where the direct coordinative binding of the monofunctional [Ru(η^6-biphenyl)(en)Cl]$^+$ complex to *N*7 of guanine bases in DNA was complemented by intercalative binding of the biphenyl ligand [43].

3.4.3. Viscosity measurements

In order to further confirm the modes of binding of complexes **1**–**3** to CT DNA, viscosity measurements of DNA solutions were performed in the presence and absence of these complexes. The viscosity of DNA is sensitive to length changes and is regarded as the least ambiguous and the most critical clues of the DNA binding mode in solution [44,45]. The addition of increasing amounts (up to r = 1.0) of complexes **1**–**3** to a DNA solution (0.01 mM) resulted in an increase in the relative viscosity of DNA (Fig. S11), which was more pronounced upon addition of complex **2**. In the case of classic intercalation, DNA base pairs are separated to host the bound compound resulting in increased DNA viscosity, the magnitude of which is usually in accordance to the strength of the interaction, because of the lengthening of the DNA helix. Therefore, the observed viscosity increase may be explained by an increase in the overall DNA length provoked by the insertion of the compounds in between the DNA base pairs due to interaction via intercalation through the aromatic chromophore of Cl-Ph-tpy and bpy ligands in the complexes. Additionally, these observations are in substantial agreement with the previously obtained results for the Cl-tpy complexes **4** and **5** [7].

3.5. Albumin-binding studies

Serum albumin, as the most abundant protein in the blood circulatory system, plays important role in the transport and delivery of many pharmaceuticals to the sites of disease [46]. Therefore, studies on the binding of biologically active compounds with proteins not only provide useful information on the structural features that determine the therapeutic effectiveness of drugs, but is also important for studying the pharmacological response of drugs and design of dosage forms. Interactions of metallodrugs with proteins are crucial for their biodistribution, toxicity, and even for their mechanism of action [47]. Furthermore, binding of drugs to proteins may affect (either enhance or reduce) the biological properties of the original drug.

We have recently shown, by means of UV–Vis and ^{1}H NMR spectroscopies supported by DFT calculations, as well as by liquid chromatography (LC) and inductively coupled plasma optical emission spectrometry (ICP-OES), that complexes **4** and **5** coordinate to BSA through the nitrogen atom of imidazole ring of several histidine (His) residues [7,8]. The binding mechanism involved the dissociation of the chloride ligand and its replacement by a water molecule, prior to binding to His. In this

study, the interaction between BSA and complexes **1**–**3** was investigated by florescence spectroscopy as this method allows a quantitative assessment of the binding strength.

BSA is the most extensively studied serum albumin because of its high structural homology with HSA (human serum albumin). HSA contains one tryptophan located at position 214, while BSA has two tryptophan residues, Trp-134 and Trp-212. BSA solution exhibits an intense fluorescence emission with $\lambda_{em,max}$ = 352 nm, when excited at 295 nm [48]. The changes and the quenching observed in the fluorescence emission spectra of tryptophan in BSA upon addition of complexes are primarily due to changes in protein conformation, subunit association, substrate binding, or denaturation.

Addition of the complexes **1**–**3** to a BSA solution (up to *r* values of 15) results in a significant quenching of BSA fluorescence at λ = 352 nm for **2** and **3**, and moderate quenching for complex **1** (Fig. 5 and Fig. S12). The observed quenching may be attributed to changes in protein tertiary structure leading to changes in tryptophan environment of BSA, and thus indicating the binding of each complex to the albumin [48–50]. Furthermore, the maximum of the bands were slightly shifted from 352 to 355, 356 or 359 nm, for **1**, **2** and **3**, respectively (Fig. S12). The red shift implies the formation of ruthenated BSA adducts, which altered the polarity of microenvironment in the vicinity of tryptophan.

In the case of all three complexes **1**–**3**, the simple Stern–Volmer plots (I_0/I versus [Q]) showed an upward curvature (Eqs. (S4), (S5) and Fig. S13). The static quenching constant *V* was obtained from the modified form of the Stern-Volmer equation (Eq. (S6)) by plotting $I_0/Ie^{V[Q]}$ versus [Q] by varying *V* until a linear plot was obtained. The highest value of correlation coefficient was used as criterion for linearity of the plot to obtain a precise value of *V*. The (dynamic) collisional quenching constant, K_{sv} was then obtained from the slope of the linear plots (inset Fig. S13). The *V* and K_{sv} values so obtained are given in Table 3. The magnitude of static quenching constant was smaller than the collisional quenching constant, but both were of the order of 10^4.

The quenching rate constant (k_q) depends on the probability of a collision between fluorophore and quencher and is a measure of the exposure of tryptophan residues to the drug. The k_q values are also given in Table 3 and indicate good quenching ability of the BSA fluorescence, with **2** exhibiting the highest k_q value (k_q = 4.6 ± (0.5) × 10^{12} M^{-1} s^{-1}). The upper limit of k_q expected for a diffusion-controlled bimolecular process is 10^{10} M^{-1} s^{-1}. The high magnitude of k_q in the present study (10^{12} M^{-1} s^{-1}) shows that the process is not entirely diffusion controlled, specific drug-protein interactions are also involved which make k_q larger [48–50].

The values of the BSA-binding constant (*K*) and the number of binding sites per albumin (n), as calculated from the Scatchard equation (Eq. (S7)) and Scatchard plot (Fig. S14) for all compounds are given in Table 3. The highest binding constant to BSA is found for complex **3**. The *n* values for the complexes **1**–**3** average out to be 1 which suggests that there is only one binding site available on the protein [51].

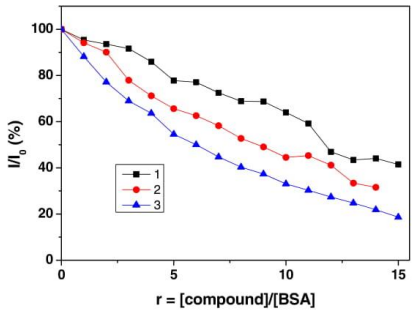

Fig. 5. Plot of % relative fluorescence intensity at λ_{em} = 352 nm vs r (r = [complex]/[BSA]) for the complexes **1**–**3** (58% of the initial fluorescence intensity for **1**, 68% for **2**, and 81% for **3**) in buffer solution (5 mM Tris and 50 mM NaCl).

The analysis of the BSA-binding constants (*K*) is rather useful to infer how a molecular species, particularly a drug, will be distributed in blood plasma. All three complexes have *K* values that are within the range which could be considered optimal; they are high enough so that the compounds bind to BSA to get transport, but nevertheless they are sufficiently low (i.e., below the value of 10^{15} M^{-1}, which is the association constant of avidin with diverse ligands; this interaction is considered the strongest among known noncovalent interactions) so that the compounds can be released from the albumin upon arrival at the target cells [52–54]. This binding might provide a path to enhance the selectivity of **1**–**3** by passive targeting to tumor tissues through BSA binding.

3.6. Hydrophobicity measurements

Lipophilicity is one of the most important factors in pharmaceutical research and can be considered a key determinant of the pharmacokinetic properties of a drug and its interaction with macromolecular targets. Octanol–water partition coefficients (log $P_{o/w}$) provide a measure of drug lipophilicity, which indicates the ability of a molecule to pass through cell membranes [55]. Knowledge of the partition coefficient is valuable, and it is frequently used in structure-activity relationship (SAR) and quantitative structure-activity relationship (QSAR) studies. The lipophilicity of complexes **1**–**3** was determined by measuring the concentration ratio of the corresponding complex in the aqueous phase at equilibrium state. After mixing with octanol and water, complexes **1**–**3** were distributed mostly in the octanol phase. All three complexes gave positive log $P_{o/w}$ values, showing them to be hydrophobic in nature. Complex **3** (0.39) tended to be more hydrophobic than **1** (0.27), and **2** (0.20), which may facilitate its cell uptake efficiency and enhance its anticancer activity.

3.7. In vitro cytotoxicity

The in vitro cytotoxicity of complexes **1**–**6**, and precursor **P1** against two selected human cancer cell lines (HeLa and A549) and one normal cell line (MRC-5) was determined by MTT assay. The widely used clinical chemotherapeutic agent cisplatin was used as a positive control. Activity was determined after incubation with investigated complexes for 72 h (Fig. 6). From Table 4, it is clear that complex **3** is generally the most active and exhibits low IC_{50} values of 12.7 μM for HeLa cells, and 4 times higher IC_{50} values (*ca.* 53.8 μM) for A549 cell line. Complexes **1** and **2** show moderate in vitro cytotoxicity against the HeLa cell line with an IC_{50} of *ca.* 84.8 and 96.3 μM, respectively, i.e. from about 7 to 8 times lower activity than that of the most potent bpy complex **3**. Conversely, **1** and **2** do not show any activity against A549 cell line. All three complexes reveal a remarkable selectivity towards the human cervix carcinoma cells (HeLa). In addition, the previously described Cl-tpy compounds [Ru(Cl-tpy)(dach)Cl]Cl (**5**) and [Ru(Cl-tpy)(bpy)Cl]Cl (**6**) [7], show lower activity in comparison with their Cl-Ph-tpy analogues **2** and **3**, respectively. Interestingly, whereas in the series of the Cl-Ph-tpy compounds **1**–**3** the bpy complex **3** is the most active, in the series of the Cl-tpy compounds **4**–**6** the en complex **4** is the uppermost. These results indicate that the biological activity of Ru(II) polypyridyl complexes depends on the nature of the meridional tridentate ligand. The introduction of chlorophenyl-substituent in the tpy ligand results in an increase in the anticancer activity. In addition, the presence of bipyridine in the coordination sphere of the ruthenium(II) chlorophenyl-substituted tpy complexes is very important for the cytotoxic activity. Compared to the pure σ-donor ligands en and dach, the π-acceptor bpy may increase the electrophilicity of the metal center and hence the reactivity of ruthenium(II) complexes. On the other hand, the possibility of bpy intercalation between the DNA bases has also been recognized [56].

Table 3
BSA constants and parameters (K_{sv}, k_q, K, n and V) derived for complexes **1–3**.

Complex	K_{sv} (M^{-1})	k_q (M^{-1} s^{-1})	K (M^{-1})	n	V (M^{-1})
1	3.7 (±0.4) × 10^4	3.7 (±0.4) × 10^{12}	2.0 × 10^4	0,81	1.0 (±0.3) × 10^4
2	4.6 (±0.5) × 10^4	4.6 (±0.5) × 10^{12}	3.0 × 10^4	1,50	1.2 (±0.4) × 10^4
3	3.5 (±0.07) × 10^4	3.5 (±0.07) × 10^{12}	5.0 × 10^4	1,34	3.0 (±0.4) × 10^4

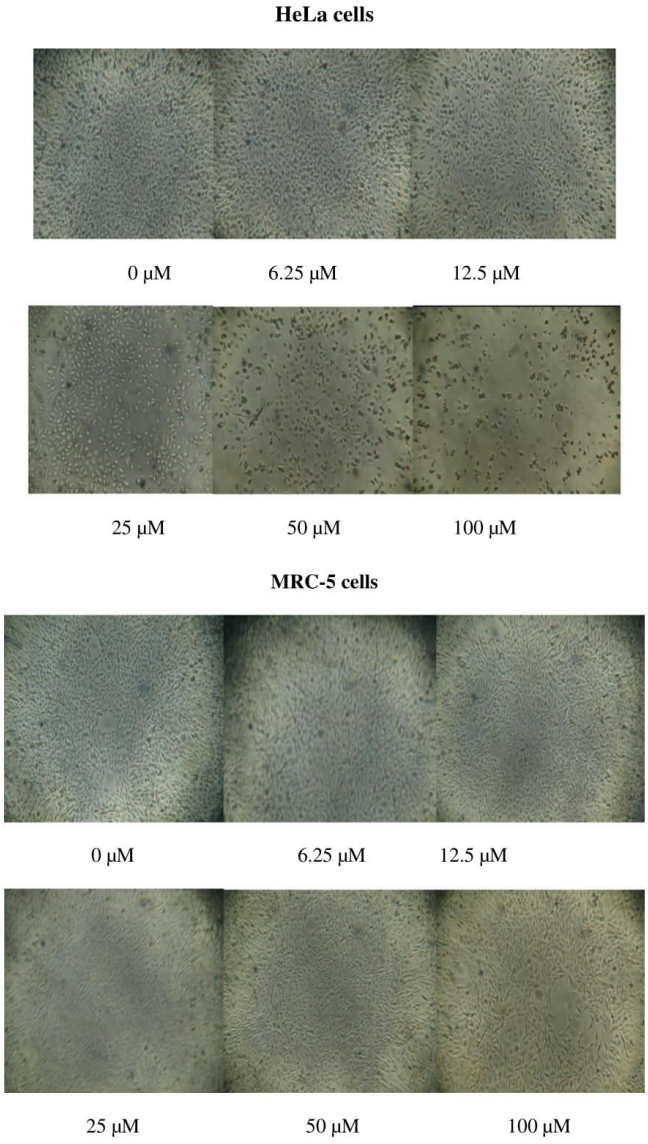

Fig. 6. Inverted microscopy examination of HeLa and MRC-5 cells after 72 h of treatment with complex **3**.

Table 4
IC_{50} values for complexes **1**–**6** and precursor **P1** towards different cell lines in comparison to cisplatin, obtained from the MTT assay, after 72 h drug exposure. In all cases, the values represent the mean of three independent experiments.

	IC_{50} [μM]		
	HeLa	A549	MRC-5
1	84.81 ± 4.67	>100	>100
2	96.28 ± 3.81	>100	>100
3	12.68 ± 1.89	53.80 ± 4.44	97.67 ± 6.93
4	71.23 ± 2.61	>100	86.66 ± 2.62
5	>100	>100	>100
6	>100	>100	>100
P1	83.05 ± 4.06	>100	64.87 ± 4.07
Cisplatin	3.33 ± 0.28	5.93 ± 0.66	7.96 ± 0.18

The in vitro activity of anticancer drugs can often be related in part, to their lipophilic character; higher hydrophobicity may contribute to an increased uptake of the complex by the cells, thereby enhancing the anticancer activity [57–60]. For example, complex **3** presents the highest lipophilicity and hence generates the strongest cytotoxicity. In contrast, complex **2** presents the lowest lipophilicity and therefore exhibits the weakest cytotoxicity. The most likely reason may be that it is easier for complex **3** to pass through the cell membrane, which induces a higher cell uptake and a higher cytotoxicity. All these findings further demonstrate that aromatic substituent on the tpy ligand has great influence on the biological activity of these complexes. Similar to Sadler and co-workers who have shown that there is a direct correlation between the lipophilicity of the arene ligand and cytotoxicity [61], in the present work we demonstrated that the cytotoxicity of the Ru-tpy complexes can be increased by using more lipophilic ligands.

3.8. Cell cycle analysis

The effect on cell cycle progression of HeLa and A549 cells after treatment with complex **3** was examined by flow cytometry, using staining with propidium iodide PI [19]. Complex **3** was selected among the other investigated complexes due to its promising profile: high cytotoxicity and selectivity towards HeLa cells, moderate cytotoxicity against A549 cells, and low cytotoxicity to normal cells (MRC-5). In comparison, the well-established drug cisplatin (CDDP) was investigated as well, under the same conditions.

The results of the cell cycle analysis of HeLa cells treated with **3**, presented in Fig. 7, show that after 48 h of action with $2IC_{50}$ and $3IC_{50}$ concentrations (IC_{50} values determined for 72 h agent action) induced barely noticeable changes: slight decrease of percent of cells in G1 phase and slight increase of percent of cells in S and G2. Simultaneously, no change of percent of cells in Sub-G1 phase (hypodiploid cells), which is considered as a marker of cell death by apoptosis [62], was observed in studied conditions (Fig. 7). On the other hand, cisplatin induced decrease of percent of cells in G1 (up to 32.8% compared to control 56.6%) and increase of percent of cells in S phase (up to 51% compared to control 18.9%). Cisplatin S phase arrest that indicates block of DNA replication is in agreement with the literature concerning the mechanism of action of CDDP and its effect on the cell cycle [63,64]. Lack of cell cycle perturbations after complex **3** action indicate that its interactions with DNA, determined by DNA binding studies, are not crucial/decisive for its cytotoxicity and perhaps a different mechanism of action compared to that of cisplatin, is implicated for the obtained activity.

The cell cycle analysis of A549 cells after 48 h treatment with **3** (with concentrations corresponding to $2IC_{50}$ and $3IC_{50}$ determined for 72 h agent action), presented in Fig. 8, show minor increase in percent of cells in G1 phase (up to 82.4% compared to control 74.3%) and decrease in S phase (up to 7.5% compared to control 12.5%). This may indicate the presence of some type of interactions with DNA that prevent the entry of cells in the synthetic phase of cell cycle. Under the same experimental conditions, cisplatin induced tremendous perturbations of cell cycle after 48 h treatment (with $2IC_{50}$ and $3IC_{50}$ concentrations), with enormous decrease of percent of cells in G1 phase (up to 15.8% compared to control 74.3%) and accumulation of cells in S and G2/M phases of the cell cycle, in agreement with previously published results [65]. In terms of the results related to the mechanism of action of our ruthenium complex **3**, although the complicated nature of A549 cell line makes difficult the interpretation of the results with respect to cisplatin, it allows us to conclude that results of cell cycle analysis confirmed again different mode of interactions of **3**, compared to cisplatin, with DNA.

4. Conclusion

In a previous work we have reported the synthesis and extensive studies including thorough investigation on their stability and behavior in aqueous solution, DNA/BSA binding activity and in vitro antiproliferative activity, of a series of new Ru(II)-tpy complexes of the general formula [Ru(Cl-tpy)(*N*-*N*)Cl]Cl (where Cl-tpy = 4′-chloro-2,2′:6′,2″-terpyridine; *N*-*N* = en (**4**), dach (**5**) or bpy (**6**)) [6–8]. We found that these compounds, in particular complex **4**, show promising antitumor activity. With the aim of expanding the structure activity relationship investigation on these polypyridyl Ru(II) complexes, we were testing another meridional tridentate ligand. In that context, we described here the synthesis and structural characterization of a series of new monofunctional ruthenium(II) complexes of the general formula *mer*-[Ru(Cl-Ph-tpy)(*N*-*N*)Cl]Cl (where *N*-*N* = en (**1**), dach (**2**) or bpy (**3**)), in which the Cl-tpy ligand was replaced by the chlorophenyl-substituted tpy ligand (Cl-Ph-tpy), while the rest of the coordination sphere remained unchanged. In view of their potential antitumor activity, their chemical behavior in aqueous solution was studied by UV–Vis

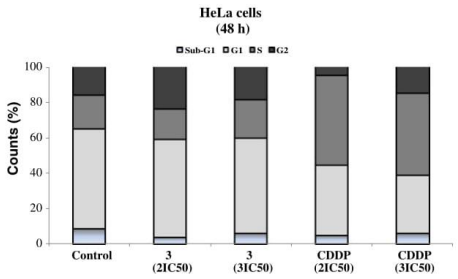

Fig. 7. Diagrams representing cell cycle phase distribution of HeLa cells treated with complex **3** or cisplatin (CDDP). IC_{50} values were determined for 72 h agent action. Bar graphs show representative experiments.

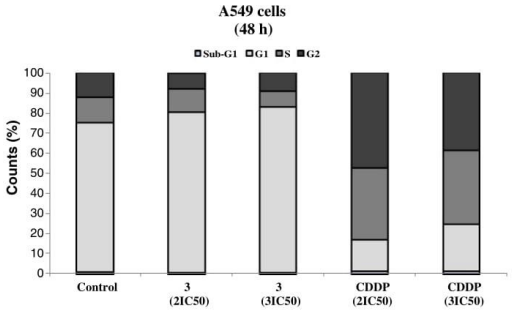

Fig. 8. Diagrams representing cell cycle phase distribution of A549 cells treated with complex **3** or cisplatin (CDDP). IC_{50} values were determined for 72 h agent action. Bar graphs show representative experiments.

and NMR spectroscopy and compared to that of the previously described analogues [Ru(Cl-tpy)(*N*-*N*)Cl]Cl. These studies showed that complexes **1**–**3** release the Cl^- ligand to form the corresponding aqua species. The rate of hydrolysis was found to depend markedly on the nature of the chelating ligand (minutes for en and dach, hours for bpy), but its extent was similar in all cases, with a *ca.* 1:9 ratio between intact and aquated species at equilibrium, at NMR concentrations.

UV–Vis spectroscopy studies and competitive binding studies with EB revealed the ability of the complexes to bind to CT DNA covalently and non-covalently through intercalation. All complexes show good binding affinity to BSA, with relatively high binding constants. The high *K* values observed for the complexes **1**–**3** suggest that these compounds can be efficiently stored and transported in the body by BSA. The cytotoxicity of **1**–**3** was evaluated against two different tumor cell lines (HeLa and A549), and one normal cell line (MRC-5) in comparison with their Cl-tpy analogues **4**–**6**, their respective precursor *mer*-[Ru(Cl-Ph-tpy)Cl_3] (**P1**) and cisplatin. Complex **3** displayed the highest cytotoxicity when tested on the HeLa cell line. Contrary to what observed for the corresponding Ru-tpy complexes **4**–**6**, that their cytotoxicity roughly correlates with their ability to hydrolyze the monodentate ligand at a reasonable rate, the most active bpy complex **3** hydrolyses slower than the other two complexes.

The present results clearly confirmed that the relatively rapid availability of one coordination position on the Ru center is not an essential requirement for observing anticancer activity, which is in contrary with the results obtained for the corresponding Ru-tpy complexes, as well as with the results obtained by Sadler and Alessio for the organoruthenium(II) half-sandwich compounds and coordination Ru(II)-[9]aneS3 complexes, respectively [5,7,20]. In addition, we showed here that the presence of a chelating ligand that is unable of making hydrogen bonds, such as bpy, not necessarily induces the loss of cytotoxic activity. In fact, the bpy complex **3** was the most active. We speculate that the activity of such complexes is relevant to their hydrophobicity and their ability to open a coordination site. These two properties largely determine their mechanism of action: by increasing the aromaticity (viz. hydrophobicity), the intercalation is the predominant mechanism, whereas in less aromatic molecules the covalent binding. The lack of correlation between cell growth inhibition, DNA and BSA binding affinity and hydrolysis stability suggests that multiple targets and multiple mechanisms involve in the anticancer process of the compounds. These differences may play very important roles in their antitumor activity and could contribute to the different mechanism for cytotoxicity compared to cisplatin.

Abbreviations

Cl-Ph-tpy	4′-(chlorophenyl)-2,2′:6′,2′-terpyridine
en	1,2-diaminoethane
dach	1,2-diaminocyclohexane
bpy	2,2′-bipyridine
CT DNA	calf thymus DNA
EB	ethidium bromide
tpy	2,2′:6′,2″-terpyridine
Cl-tpy	4′-chloro-2,2′:6′,2″-terpyridine
RPMI	Roswell Park Memorial Institute
TRIS	tris(hydroxymethyl)aminomethane
DSS	2,2-dimethyl-2,2-silapentane-5-sulfonate
DMSO	dimethyl sulfoxide
HEPES	4-(2-hydroxymethyl)piperazine-1-ethansulfonic acid
FCS	fetal calf serum
MTT	3-(4,5-dimethylthiazol-yl)-2,5-diphenyltetrazolium bromide
SDS	sodium dodecyl sulfate
ELISA	enzyme linked immunosorbent assay
PI	propidium iodide
PBS	phosphate buffer saline
FACS	fluorescence activated sorting cells
LC	liquid chromatography
ICP-OES	inductively coupled plasma optical emission spectroscopy
His	histidine
CDDR	cisplatin

Acknowledgments

The authors gratefully acknowledge financial support from the Ministry of Education, Science and Technological Development of the Republic of Serbia, Project No. 172011.

Appendix A. Supplementary data

Supplementary data to this article can be found online at doi:10.1016/j.jinorgbio.2016.10.001.

References

[1] E. Alessio, Bioinorganic Medicinal Chemistry, Wiley-VCH Verlag & Co. KGaA, Weinheim, Germany, 2011.
[2] P.E.N. Barry, J.P. Sadler, Chem. Commun. 49 (2013) 5106–5131.
[3] R. Trondl, P. Heffeter, C.R. Kowol, M.A. Jakupec, W. Berger, B.K. Keppler, Chem. Sci. 5 (2014) 2925–2932.
[4] P.C. Bruijnincx, P.J. Sadler, J. Curr. Opin. Chem. Biol. 12 (2008) 197–206.
[5] Y.K. Yan, M. Melchart, A. Habtemariam, P.J. Sadler, Chem. Commun. (2005) 4764–4776.
[6] A. Rilak, I. Bratsos, E. Zangrando, J. Kljun, I. Turel, Ž.D. Bugarčić, E. Alessio, Inorg. Chem. 53 (2014) 6113–6126.
[7] D. Lazić, A. Arsenijević, R. Puchta, Ž.D. Bugarčić, A. Rilak, Dalton Trans. 45 (2016) 4633–4646.
[8] M. Nišavić, R. Masnikosa, A. Butorac, K. Perica, A. Rilak, A. Hozić, M. Petković, M. Cindrić, J. Inorg. Biochem. 159 (2016) 89–95.
[9] L.-F. Tan, X.-J. Chen, J.-L. Shen, X.-L. Liang, J. Chem. Sci. 121 (2009) 397–405.
[10] M.-Y. Ho, M.-L. Chiou, W.-S. Du, F.Y. Chang, Y.-J. Weng, C.-C. Cheng, J. Inorg. Biochem. 105 (2011) 902–910.
[11] M.N. Patel, D.S. Gandhi, P.A. Parmar, H.N. Joshi, J. Coord. Chem. 65 (2012) 1926–1936.
[12] A. Hofmann, D. Jaganyi, O.Q. Munro, G. Liehr, R. van Eldik, Inorg. Chem. 42 (2003) 1688–1700.
[13] D. Jaganyi, D. Reddy, J.A. Gertenbach, A. Hofmann, R. van Eldik, Dalton Trans. (2004) 299–304.
[14] J. Wang, Y.-Q. Fang, G.S. Hanan, F. Loiseau, S. Campagna, Inorg. Chem. Commun. 44 (2005) 5–7.
[15] D. Reddy, K.J. Akerman, M.P. Akerman, D. Jaganyi, Transit. Met. Chem. 36 (2011) 593–602.
[16] K.A. Meadows, F. Liu, J. Sou, B.P. Hudson, D.R. McMillin, Inorg. Chem. 32 (1993) 2919–2923.
[17] A. Tarushi, E. Polatoglou, J. Kljun, I. Turel, G. Psomas, D.P. Kessissoglou, Dalton Trans. 40 (2011) 9461–9473.
[18] C.A. Puckett, J.K. Barton, J. Am. Chem. Soc. 129 (2007) 46–47.
[19] M.G. Ormerod, Analysis of DNA-General Methods. Flow Cytometry, a Practical Approach, Oxford University Press, New York, 1994 119.
[20] I. Bratsos, E. Mitri, F. Ravalico, E. Zangrando, T. Gianferrara, A. Bergamo, E. Alessio, Dalton Trans. 41 (2012) 7358–7371.
[21] I. Bratsos, C. Simonin, E. Zangrando, T. Gianferrara, A. Bergamo, E. Alessio, Dalton Trans. 40 (2011) 9533–9543.
[22] D. Chatterjee, A. Sengupta, A. Mitra, Polyhedron 26 (2007) 178–183.
[23] G.S. Papaefstathiou, A. Sofetis, C.P. Raptopoulou, A. Terzis, G.A. Spyroulias, T.F. Zafiropoulos, J. Mol. Struct. 837 (2007) 5–14.
[24] J.R. Jeitler, M.M. Turnbull, J.L. Wikaira, Inorg. Chim. Acta 351 (2003) 331–344.
[25] N. Gupta, N. Grover, G.A. Neyhart, P. Singh, H.H. Thorp, Inorg. Chem. 32 (1993) 310–316.
[26] K.J. Takeuchi, M.S. Thompson, D.W. Pipes, T.J. Meyer, Inorg. Chem. 23 (1984) 1845–1851.
[27] A. Dovletoglou, S.A. Adeyemi, T.J. Meyer, Inorg. Chem. 35 (1996) 4120–4127.
[28] M.J. Root, E. Deutsch, Inorg. Chem. 24 (1985) 1464–1471.
[29] S.E. Miller, D.A. House, Inorg. Chim. Acta 187 (1991) 125–132.
[30] J.E. Quin, J.R. Devlin, D. Cameron, K.M. Hannan, R.B. Pearson, R.D. Hannan, Biochim. Biophys. Acta Mol. basis Dis. 1842 (2014) 802–816.
[31] V. Brabec, Prog. Nucleic Acid Res. Mol. Biol. 71 (2002) 1–68.
[32] C.X. Zhang, S.J. Lippard, Curr. Opin. Chem. Biol. 7 (2003) 481–489.
[33] V. Brabec, O. Novakova, Drug Resist. Updat. 9 (2006) 111–122.
[34] J. Liu, W. Zheng, S. Shi, C. Tan, J. Chen, K. Zheng, L. Ji, J. Inorg. Biochem. 102 (2008) 193–202.
[35] T.W. Johann, J.K. Barton, Philos. Trans. R. Soc. London, A 354 (1996) 299–324.
[36] J.G. Vos, J.M. Kelly, Dalton Trans. (2006) 4869–4883.
[37] H. Huang, P. Zhang, Y. Chen, L. Ji, H. Chao, Dalton Trans. 44 (2015) 15602–15610.
[38] A. Tarushi, K. Lafazanis, J. Kljun, I. Turel, A.A. Pantazaki, G. Psomas, D.P. Kessissoglou, J. Inorg. Biochem. 121 (2013) 53–65.
[39] A. Dimitrakopoulou, C. Dendrinou-Samara, A.A. Pantazaki, M. Alexlou, E. Nordlander, D.P. Kessissoglou, J. Inorg. Biochem. 102 (2008) 618–628.

[40] C.V. Kumar, J.K. Barton, N.J. Turro, J. Am. Chem. Soc. 107 (1985) 5518–5523.
[41] A. Tarushi, G. Psomas, C.P. Raptopoulou, D.P. Kessissoglou, J. Inorg. Biochem. 103 (2009) 898–905.
[42] E.S. Koumousi, M. Zampakou, C.P. Raptopoulou, V. Psycharis, C.M. Beavers, S.J. Teat, G. Psomas, T.C. Stamatatos, Inorg. Chem. 51 (2012) 7699–7710.
[43] O. Novakova, H. Chen, O. Vrana, A. Rodger, P.J. Sadler, V. Brabec, Biochemistry 42 (2003) 11544–11554.
[44] D.D. Li, J.L. Tian, W. Gu, X. Liu, S.P. Yan, J. Inorg. Biochem. 104 (2010) 171–179.
[45] M. Jiang, Y. Li, Z. Wu, Z. Liu, C. Yan, J. Inorg. Biochem. 103 (2009) 833–844.
[46] A.R. Timerbaev, C.G. Hartinger, S.S. Aleksenko, B.K. Keppler, Chem. Rev. 106 (2006) 2224–2248.
[47] O. Dömötör, C.G. Hartinger, A.K. Bytzek, T. Kiss, B.K. Keppler, E.A. Enyedy, J. Biol. Inorg. Chem. 18 (2013) 9–17.
[48] Y. Wang, H. Zhang, G. Zhang, W. Tao, S. Tang, J. Lumin. 126 (2007) 211–218.
[49] S. Deepa, A.K. Mishra, J. Pharm. Biomed. Anal. 38 (2005) 556–563.
[50] J.R. Lakowicz, G. Weber, Biochemistry 12 (1973) 4161–4170.
[51] B. Mishra, A. Barik, K.I. Priyadarsini, H. Mohan, J. Chem. Sci. 117 (2005) 641–647.
[52] G. Psomas, D.P. Kessissoglou, Dalton Trans. 42 (2013) 6252–6276.
[53] S. Wu, W. Yuan, H. Wang, Q. Zhang, M. Liu, K. Yu, J. Inorg. Biochem. 102 (2008) 2026–2034.
[54] V. Rajendiran, R. Karthik, M. Palaniandavar, H. Stoeckli-Evans, V.S. Periasamy, M.A. Akbarsha, B.S. Srinag, H. Krishnamurthy, Inorg. Chem. 46 (2007) 8208–8221.
[55] L. Fetzer, B. Boff, M. Ali, X. Meng, J.P. Collin, C. Sirlin, C. Gaiddon, M. Pfeffer, Dalton Trans. 40 (2011) 8869–8878.
[56] B.-J. Han, G.-B. Jiang, J.-H. Yao, W. Li, J. Wang, H.-L. Huang, Y.-J. Liu, Spectrochim. Acta A 135 (2015) 840–849.
[57] M.G. Mendoza-Ferri, C.G. Hartinger, M.A. Mendoza, M. Groessl, A.E. Egger, R.E. Eichinger, J.B. Mangrum, N.P. Farrell, M. Maruszak, P.J. Bednarski, F. Klein, M.A. Jakupec, A.A. Nazarov, K. Severin, B.K. Keppler, J. Med. Chem. 52 (2009) 916–925.
[58] F. Giannini, L.E.H. Paul, J. Furrer, B. Therrienb, G. Suss-Fink, New J. Chem. 37 (2013) 3503–3511.
[59] Y. Mulyana, D.K. Weber, D.P. Buck, C.A. Motti, J.G. Collins, F.R. Keene, Dalton Trans. 40 (2011) 1510–1523.
[60] A.K. Gorle, A.J. Ammit, L. Wallace, F.R. Keene, J.G. Collins, New J. Chem. 38 (2014) 4049–4059.
[61] R.E. Aird, J. Cummings, A.A. Ritchie, M. Muir, R.E. Morris, H. Chen, P.J. Sadler, D.I. Jodrell, Br. J. Cancer 86 (2012) 1652–1657.
[62] Z. Darzynkiewicz, S. Bruno, G. Del Bino, W. Gorczyca, M.A. Hotz, P. Lassota, F. Traganos, Cytometry 13 (1992) 795–808.
[63] D. Wang, S.J. Lippard, Nat. Rev. Drug Discov. 4 (2005) 307–320.
[64] S. Nikolić, L. Rangasamy, N. Gligorijević, S. Aranđelović, S. Radulović, G. Gasser, S. Grgurić-Šipka, J. Inorg. Biochem. (2016) In Press, Available online 11 January.
[65] G.M. Almeida, T.L. Duarte, P.B. Farmer, W.P. Steward, G.D. Jones, Int. J. Cancer 122 (2008) 1810–1819.

New 4'-(4-chlorophenyl)-2,2':6',2''-terpyridine ruthenium(II) complexes: Synthesis, characterization, interaction with DNA/BSA and cytotoxicity studies

Milan M. Milutinović [a], Ana Rilak [a,*], Ioannis Bratsos [b], Olivera Klisurić [c], Milan Vraneš [d], Nevenka Gligorijević [e], Siniša Radulović [e], Živadin D. Bugarčić [a,*]

[a] *Faculty of Science, University of Kragujevac, R. Domanovića 12, P. O. Box 60, 34000 Kragujevac, Serbia.*

[b] *I.N.N., Dept. of Physical Chemistry, NCSR "Demokritos", 15310 Ag. Paraskevi, Athens, Greece.*

[c] *Department of Physics, Faculty of Sciences, University of Novi Sad, Trg Dositeja Obradovića 4, 21000 Novi Sad, Serbia.*

[d] *University of Novi Sad, Faculty of Sciences, Department of Chemistry, Biochemistry and Environmental Protection, Trg Dositeja Obradovića 3, 21000 Novi Sad, Serbia.*

[e] *Institute for Oncology and Radiology of Serbia, Pasterova 14, 11000 Belgrade, Serbia.*

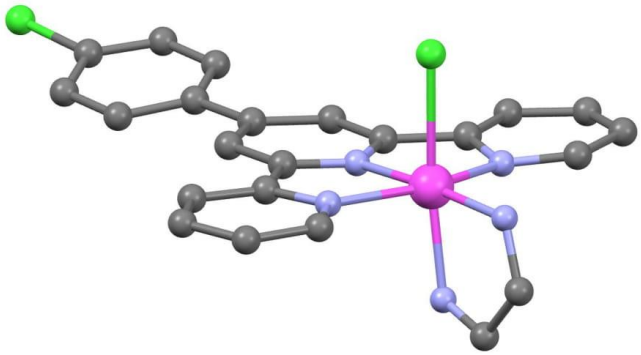

Fig. S1 Molecular structure of complex [Ru(Cl-Ph-tpy)(en)(Cl)]Cl (**1**) obtained from a crystal of low quality.

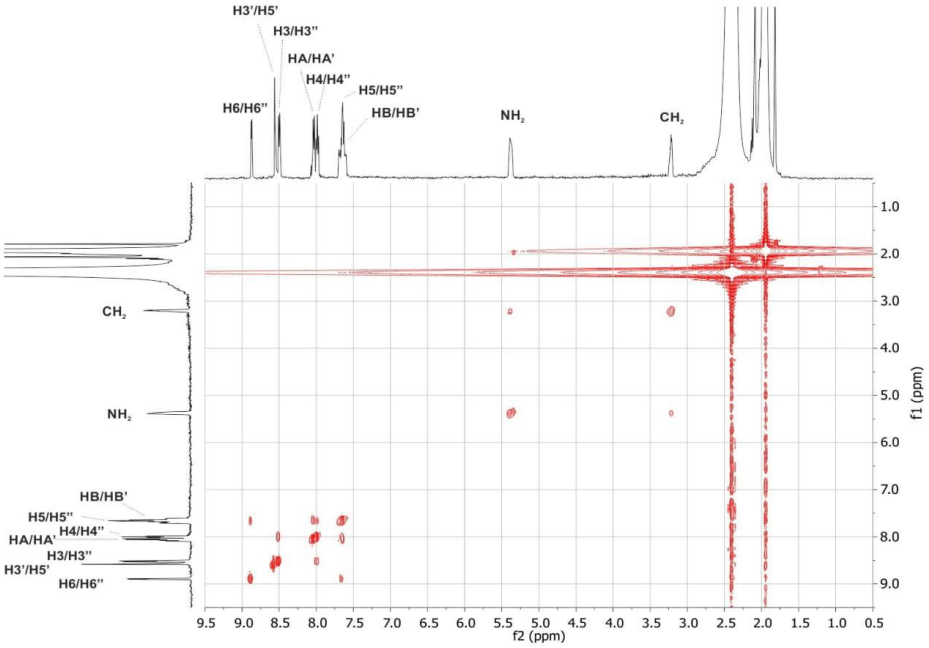

Fig. S2 The 2D homonuclear ^{1}H-^{1}H COSY NMR spectrum of [Ru(Cl-Ph-tpy)(en)Cl]Cl (**1**, 10 mM) in CD_3CN at 298 K.

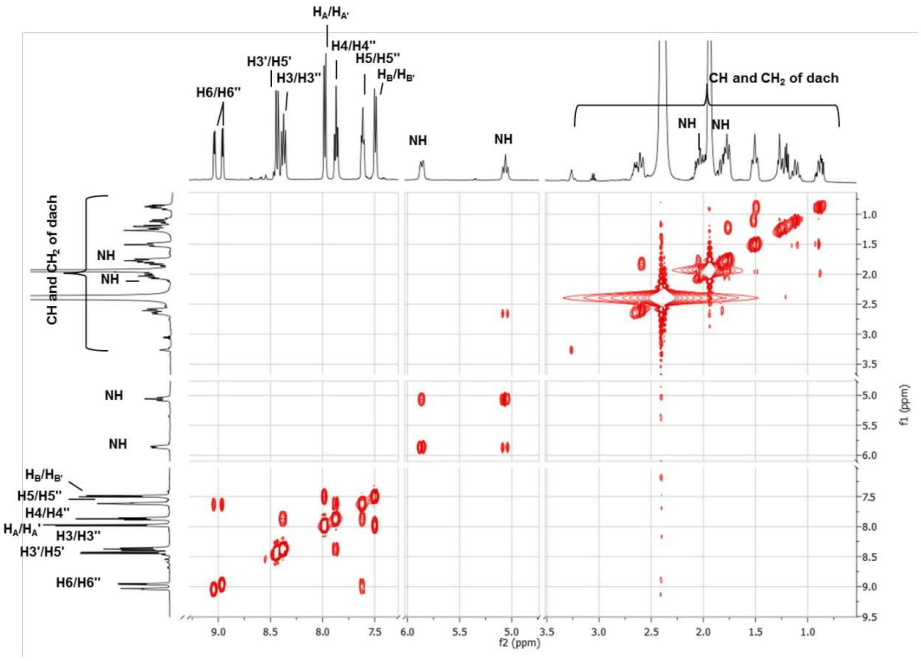

Fig. S3 The 2D homonuclear ^{1}H-^{1}H COSY NMR spectrum of [Ru(Cl-Ph-tpy)(dach)Cl]Cl (**2**, 10 mM) in CD_3CN at 298 K.

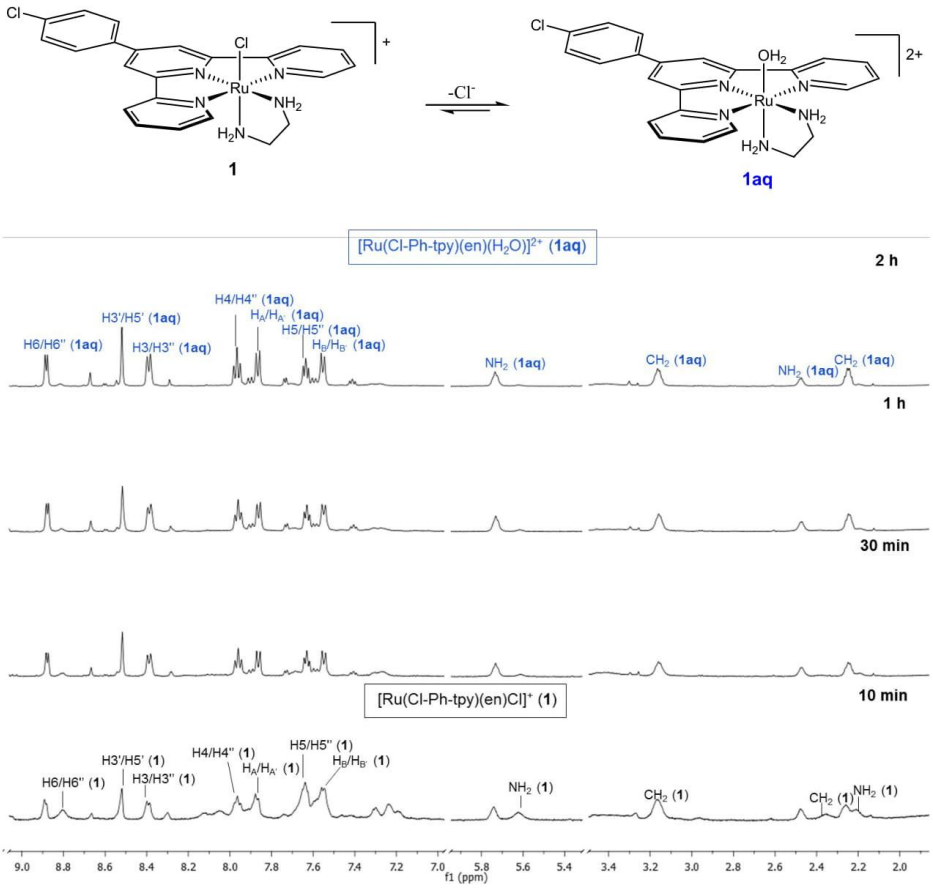

Fig. S4 Time evolution of the ^{1}H NMR spectrum of complex [Ru(Cl-Ph-tpy)(en)Cl]Cl (**1**; 4 mM) upon dissolution in D_2O at ambient temperature.

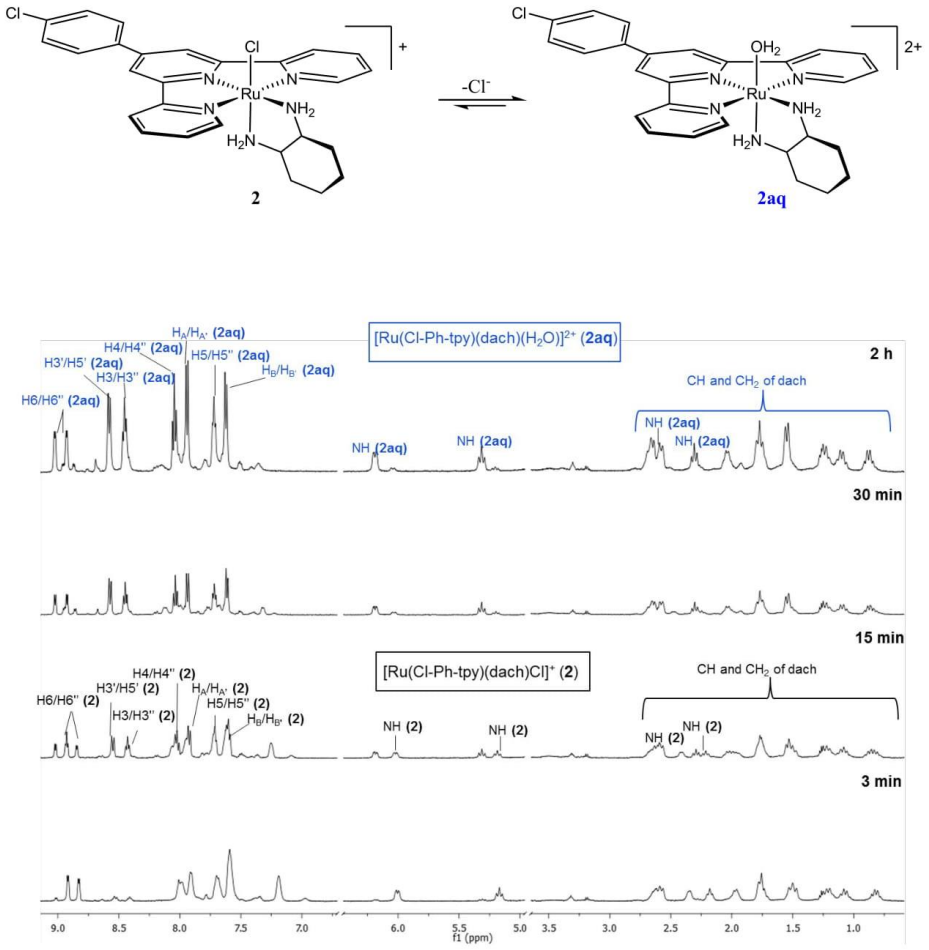

Fig. S5 Time evolution of the ^{1}H NMR spectrum of complex [Ru(Cl-Ph-tpy)(dach)Cl]Cl (**2**; 4 mM) upon dissolution in D_2O at ambient temperature.

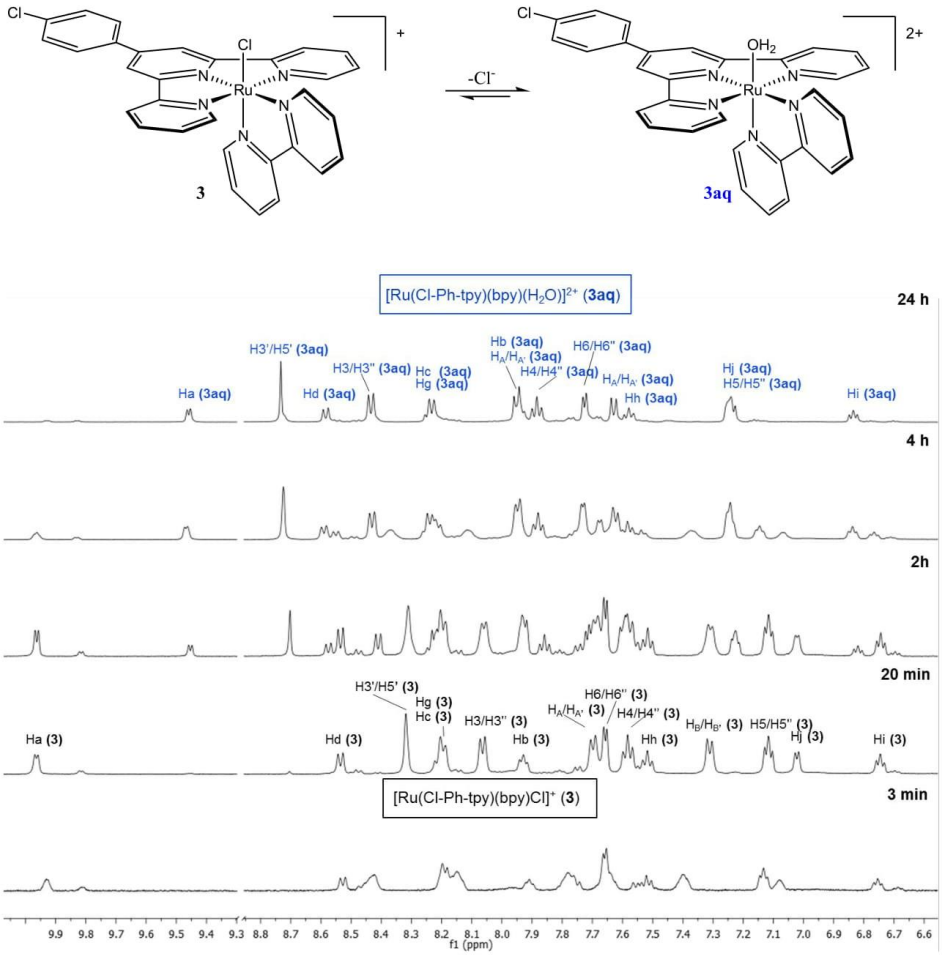

Fig. S6 Time evolution of the ^{1}H NMR spectrum of complex [Ru(Cl-Ph-tpy)(bpy)Cl]Cl (**3**; 4 mM) upon dissolution in D_2O at ambient temperature.

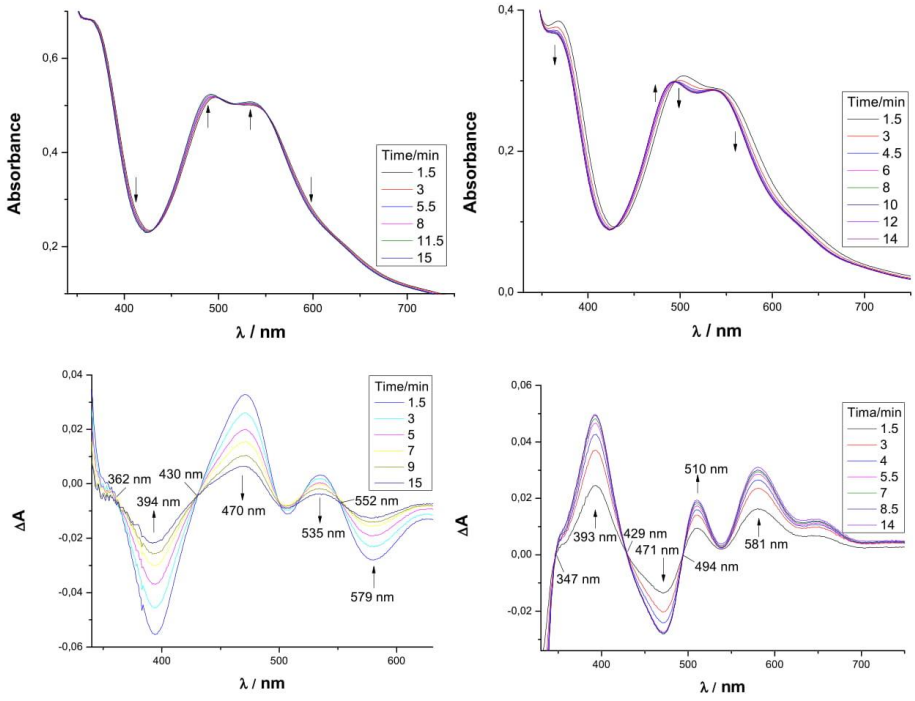

Fig. S7 Time evolution of the UV-Vis (top row) and UV-Vis difference spectra (bottom row, $\Delta A = A_t - A_0$, where A_t = absorbance at time t and A_0 = absorbance at the time at which the first spectrum was recorded) during the aquation of the complex [Ru(Cl-Ph-tpy)(en)Cl]Cl (**1**, 0.1 mM, left column) and [Ru(Cl-Ph-tpy)(dach)Cl]Cl (**2**, 0.1 mM, right column) in H_2O at 298 K.

DNA-binding studies

Calculation of DNA-binding constants

In order to compare quantitatively the binding strength of the complexes, the intrinsic binding constants K_b were determined by monitoring the changes in absorption at the MLCT band with increasing concentration of CT DNA using the following equation (S1)[S1]

$$[DNA]/(\varepsilon_A - \varepsilon_f) = [DNA]/(\varepsilon_b - \varepsilon_f) + 1/[K_b(\varepsilon_b - \varepsilon_f)] \quad (S1)$$

K_b is given by the ratio of slope to the *y* intercept in plots $[DNA]/(\varepsilon_A - \varepsilon_f)$ *versus* [DNA] (Fig. S9), where [DNA] is the concentration of DNA in base pairs, $\varepsilon_A = A_{obsd}/[complex]$, ε_f is the extinction coefficient for the unbound complex and ε_b is the extinction coefficient for the complex in the fully bound form.

Stern-Volmer equation for EB competitive studies

The relative binding of complexes to CT-DNA is described by Stern-Volmer equation[S2]:

$$I_0/I = 1 + K_{sv}[Q] \quad (S2)$$

where I_0 and I are the emission intensities in the absence and the presence of the quencher (complexes **1** – **3**), respectively, [Q] is the total concentration of quencher, K_{sv} is the dynamic quenching constant.

The simple Stern–Volmer plots were not applicable for complexes **1 – 3** as the plot between I_0/I and [Q] showed/exhibited an upward curvature (Fig. 4). Generally, a static component in the quenching mechanism leads to an upward curvature in the Stern–Volmer plots[S3] as static quenching does not require diffusion through the medium, the quenching is more efficient and the observed fluorescence intensity is lowered. A factor, $\exp^{(V[Q])}$ where *V* is the static quenching constant, can be introduced into Stern–Volmer, equation S2, in order to describe both quenching modes [S4,S5]:

$I_0/I = (1 + K_{sv}[Q])e^{V[Q]}$ (S3)

The static quenching constant, V was obtained from the equation (S3) by plotting $I_0/Ie^{V[Q]}$ versus [Q] by varying V until a linear plot was obtained. The highest value of correlation coefficient was used as criterion for linearity of the plot to obtain a precise value of V. The (dynamic) collisional quenching constant, K_{sv} was then obtained from the slope of linear plots (Fig. S10).

Stern-Volmer equation for BSA quenching studies

Fluorescence quenching is described by Stern–Volmer equation:

$I_0/I = 1+ k_q\tau_0[Q] = 1+ K_{sv}[Q]$ (S4)

where I_0 = the initial tryptophan fluorescence intensity of BSA, I = the tryptophan fluorescence intensity of BSA after the addition of the quencher, k_q = the quenching rate constants of BSA, K_{sv} = the dynamic quenching constant, τ_0 = the average lifetime of BSA without the quencher, [Q] = the concentration of the quencher respectively.

$K_{sv} = k_q\tau_0$ (S5)

and, taking as fluorescence lifetime (τ_0) of tryptophan in BSA at around 10^{-8} s, K_{sv} (M^{-1}) can be obtained by the slope of the diagram I_0/I *vs* [Q] (Stern-Volmer plots, Fig. S13), and subsequently the approximate k_q (M^{-1} s^{-1}) may be calculated.[S2]

The simple Stern–Volmer plots were not applicable for complexes **1 – 3** as the plot between I_0/I and [Q] showed/exhibited an upward curvature (Fig. S13). A factor, $\exp^{(V[Q])}$ where V is the static quenching constant, can be introduced into Stern–Volmer, equation S4, in order to describe both quenching modes [S4,S5]:

$I_0/I = (1 + K_{sv}[Q])e^{V[Q]}$ (S6)

The static quenching constant, V was obtained from the equation (S6) by plotting $I_0/Ie^{V[Q]}$ versus [Q] by varying V until a linear plot was obtained. The highest value of correlation coefficient was used as criterion for linearity of the plot to obtain a precise value of V. The (dynamic) collisional quenching constant, K_{sv} was then obtained from the slope of linear plots (inset Fig. S13).

Scatchard equation for BSA quenching studies

From Scatchard equation:

$$r/D_f = nK - rK \qquad \text{(S7)}$$

where r ($r = \Delta I/I_0$) is the moles of drug bound per mole of protein and D_f is the molar concentration of free metal complex. The association binding constant K (M^{-1}) may be calculated from the slope in the Scatchard plots r/D_f *vs* r and the number of binding sites per albumin (n) is given by the ratio of y intercept to the slope (Scatchard plots, Fig. S14).[S6]

References

S1. A. M. Pyle, J. P. Rehmann, R. Meshoyrer, C. V. Kumar, N. J. Turro and J. K. Barton, *J. Am. Chem. Soc*., 1989, **111**, 3051-3058.

S2. R. Lakowicz and G. Weber, *Biochemistry*, 1973, **12**, 4161-4170.

S3. S.S. Lehrer, Biochemistry 10 (1971) 3254 – 3263.

S4. J.R. Lakowicz, Principles of Fluorescence Spectroscopy, 3rd ed., Springer, New York, 2006, pp. 278–327, Chap.8.

S5. N. Seedher, P. Agarwal, J. Lumin. 130 (2010) 1841–1848.

S6. S. Wu, W. Yuan, H. Wang, Q. Zhang, M. Liu, K. Yu, *J. Inorg. Biochem*., 2008, **102**, 2026-2034.

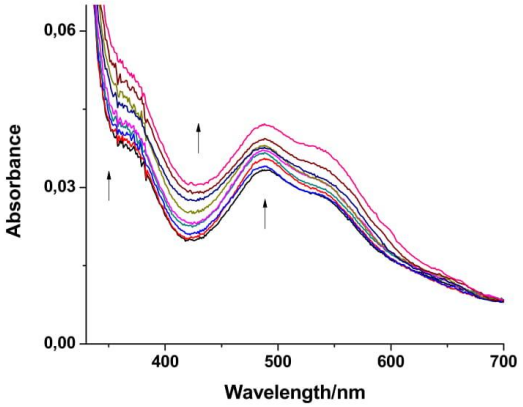
0,06
0,03
0,00
Absorbance
400
500
600
700
Wavelength/nm

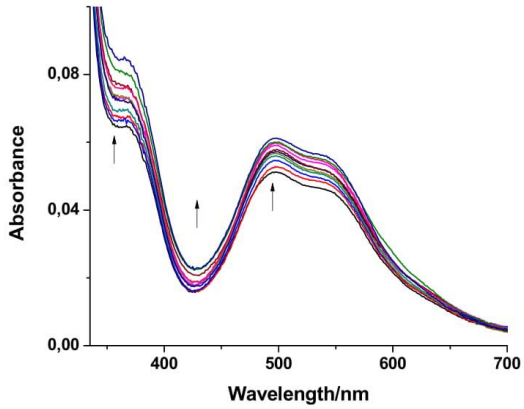
0,08
0,04
0,00
Absorbance
400
500
600
700
Wavelength/nm

12

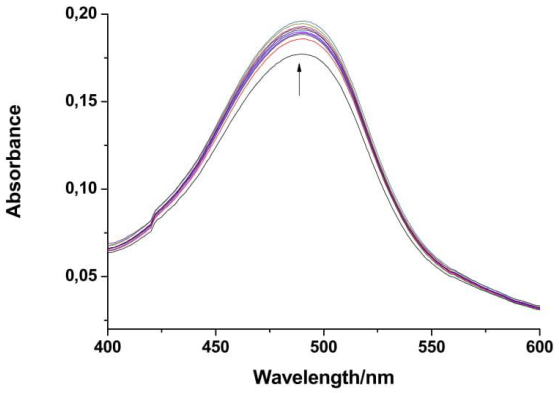

Fig. S8 Absorption spectra of the complexes **1** (top), **2** (middle) and **3** (bottom) in Tris-HCl buffer upon addition of calf thymus DNA. [Ru] = 1.25 x 10^{-5} M, [DNA] = (0.12-1.25) x 10^{-5} M. Arrow shows the absorbance changing upon increasing DNA concentrations.

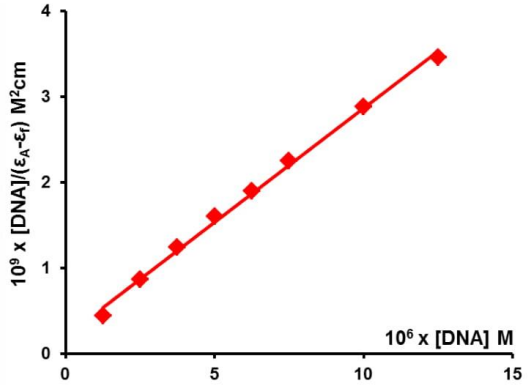

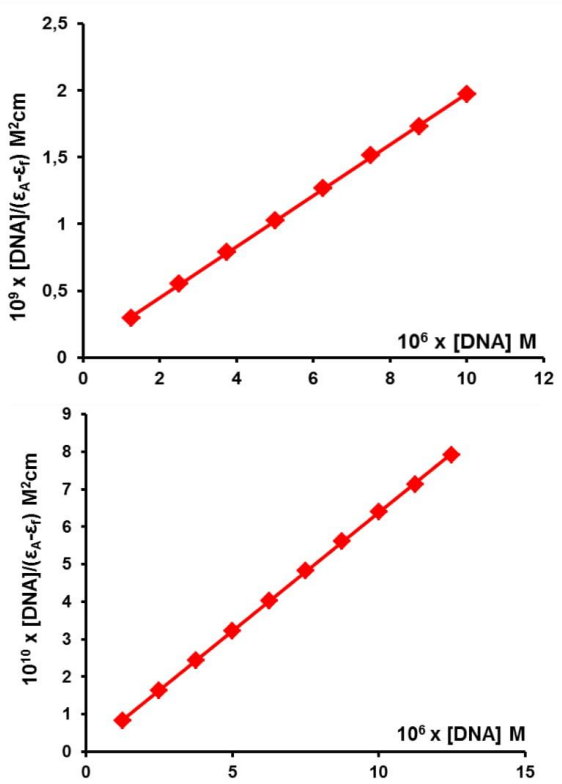

Fig. S9 Plots of [DNA]/($\varepsilon_A - \varepsilon_f$) *versus* [DNA] for the complexes **1** (top), **2** (middle) and **3** (bottom).

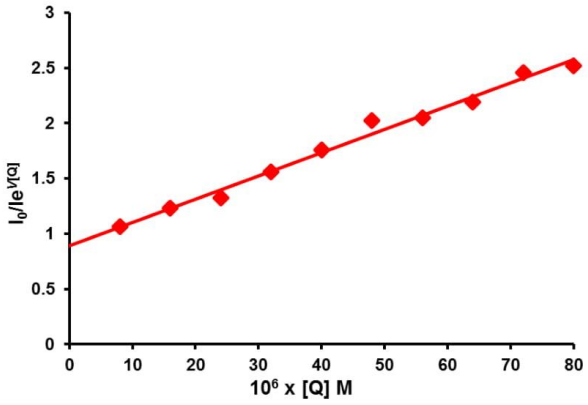

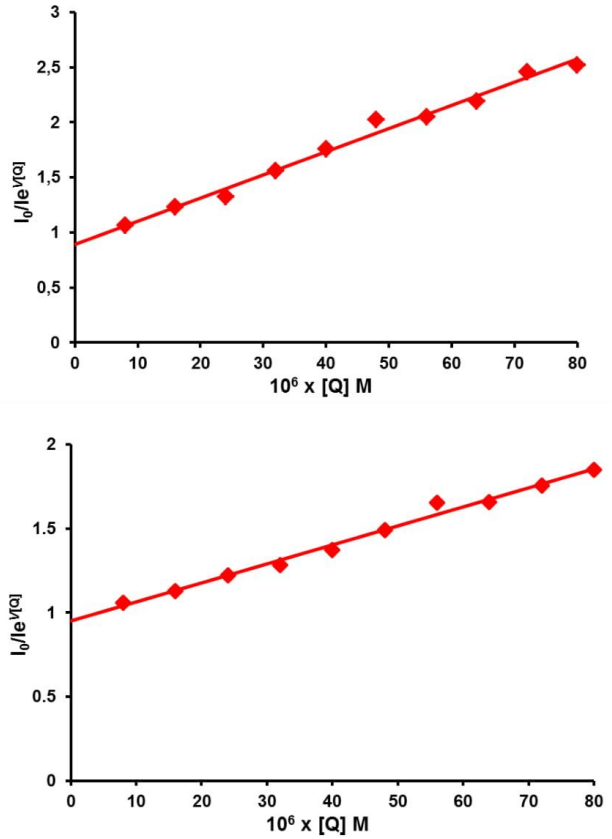

Fig. S10 Stern-Volmer quenching plot of DNA-EB for complexes **1** (top), **2** (middle) and **3** (bottom).

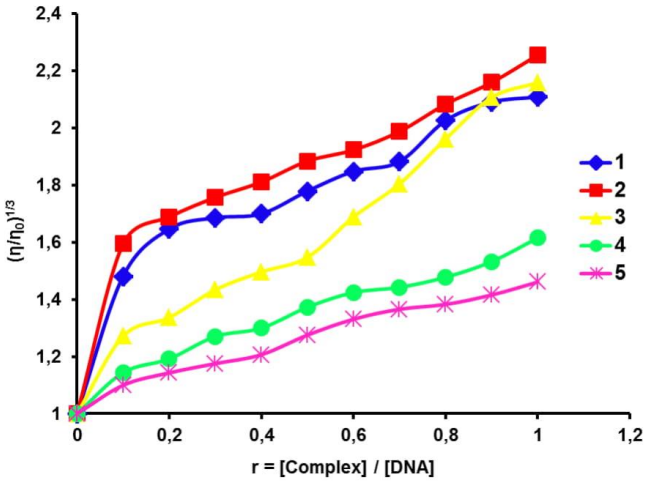

Fig. S11 Relative viscosity $(\eta/\eta_0)^{1/3}$ of CT DNA (0.01 mM) in buffer solution (50 mM NaCl and 5 mM Tris-HCl at pH 7.4) in the presence of the complexes **1** – **5** at increasing amounts (*r*).

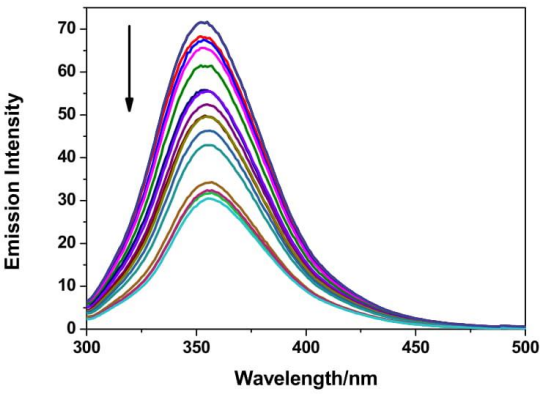
Emission Intensity
Wavelength/nm
0
10
20
30
40
50
60
70
300
350
400
450
500

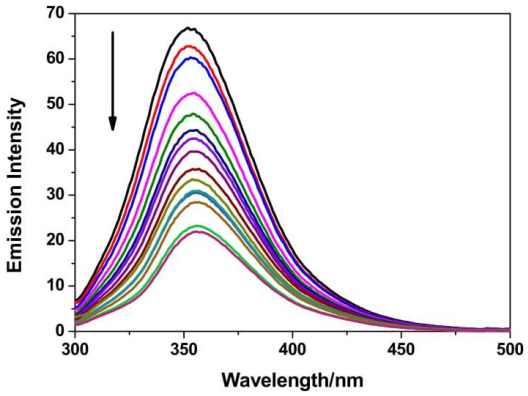
Emission Intensity
Wavelength/nm
0
10
20
30
40
50
60
70
300
350
400
450
500

17

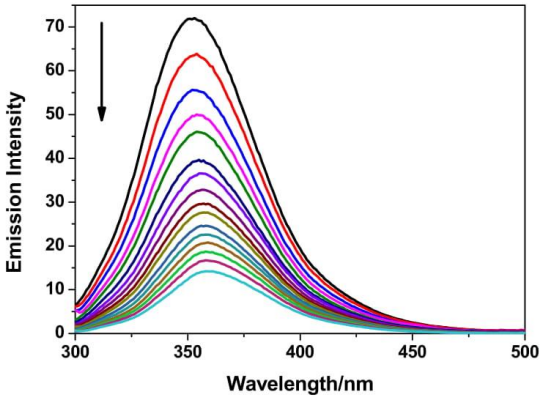

Fig. S12 Emission spectra of BSA in the presence of complexes **1** (top), **2** (middle) and **3** (bottom). [BSA] = [Ru] = 0–80 μM; λ_{ex} = 295 nm. The arrows show the intensity changes upon increasing concentrations of the complexes.

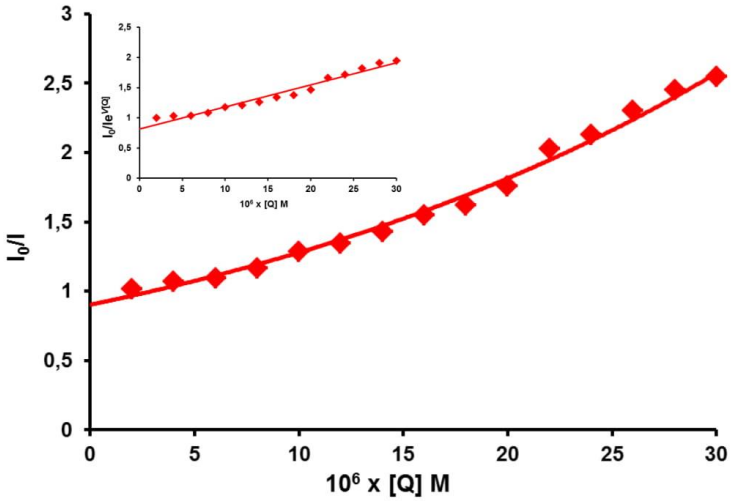

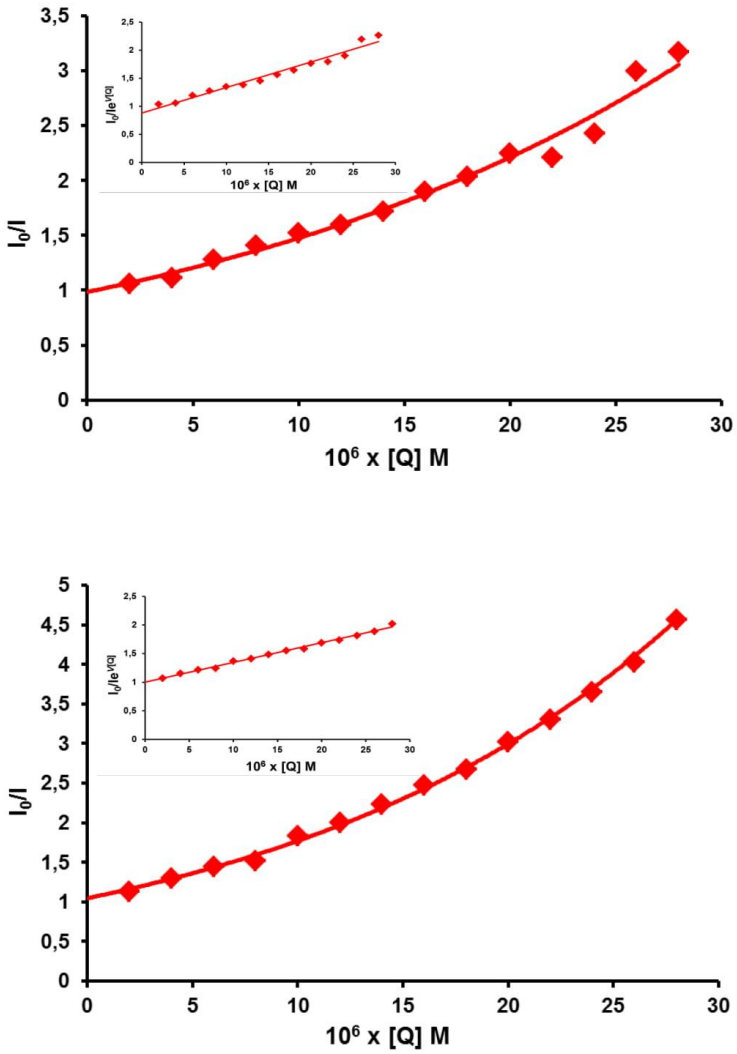

Fig. S13 Stern-Volmer quenching plot of BSA for complexes **1** (top), **2** (middle) and **3** (bottom).

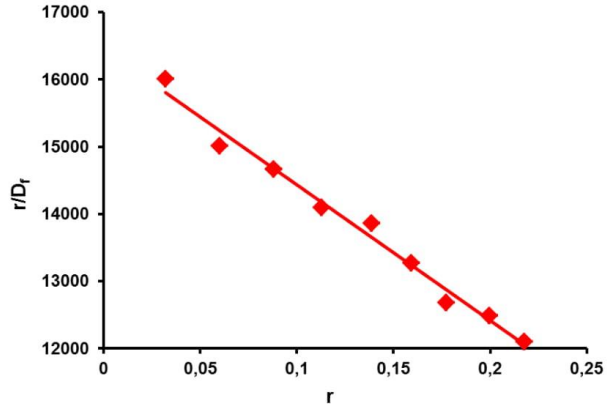
17000
16000
15000
14000
13000
12000
r/Df
0
0,05
0,1
0,15
0,2
0,25
r

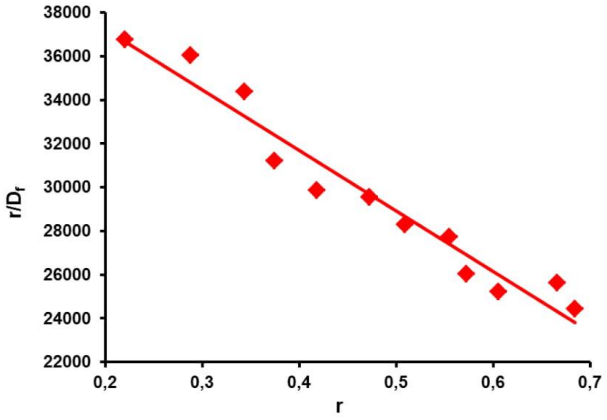
38000
36000
34000
32000
30000
28000
26000
24000
22000
r/Df
0,2
0,3
0,4
0,5
0,6
0,7
r

20

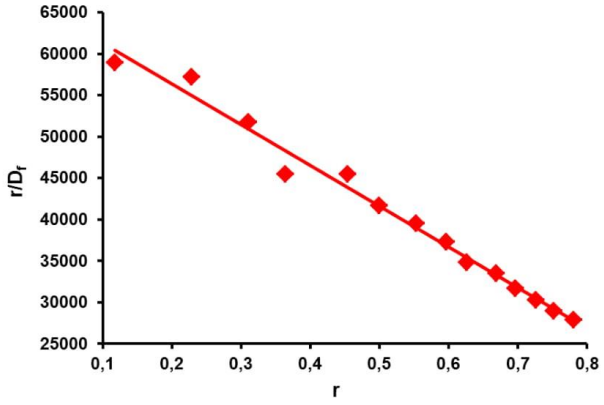

Fig. S14 Scatchard plot of BSA for complexes **1** (top), **2** (middle) and **3** (bottom).

Table S1 Assignments of selected ^{1}H resonances (δ) for the aqua species **1aq** – **3aq**.

	1aq	**2aq**	**3aq**
H6/H6''	8.89	8.98/8.88	7.81
H5/H5''	7.64	7.67	7.38-7.28
H4/H4''	7.97	8.00	7.97
H3/H3''	8.39	8.41	8.52
H3'/H5'	8.52	8.53	8.82
$H_A/H_{A'}$	7.86	7.90	8.03
$H_B/H_{B'}$	7.56	7.58	7.72
NH_2	5.73/2.47	6.14,5.27/ 2.71-2.57, 2.26	
CH_2	3.16/2.25	2.57-2.46/ 1.82-1.63/ 1.55/1.21/ 1.05/0.83	
CH		2.71-2.57/ 2.06-1.91	
Ha/Hj			9.55/7.38-7.28
Hb/Hi			8.03/6.92
Hc/Hh			8.36-8.26/ 7.67
Hd/Hg			8.67/ 8.36-8.26

2.2. Kinetic and mechanistic study on the reactions of ruthenium(II) chlorophenyl terpyridine complexes with nucleobases, oligonucleotides and DNA

Within the paper the ability of ruthenium(II) polypyridyl complexes to act as DNA binders was investigated. The substitution reactions were monitored with mononucleotide guanosine-5'-monophosphate and oligonucleotides such as fully complementary 15-mer and 22-mer duplexes with centrally located GG-binding site for DNA, and fully complementary 13-mer duplexes with centrally located GG-binding site for RNA were studied quantitatively by UV-Vis spectroscopy. Furthermore, the interactions of ruthenium(II) polypyridyl complexes with calf thymus DNA and herring testes DNA were studied by "stopped-flow" UV-Vis spectroscopy, and the reactivity of Ru-adducts was revealed by gel mobility shift assay.

Participations in the publication:

M. M. Milutinović, A. Rilak, S. K. C. Elmroth, Ž. D. Bugarčić – Kinetic investigation of DNA/RNA duplexes by UV-Vis spectroscopy, "stopped-flow" spectroscopy, gel electrophoresis, implementation of all results and writing a paper;

I. Bratsos – NMR measurements;

O. Klisurić – X-ray measurements;

DOI: 10.1039/C6DT04254F

Dalton Transactions

PAPER

View Article Online
View Journal | View Issue

Cite this: *Dalton Trans.*, 2017, **46**, 2360

Kinetic and mechanistic study on the reactions of ruthenium(II) chlorophenyl terpyridine complexes with nucleobases, oligonucleotides and DNA†‡

Milan M. Milutinović,[a,b] Sofi K. C. Elmroth,[b] Goran Davidović,[c] Ana Rilak,[a] Olivera R. Klisurić,[d] Ioannis Bratsos[e] and Živadin D. Bugarčić*[a]

Received 8th November 2016,
Accepted 30th December 2016

DOI: 10.1039/c6dt04254f

rsc.li/dalton

In this study, we investigated the ability of Ru(II) polypyridyl complexes to act as DNA binders. The substitution reactions of three Ru(II) chlorophenyl terpyridine complexes, *i.e.* [Ru(Cl-Ph-tpy)(en)Cl]Cl (**1**), [Ru(Cl-Ph-tpy)(dach)Cl]Cl (**2**) and [Ru(Cl-Ph-tpy)(bpy)Cl]Cl (**3**) (Cl-Ph-tpy = 4′-(4-chlorophenyl)-2,2′:6′,2″-terpyridine, en = 1,2-diaminoethane, dach = 1,2-diaminocyclohexane, bpy = 2,2′-bipyridine), with a mononucleotide guanosine-5′-monophosphate (5′-GMP) and oligonucleotides such as fully complementary 15-mer and 22-mer duplexes with a centrally located GG-binding site for DNA, and fully complementary 13-mer duplexes with a centrally located GG-binding site for RNA were studied quantitatively by UV-Vis spectroscopy. Duplex RNA reacts faster with complexes **1–3** than duplex DNA, while shorter duplex DNA (15mer GG) reacts faster compared with 22mer GG duplex DNA. The measured enthalpies and entropies of activation ($\Delta H^{\neq} > 0$, $\Delta S^{\neq} < 0$) support an associative mechanism for the substitution process. ^{1}H NMR spectroscopy studies performed on complex **3** demonstrated that after the hydrolysis of the Cl ligand, it is capable to interact with guanine derivatives (*i.e.*, 9-methylguanine (9MeG) and 5′-GMP) through N7, forming monofunctional adducts. The molecular structure of the cationic compound [Ru(Cl-Ph-tpy)(bpy)Cl]Cl (**3**) was determined in the solid state by X-ray crystallography. The interactions of **1–3** with calf thymus (CT) and herring testes (HT) DNA were examined by stopped-flow spectroscopy, in which HT DNA was sensibly more reactive than CT DNA. The reactivity towards the formation of Ru–DNA adducts was also revealed by a gel mobility shift assay, showing that complexes **1** and **2** have a stronger DNA unwinding ability compared to complex **3**. Overall, the complexes with bidentate aliphatic diamines proved to be superior to those with bpy in terms of capability to bind to the here studied biomolecules.

Introduction

Platinum-based drugs such as cisplatin, carboplatin, and oxaliplatin have been among the most effective chemotherapeutic agents in cancer treatment for years.[1–4] However, their high toxicity and the incidence of spontaneous or acquired drug resistance limit their clinical use. To overcome these drawbacks, a huge number of coordination compounds of transition metals other than platinum have been thoroughly studied. Ruthenium, however, stands out as a particularly attractive alternative to platinum. The rich and well-established synthetic and coordination chemistry of ruthenium compounds, combined with the fact that the metal has several oxidation states available under physiological conditions (Ru(II), Ru(III) and Ru(IV)), make ruthenium compounds in general well-suited for medicinal applications.[5–7] A key advantage of ruthenium-based metallodrugs is their ability to tune the metal–ligand exchange kinetics over many orders of magnitude *via* ligand variation. Such an influence over kinetic lability is critical for drug development and our work on ruthenium(II) complexes that is described in several previous papers showed that such a control can indeed be exerted.[8–12]

[a]*University of Kragujevac, Faculty of Science, R. Domanovića 12, P. O. Box 60, 34000 Kragujevac, Serbia. E-mail: bugarcic@kg.ac.rs; Fax: +381(0)34335040; Tel: +381(0)34300262*
[b]*Lund University, Biochemistry and Structural Biology, KILU, P.O. Box 124, SE-221 00 Lund, Sweden*
[c]*University of Kragujevac, Clinic for Cardiology, Clinical Center Kragujevac, Kragujevac, Serbia*
[d]*University of Novi Sad, Faculty of Science, Department of Physics, Trg Dositeja Obradovića 3, 21000 Novi Sad, Serbia*
[e]*I.N.N., Dept. of Physical Chemistry, NCSR "Demokritos", 15310 Ag. Paraskevi, Athens, Greece*

† This paper is dedicated to Professor Lars Ivar Elding who was the supervisor of Prof. Dr Sofi K. C. Elmroth and Prof. Dr Živadin D. Bugarčić.

‡ Electronic supplementary information (ESI) available. CCDC 1510818. For ESI and crystallographic data in CIF or other electronic format see DOI: 10.1039/c6dt04254f

Ruthenium compounds with polypyridyl ligands have emerged as leading candidates for use as anticancer drugs.[13,14] Recently, we developed a series of new polypyridyl complexes of the general formula *mer*-[Ru(L_3)(*N*–*N*)(X)][Y]$_n$ where L_3 is either tpy (2,2′:6′,2″-terpyridine) or Cl-tpy (4′-chloro-2,2′:6′,2″-terpyridine), *N*–*N* is a bidentate chelating ligand (1,2-diaminoethane (en), 1,2-diaminocyclohexane (dach), 2,2′-bipyridine (bpy)), X is a monodentate ligand (Cl or dmso-*S*), Y is the counter anion (Cl^-, PF_6^- or $CF_3SO_3^-$), and *n* depends on the nature of X.[10] Studies on the three Ru-polypyridyl complexes, *i.e.*, [Ru(Cl-tpy)(en)Cl]Cl, [Ru(Cl-tpy)(dach)Cl]Cl and [Ru(Cl-tpy)(bpy)Cl]Cl, demonstrated that after the hydrolysis of the Cl ligand, they were capable of interacting with guanine derivatives (*i.e.*, 9-methylguanine (9MeG) or guanosine-5′-monophosphate (5′-GMP)) through the N7 position, forming monofunctional adducts with rates and extents that depended strongly on the nature of the chelating ligand.[10] We have also found that these compounds strongly bind DNA by a dual function: by intercalation, interacting with the DNA helix through the insertion of the planar terpyridine ring between the DNA base pairs, and by covalent binding to guanine N7.[12] In addition, only [Ru(Cl-tpy)(en)Cl]Cl and [Ru(Cl-tpy)(dach)Cl]Cl showed high to moderate *in vitro* cytotoxicity, with IC_{50}'s of 32.80–66.30 μM and 72.80–110.80 μM, respectively.[12] With the aim of expanding the investigation of the structure activity relationship of these Ru(II) polypyridyl complexes, we tested additional functional groups on the 4′-position of the tpy ligand. Thus, using the chlorophenyl-substituted tpy ligand (Cl-Ph-tpy) in place of the Cl-tpy ligand, while the rest of the coordination sphere remained unchanged, we synthesized and characterized a series of new monofunctional ruthenium(II) complexes of the general formula *mer*-[Ru(Cl-Ph-tpy)(*N*–*N*)Cl]Cl (where *N*–*N* = en (**1**), dach (**2**) or bpy (**3**); Fig. 1).[15] It was found that the biological activity of Ru(II) polypyridyl complexes depends on the nature of the meridional tridentate ligand. The introduction of a chlorophenyl-substituent into the tpy ligand results in an increase in the anticancer activity. Compound **3** displayed high to moderate cytotoxicity against two cancer cell lines HeLa and A549 (with IC_{50} *ca.* 12.7 μM and 53.8 μM, respectively), while complexes **1** and **2** showed only moderate cytotoxicity (with IC_{50} *ca.* 84.8 μM and 96.3 μM, respectively) against HeLa cells.[15]

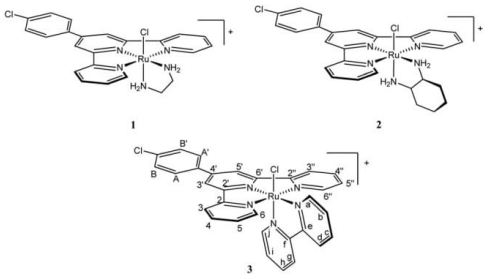

Fig. 1 Structures of complexes **1–3** with the numbering scheme of the Cl-Ph-tpy and bpy ligands.

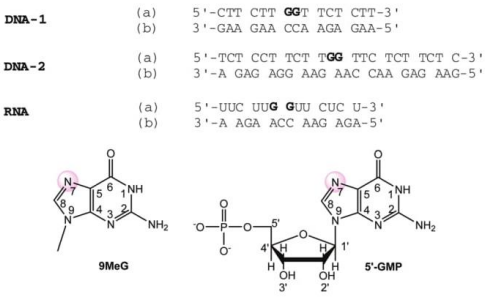

Fig. 2 Schematic representation of used duplexes of DNA or RNA and structure of 9-methylguanine (9MeG) and guanosine-5′-monophosphate (5′-GMP).

Using models able to reproduce the chemical behavior of metal–biomolecule interactions is one of the approaches most commonly used in attempting, not only to reproduce the biological activity, but also to explain the interactions between metals and biomolecules. Their interactions with DNA or small biomolecules can have a protective effect and decrease the rate of degradation or side product formation.[16,17] In continuation of our previous work,[15] herein we studied the ligand substitution reactions of ruthenium(II) chlorophenyl terpyridine complexes **1–3** with a small biomolecule such as 5′-GMP. The kinetics and thermodynamics of the investigated substitution reactions were established quantitatively by UV–Vis spectrophotometry. Focus was also directed to the interaction of selected complexes with oligonucleotides such as fully complementary 15-mer and 22-mer duplexes with a centrally located GG-binding site for DNA, and fully complementary 13-mer duplexes with a centrally located GG-binding site for RNA (Fig. 2). Furthermore, the interactions of complexes **1–3** with calf thymus (CT) and herring testes (HT) DNA were investigated using stopped-flow spectroscopy. Nuclease activity of **1–3** was studied using agarose gel electrophoresis. In addition, we report the crystal structure of the cationic complex [Ru(Cl-Ph-tpy)(bpy)Cl]Cl. It was envisaged that this study could throw more light on the impact of different inert chelating ligands on the interactions of ruthenium antitumor complexes with selected biomolecules.

Results and discussion

Crystal structure discussion

The synthesis of the complexes, the subject of this study, has been reported elsewhere.[15] These complexes were mainly characterized by various spectroscopies. Attempts to determine previously their solid state structure by single crystal X-ray diffraction were unsuccessful. However, in the course of this study we obtained crystals of the [Ru(Cl-Ph-tpy)(bpy)Cl]Cl (**3**)

complex suitable for X-ray investigation. The X-ray analysis confirmed the structure proposed for **3** on the basis of spectroscopic investigations.[15] The perspective view of molecular structure of complex **3** with the adopted atom-numbering scheme is shown in Fig. 3. Selected bond lengths, bond angles and torsion angles are listed in Table S1.‡ Complex **3** crystallizes in the triclinic crystal system and $P\bar{1}$ space group where each asymmetric unit consists of two moieties: one cationic $[Ru(Cl\text{-}Ph\text{-}tpy)(bpy)Cl]^+$ complex and Cl^- anion. The ruthenium center in the [Ru(Cl-Ph-tpy)(bpy)Cl]Cl complex is coordinated in a slightly distorted octahedral geometry. Due to the tridentate coordination of the N1,N2,N3-donor, the central nitrogen atom N2 is pushed closer to the ruthenium(II) center (Table S1‡). It therefore exerts an influence to Cl1 which explains the slightly larger value of the Ru1–Cl1 bond length (Table S1‡). The bond angles N1–Ru1–Cl1 and N2–Ru1–Cl1 approaches 90°, while the N3–Ru1–Cl1 angle is larger than 90°, showing the steric influence of the bulky chlorophenylterpyridine chelating ligand. Groups Ru1N1N2N3N4 and Ru1Cl1N2N4N5 are perfectly planar since there is no displacement from the same weighted least-squares planes. The Ru1N1N2N3N4 and Ru1Cl1N2N4N5 planes are almost perpendicular to each other with the dihedral angle of 87.91(7)° between them. The angle between the C26C27C28C29C3OC31 ring plane and the Ru1N1N2N3 plane is 18.31(7)° confirming slight distortion from the planarity of the chlorophenylterpyridine ligand's skeleton.

The crystal packing of **3** is dominantly arranged by van der Waals forces since we have not found any classic hydrogen bond in an intra or inter molecular space.

The geometrical features of complex **3** are comparable to those found in the corresponding tpy derivative [Ru(Cl-tpy)(bpy)Cl]Cl ($\mathbf{3_{Cl}}$)[10] (Table S1‡). Starting from the coordination sphere, the central nitrogen atom of Cl-tpy having the shortest Ru–N distance and the longest Ru–Cl distance, comparison of the structural features of complexes **3** and $\mathbf{3_{Cl}}$ did not reveal any significant differences in the level of the statistical significance (Table S1‡). However, there are some noticeable perturbations which could be attributable to the absence of the Ph group in $\mathbf{3_{Cl}}$ contributing to differences in the bond angles especially in the N1(N3)–Ru1–N5 and N1(N3)–Ru1–Cl1 values. Visually this result is depicted in Fig. S1,‡ which displays an overlay of complexes **3** and $\mathbf{3_{Cl}}$.

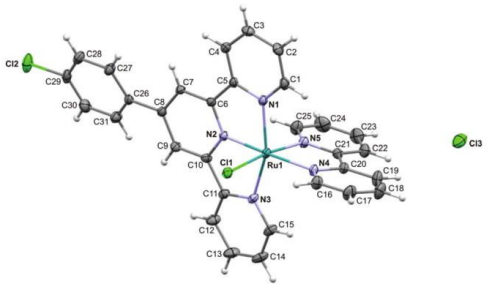

Fig. 3 ORTEP[18] drawings of the molecular structure of complex **3** with labeled non-H atoms. Displacement ellipsoids are shown at 30% probability, and H atoms are drawn as spheres of arbitrary radii. Selected bond lengths (Å) and angles (°): Ru1–N1 2.078(3), Ru1–N2 1.956(3), Ru1–N3 2.065(3), Ru1–N4 2.089(3), Ru1–N5 2.035(3), Ru1–Cl1 2.4078(9), N2–Ru1–N4 176.36(11), N1–Ru1–N3 158.70(10).

NMR studies of the reactions of complex 3 with guanine derivatives

The reactivity of compound **3** toward two guanine derivatives, *i.e.*, 9MeG and 5′-GMP, as model DNA bases, was investigated primarily by ^{1}H spectroscopy in D_2O at ambient temperature (for the numbering scheme of 9MeG and 5′-GMP, see Fig. 2).

Addition of a slight excess of 9MeG (1.1 equiv.) to an equilibrated solution of **3** (4 mM) in D_2O induced slow changes in the ^{1}H NMR spectrum (Fig. 4). A new set of resonances attributed to the product $[Ru(Cl\text{-}Ph\text{-}tpy)(bpy)(9MeG\text{-}N7)]^{2+}$ (**3-MG**) became apparent in the ^{1}H NMR spectrum within the first hours. Although binding of a ruthenium(II) center to N7 of purine moieties typically induces a downfield shift of the H8 resonance compared to the free ligand, binding of **3** to N7 of 9MeG led to a remarkable upfield shift of the H8 singlet (δ 6.63 *vs.* 7.75; $\Delta\delta = -1.12$) because of the shielding effect of the adjacent Cl-Ph-tpy. A similar shift, even though less pronounced, was observed for the CH_3 singlet (δ 3.31 *vs.* 3.63). The same behavior had been also observed for the interaction of a similar complex, *i.e.* $[Ru(Cl\text{-}tpy)(bpy)Cl]^+$, with 9MeG.[10] The system reached equilibrium after *ca.* 1 day, with *ca.* 40% of 9MeG bound to ruthenium (*i.e.* **3-MG**), 50% of **3aq**, and 10% of **3** (Fig. 4), and no spectral changes were observed afterward.

The reaction of **3** (10 mM) with 5′-GMP (1.1 equiv.) is also very slow and incomplete. More specifically, 1 h after the addition of 5′-GMP to an equilibrated solution of **3** the growth of a new set of resonances, assignable to the neutral species [Ru(Cl-tpy)(bpy)(5′-GMP-N7)] (**3-G**), was observed in the ^{1}H NMR spectrum (Fig. S2‡). Equilibrium reached after *ca.* 12 h, and the distribution of the species was *ca.* 43% of **3-G**, 40% of **3aq**, and 17% of **3**. Interestingly, the spontaneous precipitation, most likely of the neutral complex **3-G**, from the mixing solution was observed on prolonged standing at ambient temperature (*ca.* 1 day). Such a precipitation was not detected in the case of the reaction of **3** with 9MeG.

Kinetic studies of complexes 1–3 with 5′-GMP, oligonucleotides and CT and HT DNA

As DNA is considered to be a potential biological target for metal based antitumor agents, binding studies of ruthenium(II) polypyridyl complexes with nucleobases are of special interest.[17,20–22] The aim of this study was to investigate the effect of the phenyl-substituent on the terpyridyl ligand and of the nature of the inert chelating ligands on the binding mode of Ru(II)-polypyridyl complexes to DNA and to relate this to the differences in their anticancer activity. Therefore, we investigated the reactivity of complexes **1–3** with guanosine-5′-monophosphate

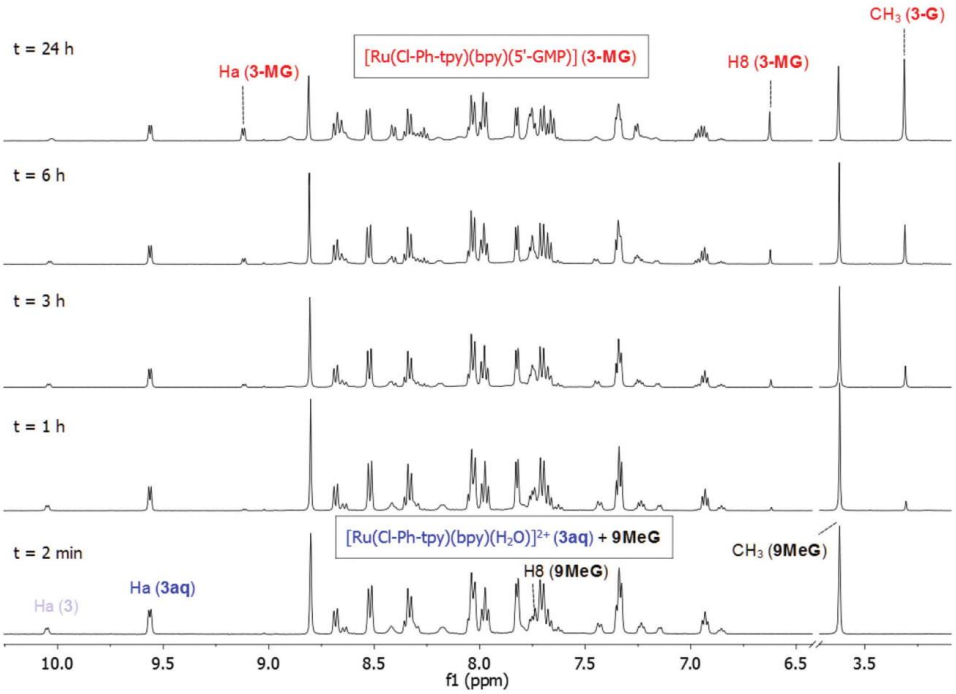

Fig. 4 ^{1}H NMR spectral changes after the addition of 9MeG (1.1 equiv.) to an equilibrated solution of [Ru(Cl-Ph-tpy)(bpy)Cl]Cl (**3**; 4 mM) in D_2O at various reaction times.

(5′-GMP), as a model DNA base. The substitution kinetics of Cl^- with 5′-GMP in complexes **1–3** were investigated UV-Vis spectrophotometrically by following the change in absorbance at selected wavelengths, corresponding to the maximum change, as a function of time in 25 mM Hepes buffer. All kinetic experiments were performed under pseudo-first-order conditions, for which the concentration of the Ru(II) complexes was always in at least a 10-fold excess. To suppress the spontaneous hydrolysis of chloride from the Ru(II) complexes, all reactions were studied in the presence of 50 mM NaCl. This value was determined prior to the kinetic measurements to be the minimum chloride concentration for which no spectral changes were observed (Fig. S3‡).

The substitution process of complexes **1–3** with 5′-GMP are represented by eqn (1):

$$[\text{Ru(Cl-Ph-tpy)}(N-N)\text{Cl}]^+ + 5'\text{-GMP} \underset{k_1}{\overset{k_2}{\rightleftharpoons}} [\text{Ru(Cl-Ph-tpy)}(N-N)(5'\text{-GMP})] + \text{Cl}^- \quad (1)$$

where *N*–*N* = en, dach or bpy.

The rate constants for the substitution were determined, under pseudo-first-order conditions, from the plot of the linear dependence of k_{obs} *versus* total complex concentration, according to eqn (2) and (3). Each pseudo-first order rate constant, k_{obs}, was calculated as the average value of two or three independent runs and the values are given in Tables S2–S4.‡

$$\frac{\text{d}[\text{Ru(Cl-Ph-tpy)}(N-N)\text{Cl}]^+}{\text{d}t} = k_{obs}[\text{Ru(Cl-Ph-tpy)}(N-N)\text{Cl}]^+ \quad (2)$$

$$k_{obs} = k_1[\text{Cl}^-] + k_2[5'\text{-GMP}] \quad (3)$$

The direct nucleophilic attack is characterized by the rate constants k_2, and the reverse reactions are presented by the rate constants k_1 where k_1 values are derived from the intercepts divided by [Cl^-] (*i.e.* 50 mM). The second-order rate constant k_2, characterizing the formation of the product, can be evaluated from the slope of a plot of k_{obs} *vs.* Ru(II) complex concentration. Their values are listed in Table 1. The experimental results for the displacement of a chloride ion from complexes **1–3** are shown in Fig. S4.‡ A linear dependence on the nucleophile concentration was observed for all reactions.

The activation parameters ($\Delta H^{\neq}$ = 46 ± 6 kJ mol^{-1} and $\Delta S^{\neq}$ = −114 ± 18 J K^{-1} mol^{-1}) were obtained from the Eyring plot, which is presented in Fig. S5.‡ It could be seen that the

Table 1 The obtained rate constants for the reactions between complexes **1–3** and 5′-GMP, oligonucleotides, and CT and HT DNA

	t °C	k_2 [M^{-1} s^{-1}]	k_1 [M^{-1} s^{-1}]	$k_{2,app}$ [M^{-1} s^{-1}]	k_{-2} [10^{-3} M^{-1} s^{-1}]
1 (en)					
5′-GMP	37	$(5.30 \pm 0.3) \times 10^{-1}$	$(13.3 \pm 3.0) \times 10^{-3}$		
DNA-1	37			12.4 ± 1.0	5.4 ± 0.8
DNA-2	37			10.5 ± 0.8	6.9 ± 0.7
RNA	37			13.6 ± 1.0	5.4 ± 0.6
CT DNA	37	$(2.1 \pm 0.1) \times 10^{3}$	1.10 ± 0.09		
HT DNA	37	$(13.0 \pm 0.9) \times 10^{3}$	1.3 ± 0.1		
2 (dach)					
5′-GMP	15	$(1.8 \pm 0.1) \times 10^{-1}$	$(3.5 \pm 0.5) \times 10^{-3}$		
	25	$(4.0 \pm 0.2) \times 10^{-1}$	$(15.0 \pm 2.0) \times 10^{-3}$		
	37	$(7.5 \pm 0.4) \times 10^{-1}$	$(12.0 \pm 3.0) \times 10^{-3}$	7.3 ± 0.9	2.8 ± 0.5
DNA-1	37			5.2 ± 0.3	3.9 ± 0.2
DNA-2	37			10.6 ± 0.7	4.4 ± 0.4
RNA	37				
CT DNA	37	$(1.3 \pm 0.2) \times 10^{3}$	0.9 ± 0.1		
HT DNA	37	$(4.9 \pm 0.4) \times 10^{3}$	1.2 ± 0.3		
3 (bpy)					
5′-GMP	37	$(3.4 \pm 0.2) \times 10^{-1}$	$(16.0 \pm 2.0) \times 10^{-3}$		
DNA-1	37			3.6 ± 0.1	0.8 ± 0.2
DNA-2	37			2.9 ± 0.3	1.1 ± 0.2
RNA	37			5.9 ± 0.4	1.5 ± 0.3
CT DNA	37	22 ± 2	$(1.0 \pm 0.1) \times 10^{-2}$		
HT DNA	37	30 ± 2	$(1.4 \pm 0.1) \times 10^{-2}$		

$\Delta S^{\neq}$ value is negative, suggesting that the activation process was strongly dominated by bond-making. The small value of $\Delta H^{\neq}$ and the negative value of $\Delta S^{\neq}$ clearly support the associative mechanism for the substitution process. Similar mechanisms have been proposed for the substitution reactions of organometallic Ru(II)-arene complexes, half sandwich Ru(II)-[9]aneS3 coordination compounds and Ru(II)-tpy complexes investigated in previous studies with biologically relevant nucleophiles, *e.g.*, 9-methylguanine (9MeG), guanosine (Guo), guanosine-5′-monophosphate(5′-GMP), L-His, thiourea (Tu), L-cysteine (L-Cys), L-methionine (L-Met), pyrazole (Pz), 1,2,4-triazole (Tz) and pyridine (Py).[8–12]

It can be seen that the rate constants depend on the nature of the inert chelating ligand: compounds **1** and **2**, which have an aliphatic diamine as a chelating ligand, react *ca.* 2 times faster than the bpy complex **3**. This could be due to the steric hindrance caused by the bulky Cl-Ph-tpy and bpy chelates on the Ru(II) center during the associative bond formation process which occurs through the transition state that has a seven coordinate character. It can be seen that the nature of the bidentate ligand *N–N* is very relevant in affecting the reactivity of the meridional complexes, since it is *trans* to the unique reactive coordination position. The steric requirements of the metal complex itself directly influence the rate of nucleobase binding. Furthermore, the π back-bonding effects of the tpy and bpy chelates increase the positive charge on the Ru(II) center giving a partial Ru(III) character that is expected to be significantly more inert than Ru(II) complexes.

It is well known that additional functional groups on the tpy fragment might enhance the binding ability of the complexes on the biomolecules.[10] For comparison, the Ru(II) tpy compounds with a general formula [Ru(Cl-tpy)(*N–N*)Cl]Cl have k_2 values (0.15–0.71 M^{-1} s^{-1})[10] that are smaller than those of complexes **1–3** for the reaction with 5′-GMP, respectively, implying that the introduction of the chlorophenyl fragment in the tpy ligand has a significant effect on the substitution behavior of the Ru(II) complexes. The chlorophenyl-substitution on the 4′-position of tpy has a strong electron-withdrawing effect on the tpy ligand and, consequently, on the metal center. This results in an increase of the reactivity of the ruthenium complexes **1–3**.

In the present study, the investigation of how the overall length and changes of base-pairing in the close vicinity of a centrally located GG-site affect the rate of ruthenium(II) binding has been performed. All reactions were studied using the conventional UV-Vis methodology by following the change in absorbance at λ = 260 nm as a function of time in 5 mM Tris-HCl buffer. For this purpose, the reactivity of two different DNA-1 (5′-CTT CTT GGT TCT CTT-3′/5′-AAG AGA ACC AAG AAG-3′) and DNA-2 (5′-TCT CCT TCT TGG TTC TCT TCT C-3′/5′-GAA GAG AAC CAA GAA GGA GAG A-3′) duplex DNAs were monitored at 37 °C. In addition, the reaction between complexes **1–3** and 13-mer duplex RNA (5′-UUC UUG GUU CUC U-3′/5′-AGA GAA CCA AGA A-3′) was also monitored at 37 °C.

Metal-induced kinetics were investigated after addition of complexes **1–3** to buffered and temperature equilibrated solutions of a preannealed duplex of either DNA or RNA. Pseudo-first order conditions were used to allow for the quantitative determination of observed reaction rate constants (k_{obs}) by a fit of a single-exponential function to the experimentally obtained ΔA-values ($\Delta A_t = A_t - A_{t=0}$). The standard expression for exponential decay according to eqn (4) was used for the determination of k_{obs}, with ΔA_∞ denoting the maximum absorbance difference reached at the end of the studied time interval. Each pseudo-first order rate constant, k_{obs}, was calculated as

the average value of two or three independent runs and the values are given in Tables S5–S13.‡

$$\Delta A_t = \Delta A_\infty(1 - \exp(-k_{obs}t)) \quad (4)$$

The obtained representative kinetic traces, together with the corresponding fitted single-exponential functions, are shown in Fig. S6–S9.‡ As can be seen here, the nature of the absorbance change is clearly dependent on the concentration of added complexes **1–3**, and also well described by a single-exponential function under investigated reaction conditions. Moreover, when the observed rate constants are plotted as a function of added complexes **1–3**, a linear dependence is observed, see Fig. S10.‡ The obtained linear dependence is in agreement with a reaction mechanism in which the interaction between complexes **1–3** and duplex DNAs or RNA creates the rate determining step, here with subsequent formation of the corresponding dissociated single-stranded DNAs or RNA ($ssDNA_a$–[**1–3**] and $ssDNA_b$; $ssRNA_a$–[**1–3**] and $ssRNA_b$) as products, see eqn (5) and (6), where $k_{2,app}$ represents the apparent second-order rate constant for the formation of the DNA–[**1–3**] or RNA–[**1–3**] adducts. In accordance to that, the second-order rate constant $k_{2,app}$ can be directly obtained from the slope of a plot of k_{obs} *vs.* $C_{\mathbf{1-3}}$.

$$\begin{aligned} &\text{dsDNA(or RNA)} + \mathbf{X} \underset{k_{-2}}{\overset{k_{2,app}}{\rightleftharpoons}} \text{ssDNA(or ssRNA)} \\ &\quad - \mathbf{X} + \text{ssDNAb(or ssRNAb)} + Cl^- \end{aligned} \quad (5)$$

$$k_{obs} = k_{2,app}[\mathbf{1}, \mathbf{2} \text{ or } \mathbf{3}] + k_{-2}[Cl^-] \quad (6)$$

The obtained rate constants for the reaction between complex **1–3** and DNA duplexes or RNA duplex are summarized in Table 1.

From the obtained data it can be seen that the investigated complexes **1–3** interact with different types of duplex DNAs as well as with RNA. The rate of the reaction for each complex decreases in the order RNA > DNA-1 > DNA-2. Concerning the length of the fragments of DNAs and RNA, it can be concluded that the shorter 13GG duplex RNA reacts faster than the longer 15GG duplex DNA-1 and 22GG duplex DNA-2, which is consistent with the previously published results.[23–25] In addition, for complexes **1–3** the rate of the reaction with each duplex decreases in the order **1** (en) > **2** (dach) > **3** (bpy). It can be seen that the rate constants depend on the nature of the inert chelating ligand: complexes **1** and **2** react *ca.* 2–4 times faster than the bpy complex **3** (Table 1). This order of reactivity can be explained by the bulky Cl-Ph-tpy and bpy chelates that causes steric hindrance during the associative bond formation process compared to the more compact en and dach ligands. The reactions with complex **2** were expected to be slower than those with **1** due to steric effects and the positive inductive effect of the cyclohexane ring that makes the Ru(II) centre less electrophilic and hence, less reactive.[26]

In the field of anticancer drug design and in particular with metallochemotherapeutics, DNA has most commonly served as the major target, either by direct interaction with the drug or indirectly by inhibition of DNA synthesis and replication.[22] On the other hand, recent research seems to favor the hypothesis that their interactions with proteins and enzymes specific for processes of cancer development and/or progress are crucial. It is thus quite possible that ruthenium complexes hit multiple targets, and a combination of their action contributes to the observed beneficial properties.[27–29] In this respect, we examined interactions of complexes **1–3** with calf thymus (CT) and herring testes (HT) DNA by stopped-flow spectroscopy. All kinetic experiments were performed under pseudo-first-order conditions.

The substitution reactions of complexes **1–3** with CT and HT DNA can be represented by eqn (7).

$$P + D \underset{k_1}{\overset{k_2}{\rightleftharpoons}} PD \quad (7)$$

where D = complex **1**, **2** or **3**; P = CT or HT DNA.

Here, k_2 is the second-order rate constant for the forward reaction, characterizing the formation of the product, and k_1 is the rate constant for the reverse reaction. The rate constants k_2 and k_1 have been already explained in the part of the interactions with 5′-GMP. Their values are listed in Table 1. The rate of the reaction is described by eqn (8).

$$k_{obs} = k_2[\mathbf{1}, \mathbf{2} \text{ or } \mathbf{3}] + k_1[Cl^-] \quad (8)$$

All kinetic runs could be fitted by a single exponential function. Each pseudo first-order rate constant, k_{obs}, was calculated as the average value of six or seven independent runs and the values are given in Tables S14–S19.‡ The experimental results for the substitution reactions of complexes **1–3** with CT and HT DNA are shown in Fig. S11–S13.‡

The experimentally obtained results clearly show that the rate constants depend on the nature of the chelating ligand. The k_2 values for the substitution reactions of complexes **1–3** with CT and HT DNA reflect the following order of reactivity: **1** (en) > **2** (dach) > **3** (bpy). Complexes **1** and **2** react two to three orders of magnitude faster than complex **3**. The same reactivity trend of selected complexes was also observed for the substitution reactions with DNA duplexes and RNA duplex. The lowest reactivity of complex **3** indicates that its interactions with DNA are not crucial for its cytotoxicity and perhaps a different mechanism of action compared to that of cisplatin, is implicated for the obtained biological activity.[15] On the other hand, taking into account the obtained rate constants for the interaction of complexes **1–3** with selected DNAs, it can be seen that the reaction goes faster with HT DNA than with CT DNA probably due to the higher percentage of guanine in herring testes DNA.

Plasmid binding studies

In order to visualize the change of the unwinding in electrophoretic mobility caused by the interaction of Ru(II) chlorophenyl terpyridine complexes with DNA in a gel mobility shift assay, electrophoresis in 1% agarose gel was used. Based on the previous results, where some of the ruthenium complexes demonstrated the ability to unwind DNA,[20,30] this study inves-

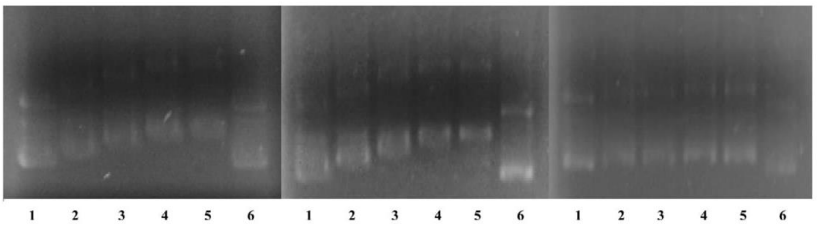

Fig. 5 Unwinding of supercoiled pUC18 plasmid DNA by ruthenium complexes. Plasmid was incubated with complexes **1–3** with r_f values 0.07, 0.14, 0.21, 0.28, 0.35 and 0 (control) (lanes 1–6, respectively).

tigated the DNA binding affinity of complexes **1–3** with the negatively supercoiled pUC 18 plasmid. For binding studies, the ratio of nucleotide concentration (C_{DNA}) and concentration of Ru(II) polypyridyl complexes (C_X, where X represents complexes **1**, **2** or **3**) ($r_f = C_X/C_{DNA}$) was varied in the range of 0–0.35 (Fig. 5). All samples were mixed in Tris-HCl buffer (pH = 7.2) and then incubated for 180 minutes in the dark at 37 °C. A compound that unwinds the DNA duplex reduces the number of supercoils so that the superhelical density of closed circular DNA decreases. This decrease upon binding of unwinding agents causes a decrease in the rate of migration through agarose gel, which makes it possible that the unwinding can be observed. As shown in Fig. 5, the increasing concentration of complexes **1–3** (line 1–5) led to unwinding of the plasmid that can be detected by the appearance of a slower migrating supercoiled plasmid band. Complexes **1** and **2** exhibit stronger unwinding efficiency than complex **3**. By comparing these three complexes it is obvious that the aliphatic diamine ligands en and dach were superior to the bipyridine ligand with respect to binding efficacy. Steric hindrance and lower conformational flexibility of the aromatic ligand system might hinder the ruthenium binding compared to the more site accessible and smaller aliphatic diamine. These results can be useful to provide a rational basis to design novel, optimized Ru-based anticancer agents, taking into account that also tiny, point structural modifications may result into markedly different reactivities, eventually determining very different *in vivo* mechanisms of action.

Experimental

Chemicals and solutions

1,2-Diaminoethane (en), (±)-*trans*-1,2-diamminocyclohexane (dach), 2,2′-bipyridine (bpy), 4′-(4-chlorophenyl)-2,2′:6′,2″-terpyridine (Cl-Ph-tpy), deoxyribonucleic acid sodium salt from calf thymus (CT DNA), deoxyribonucleic acid sodium salt from herring testes (HT DNA), pUC 18 plasmid (dsDNA) and guanosine-5′-monophosphate disodium salt hydrate (5′-GMP-Na_2) were purchased from Sigma Aldrich. Hepes (*N*-2-hydroxyethylpiperazine-*N*′-2-ethanesulfonic acid) and Tris (tris(hydroxymethyl)aminomethane) buffer are also commercially available and were used as received. All oligonucleotides (5′-CTT CTT GGT TCT CTT-3′ and 5′-AAG AGA ACC AAG AAG-3′ (DNA-1), 5′-TCT CCT TCT TGG TTC TCT TCT C-3′ and 5′-GAA GAG AAC CAA GAA GGA GAG A-3′ (DNA-2), 5′-UUC UUG GUU CUC U-3′ and 5′-AGA GAA CCA AGA A-3′ (RNA)) were purchased from IBA GmbH (IBA Nucleic Acids Synthesis, Göttingen, Germany) of HPLC grade quality. The complexes [Ru(Cl-Ph-tpy)(en)Cl]Cl (**1**), [Ru(Cl-Ph-tpy)(dach)Cl]Cl (**2**) and [Ru(Cl-Ph-tpy)(bpy)Cl]Cl (**3**) were synthesized as reported previously.[15] Microanalysis, UV-Vis spectroscopy and ^{1}H NMR spectroscopy were used to check the purity of these complexes and the spectra agreed well with the data already reported.[15] Doubly distilled water was used as the solvent throughout the experiments. The stock solutions of CT DNA and HT DNA were prepared in 5 mM Tris-HCl/50 mM NaCl buffer at pH = 7.2, which gave a ratio of UV absorbances of *ca.* 1.8–1.9 at 260 nm and 280 nm (A_{260}/A_{280}), indicating that the DNA was sufficiently free of protein and the concentration was determined by UV absorbance at 260 nm (ε = 6600 M^{-1} cm^{-1}).[31] Nucleophile stock solutions were prepared shortly before use by dissolving the chemicals.

Instrumental methods

The UV-Vis spectra were obtained on a Perkin-Elmer Lambda 25 double beam spectrophotometer or on a Cary 100 spectrophotometer equipped with a thermal control unit, using 1.0 cm path-length quartz cuvettes (3.0 ml and 1.0 ml, respectively). The stopped-flow apparatus and the associated computer system were from Applied Photophysics (model SX-20). The pH of the solutions was measured using a Mettler Delta 350 digital pH meter with a combined glass electrode. This electrode was calibrated using standard buffer solutions of pH 4, 7 and 9 obtained from Sigma Aldrich. Mono- (^{1}H; 500 MHz) and bi-dimensional (^{1}H–^{1}H COSY) NMR spectra were recorded on a Bruker Avance 500 MHz spectrometer. ^{1}H chemical shifts in D_2O were referenced to added 1,4-dioxane (δ = 3.75).

X-ray diffraction studies

Red crystals of [Ru(Cl-Ph-tpy)(bpy)Cl]Cl (**3**) suitable for X-ray analysis were obtained from the acetonitrile solution upon standing at room temperature. The diffraction data for complex **3** were collected at room temperature on an Oxford Diffraction Gemini S diffractometer. Graphite-monochromated MoKα radiation (λ = 0.7107 Å) was used for diffraction on suitable single crystals of complex **3**. CrysAlisPro and CrysAlis RED

Table 2 Experimental details: crystalographic data and refinement parameters for [Ru(Cl-Ph-tpy)(bpy)Cl]Cl complex (**3**)

Chemical formula	$C_{31}H_{22}Cl_3N_5O_0Ru$
M_r	671.95
Crystal system, space group	Triclinic, $P\bar{1}$
Temperature (K)	293
a, b, c (Å)	10.6319 (6), 11.2402 (5), 14.0886 (5)
α, β, γ (°)	80.307 (3), 84.555 (4), 69.904 (4)
V (Å^3)	1557.33 (13)
Z	2
Radiation type	Mo Kα
No. of reflections for cell measurement	4744
θ range (°) for cell measurement	3.3–28.2
μ (mm^{-1})	0.79
Crystal shape	Prism
Color	Green
Crystal size (mm)	0.23 × 0.19 × 0.10
Data collection	
Diffractometer	Xcalibur, Sapphire3, Gemini
Absorption correction	Analytical CrysAlisPro 1.171.38.41 (Rigaku Oxford Diffraction, 2015) Analytical numeric absorption correction using a multifaceted crystal model Empirical absorption correction using spherical harmonics, implemented in the SCALE3 ABSPACK scaling algorithm
T_{min}, T_{max}	0.867, 0.936
No. of measured, independent and observed [$I > 2\sigma(I)$] reflections	11 955, 7064, 5093
R_{int}	0.037
$(\sin\theta/\lambda)_{max}$ (Å^{-1})	0.683
Refinement	
$R[F^2 > 2\sigma(F^2)]$, $wR(F^2)$, S	0.047, 0.100, 0.94
No. of reflections	7064
No. of parameters	361
H-atom treatment	H-atom parameters constrained
ρ_{max}, ρ_{min} (e Å^{-3})	1.14, −0.45

Computer programs: CrysAlisPro 1.171.38.41 (Rigaku OD, 2015), SHELXL2014/6 (Sheldrick, 2014).

software packages[32] were used for data collection and data integration. The space group determinations were based on an analysis of the Laue class and the systematically absent reflections. Collected data were corrected for absorption effects by using the analytical numeric absorption correction applying a multifaceted crystal model.[33] Structure solution and refinement were carried out with the programs SHELXT and SHELXL-2014/6, respectively.[34] ORTEP-3 for Windows,[18] MERCURY[35] and PLATON[19] were employed for molecular graphics and WinGx software was used to prepare material for publication.[36] Non-hydrogen atoms were refined anisotropically, the C–H hydrogen atoms were included on calculated positions riding on their attached atoms with fixed distances C–H = 0.93 Å with U_{iso}(H) = 1.2U_{eq}(C). The crystal data and refinement parameters are summarized in Table 2.

Interactions with nucleobases

The NMR sample of complex **3** (4 mM for the reaction with 9MeG, and 10 mM for the reaction with 5′-GMP) was prepared in D_2O. When equilibrium between the intact species **3** and the aquo complex $[Ru(Cl\text{-}Ph\text{-}tpy)(bpy)(H_2O)]^{2+}$ (**3aq**) was reached (*ca.* after 3 days), 1.1 equiv. of the corresponding nucleobase, as a solid, was added.

Kinetic studies with 5′-GMP, oligonucleotides and CT and HT DNA

The kinetics of the substitution reactions of complexes **1–3** with 5′-GMP were studied spectrophotometrically. All kinetic measurements were performed under pseudo-first-order conditions (*i.e.* the concentration of the nucleophile was at least 10-fold that of the complex). The reactions were initiated by mixing a solution of each complex (0.3 mL, 1.00 mM) with 2.7 mL of a thermally equilibrated nucleophile solution (5.56 mM) in the UV-Vis cuvette. The observed pseudo-first-order rate constants, k_{obs}, represent an average value of two to three independent kinetic runs for each experimental condition. Reactions were studied at three different temperatures (15, 25 and 37 °C) in 25 mM Hepes buffer containing 50 mM NaCl at pH 7.20. The second-order rate constants, k_2, for the substitution reactions with 5′-GMP were obtained directly from the slopes of the plots of k_{obs} *versus* the concentration of the nucleophile. All kinetic data were computer-fitted to the appropriate equation using the programs Microsoft Excel 2007 and Origin 8.

The kinetics of the substitution reactions of complexes **1–3** with oligonucleotides were studied also spectrophotometrically. Equal concentrations of the (a)- and (b) strands of each duplex DNA-1, DNA-2, and RNA (Fig. 2), were mixed separately and the measurements were conducted with a total strand concentration (C_T; $C_T = C_{Xa} + C_{Xb}$; X = DNA-1, DNA-2 or RNA) of 3.0 μM in 5 mM Tris-HCl buffer (containing 50 mM NaCl). Prior to measurements, the complementary oligonucleotides were first heated to 90 °C and then allowed to hybridize by slow cooling (0.5 °C min^{-1}) to 20 °C. The annealed duplexes were then reheated to 37 °C and complexes **1–3** were added. The final concentrations of the investigated complexes were $C_{(1-3)}$ = 5, 15, 30 and 50 μM. The absorbance change was measured at λ = 260 nm after addition of complexes **1–3**.

The interactions of complexes **1–3** with CT and HT DNA were studied by stopped-flow spectroscopy. In a typical single-mixed experiment, one syringe contained various concentrations of CT or HT DNA (in the range of 5–50 mM) in 5 mM Tris-HCl buffer (pH = 7.2) containing 50 mM NaCl, and the other contained 1.0 mM complexes **1–3**. For each run, equal volumes of both solutions from separate syringes were rapidly mixed in the mixing chamber and the changes of the absorbance were monitored during a chosen period of time. The temperature of both drive syringes, the cell and the mixing chamber was maintained at 25 ± 0.2 °C by using a circulating water bath. The absorbance change was measured at λ = 260 nm after addition of complexes **1–3**.

Nuclease activity of complexes 1–3

The electrophoretic mobility experiments were carried out by agarose gel electrophoresis on a 10 μl total sample volume

solution containing pUC 18 DNA (0.2 μg) and the respective ruthenium(II) complexes. Stock solutions (0.1 mM) of **1–3** were prepared in 5 mM Tris-HCl (50 mM NaCl, pH = 7.2). Supercoiled pUC 18 DNA was treated with the complexes (5–50 μM) and the mixtures were incubated in the dark for 180 min at 37 °C. The samples were analyzed by 1% agarose gel electrophoresis in TAE (Tris-acetate-EDTA) buffer for 2 h at 100 V. The gel was stained with propidium iodide and photographed under UV light.

Table 3 IC_{50} values and partition coefficients (log $P_{o/w}$) for Cl-Ph-tpy (**1–3**) and Cl-tpy complexes[12,15]

	IC_{50} [μM]			
	HeLa	A549	MRC-5	log $P_{o/w}$
1	84.81 ± 4.67	>100	>100	0.27
2	96.28 ± 3.81	>100	>100	0.20
3	12.68 ± 1.89	53.80 ± 4.44	97.67 ± 6.93	0.39
[Ru(Cl-tpy)(en)]Cl	71.23 ± 2.61	>100	86.66 ± 2.62	−1.33
[Ru(Cl-tpy)(dach)]Cl	>100	>100	>100	−1.45
[Ru(Cl-tpy)(bpy)]Cl	>100	>100	>100	—

Conclusion

In the present work, we reported the crystal structure of the ruthenium(II) complex [Ru(Cl-Ph-tpy)(bpy)Cl]Cl (**3**), in which the Ru ion displays the typical distorted octahedral geometry with the tridentate Cl-Ph-tpy ligand coordinated with the expected meridional geometry, the bpy as the *N–N* bidentate chelating ligand, and the sixth coordination site occupied by a chloride ion. According to the previously obtained cytotoxicity results of complexes **1–3**,[15] it was of particular interest to elucidate the similarities and differences in the behavior of the chlorophenyl terpyridine ruthenium complexes towards mononucleotides, oligonucleotides and DNA, and to relate these properties to biological effects. This study provides information on the mechanism of substitution of ruthenium(II) complexes with the guanine model compound 5′-GMP. The kinetic data for the reactions of three cationic complexes [Ru(Cl-Ph-tpy)(en)Cl]Cl (**1**), [Ru(Cl-Ph-tpy)(dach)Cl]Cl (**2**) and [Ru(Cl-Ph-tpy)(bpy)Cl]Cl (**3**) with 5′-GMP clearly showed that the rate of the reaction depends on the nature of the chelating ligand: complexes **1** (en) and **2** (dach) react *ca.* 2 times faster than the bpy complex **3**.

Quantitative kinetic investigations on complexes **1–3** were also performed with oligonucleotides such as small fragments of DNAs and RNA with a centrally located GG-binding site. Concerning the length of the fragments of DNAs and RNA, it can be seen that the shorter 13GG duplex RNA reacts faster than the longer 15GG duplex DNA-1 and 22GG duplex DNA-2, which is consistent with the previously published results.[23–25] Furthermore, the interactions with calf thymus (CT) and herring testes (HT) DNA were studied by stopped-flow spectroscopy and gel mobility shift assay. According to the obtained rate constants, the complexes with bidentate aliphatic diamines proved to be superior to those with bpy in terms of reactivity and capability to bind oligonucleotides and DNA. In addition, the reactions with HT DNA were faster compared to those with CT DNA probably due to the higher percentage of guanine in herring testes DNA.

The reactivity of the complexes to DNA and their efficiency to unwind closed, negatively supercoiled DNA are not in line with their biological activity. These differences may play very important roles in their antitumor activity and could contribute to the different mechanism for cytotoxicity compared to cisplatin. The hydrophobic parameter (octanol–water partition coefficients, log $P_{o/w}$) is very important for the antitumor mechanism of these kind of Ru(II) polypyridyl complexes that contain ligands with a large aromatic area. Higher hydrophobicity may contribute to an increased uptake of the complex by the cells, thereby enhancing the anticancer activity.[37–40] It is evident from previous reports on the lipophilicity and cytotoxicity of complexes **1–3** that the cytotoxicity of the Ru-tpy complexes can be increased by using more lipophilic ligands (see Table 3).[15] In fact, complex **3** presents the highest lipophilicity (0.39) and hence generates the strongest cytotoxicity (IC_{50} *ca.* 12.7 μM).[15]

In conclusion, the present study indicates that complexes **1**, **2** and **3** are promising antitumor candidates. The results of the present work represent a further improvement in the structure–pharmacological relationship needed for the design of new antitumor ruthenium drugs and chemotherapeutic strategies.

Acknowledgements

S. K. C. Elmroth and Ž. D. Bugarčić are very thankful to prof. L. I. Elding for all his help, kindness and effort during their PhD study, and also for his continuous interest in the scientific work of S. K. C. E. and Ž. D. B. The authors gratefully acknowledge financial support from the Ministry of Education and Science of the Republic of Serbia, project No. 172011, and the Swedish Cancer foundation (Grant to S. K. C. E. No. 130317). M. M. thanks Prof. Dr Sofi K. C. Elmroth for hosting this work and continuous support at Kemicentrum, Lund University, Sweden and Dr Alak Alchikh for her support.

References

1 E. Alessio, *Bioinorganic Medicinal Chemistry*, Wiley-VCH Verlag & Co. KGaA, Weinheim, Germany, 2011.
2 P. E. N. Barry and J. P. Sadler, *Chem. Commun.*, 2013, **49**, 5106–5131.
3 L. Ronconi and J. P. Sadler, *Coord. Chem. Rev.*, 2007, **251**, 1633–1648.
4 R. Trondl, P. Heffeter, C. R. Kowol, M. A. Jakupec, W. Berger and B. K. Keppler, *Chem. Sci.*, 2014, **5**, 2925–2932.

5 C. H. Leung, H. J. Zhong, D. D. H. Chan and D. L. Ma, *Coord. Chem. Rev.*, 2013, **257**, 1764–1776.
6 A. Ghosh, A. Mandoli, D. K. Kumar, N. S. Yadav, T. Ghosh, B. Jha, J. A. Thomas and A. Das, *Dalton Trans.*, 2009, **10**, 9312–9321.
7 Y. J. Liu, H. Chao, L. F. Tau, Y. X. Yuan, W. Wei and L. N. Ji, *J. Inorg. Biochem.*, 2005, **99**, 530–537.
8 A. Rilak, B. Petrović, S. Grgurić-Šipka, Ž. Tešić and Ž. Bugarčić, *Polyhedron*, 2011, **30**, 2339–2344.
9 A. Rilak, I. Bratsos, E. Zangrando, J. Kljun, I. Turel, Ž. D. Bugarčić and E. Alessio, *Dalton Trans.*, 2012, **41**, 11608–11618.
10 A. Rilak, I. Bratsos, E. Zangrando, J. Kljun, I. Turel, Ž. D. Bugarčić and E. Alessio, *Inorg. Chem.*, 2014, **53**, 6113–6126.
11 A. Rilak, R. Pushta and Ž. D. Bugarčić, *Polyhedron*, 2015, **91**, 73–83.
12 D. Lazić, A. Arsenijević, R. Puchta, Ž. D. Bugarčić and A. Rilak, *Dalton Trans.*, 2016, **45**, 4633–4646.
13 W. H. Ang and P. J. Dyson, *Eur. J. Inorg. Chem.*, 2006, **20**, 4003–4018.
14 Z. Zhao, Z. Luo, Q. Wu, W. Zheng, Y. Feng and T. Chen, *Dalton Trans.*, 2014, **43**, 17017–17028.
15 M. M. Milutinović, A. Rilak, I. Bratsos, O. Klisurić, M. Vraneš, N. Gligorijević, S. Radulović and Ž. D. Bugarčić, *J. Inorg. Biochem.*, 2016, **169**, 1–12.
16 C. Moucheron, *New J. Chem.*, 2009, **33**, 235–245.
17 V. S. Stafford, K. Suntharalingam, A. Shivalingam, A. J. P. White, D. J. Mann and R. Vilar, *Dalton Trans.*, 2015, **44**, 3686–3700.
18 L. J. Farrugia, *J. Appl. Crystallogr.*, 1997, **30**, 565.
19 I. J. Bruno, J. C. Cole, P. R. Edgington, M. K. Kessler, C. F. Macrae, P. McCabe, J. Pearson and R. Taylor, *Acta Crystallogr., Sect. B: Struct. Sci.*, 2008, **58**, 389–397.
20 O. Novakova, J. Kasparkova, O. Vrana, P. M. van Vliet, J. Reedijk and V. Brabec, *Biochemistry*, 1995, **34**, 12369–12378.
21 N. Busto, J. Valladolid, M. Martinez-Alonso, H. J. Lozano, F. A. Jalon, B. R. Manzano, A. M. Rodriguez, M. Carmen Carrion, T. Biver, J. M. Leal, G. Espino and B. Garcia, *Inorg. Chem.*, 2013, **52**, 9962–9974.
22 J. E. Quin, J. R. Devlin, D. Cameron, K. M. Hannan, R. B. Pearson and R. D. Hannan, *Biochim. Biophys. Acta, Mol. Basis Dis.*, 2014, **1842**, 802–816.
23 C. Polonyi and S. K. C. Elmroth, *Dalton Trans.*, 2013, **42**, 14959–14962.
24 C. Polonyi, A. Alshiekh, L. A. Sarsam, M. Clausén and S. K. C. Elmroth, *Dalton Trans.*, 2014, **43**, 11941–11949.
25 M. M. Milutinović, J. Bogojeski, O. Klisurić, A. Scheurer, S. K. C. Elmroth and Ž. D. Bugarčić, *Dalton Trans.*, 2016, **45**, 15481–15491.
26 N. Summa, W. Schiessl, R. Puchta, N. van Eikema Hommes and R. van Eldik, *Inorg. Chem.*, 2006, **45**, 2948–2959.
27 K. J. Kilpin and P. J. Dyson, *Chem. Sci.*, 2013, **4**, 1410–1419.
28 W. H. Ang, A. Casini, G. Sava and P. J. Dayson, *J. Organomet. Chem.*, 2011, **696**, 989–998.
29 G. Sava, A. Bergamo and P. J. Dyson, *Dalton Trans.*, 2011, **40**, 9069–9075.
30 H. Huang, P. Zhang, Y. Chen, L. Ji and H. Chao, *Dalton Trans.*, 2015, **44**, 15602–15610.
31 K. A. Meadows, F. Liu, J. Sou, B. P. Hudson and D. R. McMillin, *Inorg. Chem.*, 1993, **32**, 2919–2923.
32 *Oxford Diffraction CrysAlis CCD and CrysAlis Red*, Oxford Diffraction, Abingdon, 2009.
33 R. C. Clark and J. S. Reid, *Acta Crystallogr., Sect. A: Fundam. Crystallogr.*, 1995, **51**, 887–897.
34 G. M. Sheldrick, *Acta Crystallogr., Sect. A: Fundam. Crystallogr.*, 2015, **71**, 3–8.
35 I. J. Bruno, J. C. Cole, P. R. Edgington, M. K. Kessler, C. F. Macrae, P. McCabe, J. Pearson and R. Taylor, *Acta Crystallogr., Sect. B: Struct. Sci.*, 2002, **58**, 389–397.
36 L. J. Farrugia, *J. Appl. Crystallogr.*, 1999, **32**, 837–838.
37 M. G. Mendoza-Ferri, C. G. Hartinger, M. A. Mendoza, M. Groessl, A. E. Egger, R. E. Eichinger, J. B. Mangrum, N. P. Farrell, M. Maruszak, P. J. Bednarski, F. Klein, M. A. Jakupec, A. A. Nazarov, K. Severin and B. K. Keppler, *J. Med. Chem.*, 2009, **52**, 916–925.
38 F. Giannini, L. E. H. Paul, J. Furrer, B. Therrienb and G. Suss-Fink, *New J. Chem.*, 2013, **37**, 3503–3511.
39 Y. Mulyana, D. K. Weber, D. P. Buck, C. A. Motti, J. G. Collin and F. R. Keene, *Dalton Trans.*, 2011, **40**, 1510–1523.
40 A. K. Gorle, A. J. Ammit, L. Wallace, F. R. Keene and J. G. Collins, *New J. Chem.*, 2014, **38**, 4049–4059.

Electronic Supplementary Material (ESI) for Dalton Transactions.

Kinetic and mechanistic study on the reactions of ruthenium(II) chlorophenyl terpyridine complexes with nucleobases, oligonucleotides and DNA

Milan M. Milutinović,[1,2] Sofi K.C. Elmroth,[2] Goran Davidović,[3] Ana Rilak,[1] Olivera R. Klisurić,[4] Ioannis Bratsos,[5] Živadin D. Bugarčić,*[1]

[1] *University of Kragujevac, Faculty of Science, R. Domanovića 12, P. O. Box 60, 34000 Kragujevac, Serbia.*

[2] *Lund University, Biochemistry and Structural Biology, KILU, P.O. Box 124 SE-221 00 Lund, Sweden.*

[3] *University of Kragujevac, Clinic for Cardiology, Clinical Center Kragujevac, Kragujevac, Serbia.*

[4] *University of Novi Sad, Faculty of Science, Department of Physics, Trg Dositeja Obradovića 3, 21000 Novi Sad, Serbia.*

[5] *I.N.N., Dept. of Physical Chemistry, NCSR "Demokritos", 15310 Ag. Paraskevi, Athens, Greece.*

**Corresponding author:* Prof. Dr. Živadin D. Bugarčić, Department of Chemistry, Faculty of Science, University of Kragujevac, Radoja Domanovića 12, Kragujevac, Serbia, Tel: +381(0)34300262, Fax: +381(0)34335040, e-mail: bugarcic@kg.ac.rs

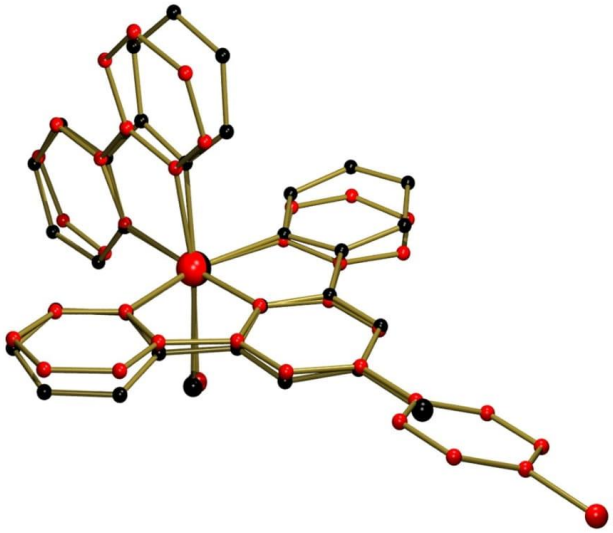

Fig. S1. PLATON[19] drawing showing an overlay of two complexes: [Ru(Cl-Ph-tpy)(bpy)Cl]Cl complex (**3**) (red atoms) and [Ru(Cl-tpy)(bpy)Cl]Cl ($\mathbf{3_{Cl}}$) (black atoms).

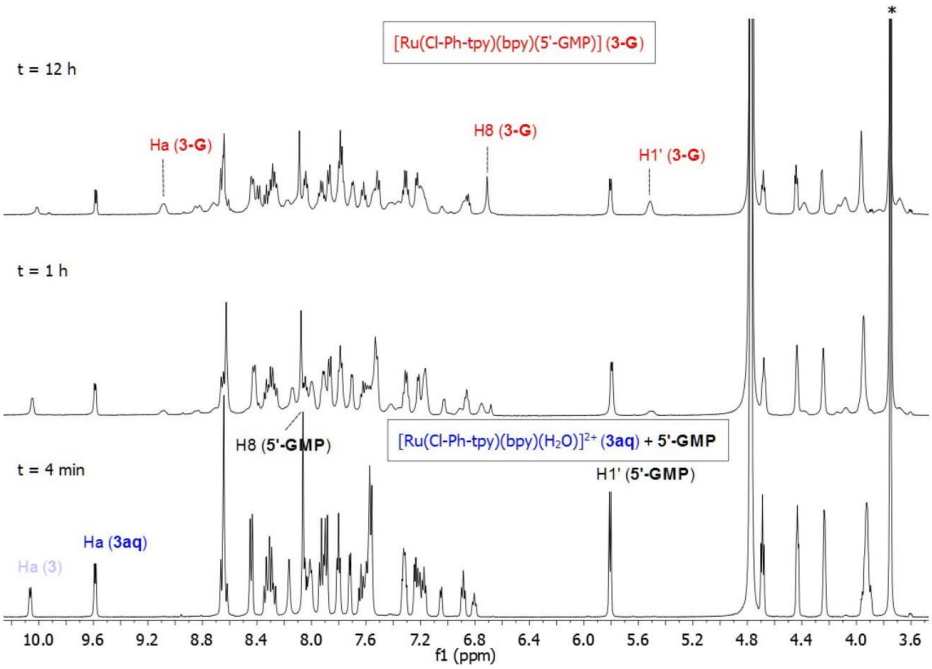

Fig. S2. ^{1}H NMR spectral changes after the addition of 5′-GMP (1.1 equiv.) to an equilibrated solution of [Ru(Cl-Ph-tpy)(bpy)Cl]Cl (**3**; 10 mM)) in D_2O at various reaction times. With * is indicated the reference resonance of 1,4 dixane.

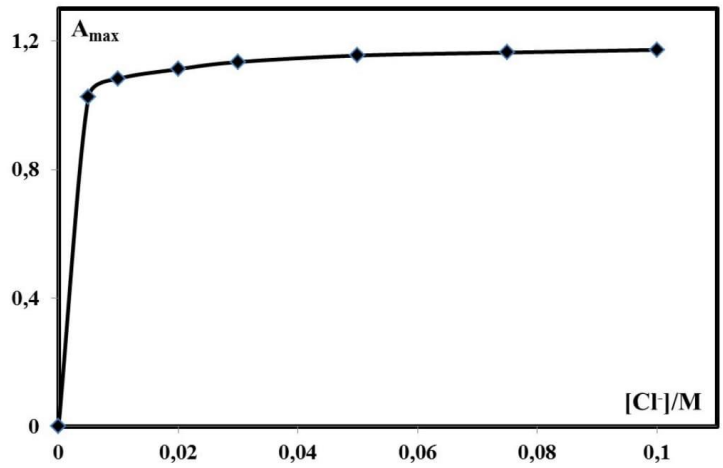

Fig. S3. The change of absorbance at 471 nm of the $[Ru(Cl\text{-}Ph\text{-}tpy)(dach)Cl]^+$ (**2**) complex *vs*. $[Cl^-]$ in 25 mM Hepes buffer at 37 ºC.

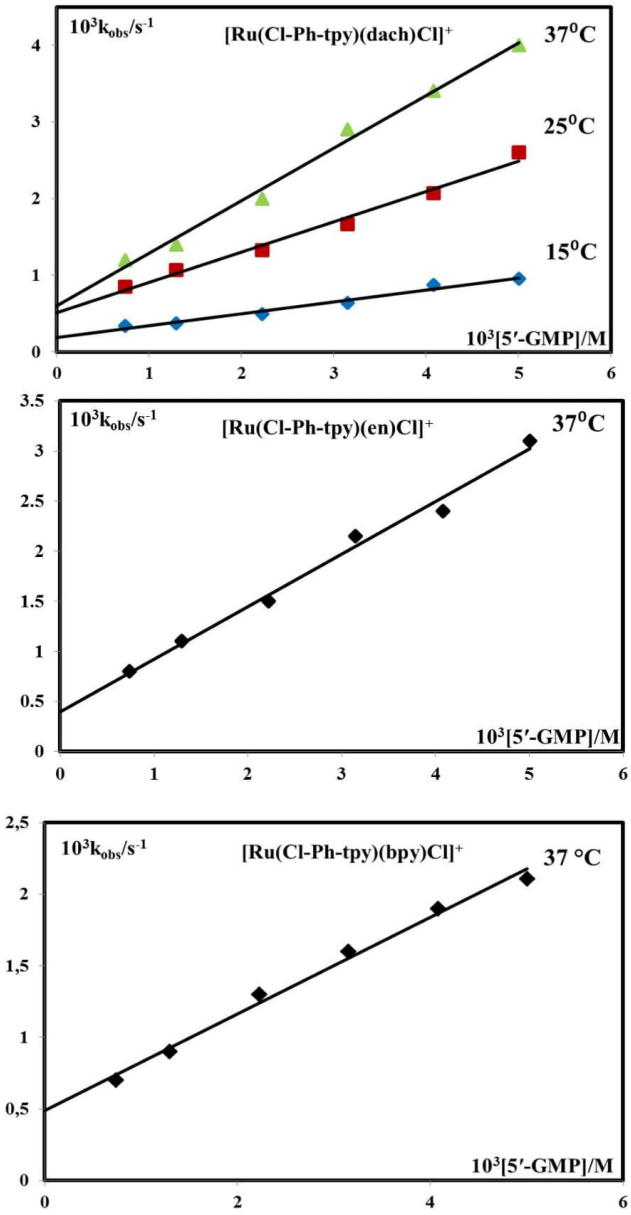
$10^3k_{obs}/s^{-1}$
[Ru(Cl-Ph-tpy)(dach)Cl]$^+$
37^{0}C
25^{0}C
15^{0}C
10^3[5′-GMP]/M
$10^3k_{obs}/s^{-1}$
[Ru(Cl-Ph-tpy)(en)Cl]$^+$
37^{0}C
10^3[5′-GMP]/M
$10^3k_{obs}/s^{-1}$
[Ru(Cl-Ph-tpy)(bpy)Cl]$^+$
37 °C
10^3[5′-GMP]/M

5

Fig. S4. *Pseudo*-first-order rate constants, k_{obs}, plotted as a function of ligand concentration and temperature for the substitution reactions of complexes **1** – **3** with 5'-GMP in 25 mM Hepes buffer (50 mM NaCl, pH = 7.2).

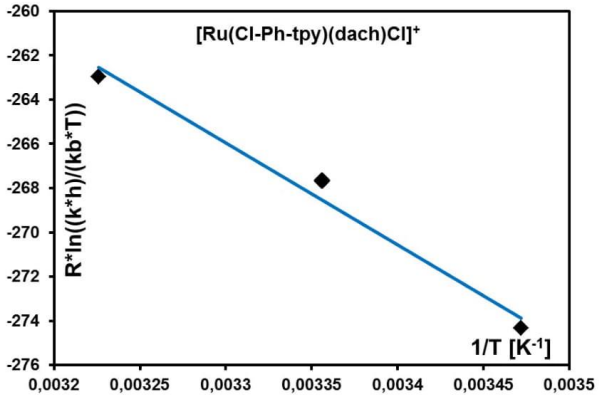

Fig. S5. Eyring plot for the reactions of complex **2** with 5'-GMP, at pH 7.20 in 25 mM Hepes buffer and 50 mM NaCl.

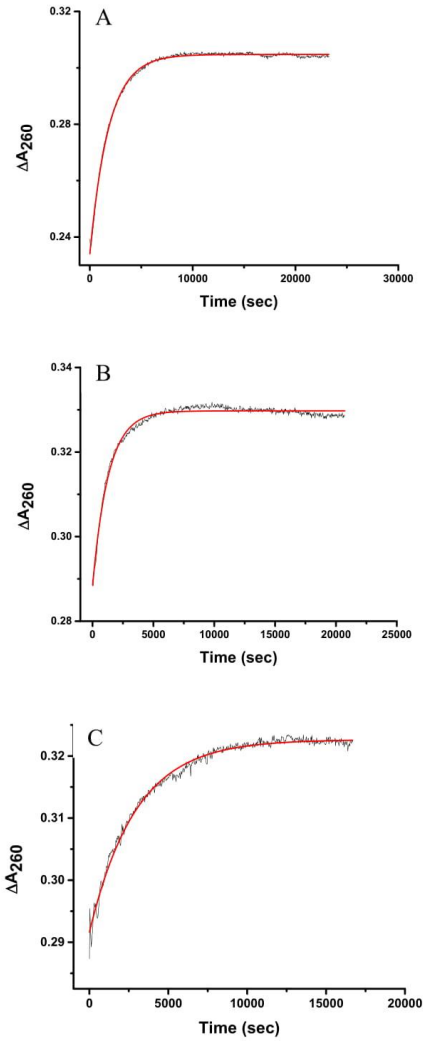

Fig. S6. Absorbance change as a function of time after the addition of complex **1** to DNA-1 (A), DNA-2 (B) and RNA (C) followed at λ = 260 nm. All measurements were conducted with $C_{\mathbf{1}}$ =

30.0 μM, C_T = 3.0 μM and T = 37 °C in Tris-HCl buffered solution, pH = 7.2. Fits of a single-exponential function to the experimental data is indicated with a solid line (red).

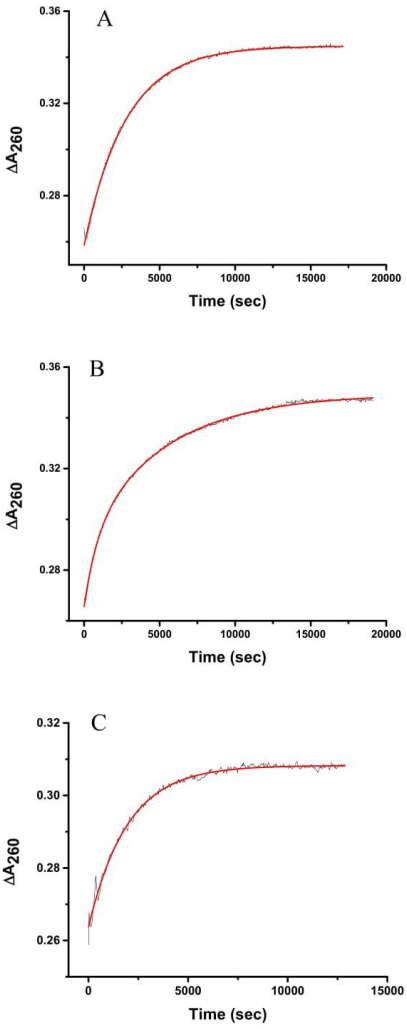

8

Fig. S7. Absorbance change as a function of time after the addition of complex **2** to DNA-1 (A), DNA-2 (B) and RNA (C) followed at λ = 260 nm. All measurements were conducted with C_2 = 30.0 μM, C_T = 3.0 μM and T = 37 °C in Tris-HCl buffered solution, pH = 7.2. Fits of a single-exponential function to the experimental data is indicated with a solid line (red).

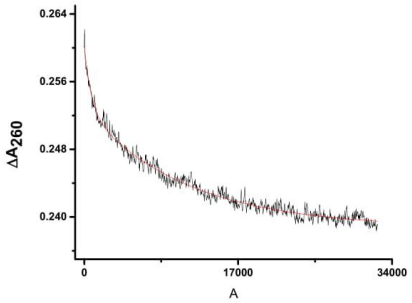

Fig. S8. Absorbance change as a function of time after the addition of complex **3** to DNA-1 followed at λ = 260 nm. All measurements were conducted with C_3 = 30.0 μM, C_T = 3.0 μM and T = 37 °C in Tris-HCl buffered solution, pH = 7.2. Fits of a single-exponential function to the experimental data is indicated with a solid line (red).

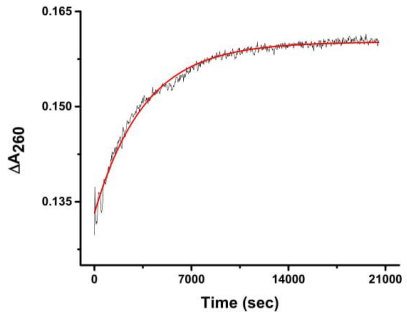

Fig. S9. Absorbance change as a function of time after the addition of complex **3** to RNA followed at λ = 260 nm. All measurements were conducted with C_3 = 30.0 μM, C_T = 3.0 μM and T = 37 °C in Tris-HCl buffered solution, pH = 7.2. Fits of a single-exponential function to the experimental data is indicated with a solid line (red).

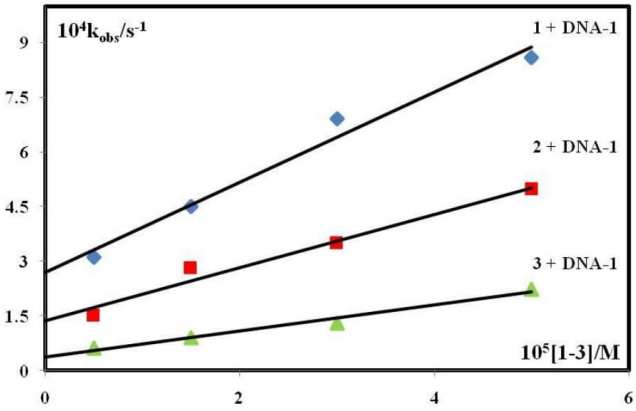
$10^4k_{obs}/s^{-1}$
1 + DNA-1
2 + DNA-1
3 + DNA-1
10^5[1-3]/M
9
7.5
6
4.5
3
1.5
0
0
2
4
6

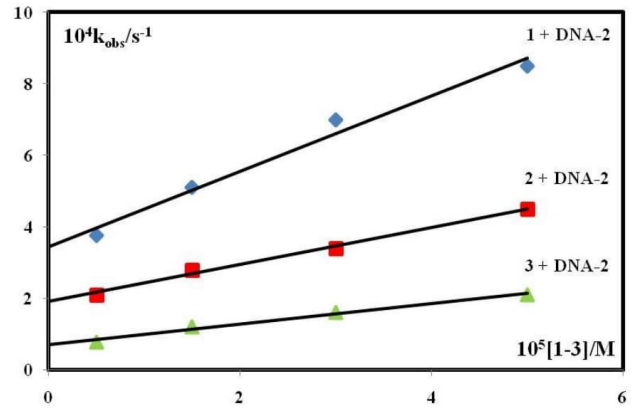
$10^4k_{obs}/s^{-1}$
1 + DNA-2
2 + DNA-2
3 + DNA-2
10^5[1-3]/M
10
8
6
4
2
0
0
2
4
6

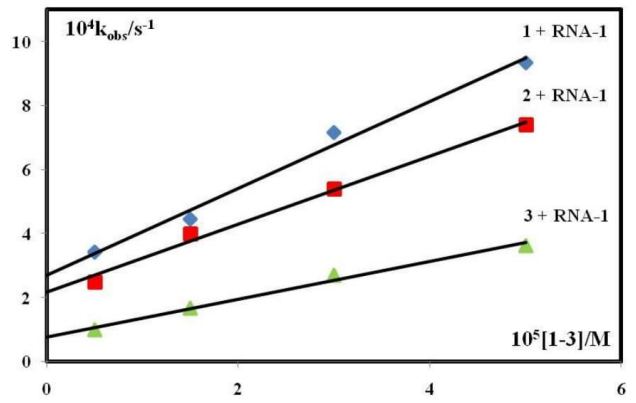
$10^4k_{obs}/s^{-1}$
1 + RNA-1
2 + RNA-1
3 + RNA-1
10^5[1-3]/M
10
8
6
4
2
0
0
2
4
6

11

Fig. S10. Observed *pseudo*-first order rate constants, k_{obs}, plotted as a function of complex concentration in the interval of 5 – 50 μM together with linear regression lines allowing for determination of $k_{2,app}$ from the slope.

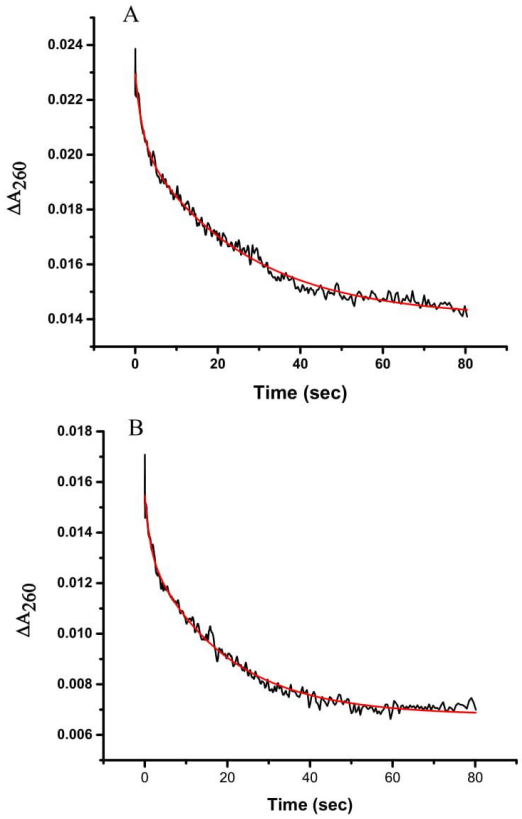

Fig. S11. Absorbance change as a function of time after the addition of complex **1** to CT DNA (A) and HT DNA (B) followed at λ = 260 nm. All measurements were conducted with $C_{\mathbf{1}}$ = 30.0 μM, C_T = 50.0 μM and T = 37 °C in Tris-HCl buffered solution, pH = 7.2. Fits of a single-exponential function to the experimental data is indicated with a solid line (red).

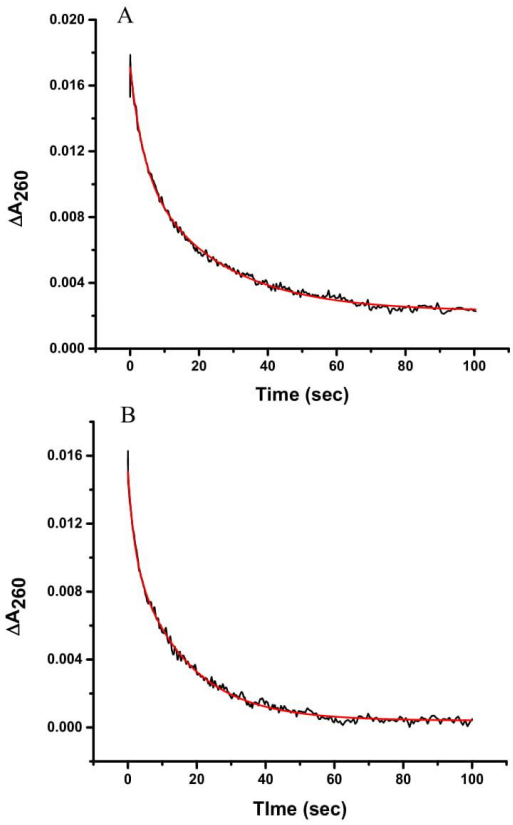

Fig. S12. Absorbance change as a function of time after the addition of complex **2** to CT DNA (A) and HT DNA (B) followed at λ = 260 nm. All measurements were conducted with C_2 = 30.0 μM, C_T = 50.0 μM and T = 37 °C in Tris-HCl buffered solution, pH = 7.2. Fits of a single-exponential function to the experimental data is indicated with a solid line (red).

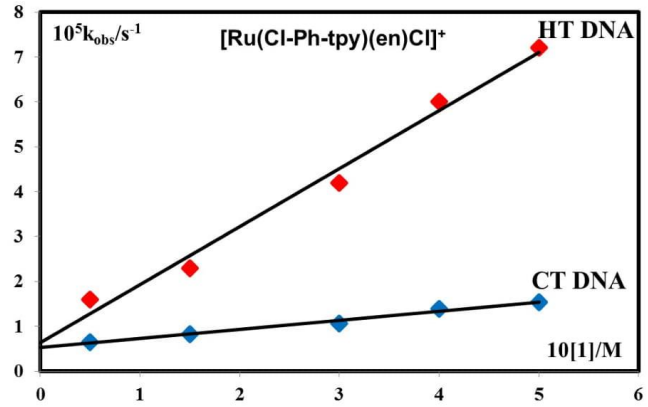
$10^5k_{obs}/s^{-1}$
[Ru(Cl-Ph-tpy)(en)Cl]+
HT DNA
CT DNA
10[1]/M

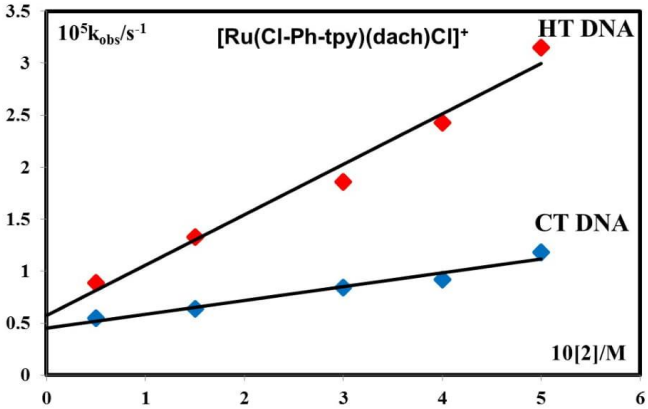
$10^5k_{obs}/s^{-1}$
[Ru(Cl-Ph-tpy)(dach)Cl]+
HT DNA
CT DNA
10[2]/M

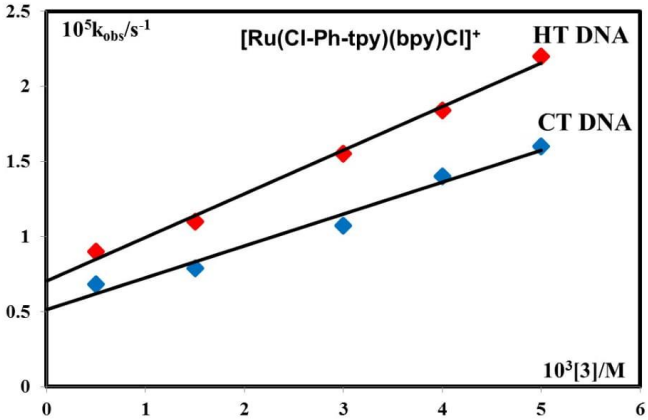
$10^5k_{obs}/s^{-1}$
[Ru(Cl-Ph-tpy)(bpy)Cl]+
HT DNA
CT DNA
10^3[3]/M

14

Fig. S13. Observed *pseudo*-first order rate constants, k_{obs}, plotted as a function of complex concentration in the interval of 5 – 50 μM together with linear regression lines allowing for determination of k_2 from the slope.

Table S1. Selected geometrical parameters for **3** and $\mathbf{3_{Cl}}$.

Bond length [°]		
	3	$\mathbf{3_{Cl}}$*
Ru1—N1	2.078(3)	2.067 (3)
Ru1—N2	1.956(3)	1.953 (3)
Ru1—N3	2.065(3)	2.064 (3)
Ru1—N4	2.089(3)	2.079 (3)
Ru1—N5	2.035(3)	2.032 (3)
Ru1—Cl1	2.4078(9)	2.4205 (9)
Bond angles [°]		
N2—Ru1—N4	176.36(11)	177.28(12)
N2—Ru1—N1	79.55(11)	79.45(12)
N4—Ru1—N1	100.27(11)	101.42(12)
N2—Ru1—N3	79.16(11)	79.62(12)
N4—Ru1—N3	100.93(11)	99.35(12)
N1—Ru1—N3	158.70(10)	158.84(12)
N2—Ru1—N5	97.83(11)	99.50(12)
N4—Ru1—N5	78.55(11)	78.06(12)
N1—Ru1—N5	95.40(11)	84.91(12)
N3—Ru1—N5	86.88(12)	95.53(12)
N2—Ru1—Cl1	89.30(8)	88.44(9)
N4—Ru1—Cl1	94.33(8)	93.99(9)
N1—Ru1—Cl1	89.78(8)	96.82(8)
N3—Ru1—Cl1	90.58(8)	85.66(8)
Torsion angles [°]		
Ru1—N1—C5—C4	175.8 (2)	
Ru1—N1—C5—C6	-4.1 (3)	
Ru1—N2—C6—C7	-178.0 (2)	
Ru1—N2—C6—C5	2.1 (4)	
Ru1—N2—C10—C9	178.1 (2)	
Ru1—N2—C10—C11	-2.3 (4)	
Ru1—N3—C11—C12	175.1 (3)	
Ru1—N3—C11—C10	-3.4 (4)	

* Data obtained from reference [10].

Table S2. Observed *pseudo*-first order rate constants as a function of complex concentration for the reaction between complex [Ru(Cl-Ph-tpy)(en)Cl]Cl (**1**) and 5'-GMP (**L**) in 25 mM Hepes buffer (50 mM NaCl, pH = 7.2) at 37 ºC.

t (ºC)	C_L [10^{-3} M]	k_{obs} [10^{-3} s^{-1}]
37.0	5.00	3.10(3)
	4.10	2.40(2)
	3.15	2.15(3)
	2.20	1.50(3)
	1.30	1.10(2)
	0.75	0.80(3)

Table S3. Observed *pseudo*-first order rate constants as a function of complex concentration and temperature for the reaction between complex [Ru(Cl-Ph-tpy)(dach)Cl]Cl (**2**) and 5'-GMP (**L**) in 25 mM Hepes buffer (50 mM NaCl, pH = 7.2).

t (ºC)	$C_{\mathbf{L}}$ [10^{-3} M]	k_{obs} [10^{-3} s^{-1}]
15.0	5.00	0.96(2)
	4.10	0.88(3)
	3.15	0.64(2)
	2.20	0.50(3)
	1.30	0.37(3)
	0.75	0.34(3)
25.0	5.00	2.60(3)
	4.10	2.07(3)
	3.15	1.67(2)
	2.20	1.33(3)
	1.30	1.07(3)
	0.75	0.85(3)
37.0	5.00	4.00(3)
	4.10	3.40(2)
	3.15	2.90(3)
	2.20	2.00(3)
	1.30	1.40(3)
	0.75	1.20(3)

Table S4. Observed *pseudo*-first order rate constants as a function of complex concentration for the reaction between complex [Ru(Cl-Ph-tpy)(bpy)Cl]Cl (**3**) and 5'-GMP (**L**) in 25 mM Hepes buffer (50 mM NaCl, pH = 7.2) at 37 ºC.

t ºC	C_L [10^{-3} M]	k_{obs} [10^{-3} s^{-1}]
37.0	5.00	2.11(2)
	4.10	1.90(3)
	3.15	1.70(2)
	2.20	1.40(3)
	1.30	0.90(3)
	0.75	0.60(3)

Table S5. Observed *pseudo*-first order rate constants as a function of complex concentration for the reaction between complex [Ru(Cl-Ph-tpy)(en)Cl]Cl (**1**) and DNA-1 in Tris-HCl buffer (50 mM NaCl, pH = 7.2).

t ºC	C_1 [10^{-5} M]	k_{obs}[10^{-4} s^{-1}]
37.0	5.0	8.60(3)
	3.0	6.90(3)
	1.5	4.50(2)
	0.5	3.10(3)

Table S6. Observed *pseudo*-first order rate constants as a function of complex concentration for the reaction between complex [Ru(Cl-Ph-tpy)(en)Cl]Cl (**1**) and DNA-2 in Tris-HCl buffer (50 mM NaCl, pH = 7.2).

t ºC	C_1 [10^{-5} M]	k_{obs} [10^{-4} s^{-1}]
37.0	5.0	8.50(2)
	3.0	7.00(2)
	1.5	5.10(3)
	0.5	3.75(3)

Table S7. Observed *pseudo*-first order rate constants as a function of complex concentration for the reaction between complex [Ru(Cl-Ph-tpy)(en)Cl]Cl (**1**) and RNA in Tris-HCl buffer (50 mM NaCl, pH = 7.2).

t ºC	C_1 [10^{-5} M]	k_{obs} [10^{-4} s^{-1}]
37.0	5.0	9.34(3)
	3.0	7.15(3)
	1.5	4.45(2)
	0.5	3.41(3)

Table S8. Observed *pseudo*-first order rate constants as a function of complex concentration for the reaction between complex [Ru(Cl-Ph-tpy)(dach)Cl]Cl (**2**) and DNA-1 in Tris-HCl buffer (50 mM NaCl, pH = 7.2).

t ºC	C_2 [10^{-5} M]	k_{obs} [10^{-4} s^{-1}]
37.0	5.0	4.97(2)
	3.0	3.50(3)
	1.5	2.80(2)
	0.5	1.50(3)

Table S9. Observed *pseudo*-first order rate constants as a function of complex concentration for the reaction between complex [Ru(Cl-Ph-tpy)(dach)Cl]Cl (**2**) and DNA-2 in Tris-HCl buffer (50 mM NaCl, pH = 7.2).

t ºC	C_2 [10^{-5} M]	k_{obs} [10^{-4} s^{-1}]
37.0	5.0	4.50(3)
	3.0	3.40(2)
	1.5	2.80(2)
	0.5	2.10(3)

Table S10. Observed *pseudo*-first order rate constants as a function of complex concentration for the reaction between complex [Ru(Cl-Ph-tpy)(dach)Cl]Cl (**2**) and RNA in Tris-HCl buffer (50 mM NaCl, pH = 7.2).

t ºC	C_2 [10^{-5} M]	k_{obs} [10^{-4} s^{-1}]
37.0	5.0	7.40(2)
	3.0	5.40(3)
	1.5	4.00(3)
	0.5	2.50(3)

Table S11. Observed *pseudo*-first order rate constants as a function of complex concentration for the reaction between complex [Ru(Cl-Ph-tpy)(bpy)Cl]Cl (**3**) and DNA-1 in Tris-HCl buffer (50 mM NaCl, pH = 7.2).

t ºC	C_3 [10^{-5} M]	10^4 k_{obs}/s^{-1}
37.0	5.0	2.23(3)
	3.0	1.30(3)
	1.5	0.89(3)
	0.5	0.61 (2)

Table S12. Observed *pseudo*-first order rate constants as a function of complex concentration for the reaction between complex [Ru(Cl-Ph-tpy)(bpy)Cl]Cl (**3**) and DNA-2 in Tris-HCl buffer (50 mM NaCl, pH = 7.2).

t ºC	C_3 [10^{-5} M]	k_{obs} [10^{-4} s^{-1}]
37.0	5.0	2.10(2)
	3.0	1.60(2)
	1.5	1.20(3)
	0.5	0.78(3)

Table S13. Observed *pseudo*-first order rate constants as a function of complex concentration for the reaction between complex [Ru(Cl-Ph-tpy)(bpy)Cl]Cl (**3**) and RNA in Tris-HCl buffer (50 mM NaCl, pH = 7.2).

t ºC	C_3 [10^{-5} M]	k_{obs} [10^{-4} s^{-1}]
37.0	5.0	3.63(3)
	3.0	2.70(3)
	1.5	1.65(3)
	0.5	0.98(3)

Table S14. Observed *pseudo*-first order rate constants as a function of complex concentration for the reaction between complex [Ru(Cl-Ph-tpy)(en)Cl]Cl (**1**) and CT DNA in Tris-HCl buffer (50 mM NaCl, pH = 7.2).

t ºC	C_1 [10^{-5} M]	k_{obs} [10^{-1} s^{-1}]
37.0	5.00	1.54(2)
	4.00	1.39(3)
	3.00	1.07(3)
	1.50	0.83(2)
	0.50	0.65(3)

Table S15. Observed *pseudo*-first order rate constants as a function of complex concentration for the reaction between complex [Ru(Cl-Ph-tpy)(en)Cl]Cl (**1**) and HT DNA in Tris-HCl buffer (50 mM NaCl, pH = 7.2).

t ºC	C_1 [10^{-5} M]	k_{obs} [10^{-1} s^{-1}]
37.0	5.00	7.20(3)
	4.00	6.00(3)
	3.00	4.20(3)
	1.50	2.29(3)
	0.50	1.60(3)

Table S16. Observed *pseudo*-first order rate constants as a function of complex concentration for the reaction between complex [Ru(Cl-Ph-tpy)(dach)Cl]Cl (**2**) and CT DNA in Tris-HCl buffer (50 mM NaCl, pH = 7.2).

t ºC	C_2 [10^{-5} M]	k_{obs} [10^{-1} s^{-1}]
37.0	5.00	1.18(3)
	4.00	0.92(3)
	3.00	0.84(2)
	1.50	0.64(3)
	0.50	0.55(3)

Table S17. Observed *pseudo*-first order rate constants as a function of complex concentration for the reaction between complex [Ru(Cl-Ph-tpy)(dach)Cl]Cl (**2**) and HT DNA in Tris-HCl buffer (50 mM NaCl, pH = 7.2).

t ºC	C_2 [10^{-5} M]	k_{obs} [10^{-1} s^{-1}]
37.0	5.00	3.15(2)
	4.00	2.43(3)
	3.00	1.86(3)
	1.50	1.33(3)
	0.50	0.89(3)

Table S18. Observed *pseudo*-first order rate constants as a function of complex concentration for the reaction between complex [Ru(Cl-Ph-tpy)(bpy)Cl]Cl (**3**) and CT DNA in Tris-HCl buffer (50 mM NaCl, pH = 7.2).

t ºC	C_3 [10^{-5} M]	k_{obs} [10^{-3} s^{-1}]
37.0	5.00	1.60(2)
	4.00	1.40(2)
	3.00	1.07(2)
	1.50	0.79(3)
	0.50	0.68(3)

Table S19. Observed *pseudo*-first order rate constants as a function of complex concentration for the reaction between complex [Ru(Cl-Ph-tpy)(bpy)Cl]Cl (**3**) and HT DNA in Tris-HCl buffer (50 mM NaCl, pH = 7.2).

t ºC	C_3 [10^{-5} M]	k_{obs} [10^{-3} s^{-1}]
37.0	5.00	2.20(3)
	4.00	1.84(3)
	3.00	1.55(3)
	1.50	1.10(3)
	0.50	0.90(2)

2.3. A camphor based 1,3-diamine Ru(II) terpyridine complex: synthesis, characterization, kinetic investigation and DNA binding

Within the paper the synthesis and reactivity of a new ruthenium(II) complex with a bidentate enantiopure camphor based diamine ligand was described. UV-Vis and NMR measurements were performed for the characterization of the new complex, and also the kinetic studies with guanosine-5'-monophosphate were monitored by the UV-Vis spectroscopy. DNA interactions were performed with new ruthenium(II) complex and calf thymus DNA.

Participations in the publication:

M. M. Milutinović, R. Wilhelm – Synthesis, characterization, kinetic investigation by UV-Vis spectroscopy, implementation of all results and writing paper.

DOI: 10.1039/C7NJ04674J

NJC

LETTER

View Article Online
View Journal | View Issue

Cite this: *New J. Chem.*, 2018, **42**, 7607

Received 29th November 2017,
Accepted 24th January 2018

DOI: 10.1039/c7nj04674j

rsc.li/njc

A camphor based 1,3-diamine Ru(II) terpyridine complex: synthesis, characterization, kinetic investigation and DNA binding†

Milan M. Milutinović, [ab] Živadin D. Bugarčić ‡[b] and René Wilhelm *[a]

The synthesis and reactivity of a new ruthenium(II) terpyridine complex with a bidentate enantiopure camphor based diamine ligand is described. Reactivity measurements of the Ru(II) complex showed a high affinity towards guanosine-5′-monophosphate as a model for DNA bases. Furthermore, the Ru(II) complex was found to interact with CT-DNA. This suggests the high potential of the newly synthesized ruthenium complex as an antitumor agent.

Over the last few decades, the investigation of compounds that show great potential as anticancer agents has become more and more important.[1–4] Recently, ruthenium complexes have shown to be leading candidates as anticancer agents.[5–8] Simultaneously, many chiral based diamines have found application in areas such as pharmaceuticals, fine chemistry and perfumes.[9] The nature of both ligand and metal plays a crucial role in metal complexes. The biological activities of many Schiff base metal complexes have been recognized for their antifungal, antiviral, antimicrobial, antioxidant, anti-inflammatory, insecticidal and plant growth regulation activities.[9] Camphor based ligands can be electronically and sterically fine-tuned by varying the structures of the amine substituents. Camphoric 1,3-diamine **B** (Scheme 1) has been applied for the synthesis of functional Schiff-base metal complexes, *N*-heterocyclic carbenes and supramolecular complexes.[10] Various types of metals such as Ni, Co, Zn, Fe, Cu, *etc.*, which are considered essential to life, have been used in the synthesis with these types of ligands.[11] In contrast, ruthenium complexes with 1,3-diamine camphor based ligands are relatively limited.[12] Ruthenium complexes with tridentate polypyridyl ligands have emerged as leading candidates for their use as anticancer drugs.[13] The roles of both the metal and the ligands in recognition processes under conditions of biological relevance

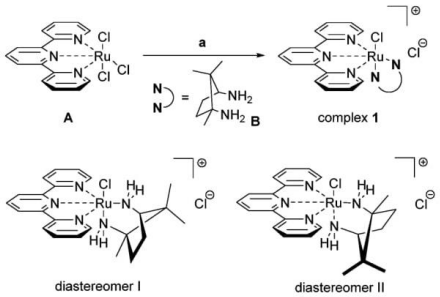

Scheme 1 Synthetic pathways for the preparation of complex **1**. *Reagents and conditions*: (**a**) *N*–*N* (1.2 eq.; *N*–*N* = κ^2(1*S*,3*R*)-NH_2/NH_2), EtOH/H_2O (3 : 1), Et_3N (3.0 eq.), and LiCl (10.0 eq.).

is the key to such discovery. The understanding of thermodynamics and kinetics of metal complex reactions is considered to be of importance as well.[14,15]

With the aim of expanding the structure–activity relationship of ruthenium(II) complexes and investigating bidentate chiral enantiopure diamine camphor based ligands, a Ru(II) terpyridine complex **1** of the type $[Ru(tpy)(N–N)Cl]^+$ was synthesized (where tpy = 2,2′:6′,2″-terpyridine, *N*–*N* = κ^2(1*S*,3*R*)-$NH_2 \cap NH_2$)[16,17] by the treatment of $[Ru^{III}(tpy)Cl_3]$ **A** with the camphor based 1,3-diamine ligand **B** in a mixture of EtOH/H_2O (3 : 1) under reflux in the presence of Et_3N and LiCl (Scheme 1). The resulting new ruthenium(II) terpyridine complex **1** was fully characterized by NMR spectroscopy, ESI-MS spectrometry and UV-Vis spectrophotometry. The chemical behaviour of the new complex in aqueous solution and its binding properties towards biomolecules as model DNA bases such as 5′-GMP were investigated by UV-Vis spectroscopy. In addition, the DNA binding ability (CT-DNA) and properties of the new complex have been investigated.

Electrospray (ESI)-MS analysis of the complex demonstrated the formation of the desired complex by displaying a prominent peak at *m*/*z* 512.1170 corresponding to a molecular ion peak

[a] *Department of Organic Chemistry, University of Paderborn, Warburgerstraße 100, 33098 Paderborn, Germany. E-mail: rene.wilhelm@uni-paderborn.de*
[b] *Faculty of Science, University of Kragujevac, R. Domanovića 12, 34000 Kragujevac, Serbia*

† Electronic supplementary information (ESI) available: Experimental details and spectral data, Fig. S1–S4. See DOI: 10.1039/c7nj04674j

‡ Sadly, Prof. Živadin D. Bugarčić died in September 2017.

$[C_{23}H_{29}ClN_5Ru]^+$ (Fig. S2, ESI†). In the NMR spectra it could be observed by COSY and HMBC that two diastereomers of complex **1** were formed in a ratio of 1 : 1 (Fig. S1, ESI†). Interestingly, the 10-methyl group of the camphor fragment of diastereomer II was significantly shifted downfield to 1.75. This can be due to the *trans*-effect. In diastereomer II the 10-methyl group is next to the amino function *trans* to the terpyridine ligand of the ruthenium resulting in a larger downfield shift of the methyl group. In comparison, this signal occurs for diastereomer I at 0.83. Complementarily, it can be found that the single proton on the opposite side of the camphor fragment of diastereomer I is significantly shifted downfield and occurs between 3.80 and 3.78 while for diastereomer 2 between 2.48 and 2.43.

Complex **1** was investigated quantitatively in the kinetics of aquation by UV-Vis spectroscopy at 25 °C in a 0.1 mM solution. The calculation of the equilibrium constants K_{aq} was achieved *via* rapid reversion of the equilibrium. The UV-Vis spectra of complex **1** showed a significant time-dependent change in the region 200–800 nm (Fig. S3, ESI†) with clean isosbestic points that suggest the occurrence of a single hydrolytic process (*i.e.* conversion of the initial chlorido complex into the corresponding aqua species **1aq**, respectively). The wavelength corresponding to the maximum change in the absorption (difference spectra) was selected for kinetic studies (464 nm for complex **1**). The time course of the absorbance followed the first-order kinetics (Fig. 1), which afforded the rate constant k_{H_2O} provided in Table 1.

It can be seen that complex **1** hydrolyses slightly slower than similar Ru-tpy analogues like [Ru(Cl-tpy)(en)Cl]Cl[18] and [Ru(Cl-tpy)(dach)Cl]Cl ($2.52–3.94 \times 10^{-3}$ s^{-1})[19] but slightly faster like [Ru(tpy)(en)Cl]Cl[20] as well as other similar ruthenium analogues such as [Ru(Cl-Ph-tpy)(en)]Cl and [Ru(Cl-Ph-tpy)(dach)]Cl ($4.90–6.10 \times 10^{-3}$ s^{-1}),[16] and *ca.* two orders of magnitude higher than those of the established anticancer drug cisplatin (6.32×10^{-5} s^{-1} and 2.5×10^{-5} s^{-1} for the first and second aquation process, respectively).[21] It has been proved that fast aquation of complexes might lead to reduced activity and/or to increased toxicity due to their fast binding to biomolecules other than those responsible for tumour proliferation such as DNA. Considering this fact and the implications of our results, the new complex **1** can be suggested as a potential candidate as an anticancer drug with low toxicity. The aquation studies of complex **1** in other biologically relevant solutions such as a buffer solution (5 mM tris–HCl, pH ≈ 7.4) was investigated next. The results show that complex **1** has poor stability in the selected buffer solutions, which is indicated by a decrease in the intensity of the bands and a hypsochromic shift of the MLCT transition band in the spectrum.[22]

Table 1 Rate constants for aquation and half-life at 25 °C in H_2O for complex **1**

	Isosbestic points (nm)	k_{obs} (10^{-3} s^{-1})	$(t_{1/2})_{H_2O}$ (min)
1	358, 402, 500	2.00 ± 0.01	5.80 ± 0.03

Further investigation of complex **1** was related to the addition of excess of chloride (NaCl) where the observed spectral changes are the characteristics of the reformation of the chloride complex (Fig. 2). Based on eqn (1), the rate law for the reversible aquation of complex **1** is given in eqn (2) with $k_2 = 1.51 \times 10^{-3}$ s^{-1} and $k_1 = 3.42 \times 10^{-3}$ M^{-3} s^{-1} at ambient temperature based on the plot shown in Fig. 3.

Based on this data, the equilibrium constant for the aquation reaction is $K_1 = k_2/k_1$, where $K_1 = 0.44 \pm 0.02$ M at ambient temperature. It can be seen from K_1 that a high concentration of chloride is required to prevent the spontaneous aquation reaction. To reach an equilibrium mixture of the aqua and chlorido complex, 250 mM to 1.5 M of chlorides is necessary, which is presented in Table 2. Typical spectral values were obtained for the aquation reactions at different added chloride concentrations.

$$[Ru(tpy)(N{-}N)Cl]^+ + H_2O \underset{k_1}{\overset{k_2}{\rightleftharpoons}} [Ru(tpy)(N{-}N)(H_2O)] + Cl^- \quad (1)$$

$$k_{obs} = k_2 + k_1[Cl^-] \quad (2)$$

The substitution reactions of Cl^- with 5′-GMP in complex **1** were investigated by UV-Vis spectrophotometrically following the change in absorbance at selected wavelengths, corresponding to

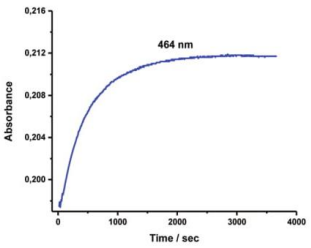

Fig. 1 Time-dependence of the absorbance during the aquation of complex **1** at 464 nm and 0.01 mM in H_2O at room temperature. The full line represents the computer fit giving the first-order rate constant for the aquation of complex **1** ($k_{obs} = 2.0 \pm 0.01 \times 10^{-3}$ s^{-1}).

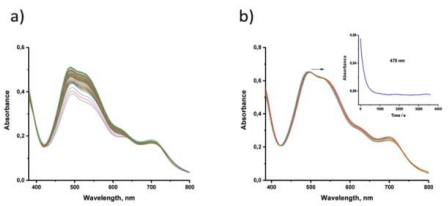

Fig. 2 (a) Typical UV/Vis spectral changes observed during the spontaneous aquation of complex **1** in the absence of added chloride (NaCl). Experimental conditions: [**1**] = 2.5×10^{-4} M and t = 25 °C; spectra recorded every 40 s; (b) spectral changes recorded for the anation of complex **1** by chloride (NaCl). Experimental conditions: [**1**] = 2.5×10^{-4} M, t = 25 °C, and [Cl^-] = 0–3.0 M; spectra recorded every 40 s.

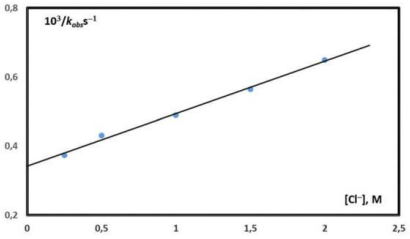

Fig. 3 Dependence of k_{obs} on [Cl⁻] for the anation of complex **1** by chloride in H_2O: experimental conditions: [**1**] = 2.5 × 10^{-4} M at ambient temperature.

Table 2 Wavelength maximum shifts of major peaks observed as a result of aquation of complex **1** at different chloride (NaCl) concentrations at 25 °C

[Cl⁻], M	0	0.03	0.06	0.12	0.25	0.5	1.0	1.5	>3.0
λ (nm)	489.0	489.2	491.7	492.8	495.2	495.5	497.1	497.3	497.4
	526.0	526.3	528.1	530.5	533.0	534.7	536.9	537.0	537.1

the maximum change as a function of time in water. In the present study, the direct nucleophilic attack proceeds in a reversible manner which can be seen from the proposed reaction pathways for the observed substitution processes using eqn (3). All kinetic experiments were performed under *pseudo*-first-order conditions, for which the concentration of the Ru^{II} complex was always in at least a 10-fold excess (Fig. 4).

$$[\mathrm{Ru(tpy)}(N\!-\!N)(\mathrm{H_2O})]^{2+} + 5'\text{-GMP} \xrightarrow{k_2} [\mathrm{Ru(tpy)}(N\!-\!N)(5'\text{-GMP})] + \mathrm{H_2O} \quad (3)$$

$$k_{obs} = k_2[5'\text{-GMP}] \quad (4)$$

The rate constants for the substitution were determined from the plot of the linear dependence of k_{obs} *versus* the total complex concentration, according to eqn (4), under *pseudo*-first-order conditions. The rate constants for the substitution reaction between complex **1** and 5′-GMP are presented in Table 3. The activation parameters $\Delta H_2^{\neq}$ and $\Delta S_2^{\neq}$ were calculated for complex **1** using the Eyring equation (Fig. S4, ESI†). For the reaction with 5′-GMP, $\Delta H_2^{\neq} = 41 \pm 3$ kJ mol^{-1} and $\Delta S_2^{\neq} = -130 \pm 10$ J K^{-1} mol^{-1} were found. The negative value of $\Delta S_2^{\neq}$ clearly suggests and supports an associative mechanism for the substitution process.

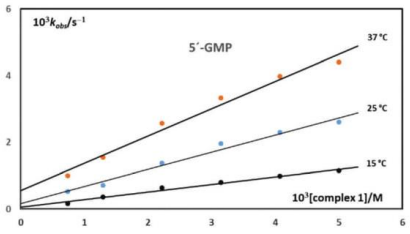

Fig. 4 *Pseudo*-first-order rate constants plotted as a function of complex **1** concentration for the substitution reactions of complex **1** with 5′-GMP in H_2O.

Due to the obtained results for the rate constants with 5′-GMP, it can be concluded that the activity of the complex **1** is influenced by the size of the new chelating diamine ligand. Next to the sterical influence of the diamine ligand **B**, a slight increase in electron density can also be anticipated compared to the often applied ethylenediamine ligands in similar complexes.[23,24] The increased electron density in ligand **B** would be due to the fact that the amino groups are attached to a secondary carbon atom and a tertiary carbon atom, which results in a stronger +*I* effect. Complex **1** reacts in a similar way to the reported [Ru(Cl-tpy)(en)Cl]Cl and [Ru(Cl-tpy)(bpy)Cl]Cl complexes, but faster than a [Ru(Cl-Ph-tpy)(bpy)Cl]Cl complex.[23,24] It could be that the steric requirements of metal complex **1** itself directly influence the rate of 5′-GMP binding.

As shown in our previous work, Ru-(Ph-tpy-Cl) complexes both intercalate and covalently bind to CT-DNA.[16,24] Considering these facts, we have extended here the investigation of complex **1** with DNA-binding studies. DNA is a critical therapeutic target that is responsible for a wide variety of intracellular interactions.[25–29] Using complex **1**, UV-Vis titrations were carried out. The intrinsic equilibrium binding constant (K_b) was evaluated. The metal complex absorption titration studies were carried out at room temperature using a fixed concentration of complex **1** (12.5 μM) in PBS buffer and varying the amount of CT-DNA (0–20 μM).[30] The absorption intensity of the complex may decrease (hypsochromism) or increase (hyperchromism) with a slight increase in the absorption wavelength (bathochromism) upon addition of DNA.[16] The three new bands at 275 nm, 318 nm and 495 nm present a hyperchromism upon addition of increasing amounts of CT-DNA (Fig. S5, ESI†), suggesting a strong binding to CT-DNA. Moreover, the band at 495 nm presents a red shift (bathochromism) of 5 nm (up to 490 nm), suggesting the stabilization of the CT-DNA duplex. Nevertheless, the exact mode of binding cannot be surely proposed using UV-Vis spectroscopic methods.[16,31,32] The value of K_b of complex **1** was (2.2 ± 0.2) × 10^5 M^{-1} (Table 4) and was calculated using the equation (Fig. S1, ESI†) and the plot shown in Fig. S6 of the ESI†. K_b is similar to Ru^{II} analogues,[23] which are also believed to bind to DNA in a bifunctional manner (covalently and non-covalently) and have K_b values (2.1–10.0 × 10^4 M^{-1}) which are *ca.* one order of magnitude lower than our complex **1**. Therefore, we can suggest the great importance of the bidentate diamine camphor based ligand **B** due to the possible significant effect on the DNA binding activity.

Table 3 Rate constants for the substitution reactions of complex **1** with 5′-GMP in H_2O with different temperatures

	t (°C)	k_2 (10^{-1} M^{-1} s^{-1})	$\Delta H_2^{\neq}$ (kJ mol^{-1})	$\Delta S_2^{\neq}$ (J K^{-1} mol^{-1})
1	37	8.16 ± 0.20		
	25	5.14 ± 0.10	41 ± 3	−130 ± 10
	15	2.28 ± 0.30		

Table 4 The DNA-binding constant (K_b) and the Stern–Volmer constant (K_{SV}) from the EthBr–DNA fluorescence for complex **1**

1	K_b (M^{-1})	K_{SV} (M^{-1})
CT-DNA	$(2.2 \pm 0.2) \times 10^5$	$(4.6 \pm 0.1) \times 10^4$

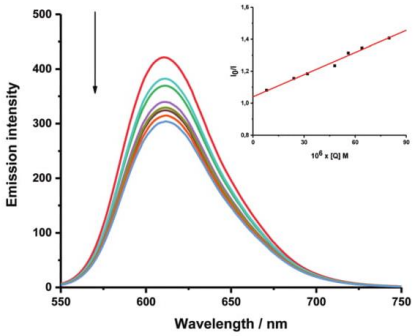

Fig. 5 Emission spectra of EthBr bound to DNA in the presence of complex **1**. [EthBr] = 80 μM, [DNA] = 80 μM, and [**1**] = 0–80 μM. λ_{ex} = 527 nm. The arrow shows the intensity changes upon increased concentrations of complex **1**. Inset: Plot of I_0/I *versus* [Q].

The interaction of complex **1** with CT-DNA has also been investigated by ethidium bromide (EthBr) displacement studies, which provides strong evidence about the competitive binding of drugs with CT-DNA. EthBr is a classical intercalator that exhibits a significant fluorescence emission intensity when it intercalates into the base pairs of DNA. DNA-induced EthBr fluorescence emission could be quenched after the addition of complexes capable to form strong interactions with DNA, replacing EthBr.[33] The significant decrease of the intensity of the emission band at 612 nm after the addition of increasing amounts of complex **1** shows the competition of complex **1** in binding to DNA (Fig. 5). The Stern–Volmer quenching constant (K_{SV}) is calculated from the slopes of the plots I_0/I *vs.* [Q] (see the inset in Fig. 5) using eqn ((S2), ESI†). The value of K_{SV} is presented in Table 4.

Conclusions

We have synthesized a new ruthenium(II) terpyridine complex **1** with a bidentate diamine camphor based ligand. Complex **1** was characterized with different spectroscopic techniques. Our constant interest to design efficient compounds for possible anticancer treatment motivated us to study the chemical behaviour of complex **1** in aqueous solutions. The influence of chloride ions in an aqueous solution, the binding affinity toward the nitrogen donor biomolecule 5′-GMP, and the affinity to bind with DNA were studied. Chiral ancillary ligands that have more steric bulk or the addition of stereospecific functional groups may result in an increase in reactivity with biomolecules and DNA, which would further result in an increase of cytotoxicity as well. Complex **1** bears novelty as a good binding agent with CT-DNA and it is a promising candidate to be a potential antitumor agent. The obtained results represent a further improvement in the structural–pharmacological relationship needed for the design of new ruthenium agents.

Conflicts of interest

There are no conflicts to declare.

Acknowledgements

This publication has been funded with support from the European Commission under the Erasmus Mundus project Green-Tech-WB: Smart and Green technologies for Innovative and Sustainable Societies in Western Balkans (551984-EM-1-2014-1-ES-ERA MUNDUS-EMA2). This publication is dedicated to Prof. Dr Živadin D. Bugarčić who passed away and was one of the supervisors of M. Milutinović.

Notes and references

1 *Bioinorganic Medicinal Chemistry*, ed. E. Alessio, Wiley-VCH, Weinheim, 2011, ch. 1–4.
2 P. E. N. Barry and J. P. Sadler, *Chem. Commun.*, 2013, **49**, 5106; L. Ronconi and J. P. Sadler, *Coord. Chem. Rev.*, 2007, **251**, 1633.
3 R. Trondl, P. Heffeter, C. R. Kowol, M. A. Jakupec, W. Berger and B. K. Keppler, *Chem. Sci.*, 2014, **5**, 2925.
4 C.-H. Leung, H.-J. Zhong, D. D.-H. Chan and D.-L. Ma, *Coord. Chem. Rev.*, 2013, **257**, 1764.
5 E. Antonarakis and A. Emadi, *Cancer Chemother. Pharmacol.*, 2010, **66**, 1.
6 R. E. Aird, J. Cummings, A. A. Ritchie, M. Muir, R. E. Morris, H. Chen, P. J. Sadler and D. I. Jodrell, *Br. J. Cancer*, 2002, **86**, 1652.
7 O. Novakova, J. Kasparkova, O. Vrana, P. M. van Vliet, J. Reedijk and V. Brabec, *Biochemistry*, 1995, **34**, 12369.
8 E. Corral, A. C. G. Hotze, H. D. Dulk, A. Leczkowska, A. Rodger, M. J. Hannon and J. Reedijk, *J. Biol. Inorg. Chem.*, 2009, **14**, 439.
9 X. Ji and H. Huang, *Org. Biomol. Chem.*, 2016, **14**, 10557; A. Prakash and D. Adhikari, *Int. J. ChemTech Res.*, 2011, **3**, 1891; D. Murtinho, Z. N. da Rocha, A. S. Pires, R. P. Jimenez, A. M. Abrantes, M. Laranjo, A. C. Mamede, J. E. Casalta-Lopes, M. F. Botelho, A. A. C. C. Pais, S. C. C. Nunes, H. D. Burrows, T. Costa and M. E. S. Serra, *Appl. Organometal. Chem.*, 2015, **29**, 425.
10 E. Rais, U. Flörke and R. Wilhelm, *Synthesis*, 2017, 2852; P. D. Newman, K. J. Cavell and B. M. Kariuki, *Organometallics*, 2010, **29**, 2724; P. D. Newman, K. J. Cavell and B. M. Kariuki, *Dalton Trans.*, 2012, **41**, 12395.
11 M. E. S. Serra, D. Murtinho, Z. N. da Rocha, A. S. Pires, J. G. Baptista, A. M. Abrantes, M. Laranjo, J. E. Casalta-Lopes, M. F. Botelho, A. A. C. C. Pais, S. C. C. Nunes, H. D. Burrows

and T. Costa, *Polyhedron*, 2017, **137**, 147; D. Jaramillo, D. P. Buck, J. G. Collins, R. R. Fenton, F. H. Stootman, N. J. Wheate and J. R. Aldrich-Wright, *Eur. J. Inorg. Chem.*, 2006, 839.
12 J.-L. Yu., R. Guo, H. Wang, Z.-T. Li and D.-W. Zhang, *J. Organomet. Chem.*, 2014, **768**, 36.
13 W. H. Ang. and P. J. Dyson, *Eur. J. Inorg. Chem.*, 2006, 4003; Z. Zhao, Z. Luo, Q. Wu, W. Zheng, Y. Feng and T. Chen, *Dalton Trans.*, 2014, **43**, 1.
14 N. P. E. Barry and P. J. Sadler, *Pure Appl. Chem.*, 2014, **86**, 1897.
15 F. C. Abreu, P. A. L. Ferraz and M. O. F. Goulart, *J. Braz. Chem. Soc.*, 2002, **13**, 19.
16 M. M. Milutinović, A. Rilak, I. Bratsos, O. Klisurić, M. Vraneš, N. Gligorijević, S. Radulović and Ž. D. Bugarčić, *J. Inorg. Biochem.*, 2017, **169**, 1.
17 M. Koppenwallner, E. Rais, M. Uzarewicz-Baig, S. Tabassum, M.-A. Gilani and R. Wilhelm, *Synthesis*, 2015, 789.
18 P. C. Bruijnincx and P. J. Sadler, *Curr. Opin. Chem. Biol.*, 2008, **12**, 197.
19 Y. K. Yan, M. Melchart, A. Habtemariam and P. J. Sadler, *Chem. Commun.*, 2005, 4764.
20 M. Chrzanowska, A. Katafias, O. Impert, A. Kozakiewicz, A. Surdykowski, P. Brzozowska, A. Franke, A. Zahl, R. Puchta and R. Eldik, *Dalton Trans.*, 2017, **46**, 10264.
21 S. E. Miller and D. A. House, *Inorg. Chim. Acta*, 1991, **187**, 125.
22 P. Čanović, A. Rilak Simović, S. Radisavljević, I. Bratsos, N. Demitri, M. Mitrović, I. Zelen and Ž. D. Bugarčić, *J. Biol. Inorg. Chem.*, 2017, **22**, 1007.
23 A. Rilak, I. Bratsos, E. Zangrando, J. Kljun, I. Turel, Ž. D. Bugarčić and E. Alessio, *Inorg. Chem.*, 2014, **53**, 9069.
24 M. M. Milutinović, S. K. C. Elmroth, G. Davidović, A. Rilak, O. Klisurić, I. Bratsos and Ž. D. Bugarčić, *Dalton Trans.*, 2017, **46**, 2360.
25 J. E. Quin, J. R. Devlin, D. Cameron, K. M. Hannan, R. B. Pearson and R. D. Hannan, *Biochim. Biophys. Acta, Mol. Basis Dis.*, 2014, **1842**, 802.
26 V. Brabec, *Prog. Nucleic Acid Res. Mol. Biol.*, 2002, **71**, 1.
27 C. X. Zhang and S. J. Lippard, *Curr. Opin. Chem. Biol.*, 2003, **7**, 481.
28 V. Brabec and O. Novakova, *Drug Resist. Updat.*, 2006, **9**, 111.
29 J. Liu, W. Zheng, S. Shi, C. Tan, J. Chen, K. Zheng and L. Ji, *J. Inorg. Biochem.*, 2008, **102**, 193.
30 E. C. Long and J. K. Barton, *Acc. Chem. Res.*, 1990, **23**, 271; R. F. Pasternack, E. J. Gibbs and J. Villafranca, *J. Biochem.*, 1983, **22**, 251.
31 A. Tarushi, E. Polatoglou, J. Kljun, I. Turel, G. Psomas and D. P. Kessissoglou, *Dalton Trans.*, 2011, **40**, 9461.
32 A. Tarushi, K. Lafazanis, J. Kljun, I. Turel, A. A. Pantazaki, G. Psomas and D. P. Kessissoglou, *J. Inorg. Biochem.*, 2013, **121**, 53.
33 S. Dhar, M. Nethaji and A. R. Chakravarty, *J. Inorg. Biochem.*, 2005, **99**, 805.

Electronic Supplementary Information (ESI)

Camphor based 1,3-diamine Ru(II) terpyridin complex: Synthesis, characterization, kinetic investigation and DNA binding

Milan M. Milutinović,[a,b] Živadin D. Bugarčić [b,†] and René Wilhelm[a,*]

[a] Department of Organic Chemistry, University of Paderborn, Warburger Straße 100, 33098 Paderborn, Germany, email: rene.wilhelm@uni-paderborn.de

[b] Faculty of Science, University of Kragujevac, R. Domanovića 12, 34000 Kragujevac, Serbia

Electronic Supplementary Information (ESI)

Experimental part:

General Experimental. All commercially available chemicals were used without further purification. Silica gel 60 (0.063-0.040 mm particle size) was used for column chromatography. Thin layer chromatography was performed on plates from Merck (Silica gel 60, F254). Substances were detected under UV-light at 254 nm. NMR spectra were recorded at 30 °C on a Bruker Avance 500 spectrometer (^{1}H-NMR: 700 MHz; ^{13}C-NMR: 175 MHz; ^{15}N-NMR: 70 MHz). The NMR signals are referenced to the residual proton or carbon signals of the deuterated solvent (^{1}H- and ^{13}C-NMR) and are reported in ppm relative to TMS. Liquid ammonia was used as an external reference for ^{15}N-NMR. Mass spectrometry was carried out on Waters Quadrupole-ToF Synapt 2G using electrospray ionization (ESI). Synthesis of the ligand is prepared according to the literature procedure.[S1]

Preparation of the ligand and complex

Ruthenium(II) terprydine complex **1** was synthesized by a literature method described earlier.[S2] $RuCl_3$ x 3 H_2O (1 mmol) was dissolved in 139.0 mL of ethanol and the solution was refluxed until the color of the solution changed from brown to green (*ca.* 2h). Terpyridine, tpy, (1 mmol) was added and reflux continued for 5 h where the color of the solution turned again to brown with a formation of the product as a brown solid. The brown solid is [Ru(tpy)Cl_3] complex **A** which was used without further purification. **A** (0.181 mmol), *N-N* ligand (0.218 mmol) **B**, LiCl (1,814 mmol) and Et_3N (0.544 mmol) were mixed in a 20 mL solution of EtOH/H_2O which afforded ruthenium(II) complex **1** as a dark purple liquid. The product was purified via column chromatography on silica gel using dichloromethane/methanol (75:25, *v/v*) as eluent. The purple fraction was collected and the solvent removed to give a purple solid of complex **1** (yield 68%, 0.123 mmol) (Scheme 1).

^{1}H-NMR (CD_3OD) δ [ppm] = 9.35 (d, *J* = 5 Hz, 1H, Dia2), 9.29 (d, *J* = 5 Hz, 1H, Dia1), 9.18 (d, *J* = 5 Hz, 1H, Dia2), 9.12 (d, *J* = 5 Hz, 1H, Dia1), 8.43-8.37 (m, 8H, Dia1+Dia2), 7.98-7.93 (m, 4H, Dia1+Dia2), 7.77-7.73 (m, 2H, Dia1+Dia2), 7.63-7.60 (m, 4H, Dia1+Dia2), 4.48 (s, br, NH), 3.80-3.78 (m, 1H, Dia1), 2.48-2.43 (m, 1H, Dia2), 2.40-2.39 (m, 1H, Dia2), 2.26-2.23 (m, 2H, Dia1), 2.07-2.02 (m, 1H, Dia2), 1.75 (s, 3H, Dia2), 1.70-1.67 (m, 1H, Dia2), 1.51-1.46 (m, 1H, Dia1), 0.93 (s, 3H, Dia1), 0.91 (s, 3H, Dia2), 0.90 (s, 3H, Dia1), 0.86 (s, 3H, Dia2), 0.83 (s, 3H, Dia1), 0.74-0.71 (m, 1H, Dia1), 0.47-0.42 (m, 1H, Dia2)

^{13}C-NMR (CD_3OD) δ [ppm] = 162.6 (q), 162.4 (q), 162.3 (q), 162.2 (q), 162.1 (q), 162.0 (q), 161.8 (q), 161.5 (q), 155.7 (+), 155.4 (+), 155.2 (+), 137.4 (+), 137.2 (+), 137.1 (+), 137.0 (+), 131.3 (+), 131.2 (+), 127.4 (+), 127.3 (+), 127.1 (+), 123.7 (+), 123.6 (+), 123.5 (+), 122.9 (+), 122.8 (+), 122.3 (+), 122.2 (+), 65.6 (+), 65.5 (q), 64.5 (q), 63.8 (+), 48.6 (+), 48.4 (+), 36.7 (-), 36.3 (-), 28.8 (-), 27.7 (-), 27.3 (+), 26.9 (+), 24.4 (+), 23.1 (+), 16.9 (+), 16.5 (+), 9.2 (q).

^{15}N-NMR (CD_3OD) δ [ppm] = 294, 248, 247, 19, –5.

HRMS (ESI) m/z calcd for $C_{23}H_{29}ClN_5Ru$ 512.1155 $[M]^+$, found: 512.1170.

Electronic Supplementary Information (ESI)

Fig. S1 NMR spectrums of complex **1** in CD_3OD at ambient temperature.

1H-NMR

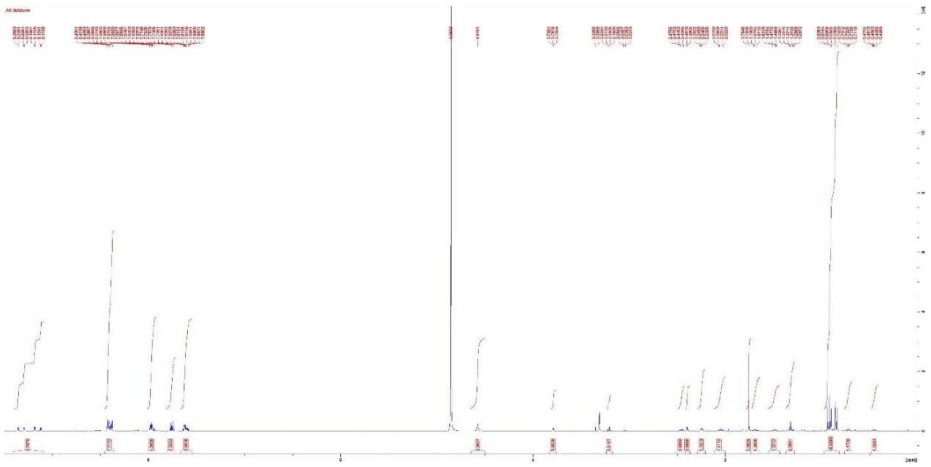

13C-NMR

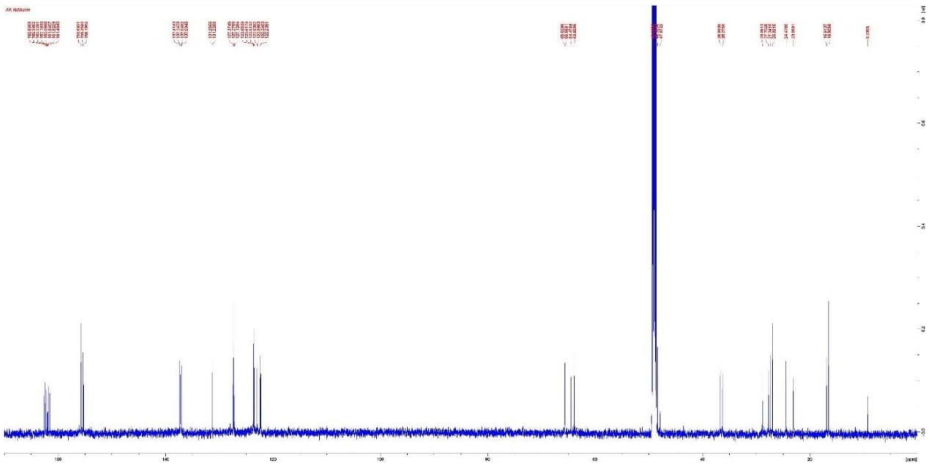

Fig. S2 Electrospray (ESI)-MS spectrum of complex **1**.

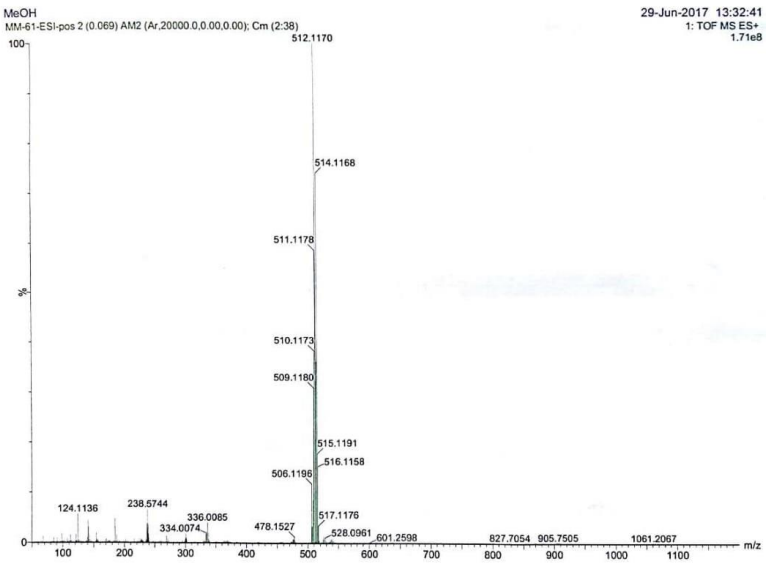

Elemental Composition Report **Page 1**

Single Mass Analysis
Tolerance = 10.0 PPM / DBE: min = -1.5, max = 50.0
Element prediction: Off
Number of isotope peaks used for i-FIT = 3

Monoisotopic Mass, Odd and Even Electron Ions
22 formula(e) evaluated with 1 results within limits (up to 50 closest results for each mass)
Elements Used:
C: 0-23 H: 0-29 N: 0-5 Cl: 0-1 Ru: 0-1

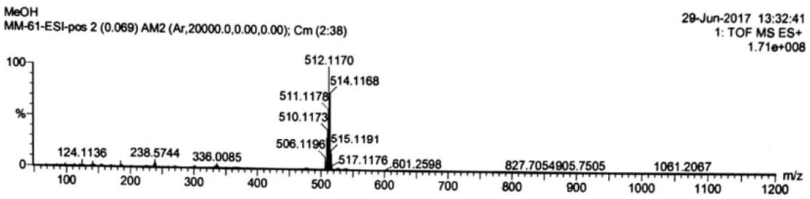

Minimum:				-1.5				
Maximum:		5.0	10.0	50.0				
Mass	Calc. Mass	mDa	PPM	DBE	i-FIT	Norm	Conf(%)	Formula
512.1170	512.1155	1.5	2.9	11.5	695.3	n/a	n/a	C23 H29 N5 Cl Ru

Fig. S3 Time evolution of the UV-Vis (top row). Experimental conditions and UV-Vis difference spectra (bottom row, $\Delta A = A_t - A_0$, where A_t = absorbance at time t and A_0 = absorbance at the time at which the first spectrum was recorded) during the aquation of the complex **1** (0.1 mM) in H_2O at room temperature.

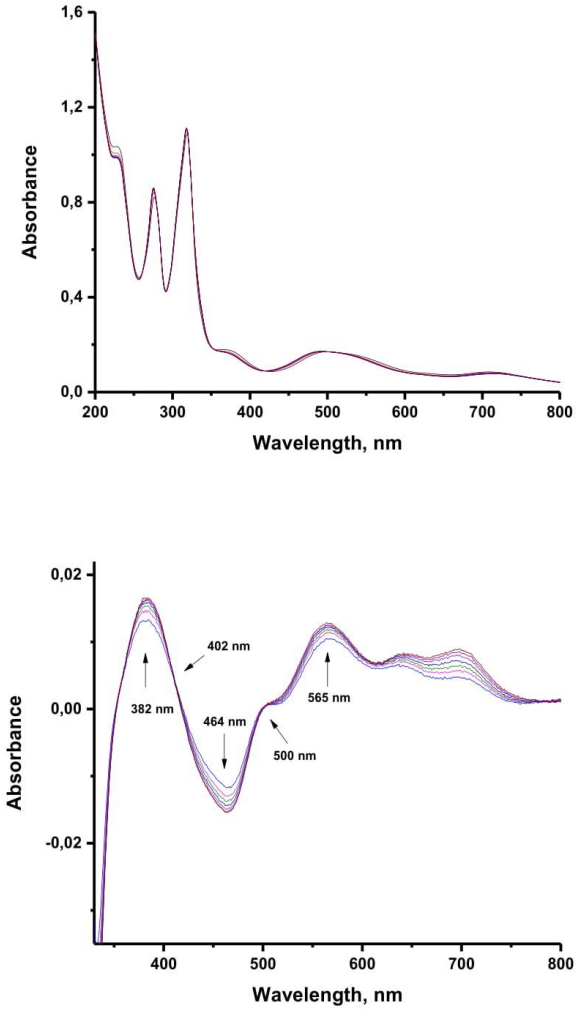

Fig. S4 *Eyring* plot for the reactions of complex **1** with 5'-GMP in H_2O.

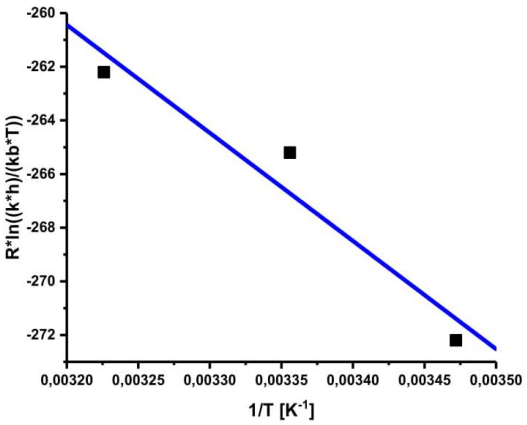

DNA-binding studies

Calculation of DNA-binding constant

In order to compare quantitatively the binding strength of the complexes, the intrinsic binding constants K_b were determined by monitoring the changes in absorption at the MLCT band with increasing concentration of CT-DNA using the following equation (S1):[S3]

$$[DNA]/(\varepsilon_a - \varepsilon_f) = [DNA]/(\varepsilon_b - \varepsilon_f) + 1/[K_b(\varepsilon_b - \varepsilon_f)] \quad (S1)$$

K_b is given by the ratio of slope to the *y* intercept in plots $[DNA]/(\varepsilon_a - \varepsilon_f)$ *versus* [DNA] (**Fig. S6**), where [DNA] is the concentration of DNA in base pairs, $\varepsilon A = A_{obs}/[complex]$, ε_f is the extinction coefficient for the unbound complex and ε_b is the extinction coefficient for the complex in the fully bound form.

Stern-Volmer equation for EB competitive studies

The relative binding of complexes to CT-DNA is described by Stern-Volmer equation (S2):[S4]

$$I_0/I = 1 + K_{sv}[Q] \quad (S2)$$

Where, I_0 and I are the emission intensities in the absence and the presence of the quencher (complex **1**), respectively, [Q] is the total concentration of quencher, K_{sv} is the dynamic quenching constant. (**Fig. 5**).

Fig. S5 Absorption spectra of the complex **1** in PBS buffer upon addition of calf thymus DNA; [**1**] = 1.25 x 10^{-5} M, [CT-DNA] = (0.12-1.25) x 10^{-5} M. Arrow shows the absorbance changing upon increasing DNA concentrations.

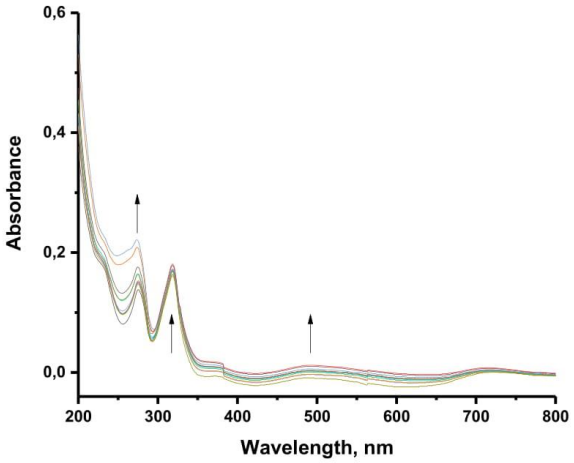

Fig. S6 Plot of [DNA]/($\varepsilon_a - \varepsilon_f$) versus [DNA] for the complexes **1**.

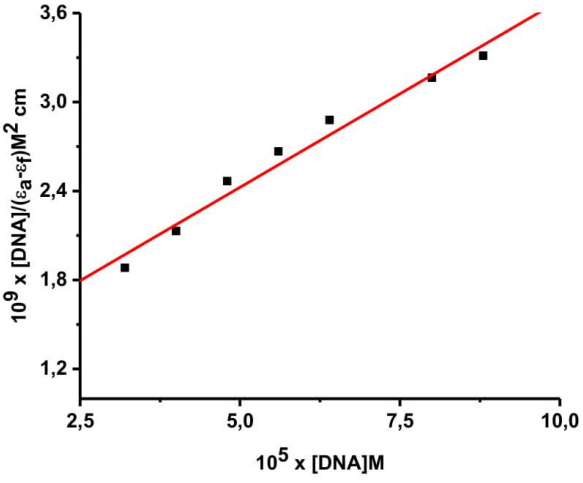

References

S1. M. Koppenwallner, E. Rais, M. Uzarewicz-Baig, S. Tabassum, M.-A. Gilani, R. Wilhelm, *Synthesis*, 2015, **47**, 789.

S2. M. M. Milutinović, A. Rilak, I. Bratsos, O. Klisurić, M. Vraneš, N. Gligorijević, S. Radulović, Ž. D. Bugarčić, *J. Inorg. Biochem.*, 2017, **169**, 1.

S3. A. M. Pyle, J. P. Rehmann, R. Meshoyrer, C. V. Kumar, N. J. Turro and J. K. Barton, *J. Am. Chem. Soc.*, 1989, **111**, 3051-3058.

S4. R. Lakowicz and G. Weber, *Biochemistry*, 1973, **12**, 4161-4170.

2.4. Newly synthesized heteronuclear ruthenium(II)/ferrocene complexes suppress 4T1 mammary carcinoma growth in BALB/c mice by promoting activation of anti-tumor immunity

Within the paper two new heteromettalic Ru(II)-terpyridine/ferrocene complexes were synthesized and characterized by elemental analysis, spectroscopic techniques (IR, UV-Vis, 1D and 2D NMR) and mass spectrometry (MALDI TOF MS). The chemical behavior of the complexes was monitored by UV-Vis spectroscopy. Also DNA/BSA interactions were studied with newly synthesized Ru(II)-terpyridine/ferrocene complexes, and molecular docking was performed as well. Cytotoxic studies were made on human and murine breast cancer cells, as well as the *in vivo* studies on mice.

Participations in the publication:

M. M. Milutinović, A. Rilak Simović – Synthesis of ruthenium complexes, UV-Vis spectroscopy, NMR measurements, viscosity measurements, DNA/BSA interaction measurements, implementation of all results and writing a paper;

D. Stevanović – synthesis of desired ferrocene ligands;

R. Masnikosa – MALDI TOF MS measurements;

M. Vraneš, A. Tot – Molecular docking measurements;

P. Čanović, M. Zarić, B. Simović Marković, V. Volarević, T. Kanjevac, M. Misirkić Marjanović, Lj. Vučićević, M. Savić, V. Jakovljević, V. Trajković – *In vitro* and *in vivo* cytotoxic studies.

DOI: https://pubs.acs.org/doi/10.1021/acs.organomet.8b00604

ORGANOMETALLICS
Article
Cite This: Organometallics 2018, 37, 4250−4266
pubs.acs.org/Organometallics

Newly Synthesized Heteronuclear Ruthenium(II)/Ferrocene Complexes Suppress the Growth of Mammary Carcinoma in 4T1-Treated BALB/c Mice by Promoting Activation of Antitumor Immunity

Milan M. Milutinović,[†,‡,@] Petar P. Čanović,[§,@] Dragana Stevanović,[†] Romana Masnikosa,[∥] Milan Vraneš,[⊥] Aleksandar Tot,[⊥] Milan M. Zarić,[§] Bojana Simović Marković,[#] Maja Misirkić Marjanović,[▽] Ljubica Vučićević,[▽] Maja Savić,[$] Vladimir Jakovljević,[&] Vladimir Trajković,[▽] Vladislav Volarević,[#] Tatjana Kanjevac,[*,%] and Ana Rilak Simović[*,†]

[†]University of Kragujevac, Faculty of Science, R. Domanovića 12, P.O. Box 60, 34000 Kragujevac, Serbia
[‡]University of Paderborn, Department of Organic Chemistry, Warburgerstraße 100, 33098 Paderborn, Germany
[§]University of Kragujevac, Serbia, Faculty of Medical Sciences, Department of Biochemistry, S. Markovića 69, 34000 Kragujevac, Serbia
[∥]University of Belgrade, Vinča Institute of Nuclear Sciences, Department of Physical Chemistry, Mike Petrovića Alasa 12-14, 11000 Belgrade, Serbia
[⊥]University of Novi Sad, Faculty of Sciences, Department of Chemistry, Biochemistry and Environmental Protection, Trg Dositeja Obradovića 3, 21000 Novi Sad, Serbia
[#]University of Kragujevac, Serbia, Faculty of Medical Sciences, Department of Microbiology and Immunology, Center for Molecular Medicine and Stem Cell Research, S. Markovića 69, 34000 Kragujevac, Serbia
[▽]University of Belgrade, Serbia, School of Medicine, Institute of Microbiology and Immunology, Dr Subotića 1, 11000 Belgrade, Serbia
[&]University of Kragujevac, Serbia, Faculty of Medical Sciences, Department of Physiology, S. Markovića 69, 34000 Kragujevac, Serbia
[$]University of Kragujevac, Serbia, Faculty of Medical Sciences, Department of Pharmacy, S. Markovića 69, 34000 Kragujevac, Serbia
[%]University of Kragujevac, Serbia, Faculty of Medical Sciences, Department of Dentistry, S. Markovića 69, 34000 Kragujevac, Serbia

Supporting Information

ABSTRACT: The two new heterometallic Ru(II)-tpy/ferrocene complexes [Ru(tpy)Cl_2(mtefc)] (**1**) and [Ru(tpy)-Cl_2(mtpfc)] (**2**) (where tpy = 2,2′:6′,2″-terpyridine, mtefc = (2-(methylthio)ethyl)ferrocene, and mtpfc = (3-(methylthio)-propyl)ferrocene) have been synthesized and then characterized through elemental analysis, followed by various spectroscopic (IR, UV−vis, 1D and 2D NMR) and mass spectrometric techniques (MALDI TOF and ESI Q-TOF MS). UV−vis and fluorescence spectroscopy and viscometry were employed to study the interactions of the complexes **1** and **2** with calf thymus DNA. Both **1** and **2** expelled ethidium bromide (EB) from the EB/DNA complex (K_{sv} = (1.5−1.8) × 10^4 M^{-1}), which suggested that the complexes intercalated into the double helix of DNA. Both complexes strongly quenched the fluorescence of tryptophan residues in serum albumin through both static and dynamic quenching. Molecular docking confirmed the intercalative mode of complex interaction with DNA. The docking results implied that **1** and **2** interacted with hydrophobic residues of albumin, particularly with those lying in the proximity of Tyr 160. We here demonstrate the high cytotoxic potential of complexes **1** and **2** against the breast cancer cells that originated either from humans (MDA-MB-231) or from mice (4T1), with apoptosis being the main mechanism of
continued...

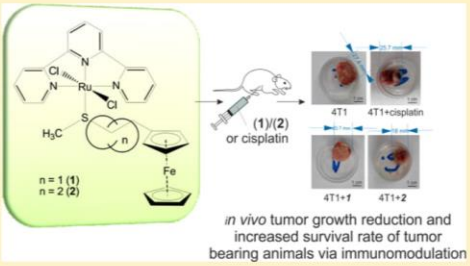

Received: August 22, 2018
Published: November 12, 2018

DOI: 10.1021/acs.organomet.8b00604
Organometallics 2018, 37, 4250−4266

complex-induced cell death. It is worth noting that both complexes promoted activation of innate and acquired antitumor immunity, which contributed to the reduced growth and progression of mammary carcinoma in vivo.

INTRODUCTION

Currently, a major focus of chemical research is the design and synthesis of compounds that could become antitumor drugs. Many of these compounds are coordination complexes of transition metals, which could be widely applied in diverse areas.[1−5] Platinum-based drugs are known for their toxicity and numerous side effects, and drug resistance often develops in patients. Being aware of these drawbacks of platinum drugs in use, chemists have been motivated to synthesize coordination compounds based on other (transition) metals.[6] In the past decade, a large number of metallo complexes have been synthesized and extensively studied for their anticancer activities. Many inorganic chemists turned their attention toward ruthenium complexes, having in mind not only their uncomplicated synthesis but also a wide span of Ru oxidation states and the kinetic aspects that are similar to those of Pt(II).[7,8] Hundreds of octahedral organometallic Ru(II) complexes have been synthesized, which enclosed both aromatic rings and mono- or bidentate chelating ligands (−N,N, −C,N, −N,O, −O,O, −O,S donors). The great majority of these compounds were tested for anticancer activity, mostly in vitro.[9−11] It has been long believed that most metallo complexes exert their anticancer activities by virtue of their binding to DNA, which result in its structural changes. An altered DNA molecule represents a signal for the cancer cell to start the suicidal cell program, apoptosis.[12] The results of many, particularly novel, studies pointed out that metallo complexes strongly interacted with cellular proteins, apart from their binding to cell DNA.[1,13−16] In light of this information, one seeks to develop anticancer agents that would ideally target both intracellular proteins and nuclear DNA.[13−16]

Many chemists have shown particular interest in ferrocenyl derivatives that contain one or more heteroatoms, such as monodentate ligands that form coordinative bonds with transition metals or polydentate ligands that form several bonds with metal atoms (chelates).[13,17] Ever since Woodward reported Friedel−Crafts acylation of ferrocene,[18] various ferrocenyl derivatives have been synthesized using classical organic synthesis.[19,20] Ferrocenyl derivatives have appeared as attractive candidates for potential treatment of not only human cancers[21] but also infective diseases such as malaria,[22] fungal and bacterial infections,[23] and human immunodeficiency virus (HIV).[24] The biological attractiveness of ferrocene-based metallo complexes should be sought in their stability in aqueous solutions and air and then, in their ability to enter cells, in their ease of chemical modification and their redox activity.[25−27] Ferrocene itself is not cytotoxic, but the ferrocenium ion—its singly charged cation—is cytotoxic.[28] It seems that a potent system for killing cancer cells (i.e., a metallodrug) could be created by the inclusion of a ferrocenyl unit into a complex structure.[29] Incorporation of the ferrocenyl unit could increase drug cytotoxicity and/or cell permeability; this might promote intercalation and/or noncovalent interactions with DNA and proteins as well.

Ruthenium(II) polypyridyl complexes possess the potential to serve as anticancer agents, due to their redox and photophysical properties, relatively low toxicity, and proven antitumor effectiveness.[30] We have recently described the synthesis of a series of Ru(II) coordination compounds which contained a terpyridine ligand, with the general formula *mer*-$[Ru(L_3)(N{-}N)(X)][Y]_n$, in which L_3 was 2,2′:6′,2″-terpyridine (tpy), 4′-chloro-2,2′:6′,2″-terpyridine (Cl-tpy), or 4′-(4-chlorophenyl)-2,2′:6′,2″-terpyridine (Cl-Ph-tpy), *N*−*N* was a bidentate chelating ligand (1,2-diaminoethane (en), 1,2-diaminocyclohexane (dach), 2,2′-bipyridine (bpy), 1,10-phenanthroline (phen), or *o*-benzoquinonediimine (*o*-bqdi)), X was a monodentate ligand (Cl or dmso-S), Y was a counteranion (Cl^-, PF_6^-, or $CF_3SO_3^-$), and *n* depended on the nature of the chelator and X.[14,16,31,32] Following the hydrolysis of Cl, these compounds formed monofunctional adducts with N7 atoms of two examined guanine derivatives: 9-methylguanine (9MeG) and guanosine-5′-monophosphate (5′-GMP). The rate and yield of these substitution reactions strongly depended on the nature of the chelating ligands.[14,16,31,32] We then analyzed the interactions of these complexes with DNA fragments (oligonucleotides), as well as with entire DNA molecules such as calf thymus DNA (CT DNA) and herring testes DNA (HT DNA).[33] The interactions of these complexes with two major metal transporters from human plasma, human serum albumin (HSA) and transferrin, were also studied in detail.[15] All in all, the recent studies done by our group indicated that either DNA or proteins, or both of them, might be potential cellular targets of the Ru(II) polypyridyl complexes.

It can be drawn from our previous studies that the nature of tridentate and bidentate ligands inside the Ru(II) polypyridyl complexes governed their mechanism of action in cells: i.e., their biological activity. Among the studied Ru(II) complexes bearing a tpy or Cl-tpy ligand, those from which chloride ion dissociated at a reasonable rate showed the greatest biological activity. The bidentate ligands of these compounds (en or dach) formed hydrogen bonds with derivatives of guanine. This finding suggested that the covalent binding of the Ru(II) polypyridyl complexes to DNA might be the predominant mode of their biological action. The other way around, the most active compound among those with an additional aromatic ring attached to the tridentate ligand (Cl-Ph-tpy), appeared to be the one that had bpy as a chelating ligand. This fact is highly suggestive of intercalation into DNA being their major mechanism of action.

Due to the medicinal value attributed to both ruthenium- and iron-based drugs, antitumor effects of the coordination complexes that contain both iron and ruthenium are worth studying. The main hypothesis of our study was that the attachment of a ferrocenyl unit to a complexed Ru(II) center would produce a combined compound that possesses an enhanced ability to induce DNA damage. Considering all the above, we synthesized and thoroughly characterized two heterometallic Ru(II)-tpy complexes containing two monosubstituted ferrocenyl ligands, $[Ru(tpy)Cl_2(mtefc)]$ (**1**) and $[Ru(tpy)Cl_2(mtpfc)]$ (**2**) (where mtefc = (2-(methylthio)ethyl)ferrocene and mtpfc = (3-(methylthio)propyl)ferrocene; Figure 1). We performed a competition binding study using a well-known intercalative agent, ethidium bromide (EB), with the aim of evaluating interaction of the complexes with CT DNA. Second, the affinity of **1** and **2** toward serum albumin (BSA) was investigated, and the binding constants were determined. In addition, molecular docking studies were carried out to get a glimpse of the binding sites of complexes **1** and **2** on both DNA and serum albumin. Finally, we analyzed the biological actions of complexes **1** and **2** against human (MDA-MB-231) and murine (4T1) breast

DOI: 10.1021/acs.organomet.8b00604
Organometallics 2018, 37, 4250−4266

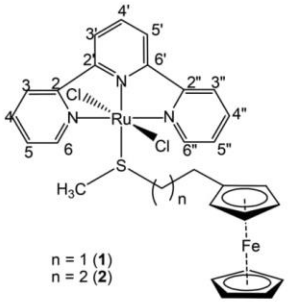

Figure 1. Structures of complexes **1** and **2** with the NMR numbering scheme.

cancer cells in vitro and in vivo. By using a 4T1 orthotopic model of breast cancer, we showed that the novel Ru(II) ferrocenyl complexes significantly reduced the growth of the breast cancer by modulating innate and acquired antitumor immune response, which suggested their therapeutic potential.

RESULTS AND DISCUSSION

Synthesis and Characterization. The sulfur-containing acylferrocenes were synthesized from ferrocene via Friedel–Crafts acylation using chlorides of the corresponding carboxylic acids.[34] Starting from these acylferrocenes, two ligands, (2-(methylthio)ethyl)ferrocene (mtefc) and (3-(methylthio)-propyl)ferrocene (mtpfc), were synthesized following modified literature procedures.[35] A borane dimethyl sulfide complex solution was added to a solution of the corresponding acylferrocene in dry THF in a Schlenk tube, and the reaction mixture was stirred at reflux for 2.5 h. The resultant mixture was extracted using ethyl acetate (EtOAc). Both ferrocenyl ligands were purified by liquid chromatography (SiO_2; *n*-hexane/EtOAc mixture). In the present work, we prepared the two new heteronuclear ruthenium(II)/ferrocene complexes $[Ru(tpy)Cl_2(mtefc)]$ (**1**) and $[Ru(tpy)Cl_2(mtpfc)]$ (**2**). The synthesis of the ferrocenyl ligands and their complexes is depicted in Scheme 1. Complexes

Scheme 1. Pathways of Synthesis of the Ferrocenyl Ligands and Complexes 1 and 2

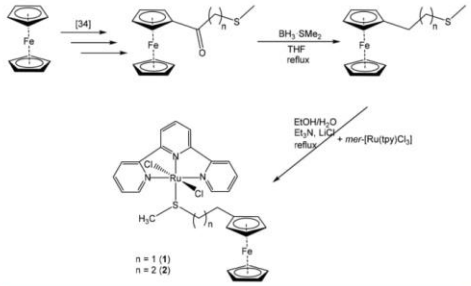

1 and **2** were prepared by the reaction between the neutral Ru(III) precursor *mer*-$[Ru(tpy)Cl_3]$ and the corresponding ferrocenyl ligand under reflux. Both complexes were obtained in good yields (69–72%) as air- and moisture-stable solids. The new complexes were characterized by elemental analysis and various spectroscopic techniques such as IR, UV–vis, and 1D (^1H and ^{13}C) and 2D (^1H–^1H NOESY, ^1H–^{13}C HSQC, and ^1H–^{13}C HMBC) NMR, and also by mass spectrometry (MALDI TOF MS and ESI Q-TOF MS). Both complexes were purified with the aid of liquid column chromatography on silica gel, where a dichloromethane/methanol mixture (90/10, v/v) was used as eluent.

NMR spectroscopy revealed that both complexes had *Cs* symmetry, which confirmed a proposed octahedral geometry with tpy as a tridentate chelating ligand. There were six aromatic resonances in the ^1H NMR spectrum of complex **1**, which were assigned to the equal halves of the tpy, along with the characteristic pattern for monosubstituted ferrocenes (a singlet for the C_5H_5 protons and two pseudotriplets for the C_5H_4 moiety; Figure 2). Two protons from $-CH_2-$ and one proton from

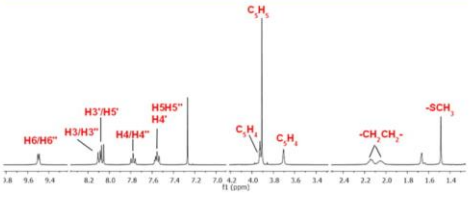

Figure 2. ^1H NMR spectrum of complex **1** in $CDCl_3$ at ambient temperature.

$-SCH_3$ (δ 2.19–2.10, 2.10–1.98, and 1.48, respectively) belonging to the mtefc ligand of **1** were significantly shifted in comparison to the corresponding signals of the free ligand (δ 2.69–2.56, and 2.12, respectively; Figure S1 and Table S1), which was due to the shielding effect of the tpy ligand. Similarly, the ^{13}C NMR spectrum of **1** displayed 12 resolved resonances in the downfield region, which originated from the aromatic carbon atoms, and 3 upfield resonances assigned to the carbon atoms of the $-CH_2-$ and $-SCH_3$ groups (Figure S2 and Table S2). The full assignments of the protonated and quaternary carbon atoms were achieved by 2D heteronuclear ^1H–^{13}C HSQC and long-range ^1H–^{13}C HMBC experiments, respectively (Figures S3 and S4). When the full assignments of the carbon atoms were finished, the correlation between H6/H6″ protons due to the tpy ligand of complex **1** and the $-CH_2-$ and $-SCH_3$ protons due to the mtefc ligand of complex **1** was achieved by a 2D homonuclear ^1H–^1H NOESY experiment (Figure S5).

The ^1H NMR spectrum of complex **2** in $CDCl_3$ was very similar to that of **1**, with the obvious presence of relatively upfield resonances (δ 2.19–1.98, 1.98–1.70, 1.35–1.10, and 1.45, respectively), which were assigned to three $-CH_2-$ protons and one $-SCH_3$ proton, respectively (Figure S6). ^{13}C NMR spectral data further supported the formation of complex **2** (Figure S7 and Table S2).

The solid-state IR spectra of complexes **1** and **2** showed typical bands of the tpy ligands and ferrocene moiety: the aromatic C–H stretching at 3053 cm^{-1} and the most characteristic strong band in the region 1378–1629 cm^{-1} assigned to ν(C=N) and ν(C=C) stretching (Figure S8).[36,37] The bands in the region 2920–2855 cm^{-1} were attributed to the antisymmetric and symmetric stretching vibrations of the alkyl group.[38,39]

The solution electronic absorption spectra of complexes **1** and **2** were almost identical, both displaying intense bands in the UV

DOI: 10.1021/acs.organomet.8b00604
Organometallics 2018, 37, 4250–4266

(**1**, 272 and 313 nm; **2**, 272 and 313 nm) and visible (**1**, 499 nm; **2**, 500 nm) regions (Figure 3). These absorbances were ascribed

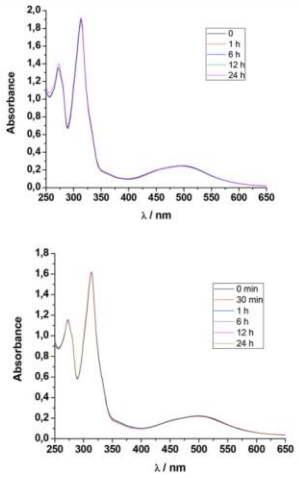

Figure 3. UV−vis spectra of complexes **1** and **2** in PBS (137 mM NaCl, pH 7.4) over a 24 h period. Conditions: [Ru(II)] = 1×10^{-4} M, T = 25 °C.

to intraligand ($\pi \rightarrow \pi^*$) charge transfer and to metal to ligand dπ(Ru) $\rightarrow$ π^*(polypyridyl) charge transfer (MLCT) transitions, respectively.[36,38,40−42]

Apart from the spectroscopic techniques, we checked the purity and stability of the novel ruthenium complexes by using two mass spectrometric techniques: MALDI TOF MS and ESI Q-TOF MS. MALDI TOF MS is an efficient tool for the fast analysis of metal-containing coordination compounds.[43−45] The MALDI TOF mass spectra of complexes **1** and **2** are shown in Figure S9, and the assigned mass signals are given in Table S3. Ruthenium is composed of seven stable isotopes; hence, all of the signals that arise from the Ru-containing ions appear as multiple lines. The mass spectrum of complex **2** in Figure S9B appears quite similar to that of **1**, except for the difference between the corresponding m/z values, which is a mass of the CH_2 group. The spectra do not contain signals derived from the tpy ligand alone, which confirms the high stability of the Ru−N bond. The Ru−Cl bond is particularly sensitive to the laser shot, and Cl anions are the first to leave the complex ions in the gas phase. Still, we managed to obtain the signals for the protonated molecular ions ($[M + H^+]^+$) in both spectra on applying mild instrumental settings (low laser intensity, low accelerating voltage). It seems that the Ru−S bond is not as stable as the Ru−N bond, according to the appearance of signals at m/z 334.5216 ($[Ru(tpy)]^{\cdot+}$), m/z 349.2192 ($[Ru(tpy)(CH_3) - H^+]^+$), m/z 546.4862 ($[Ru(tpy)(C_2H_4)(ferrocene) - H]^{\cdot+}$) and m/z 561.2012 ($[Ru(tpy)(C_3H_6)(ferrocene) - H]^{\cdot+}$) (Table S3). Finally, the laser shots in the MALDI source caused the loss of the cyclopentadienyl moiety bound to the Fe atom, giving rise to the most intense signals in both spectra (m/z 530.6500 and m/z 545.3434).

The ESI Q-TOF mass spectra of complexes **1** and **2**, together with the isotopic distributions (both theoretically and experimentally obtained) of the major m/z signals are shown in Figure S10. The signals at m/z 644.0156 and m/z 629.9998 both originated from the $[M - Cl]^+$ molecular ions. The appearance of these two ions was expected, since the mass spectra were acquired in positive mode. The complex molecules of **1** and **2** carry no charges; therefore, they cannot be detected by mass spectrometry. The theoretical and experimental isotopic distributions of the $[M - Cl]^+$ molecular ions were almost identical (Figure S10B,D), confirming the identity of the major signals.

Chemical Behavior of the Complexes in Aqueous Solution. We carried out a preliminary study of the stability of **1** and **2** in aqueous solution (using UV−vis spectrophotometry), having in mind that the complexes are meant to be tested for their anticancer properties in a cell-friendly, aqueous solution. Complexes **1** and **2** were independently dissolved in a minimum amount of methanol, from which two aliquots were taken and then diluted with water to make a final ruthenium concentration of 1×10^{-4} M. These solutions were immediately analyzed by UV−vis spectrophotometry, but we also kept collecting the spectra over 24 h. The absorption maxima of the ruthenium complexes decreased over time, which was attributed to hydrolysis of the Ru(II)-bound chloride ion (Figure S11). In a change from the chlorido complexes **1** and **2** to their corresponding aqua species, the MLCT bands underwent blue shifts from 497 to 488 nm and from 498 to 490 nm for **1** and **2**, respectively, which was a result of the stabilization of ruthenium dπ orbitals.

The stability of complexes **1** and **2** in 10 mM phosphate buffer (137 mM NaCl, pH 7.4) was also investigated (Figure 3). Electronic absorption spectra of both complexes remained unaltered for 24 h after the dissolution, suggesting a good stability of complexes **1** and **2**.

We have also studied the chemical behavior of **1** and **2** in aqueous solution at room temperature by means of ^{1}H NMR spectroscopy (Figures S12 and S13). Complexes **1** and **2** proved to be poorly soluble in aqueous solution, behaving quite similarly to other ruthenium terpyridine compounds. The complexes were unstable when we dissolved them in 70% MeOD-d4/30% D_2O (v/v). The presence of methanol ensured the solubility of the complexes. After the dissolution, slow, time-dependent alterations in the ^{1}H NMR spectra of **1** and **2** were noticed, which were due to ligand exchange reactions forming the respective hydrolyzed species (Figures S12 and S13). In addition, we observed that a new set of resonances grew both in the aromatic (tpy resonances) and in the aliphatic ($-CH_2-$ and $-SCH_3$ resonances) regions of the ^{1}H NMR spectra. The quantitative formation of hydrolyzed species was complete after ca. 24 h, with no further changes (including release of the ferrocenyl ligands) afterward. The assignment of the new resonances was not achieved due to the spontaneous precipitation of the complexes.

DNA Binding Titration Studies. *Absorption Spectroscopic Studies.* The potential interactions of complexes **1** and **2** with CT DNA were monitored through changes in their MLCT absorption bands upon mixing with solutions of CT DNA, using increasing [complex]/[DNA] mixing molar ratios (r values). In addition to that, the pattern of observed UV−vis spectral changes during this titration gave us information on their interaction mode.

The UV−vis spectra of **1** and **2** in the absence and presence of increasing amounts of CT DNA are displayed in Figure S14. The hypochromism of the band at 499 nm, seen in the spectrum of **1** upon titration with CT DNA, suggested the tight binding of this complex to CT DNA, quite possibly through intercalation.[44,46]

DOI: 10.1021/acs.organomet.8b00604
Organometallics 2018, 37, 4250−4266

Similarly, in the case of complex **2**, we observed the hypochromism of the band centered at 502 nm.

The results from the absorption titration experiments strongly support the binding of the studied complexes to CT DNA, followed by a stabilization of DNA duplex. However, the nature of their interactions cannot be unambiguously determined, if we take into account solely UV−vis spectral changes.[47,48] It is worth mentioning that complexes **1** and **2** contain both a leaving group and an intercalating ligand, which means they have the potential for a bifunctional interaction with DNA: i.e., to form a covalent bond and to intercalate into the DNA double helix.

The intrinsic CT DNA binding constants, K_b, of complexes **1** and **2**, which were calculated using eq S1 and plots of [DNA]/(ε_A-ε_f) vs [DNA] (Figure S15), were (7.2 ± 0.1) × 10^3 and (5.2 ± 0.1) × 10^3 M^{-1}, respectively (Table 1). These values

Table 1. DNA-Binding Constants (K_b) and Stern−Volmer Constants (K_{sv}) from EB−DNA Fluorescence for 1 and 2

complex	K_b (10^3 M^{-1})	K_{sv} (10^4 M^{-1})
1	7.2 ± 0.2	1.75 ± 0.1
2	5.2 ± 0.1	1.50 ± 0.1

suggested a moderate binding of **1** and **2** to CT DNA, and **1** exhibited higher K_b values in comparison to complex **2**. Additionally, the obtained K_b values lay within the range reported for other tpy-containing Ru complexes.[14,16,32]

Ethidium Bromide (EB) Displacement Studies. It is widely known that ethidium bromide (EB = 3,8-diamino-5-ethyl-6-phenylphenanthridinium bromide) forms a strong noncovalent bond with the double-helical DNA molecule. EB practically inserts itself between adjacent DNA base pairs using its planar phenanthridine ring, and this interaction is called intercalation. When the EB−DNA adduct is formed, it is readily detected as an intense fluorescence emission of EB at 612 nm (upon excitation at 527 nm). Hence, the mode of interaction between a metallocomplex and CT DNA can be revealed by monitoring changes in the fluorescence spectrum of the EB−CT DNA adduct, which is titrated with increasing amounts of that metallocomplex. Namely, a metallocomplex that is able to intercalate with the same or greater affinity for DNA than that of EB will displace EB from its binding sites and the intensity of the 612 nm band will decrease. The studied complexes must not emit their own fluorescence at around 612 nm, neither in the absence nor in the presence of DNA. We emphasize that **1** and **2** did not emit any significant fluorescence upon excitation at 527 nm, neither in the absence nor in the presence of CT DNA. What is more, the complexes did not bind to EB, which was tested by the addition of **1** or **2** to the EB solution. The mixing did not provoke quenching of free EB fluorescence emission, and no new peaks appeared in the spectra.

The intensity of the 612 nm band significantly decreased upon the addition of increasing amounts (up to r = 1.0, where r = [complex]/[CT DNA]) of **1** or **2** to a solution of EB−CT DNA adduct. This finding clearly showed the capability of both **1** and **2** to displace EB molecules that are inside CT DNA (Figure S16). On displacement from CT DNA, EB fluorescent emission dropped to 42% and 49% of its initial/maximum value (I_0) for **1** and **2**, respectively. Figure S17 depicts the fluorescence quenching curves of EB−CT DNA adducts upon titration with **1** or **2**. Taking into account the results in Figure 4 and Figure S12, we concluded that the binding of **1** or **2** to CT DNA resulted in the ejection of EB from the EB−CT DNA adduct. This fact further implied that the interaction between the Ru(II) ferrocenyl complexes and double-helical DNA might be intercalation.[48−50]

The Stern−Volmer plots of the EB−DNA quenching (Figure S18) were all linear, which was in good agreement (R = 0.99) with the linear form of Stern−Volmer eq S2. Looking

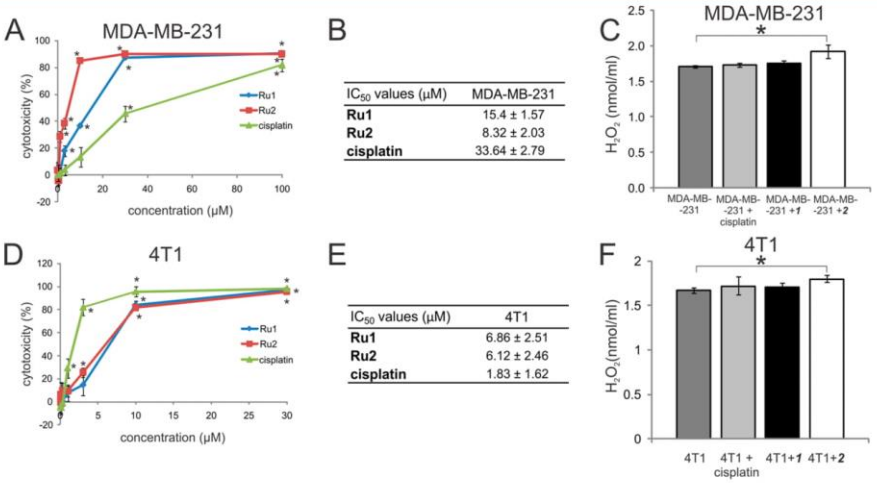

Figure 4. In vitro cytotoxicity of complexes **1** and **2** and cisplatin against human (A−C) and murine (D, E) breast cancer cell lines. The cytotoxicity of **1**, **2**, and cisplatin against MDA-MB-231 (A) and 4T1 (D) cells after 48 h was determined by MTT assay. Concentrations that induced a 50% decrease in viability of MDA-MB-231 (B) and 4T1 (E) cells were determined after 48 h. IC_{50} values (μM) were calculated from the MTT assay results. Data are expressed as the mean ± standard deviation (mean ± SD). The production of hydrogen peroxide (H_2O_2) was measured in MDA-MB-231 (C) and 4T1 (F) cell cultures after treatment with the respective compounds at their IC_{50} values.

DOI: 10.1021/acs.organomet.8b00604
Organometallics 2018, 37, 4250−4266

Table 2. BSA Constants and Parameters (K_{SV}, k_q, K, n, and V) Derived for Complexes 1 and 2

complex	K_{SV} (M^{-1})	k_q (M^{-1} s^{-1})	K (10^4 M^{-1})	N	V (10^4 M^{-1})
1	$(1.40 \pm 0.5) \times 10^5$	$(1.40 \pm 0.5) \times 10^{13}$	9.0	1.30	3.50 ± 0.4
2	$(7.50 \pm 0.4) \times 10^4$	$(7.50 \pm 0.4) \times 10^{12}$	7.8	1.40	7.00 ± 0.3

at the values of the Stern−Volmer constants (K_{SV} in Table 1), we strongly suggest that **1** and **2** dislocated EB from its binding sites inside DNA. Moreover, the values of quenching constants lay within the range reported for the other ruthenium complexes containing tpy.[14,16,32]

Viscosity Measurements. The previously mentioned displacement of EB from its adduct with CT DNA by **1** or **2** was highly suggestive of their intercalative mode of binding to DNA. To confirm the intercalation, we carried out viscosity measurements of DNA solutions alone and those exposed to the presence of **1** or **2**. The change in viscosity of a DNA solution reflects changes in the length of the DNA molecule. A change in DNA viscosity is, thus, regarded as the least ambiguous proof of intercalation.[51,52] In our experimental system, the addition of increasing amounts (up to r = 1.0) of **1** or **2** to a CT DNA solution (0.01 mM) caused its relative viscosity to increase (Figure S19). The increase was more pronounced in the case of **2**. When a classical intercalation occurs, DNA base pairs move apart (i.e., DNA helix stretches) to accommodate the bound compound, which leads to increased DNA viscosity, the magnitude of which is usually in accordance with the strength of the interaction. Hence, the increase in viscosity detected in our study may be explained by lengthening of the CT DNA molecule, which was caused by the insertion of the ferrocenyl metallocomplexes **1** and **2** between base pairs. The best candidates for the intercalation are the aromatic tpy and ferrocenyl ligands of the complexes.

Albumin-Binding Studies. Studying interactions between a newly synthesized therapeutic and major plasma proteins is of special importance, since they greatly affect the pharmacokinetics of the drug. Serum albumin is the most abundant protein in plasma. Binding of a drug to albumin may augment or lessen its pharmacological properties and/or provide the drug trafficking route. We have investigated the interactions of **1** and **2** with serum albumin by means of fluorescence spectroscopy, knowing that it enables a quantitative assessment of the binding strength. BSA was chosen because its amino acid sequence shares a high degree of homology with human serum albumin. The quenching of the fluorescence emission seen in the spectra of BSA, which occurs upon the addition of metallocomplexes, can be attributed to changes in the protein conformation, ligand binding, or denaturation.

The fluorescence intensity of BSA at its emission maximum of λ 365 nm was significantly reduced after the addition of complexes **1** and **2** to a BSA solution (up to r values of 15). (Figures S20 and S21). The observed quenching might be due to changes in the tertiary structure of BSA. It often causes changes in amino acids that surround two tryptophan residues in BSA, indicating the binding event.[53] Furthermore, the maxima of the fluorescence emission curves were slightly red shifted for both complexes (Figure S21). This fact is consistent with the formation of ruthenated BSA adducts.

The Stern−Volmer plots (I_0/I versus [Q]) showed upward curvatures for both complexes (eqs S3 and S4 and Figure S22). The static quenching constant V was calculated from the modified Stern−Volmer equation (S5), by plotting $I_0/Ie^{V[Q]}$ versus [Q] by varying V until we obtained a linear plot. In order to obtain a precise value of V, we used the highest value of the correlation coefficient as a criterion for the plot linearity. We then used the slope of the linear plots (inset in Figure S22) to calculate the (dynamic) collisional quenching constant, K_{SV}. The V and K_{SV} values are shown in Table 2. It should be noted that the magnitudes of both static quenching constants were smaller than the collisional quenching constants for **1** and **2**.

The quenching rate constant (k_q) depends on the probability of a collision between the fluorophore (Trp residues in BSA) and a quencher (metallocomplex): i.e., it reflects a degree of exposure of the Trp residues to the drug. The k_q values are also given in Table 2. The tested complexes demonstrated a good quenching ability, with **2** having a higher k_q value ($k_q = (1.40 \pm 0.4) \times 10^{13}$ M^{-1} s^{-1}) than **1**. The upper limit of k_q reported for a diffusion-controlled bimolecular process is 10^{10} M^{-1} s^{-1}. The high value of k_q found in the present study (10^{13} M^{-1} s^{-1}) suggested that specific metallocomplex−BSA interactions occurred, which made k_q larger.[49,50] The values of quenching constants were within the range reported for other ruthenium complexes with tpy as a ligand.[14,16]

The BSA-binding constants (K) and the number of the binding sites (n), as calculated from the Scatchard equation (S6) and Scatchard plot (Figure S23), are given in Table 2. The metallocomplex **1** had a higher binding constant than **2**. The n values for both complexes were close to 1, which suggested one binding site on BSA.[49] To sum up, the obtained K values were within $(7.8–9.0) \times 10^4$ M^{-1} and, hence, high enough to suggest the binding of **1** and **2** to BSA and their possible transfer to target tissues. Fortunately, the K values were not too high (they are quite below the association constant of the avidin−biotin interaction with $K = 10^{15}$ M^{-1}); therefore, they could be detached from BSA upon their arrival to the target.[54]

Molecular Docking with DNA. We conducted in silico studies of preferred binding sites for **1** and **2** on DNA, as well as the nature of interactions between the complexes and DNA using molecular docking. To do this, we employed a synthetic dodecamer, known as 1BNA ($d(CGCGAATTCGCG)_2$), that forms slightly more than one complete turn of a right-handed double-stranded B DNA helix. In other words, 1BNA possesses a minimal double-helical structure of the native DNA.

According to literature data, it could be assumed that interactions of metallocomplexes with 1BNA parralel those with CT DNA. The best-docked poses of **1** and **2** with 1BNA are depicted in Figure S24. The binding energies and docked inhibition constants are summarized in Table 3. The docking results suggested that intercalation is the major mode of interaction between the studied ferrocenyl Ru(II) complexes and 1BNA. The strong $\pi-\pi$ stacking interactions occurred between metallocomplexes and 1BNA due to the planarity of the pyridine core that fits inside DNA strands by van der Waals interactions (Figure S24). The calculated free energies of binding were very similar for docked structures **1** and **2** (Table 3). These results clearly indicated that the prolongation of the alkyl chain does not contribute significantly to the binding affinity of the complexes. Therefore, our results from the molecular docking using model B-DNA were in accordance with the results obtained using the whole DNA molecule (the fluorescence measurements with CT DNA).

DOI: 10.1021/acs.organomet.8b00604
Organometallics 2018, 37, 4250−4266

Table 3. Docking Scores, Free Energies of Binding, and Docked Inhibition Constants of Ru(II) Ferrocenyl Complexes 1 and 2

complex	docking score	free energy of binding ΔG (kJ mol^{-1})	docked inhibition constant K_i (μM)
		DNA	
1	−4.884	−48.96	0.003
2	−4.906	−49.22	0.002
		BSA	
1	−5.231	−33.58	1.308
2	−5.269	−34.04	1.087

Molecular Docking with BSA. As with DNA, we sought to predict the potential binding sites for **1** and **2** on the BSA molecule with the aid of molecular docking. We found that the most probable binding sides for **1** and **2** were located in the proximity of the hydrophobic domain around the Tyr 160 residue. The results obtained for the best-docked poses of **1** and **2** are displayed in Figure S25. The amino acid residues close to this binding site are Leu 112, Lys 116, Pro 119, Glu 125, Lys 136, Arg 144, Lys 159, Asn 161, and Arg 185 (within 4 Å). In addition to the mentioned residues, the binding was additionally stabilized via $\pi-\pi$ stacking interactions that occurred between the ferrocene ring and amino acids Phe 133 and Trp 134. The calculated values of free binding energy for the investigated docked structures are presented in Table 3. The small difference in binding energy between **1** and **2** was probably due to a greater number of van der Waals interactions between **2** and 1BNA.

Higher Cytotoxic Potential of Complexes 1 and 2 in Comparison to Cisplatin against Human and Murine Breast Carcinoma Cells in Vitro. A cytotoxicity assay (Figure 4A) and IC_{50} values (Figure 4B) showed a dose-dependent correlation between the concentration of complexes **1** and **2** and the cell viability of MDA-MB-231 human breast cancer cells. Importantly, both complexes showed significantly higher cytotoxicity in comparison to cisplatin at the lowest tested concentrations (0.1, 0.3, and 1 μM, Figure 4A) that are suitable for a potential in vivo application. These results were accompanied by significantly lower values of IC_{50} in comparison to cisplatin (Figure 4B).

Having in mind that a ferrocene unit, when in the presence of H_2O_2, undergoes an oxidation to form the ferrocenyl cation, we have also analyzed the production of reactive hydrogen peroxide (H_2O_2), and these results are presented in Figure 4C,F. We noticed an increased concentration of H_2O_2 in MDA-MB-231 and 4T1 cell culture after treatment with **2**. We assumed that this oxidation process was, at least, partially responsible for the cytotoxic effects of **2**.

To confirm the cytotoxic potential of complexes **1** and **2** against murine breast carcinoma cells and to determine their applicability for in vivo testing in an animal model of breast cancer, the cytotoxicity of **1** and **2** was further tested against 4T1 cells in parallel to cisplatin.

Similarly, when they were applied to 4T1 cells, **1** and **2** at their lowest tested concentrations (0.1, 0.3 μM) displayed higher cytotoxicity in comparison to cisplatin (1 μM) (Figure 4D,E).

Apoptosis and Cell Cycle Arrest Induced by Complexes 1 and 2 in Human and Murine Breast Carcinoma Cells in Vitro. Complexes **1** and **2** mainly decreased viability by inducing apoptosis of MDA-MB-231 cells. The results, presented in Figure 5, showed that a majority of nonviable MDA-MB-231 cells were apoptotic 48 h after the treatment with **1**, **2**, or cisplatin (Figure 5A,B). Importantly, 94.7% of nonviable **1**-treated MDA-MB-231 cells were apoptotic, whereas 5.3% of them were necrotic. Almost all nonviable MDA-MB-231 cells treated with **2** (98.6%) were in apoptosis, while only 1.4% of nonviable MDA-MB-231 cells were necrotic after their treatment with **2** (Figure 5B). Induction of apoptosis in MDA-MB-231 cells was the main mechanism of the cisplatin action as well, although it is important to highlight that the percentage of apoptotic MDA-MB-231 cells was notably lower after the cisplatin treatment than after the exposure of these cells to **1** and **2** (Figure 5B).

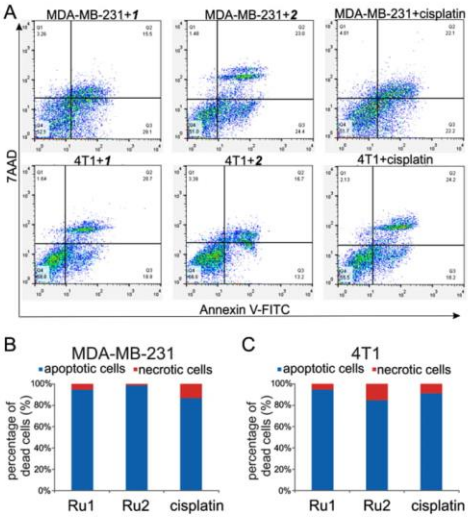

Figure 5. Inducement of apoptosis of human and murine breast cancer cells bt ruthenium complexes **1** and **2** in vitro. Histograms presenting the results of Annexin-7AAD assay (A). The relative percentage of apoptotic and necrotic MDA-MB-231 (B) and 4T1 (C) cells was determined by Annexin V-7AAD assay. Results were calculated as the ratio of the percentage of necrotic or apoptotic cells to the total percentage of nonviable cells.

Similarly, complexes **1** and **2** at the tested IC_{50} concentrations mainly induced cell death of 4T1 by induction of apoptosis (Figure 5C).

We found a significantly greater percentage of 4T1 cells in S phase after their treatment with IC_{50} values of **1** and **2** during 48 h. This finding was accompanied by a decrease in percentage of cells in G0/G1 phase (2N) ($p < 0.05$). After the treatment of MDA-MB-231 cells with IC_{50} values of **1** ($p < 0.05$) (Figure 6) we obtained similar results. However, **2** induced cell cycle arrest in G2/M phase in comparison to untreated cells (4N) ($p < 0.05$) (Figure 6). These results demonstrated that both **1** and **2** arrested mitosis in 4T1 and MDA-MB-231 tumor cells. The apoptosis and cell cycle are closely related. The cell cycle machinery possesses a set of regulatory molecules that serve to induce a cell cycle arrest, which gives a cell time needed to fix the damage. When the cell is unable to fix the defect, an apoptotic program starts. The G2/M phase arrest, induced by complex **2** in MDA-MB-231 cells, thus can be a key event that triggers the apoptosis. However, the S phase arrest, induced by **1** and **2** in 4T1 cells and **1** in MDA-MB-231 cells, suggested that a potential

DOI: 10.1021/acs.organomet.8b00604
Organometallics 2018, 37, 4250−4266

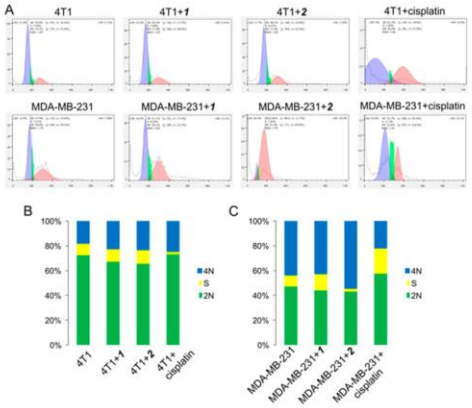

Figure 6. Flow cytometric analysis of the cell cycle. (A) Histograms presenting cell cycle distribution in the untreated cells and cells treated with **1**, **2**. or cisplatin at their IC50 values. (B) Similar increase in percentage of 4T1 cells in the S phase induced by both **1** and **2**. (C) Inducement of an increase in the number of S-phase cells by complex **1** and inducement of an increase in the number of G2/M phase cells (4N) in MDA-MB-231 cells by complex **2**.

trigger of the apoptosis might be a blockade of DNA replication. It should be emphasized that the apoptosis which mostly affects cells in the S phase of the cell cycle points to the inhibition of topoisomerase I.

Significant Reduction of Tumor Growth and Increase in Survival Rate of Tumor-Bearing Animals on Treatment with Complexes 1 and 2. The complexes **1** and **2** were given to mice bearing 4T1 tumors twice per week. The tumor growth and progression were monitored over 35 days after the administration of metallocomplexes (Figure 7A). One control group of tumor-bearing mice was left untreated, whereas the other group was given cisplatin. Both complexes were tolerated well by the animals. We did not observe any changes in the pattern of food/water consumption by the treated animals. No measurable change in body weight of mice could be observed during the treatment. Importantly, **1** and **2** significantly inhibited the tumor growth (Figure 7B,C). The capacity of **2** to suppress the breast tumor growth in mice was significantly higher than that of cisplatin injection (Figure 7B,C). In line with these findings, there was a significantly better survival rate in mice treated with either **1** or **2** than in the cisplatin-treated control group (Figure 7D).

Reduced tumor growth in mice treated with the Ru(II) ferrocenyl complexes **1** and **2** may be due to modulation of the antitumor immune response. To check this hypothesis, we studied the effect of the complexes on immune cells: i.e., we analyzed the cellular makeup of the tumors. The increased presence of interleukin 10 (IL-10) producing, alternatively activated (M2) macrophages correlates with primary growth and metastasis of 4T1 murine breast cancer. In contrast, the enhanced presence of IL-12 producing (M1) macrophages reduces the breast tumor progression.[58,59] Additionally, through the production of TNF-α (tumor necrosis factor alpha), tumor-infiltrating M1 macrophages promote necrosis of breast cancer cells and attenuate mammary tumor growth.[60,61]

To check whether complexes **1** and **2** modulated cytokine production by tumor-associated macrophages in mice, we first isolated tumor-infiltrated immune cells (leukocytes) from the breast tumors, as well as splenocytes from the murine spleens. We then stained these immune cells for their intracellular content of specific molecules such as TNF-α, interleukins IL-10, IL-17, and IL-12, interferon γ (IFN-γ), and forkhead box P3 (Fox P3) and counted them using flow cytometry. This way we were able to compare the number of particular immune cells, which were infiltrated in tumors and spleens taken from the control, nontreated, cisplatin-treated, complex **1** treated, and complex **2** treated mice. Both the percentage of TNFα producing ($p < 0.05$; Figure 8A) and IL-12 producing F4/80+ macrophages ($p < 0.05$; Figure 8B) were notably higher in tumors of complex **1** treated mice than in cisplatin-treated and nontreated animals. In contrast, there was a significantly lower percentage of tumor-associated macrophages that produced immunosuppressive IL-10 in Ru(II) complex treated tumor bearing mice in comparison to cisplatin-treated and nontreated mice ($p < 0.01$; Figure 8C).

To sum up, complexes **1** and **2** remarkably modulated cytokine production of tumor-associated macrophages by promoting the production of antitumor TNFα and pro-Th1 cytokine IL-12. It was observed that tumor-associated macrophages, in an IL-10 dependent manner, regulate expression of IL-12 in tumor-infiltrating dendritic cells (DCs).[62] An increased presence of IL-12 producing DCs in breast cancer tissue was found to be crucially important for an enhanced activation of CTLs and improved survival of tumor-bearing animals, and most of the newly designed anticancer drugs promoted pro-inflammatory phenotype in DCs.[62] Furthermore, a grat deal of evidence suggests that breast cancer cells evade host immunity by converting DCs from potent stimulators to negative modulators of immunity.[63,64] Breast cancer cells induce generation of regulatory phenotype in tumor-infiltrating DCs by promoting the production of immunosuppressive IL-10,[65] and DC-based immunotherapy of tumors is focused on the promotion of IL-12 secretion and inhibition of IL-10 expression in DCs.[66] In line with the literature data, the results presented herein highly suggested that the novel complexes **1** and **2** polarized tumor-infiltrated DCs toward proinflammatory antitumor phenotype. What is more, we observed a significantly higher percentage of inflammatory, IL-12 producing CD11c+ DCs ($p < 0.05$; Figure 8D) along with a significantly lower percentage of regulatory IL-10 producing CD11c+ DCs ($p < 0.05$; Figure 8E) in mice with breast tumors that received **1** or **2**, in comparison to in mice that received cisplatin.

We have also assessed the percentage of two populations of antitumor cells that produce IL-17: CD4+ and CD8+ T cells, which were present in tumors extracted from mice. We observed a significantly higher percentages of IL-17 producing CD4+ ($p < 0.05$; Figure 8F) and CD8+ T cells ($p < 0.05$; Figure 8G) in tumors from mice that received complex **1** or **2**. It is known that an increased presence of IL-17 producing T cells in breast cancer tissue means a decreased proliferative capacity and a decreased invasion of both blood and lymphatic vessels by breast cancer cells. An increased number of IL-17 T cells is regarded as a favorable prognostic factor in breast cancer patients.[67] In light of these facts it is highly possible that the capacity of complexes **1** and **2** to attenuate the breast cancer growth in mice (and, hence, to increase the survival rate of tumor-bearing mice) is due to their ability to promote T cell dependent antitumor immunity.

We then counted a number of immunosuppressive T cells in the tumors extracted from mice that were treated with **1** or **2** (cisplatin also in parallel). In comparison to untreated and

DOI: 10.1021/acs.organomet.8b00604
Organometallics 2018, 37, 4250−4266

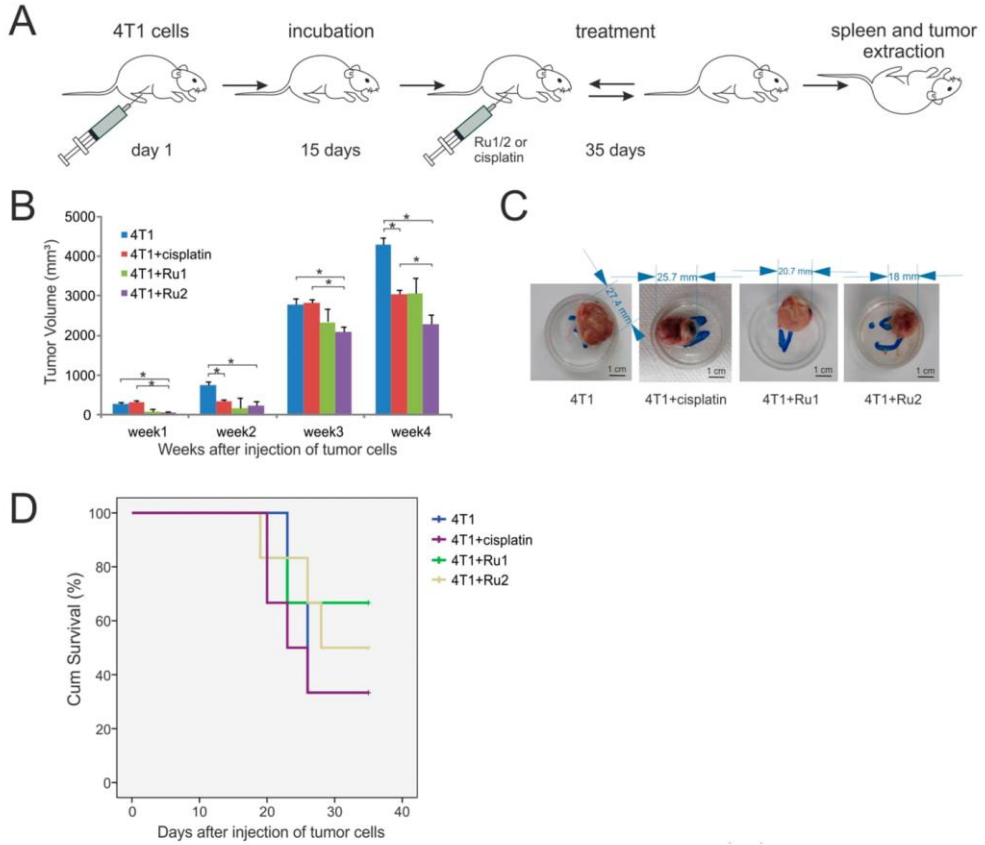

Figure 7. In vivo antitumor effects of complexes **1** and **2** (A) demonstrating significantly reduced tumor growth (B, C) and increased survival rate (D) of tumor-bearing animals treated with **1** or **2**. (A) On the first day of the experiment, the mice were inoculated with breast tumor cells 4T1. After 15 days of incubation, palpable tumors were detected and mice began to receive treatment with complex **1** or **2** or cisplatin. Fifty days from the start of the experiment, mice were sacrificed and their tumors and spleens were extracted for further analysis. (B) The results represent average tumor volume values per week in the control group of untreated mice (4T1) as well as in mice treated with complex **1** or **2** or cisplatin. Results are presented as mean ± SD; $*p < 0.05$. (C) Representative photographs of tumors extracted from the treatment and control groups of mice with their respective dimensions. There is a clear indication of the difference in tumor diameters between the untreated mice (4T1) and those from the treated mice. (D) Cumulative survival of mice from the moment of therapy initiation.

cisplatin-treated mice, we observed that a significantly lower percentage of immunosuppressive CD4+ FoxP3+ T regulatory cells (Tregs) ($p < 0.05$; Figure 8H), as well as IL-10 producing CD4+ T cells ($p < 0.05$; Figure 8I) were present in tumors from mice treated with **1** or **2**. CD4+FoxP3+ Tregs are the main population of immunoregulatory cells that, either in a contact dependent manner or through the production of immunosuppressive cytokines (IL-10 and TGF-β), suppress acquired antitumor immunity in breast cancer.[68−70] The results recently obtained by Montani and colleagues[71] suggested the potential of some Ru(II) complexes to suppress infiltration of immunosuppressive Tregs within murine breast tumors. Accordingly, our findings that complexes **1** and **2** suppressed presence of Tregs within breast tumors could be one of the main reasons for the beneficient, antitumor effects of these complexes in the treatment of murine mammary carcinoma.

Promotion of Systemic Antitumor Immunity in 4T1-Treated Mice by Complexes 1 and 2. To sum up, Ru(II) ferrocenyl complexes **1** and **2** exerted significantly more pronounced effects on both innate (macrophages and DCs) and acquired immunity cells (effector T cells, Tregs) from breast cancer bearing animals in comparison to the effects of cisplatin. In other words, our novel complexes demonstrated more potent immunostimulatory activity than cisplatin.

Finally, we tested the ability of complexes **1** and **2** to induce a strong systemic innate and acquired antitumor immunity (Figure 9). A significantly higher percentage of IL-12 producing F4/80+ macrophages ($p < 0.05$; Figure 9A) and CD11c+ DCs

DOI: 10.1021/acs.organomet.8b00604
Organometallics 2018, 37, 4250−4266

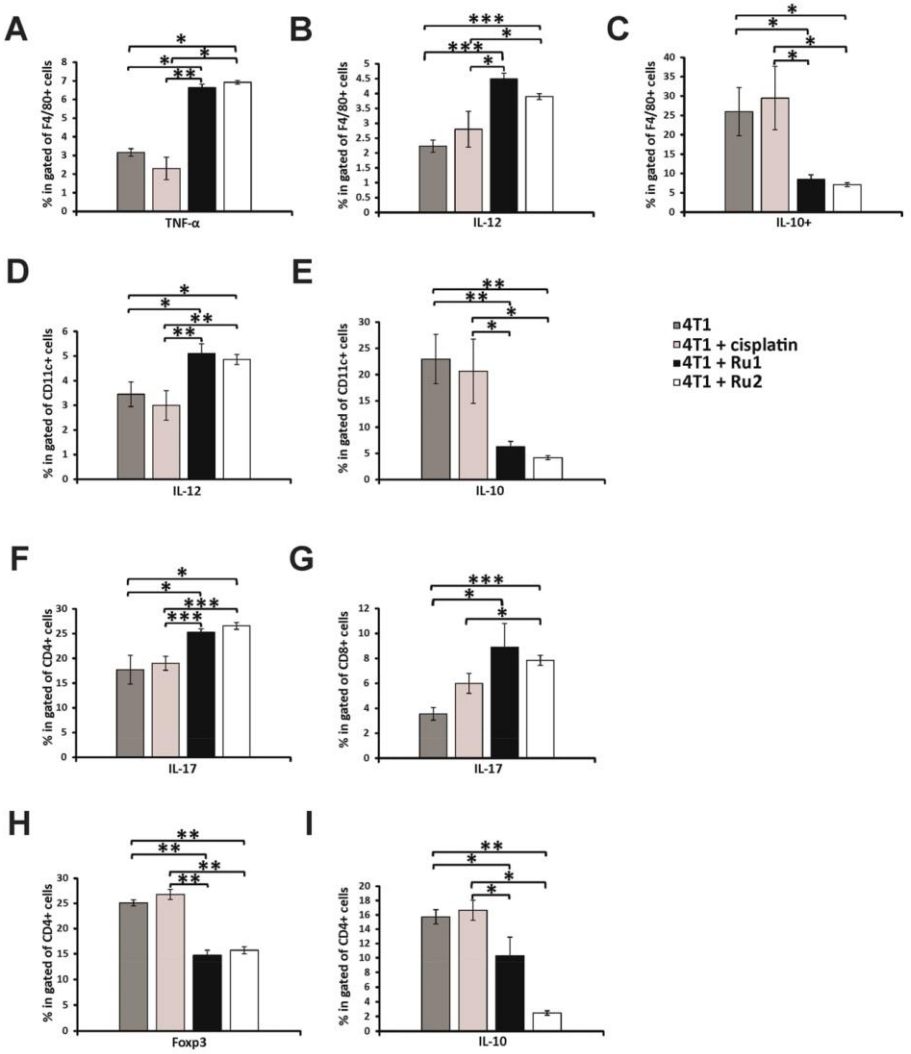

Figure 8. Ru(II) ferrocene complex reduction of tumor growth through affecting antitumor immune response. Cellular makeup of the tumor, determined by flow cytometry, shows (A−C) the percentage of TNF-α, IL-12, and IL-10 producing F4/80+ macrophages, (D, E) IL-12 and IL-10 producing CD11c+ dendritic cells, (F, G) IL-17 producing CD4+ T helper cells and CD8+CTLs, and (H, I) regulatory cells CD4+Foxp3+ and CD4+IL-10+. Data are presented as mean ± SEM (n = 10 per group); *p < 0.05, **p < 0.01; ***p < 0.001.

(p < 0.05; Figure 9B), as well as IL-17 producing CD4+ (p < 0.05; Figure 9C) and CD8+T cells (p < 0.05; Figure 9D), was noticed in the spleens of tumor-bearing animals that received **1** and **2**, in comparison to the control and cisplatin-treated groups. Additionally, percentages of immunosuppressive, IL-10 producing F4/80+ macrophages (p < 0.05; Figure 9E), IL-10 producing CD11c+ DCs (p < 0.05; Figure 9F) and CD4+FoxP3+ Tregs (p < 0.05; Figure 9G) were significantly lower in the spleens of 4T1+complex **1** or **2** treated mice when compared to cisplatin-treated and nontreated tumor bearing mice.

■ CONCLUSION

Ruthenium-ferrocenyl complexes have been attracting the attention of chemists ever since they showed a chemotherapeutic potential. Introducing a ferrocene molecule into a

DOI: 10.1021/acs.organomet.8b00604
Organometallics 2018, 37, 4250−4266

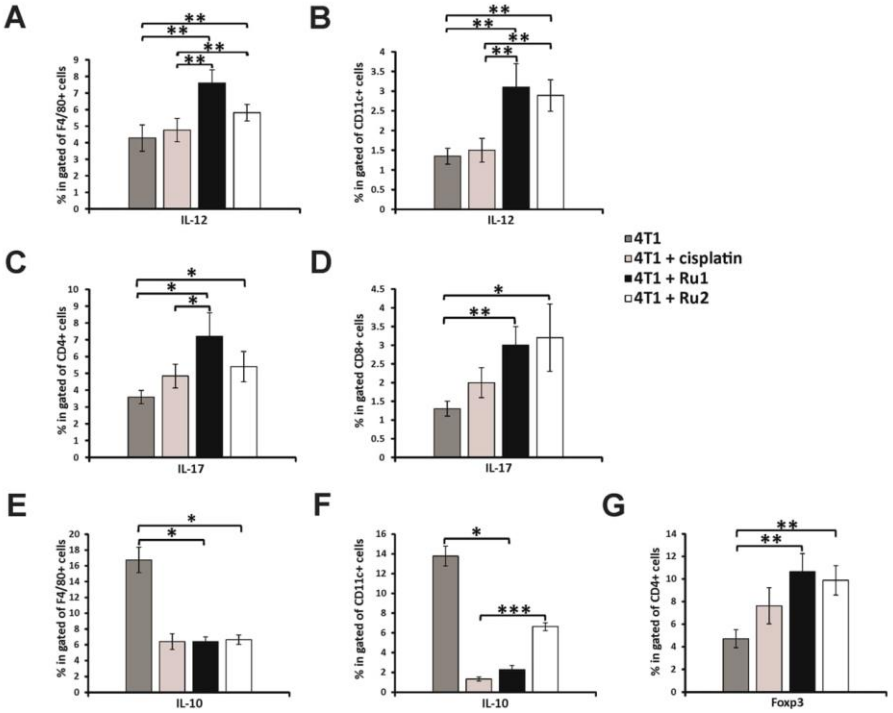

Figure 9. Promotion of systemic antitumor immunity in 4T1-treated mice by Ru(II) complexes. Flow cytometry analysis of the splenocytes is shown. The percentages of (A, B) IL-12 producing macrophages and dendritic cells, (C, D) IL-17-producing CD4+ T helper cells and CD8+CTLs, and (E−G) regulatory cells (F4/80+IL-10+, CD11c+IL-10+, and CD4+Foxp3+) are presented. Values are mean ± SEM (n = 10 per group); $^{*}p < 0.05$, $^{**}p < 0.01$, $^{***}p < 0.001$.

ruthenium(II) coordination sphere is expected to alter the photophysical properties of the ruthenium(II) center as well as the DNA/serum albumin binding properties of the ruthenium-(II) complexes. In the study presented herein, we described the synthesis and structural characterization of the two novel heterometallic Ru(II)-tpy/ferrocene complexes [Ru(tpy)Cl_2(mtefc)] (**1**) and [Ru(tpy)Cl_2(mtpfc)] (**2**) (where mtefc = (2-(methylthio)-ethyl)ferrocene and mtpfc = (3-(methylthio)propyl)ferrocene). First we studied their solution behavior in water and under physiologically relevant conditions. Both complexes were proved to be sufficiently stable within a physiological-like environment, this representing the essential prerequisite for any further pharmacological evaluation.

The interactions of complexes **1** and **2** with CT DNA were examined not only by absorption (UV−vis) and fluorescence emission spectral studies (EB displacement studies) but also by viscosity measurements and molecular docking. We demonstrated the binding of the complexes to CT DNA and, also, a stabilization of the CT DNA duplex. The ability of complexes **1** and **2** to displace EB from the DNA−EB adduct was highly suggestive of intercalation, which was confirmed by the viscosity measurements. Both complexes showed a moderate affinity for serum albumin. Molecular docking studies were consistent with intercalation of the complexes into DNA. They also proposed that **1** and **2** interacted with albumin through its hydrophobic residues, particularly those lying in the proximity of Tyr 160. Overall, our study implied that biomolecules such as DNA and proteins might be the biological targets of the heterometallic Ru(II)-tpy compounds that contain ferrocenyl ligands such as (2-(methylthio)ethyl)ferrocene and (3-(methylthio)propyl)-ferrocene.

Having in mind our finding that the main mechanism of action of complexes **1** and **2** was apoptotic cell death of breast cancer cells and the literature data that the death of the tumor cells was closely related to induction of particular immune response,[71] we assumed that **1** and **2** significantly enhanced the immunogenicity of 4T1 cells and, hence, favored the transfer of tumor antigens to professional antigen presenting cells (macrophages and DCs). This event probably ultimately "cross-primed" and activated the antitumorigenic CD4+/CD8+T-cell immunity, which contributed to the reduced tumor growth and progression. To sum up, we demonstrated the potential of complexes **1** and **2** to be promising candidates for future pharmacological research in the field of breast cancer research. Although several studies have already described the potential of Ru(II) complexes to modulate microbicidal characteristics of macrophages,[55−57] herewith, we first demonstrated Ru(II) complex based polarization of tumor-infiltrating macrophages.

DOI: 10.1021/acs.organomet.8b00604
Organometallics 2018, 37, 4250−4266

EXPERIMENTAL SECTION

Chemicals and Solutions. 2,2′:6′,2′′-Terpyridine (tpy), ethidium bromide (EB), DNA sodium salt from calf thymus (CT DNA), and bovine serum albumin (BSA) are commercially available and were used as received. 1-Ferrocenyl-2-(methylthio)ethan-1-one and 1-ferrocenyl-3-(methylthio)propan-1-one were synthesized according to a previously described procedure.[34] The procedure for the synthesis of the ferrocenyl ligands was carried out under an argon atmosphere using Schlenk techniques. The complex $[Ru(tpy)Cl_3]$ was synthesized as reported previously.[72] All other chemicals were used as purchased without further purification. Doubly distilled water was used as the solvent throughout the experiments. Methanol solutions of the complexes (approximately 5 mM) were prepared for MALDI MS analysis. The solution of the matrix—dithranol in tetrahydrofuran—was freshly prepared prior to each use (10 mg mL^{-1}). A 0.5 μL portion of the complex solution was applied to the 100-well sample plate and left to dry at room temperature, and then 0.5 μL of the matrix solution was laid over the complex and left at room temperature to crystallize. The stock solution of CT-DNA was prepared in 10 mM phosphate buffer at pH 7.4, which gave a ratio of UV absorbances at 260 and 280 nm (A_{260}/A_{280}) of ca. 1.8−1.9, indicating that the DNA was sufficiently free of protein and the concentration was determined by UV absorbance at 260 nm (ε = 6600 M^{-1} cm^{-1}). The stock solution of BSA was prepared by dissolving the solid BSA in 10 mM phosphate buffer at pH 7.4, and the concentration was kept fixed at 2 μM. All stock solutions were stored at 4 °C and used within 5 days.

Instrumental Methods. Mono (^{1}H and ^{13}C)- and bidimensional (^{1}H−^{1}H NOESY, ^{1}H−^{13}C HSQC, and ^{1}H−^{13}C HMBC) NMR spectra were recorded on a Bruker Avance III 400 MHz and Varian Gemini 200 MHz (^{1}H at 400 and 200 MHz, ^{13}C at 101 MHz) NMR spectrometer. ^{1}H and ^{13}C chemical shifts in $CDCl_3$ were referenced to the peak of the residual nondeuterated solvent (δ 7.26 and 77.36, respectively). All NMR spectra were run at 298 K. The UV−vis spectra were obtained on a PerkinElmer Lambda 35 double-beam spectrophotometer, using 1.0 cm path length quartz cuvettes (3.0 mL). Infrared spectra were recorded on a PerkinElmer 983G spectrometer. Fluorescence measurements were carried out on an RF-1501 PC spectrofluorometer (Shimadzu, Japan). The excitation and emission bandwidths were both 10 nm. Matrix-assisted laser desorption/ionization time-of-flight (MALDI TOF) mass spectra were acquired on a Voyager-DE Pro instrument (Sciex, USA) equipped with a 50 Hz pulsed nitrogen laser operating at 337 nm. The instrumental settings were as follows: extraction voltage 9000 V, grid voltage 40%, guide wire 0.05%, extraction delay time 185 ns (complex **1**) or 120 ns (complex **2**), acquisition mass range m/z 300−800, laser intensity 2825, low mass gate OFF. The spectra were recorded in positive reflectron mode. Each spectrum represents an average of at least 300 laser shots. Electrospray ionization hybrid quadrupole time-of-flight (ESI Q-TOF) mass spectra were acquired on a Synapt G2-Si instrument (Waters). The instrumental settings were as follows: capillary voltage 2.8 kV, cone voltage 32 V, desolvation gas 650 L/h, desolvation temperature 350 °C, source temperature 120 °C. The pH of the solutions was measured using a Mettler Delta 350 digital pH meter with a combined glass electrode. This electrode was calibrated using standard buffer solutions of pH 4, 7, and 9 obtained from Sigma-Aldrich.

General Synthetic Procedure for Ferrocenyl Ligands.[34,35] To a solution of the corresponding acylferrocene (1 mmol) in dry THF (5 mL) in a Schlenk tube was added borane dimethyl sulfide complex solution (BH_3·SMe_2, 1 mL, 2 M in THF) under an argon atmosphere and the progress of the reaction monitored by TLC. The reaction mixture was stirred at reflux for 2.5 h and then cooled to room temperature. After the evaporation of the solvent, the residue was quenched by a 10% aqueous solution of HCl (30 mL) and the resultant mixture extracted with ethyl acetate (EtOAc) (two 20 mL portions). The combined organic layer was then washed with brine and dried over anhydrous Na_2SO_4. The solvent was removed under reduced pressure, and the crude product was purified by column chromatography (SiO_2; *n*-hexane/EtOAc mixture).

(2-(Methylthio)ethyl)ferrocene (mtefc). In a Schlenk tube under an argon atmosphere, 1-ferrocenyl-2-(methylthio)ethan-1-one (274 mg, 1 mmol) was dissolved in dry THF (5 mL) and then BH_3·SMe_2 (1 mL, 2 M in THF) was added. After the mixture was stirred at reflux for 2.5 h, the solvent was removed under reduced pressure and the residue was quenched by a 10% aqueous solution of HCl (30 mL). The resultant mixture was extracted with EtOAc (two 20 mL portions), and the combined organic layer was then washed with brine and dried over anhydrous Na_2SO_4. The solvent was evaporated, and the crude product was purified by column chromatography (SiO_2; *n*-hexane/EtOAc 85/15 (v/v)). The pure product was obtained in 88% yield. ^{1}H NMR (400 MHz, $CDCl_3$): δ 4.11 (s, 5H, C_5H_5), 4.11−4.09 (m, 2H, 2 × CH, C_5H_4), 4.08−4.06 (m, 1H, 2 × CH, C_5H_4), 2.69−2.56 (m, 4H, $-CH_2CH_2-$), 2.12 (s, 3H, -SCH_3). ^{13}C NMR (101 MHz, $CDCl_3$): δ 87.3 (C_5H_4), 68.6 (C_5H_5), 68.1 (C_5H_4), 67.4 (C_5H_4), 35.0 ($-CH_2CH_2-$), 29.9 ($-CH_2CH_2-$), 15.8 ($-SCH_3$). Selected IR (KBr, cm^{-1}): 3091 (w), 2916 (s), 2847 (w), 1630 (m), 1436 (s), 1001 (m), 819 (s), 486 (s). UV/visible spectrum (CH_3OH; λ_{max}, nm (ε, M^{-1} cm^{-1})): 442 (2184).

(3-(Methylthio)propyl)ferrocene (mtpfc). In a Schlenk tube under an argon atmosphere, 1-ferrocenyl-3-(methylthio)propan-1-one (288 mg, 1 mmol) was dissolved in dry THF (5 mL) and then BH_3·SMe_2 (1 mL, 2 M in THF) was added. After the mixture was stirred at reflux for 2.5 h, the solvent was removed under reduced pressure and the residue was quenched by a 10% aqueous solution of HCl (30 mL). The resultant mixture was extracted with EtOAc (two 20 mL portions), and the combined organic layer was then washed with brine and dried over anhydrous Na_2SO_4. The solvent was evaporated, and the crude product was purified by column chromatography (SiO_2; *n*-hexane/EtOAc 8/2 (v/v)). The pure product was obtained in 97% yield. ^{1}H NMR (200 MHz, $CDCl_3$): δ 4.13 (s, 5H, C_5H_5), 4.11−4.03 (m, 4H, 4 × CH, C_5H_4), 2.51 (t, J = 7.2 Hz, 2H, $-CH_2CH_2CH_2-$), 2.46−2.35 (m, 2H, $-CH_2CH_2CH_2-$), 2.10 (s, 3H, -SCH_3), 1.87−1.69 (m, 2H, $-CH_2CH_2CH_2-$). ^{13}C NMR (50 MHz, $CDCl_3$): δ 88.6 (C_5H_4), 68.7 (C_5H_5), 68.3 (C_5H_4), 67.4 (C_5H_4), 34.0 ($-CH_2CH_2CH_2-$), 30.3 ($-CH_2CH_2CH_2-$), 28.5 ($-CH_2CH_2CH_2-$), 15.5 ($-SCH_3$). Selected IR (KBr, cm^{-1}): 3092 (w), 2913 (s), 2851 (w), 1436 (s), 1000 (m), 818 (s), 486 (s). UV/visible spectrum (CH_3OH; λ_{max}, nm (ε, M^{-1} cm^{-1})): 442 (2524).

General Synthetic Procedure for Complexes [Ru(tpy)Cl$_2$(mtefc)] (1) and [Ru(tpy)Cl$_2$(mtpfc)] (2). A weighed amount of $[Ru(tpy)Cl_3]$ was suspended in an ethanol/H_2O (3/1) mixture containing 10 equiv of LiCl and 3 equiv of triethylamine (Et_3N). A ferrocenyl ligand (1.0 equiv; mtefc, mtpfc) was then added, and the mixture was refluxed under argon for ca. 6 h with vigorous stirring. The dark purple solution was filtered while hot to remove any undissolved material. Rotary concentration under reduced pressure to ca. 1/4 of the initial volume and storage at 4.0 °C for 24 h induced the formation of the product as a dark solid. It was collected by filtration, washed with ice-cold H_2O, cold acetone, and diethyl ether, vacuum-dried, and purified via column chromatography.

[Ru(tpy)Cl$_2$(mtefc)] (1). A 100.0 mg (0.181 mmol) portion of $[Ru(tpy)Cl_3]$, 58.8 mg (0.181 mmol) of mtefc, 96.2 mg (1.814 mmol) of LiCl, and 94.9 μL (0.544 mmol) of Et_3N in 20 mL of ethanol/H_2O afforded **1** as a dark purple solid. The product was purified via column chromatography on silica gel using dichloromethane/methanol (90/10, v/v) as eluent. The purple fraction was collected and the solvent removed to give a purple solid. Yield: 107.3 mg (71.6%). Anal. Calcd for $C_{28}H_{27}Cl_2FeN_3RuS$ (665.42): C, 50.54; H, 4.09; N, 6.31. Found: C, 50.84; H, 3.98; N, 6.39. Complex **1** is soluble in methanol, acetone, chloroform, dichloromethane, acetonitrile, and DMSO, partially soluble in ethanol, and slightly soluble in water. ^{1}H NMR (400 MHz, $CDCl_3$): 9.49 (d, 2H, J = 5.3 Hz, C6*H*/C6′′*H*), 8.10 (d, 2H, J = 8.0 Hz, C3*H*/C3′′*H*), 8.07 (d, 2H, J = 8.0 Hz, C3′*H*/C5′*H*), 7.78 (t, 2H, J = 7.3 Hz, C4*H*/C4′′*H*), 7.54 (dd, 3H, J = 7.3, 5.5 Hz, C5*H*/C5′′*H*, C4′*H*), 3.92 (br s, 2H, 2 × CH, C_5H_4), 3.91 (s, J = 4.4 Hz, 5H, C_5H_5), 3.70 (br s, 2H, 2 × CH, C_5H_4), 2.19−2.10 (m, 2H, $-CH_2CH_2-$), 2.10−1.98 (m, 2H, $-CH_2CH_2-$), 1.48 (s, 3H, $-SCH_3$). ^{13}C NMR ($CDCl_3$): 161.1 (*C*2′/*C*6′), 159.2 (*C*2/*C*2′′), 153.8 (*C*6H/*C*6′′H), 135.4 (*C*4H/*C*4′′H), 129.2 (*C*4′H), 127.0 (*C*5H/*C*5′′H), 121.9 (*C*3H/*C*3′′H), 121.3 (*C*3′H/*C*5′H), 85.8 (C_5H_4), 68.54 (C_5H_5). 67.7 (C_5H_4), 67.48 (C_5H_4), 36.5

DOI: 10.1021/acs.organomet.8b00604
Organometallics 2018, 37, 4250−4266

($-CH_2CH_2-$), 27.1 ($-CH_2CH_2-$), 17.1 ($-SCH_3$). Selected IR (KBr, cm^{-1}): 3054 (w), 2920 (m), 2855 (m), 1597(s), 1445 (s), 1378 (s). UV/visible spectrum (CH_3OH; λ_{max}, nm (ε, $M^{-1}cm^{-1}$)): 272 (13520), 313 (18850), 442 (2416).

*[Ru(tpy)Cl$_2$(mtpfc)] (**2**).* A 100.0 mg portion (0.181 mmol) of [Ru(tpy)Cl_3], 62.4 mg (0.181 mmol) of mtpfc, 96.2 mg (1.814 mmol) of LiCl, and 94.9 μL (0.544 mmol) of Et_3N in 20 mL of ethanol/H_2O afforded **2** as a dark purple solid. The product was purified via column chromatography on silica gel using dichloromethane/methanol (90/10, v/v) as eluent. The purple fraction was collected and the solvent removed to give a purple solid. Yield: 106.2 mg (69.0%). Anal. Calcd for $C_{29}H_{29}Cl_2FeN_3RuS$ (679.45): C, 51.26; H, 4.30; N, 6.18. Found: C, 51.30; H, 4.25; N, 6.24. Complex **2** is soluble in methanol, acetone, chloroform, dichloromethane, acetonitrile, and DMSO, partially soluble in ethanol, and slightly soluble in water. ^{1}H NMR (200 MHz, $CDCl_3$): 9.36 (d, 2H, J = 5.1 Hz, C6*H*/C6′′*H*), 8.30−8.06 (m, 4H, C3*H*/C3′′*H*, C3′*H*/C5′*H*), 8.14 (d, 2H, J = 8.0 Hz, C3′*H*/C5′*H*), 7.84 (t, 2H, J = 7.0 Hz, C4*H*/C4′′*H*), 7.67−7.50 (m, 3H, C5*H*/C5′′*H*, C4′*H*), 4.00 (s, J = 4.4 Hz, 5H, C_5H_5), 3.98−3.92 (m, 2H, 2 × CH, C_5H_4), 3.79−3.69 (m, 2H, 2 × CH, C_5H_4), 2.19−1.98 (m, 2H, $-CH_2CH_2CH_2-$), 1.98−1.70 (m, 2H, $-CH_2CH_2CH_2-$), 1.45 (s, 3H, $-SCH_3$), 1.35−1.10 (m, 2H, $-CH_2CH_2CH_2-$). ^{13}C NMR ($CDCl_3$): 161.0 (*C*2′/*C*6′), 159.2 (*C*2/*C*2′′), 153.6 (*C*6H/*C*6′′H), 135.5 (*C*4H/*C*4′′H), 129.3 (*C*4′H), 126.9 (*C*5H/*C*5′′H), 122.2 (*C*3H/*C*3′′H), 121.6 (C3′H/C5′H), 86.9 (C_5H_4), 68.5 (C_5H_5), 67.7 (C_5H_4), 67.5 (C_5H_4), 35.1 ($-CH_2CH_2CH_2-$), 30.3 ($-CH_2CH_2CH_2-$), 28.1 ($-CH_2CH_2CH_2-$), 16.4 ($-SCH_3$). Selected IR (KBr, cm^{-1}): 3054 (w), 2920 (m), 2854 (m), 1597(s), 1446 (s), 1378 (s). UV/visible spectrum (CH_3OH; λ_{max}, nm (ε, $M^{-1}cm^{-1}$)): 272 (11505), 313 (16180), 500 (2175).

Solution Studies. The solution chemistry of complexes **1** and **2** was analyzed by absorption UV−vis spectroscopy. The electronic spectra were recorded by diluting small amounts of freshly prepared concentrated solutions of the individual complexes in methanol in water and a buffer solution, 10 mM phosphate buffer (containing 137 mM NaCl, pH 7.4). The concentration of each complex in the final sample was 1 × 10^{-4} M. The resulting solutions were monitored by recording the electronic spectra over 24 h at room temperature.

DNA-Binding Studies. *Absorption Spectroscopic Studies.* The interaction of complexes **1** and **2** with CT DNA was studied using UV−vis spectroscopy. The DNA-binding experiments were performed at 37 °C. The absorption titration of the ruthenium(II) complex in 10 mM phosphate buffer (137 mM NaCl, pH 7.4) was performed by using a fixed complex concentration (12.5 μM) to which increments of the DNA stock solution were added (2.0 mM).

Fluorescence Quenching Measurements. The binding interaction of the complexes with CT DNA was also studied by fluorescence spectroscopy. The fluorescence intensities were measured with the excitation wavelength set at 527 nm and the fluorescence emission at 612 nm. The excitation and emission slit widths (each 10 nm) and scan rate were maintained constant for all the experiments. Stock solutions of DNA (2.0 mM) and complexes (0.1 mM) were prepared in 10 mM PBS buffer (137 mM NaCl, pH 7.4). A series of complex−DNA solutions were prepared by mixing DNA solutions with a different concentration of complexes. For fluorescence determination, the final DNA concentration was 80.0 μM, and the complex concentrations varied from 8.0 to 80.0 μM. Before measurements, the system was shaken and incubated at room temperature for 5 min. The emission was recorded at 550−750 nm.

Viscosity Measurements. The viscosity of a DNA solution was measured in the presence of increasing amounts of complexes **1** and **2**. The flow time was measured with a digital stopwatch, each sample was measured six times, and the average flow time was calculated. The data are presented as $(\eta/\eta_0)^{1/3}$ against r, where η is the viscosity of DNA in the presence of complex and η_0 is the viscosity of DNA alone in the buffered solution. The viscosity values were calculated from the observed flow time of the DNA-containing solutions (t) corrected for the flow time of the buffer alone (t_0): $\eta = (t - t_0)/t_0$.

Albumin-Binding Studies. The protein binding study was performed by tryptophan fluorescence quenching experiments using bovine serum albumin (BSA, 2 μM) in 10 mM PBS (137 mM NaCl, pH 7.4). Quenching of the emission intensity of tryptophan residues of BSA at 365 nm was monitored using complexes **1** and **2** as quenchers with increasing concentration (up to 3.0 × 10^{-5} M). Fluorescence spectra were recorded in the range 300−500 nm at an excitation wavelength of 295 nm. The fluorescence spectra of the compounds in buffered solutions were recorded under the same experimental conditions, and no fluorescence emission was detected. The Stern−Volmer and Scatchard equations (Supporting Information, eqs S3−S6) and graphs have been used to study the interaction of the complexes with serum albumin and to calculate the corresponding constants.

Molecular Docking with DNA and BSA. The initial three-dimensional structures of B-DNA dodecamer and BSA were retrieved from the protein data bank with PDB ID 1BNA and 3V03, respectively. The structures were processed using Protein Preparation Wizard and Glide model as a part of the Schrödinger package suite.[73] The structural integrity was checked and adjusted using Prime, by implying the parameters such as assigning bond orders to hydrogens; zero-order bonds were created to metal atoms, and capping of the termini and desolvation were carried out by deleting the crystallized free water molecules beyond 5 Å. The protonation and tautomeric states of residues were adjusted to match pH 7 performed using PROPKA.[74] The receptors (receptor = 1BNA or BSA) were subjected to a geometry refinement using an OPLS-2005 force field restrained minimization with the convergence of heavy atoms to an RMSD of 0.3 Å.[75] Before the docking procedure ligands (ligand = complex **1** or **2**) were prepared and optimized using MacroModel/Conformation Search and LigPrep options. For docking calculations, Lamarckian genetic algorithms were used and the grid size was set at 35 × 35 × 35 for DNA and 40 × 40 × 40 Å for BSA with flexible ligand sampling and extra precision. Docking parameters were as follows: population size 50, maximum number of iterations 2000, maximum number of steps 500, van der Waals scaling factor of 0.8, and partial charge cutoff 0.15. The number of generated poses was 10. At the end of the docking runs, the diverse binding energy of the complexes was obtained with their respective conformations; the stable conformation which corresponds to the lowest binding energy was chosen as the best pose and was used in the docking analysis. The lowest energy poses were presented using Maestro Pose Viewer.

Preparation of Drug Solution. Stock solution of complexes **1** and **2** were dissolved in DMSO (Sigma-Aldrich, Germany) at a concentration of 40 mM, filtered through a 0.22 mm Millipore filter before use, and diluted by a nutrient cell medium (Dulbecco's Modified Eagle's medium (DMEM), Sigma-Aldrich, Germany) to various working concentrations (0.3, 1, 3, 10, 30, and 100 μM), so that the final concentration of DMSO in the cell culture medium never exceeded 0.5% (v/v). All solutions were prepared on the day of the treatment of the cells.

Cell Lines. Human (MDA-MB-231) and murine (4T1) breast cancer cell lines were purchased from American Type Culture Collection (ATCC, Manassas, USA). All cells were maintained in complete growth medium, which consisted of high-glucose DMEM (Sigma-Aldrich, Munich, Germany) supplemented with 10% fetal bovine serum (FBS, Sigma-Aldrich, Munich, Germany), penicillin G (100 IU/mL, Sigma-Aldrich, Munich, Germany), and streptomycin (100 μg/mL, Sigma-Aldrich, Munchen, Germany), and under an atmosphere containing 5% CO_2 at 37 °C at absolute humidity. The number of viable tumor cells was determined by trypan blue exclusion, and only cell suspensions with ≥95% viable cells were used.

MTT (3-(4,5-Dimethylthiazol-2-yl)-2,5-diphenyltetrazolium Bromide) Tetrazolium Reduction Assay. The cytotoxicities of **1** and **2** on experimental cells were evaluated by an MTT assay and compared with the cytotoxicity of cisplatin.[76] Tumor cells were harvested from the culture flasks during the exponential growth phase, and 5 × 10^3 cells/well were seeded into 96-well cell culture plates. The cells were allowed to adhere, and after 24 h, the cells were treated with selected concentrations of **1**, **2**, and cisplatin (0.3, 1, 3, 10, 30, and 100 μM). Control wells were prepared by the addition of complete cell culture medium alone. All cell lines were incubated at 37 °C under an atmosphere containing 5% CO_2 at absolute humidity for 72 h. After

DOI: 10.1021/acs.organomet.8b00604
Organometallics 2018, 37, 4250−4266

incubation, the drug-containing medium was removed from each well and MTT solution (final concentration of 0.5 mg/mL) was added to each well. After an additional 4 h of incubation at 37 °C in the 5% CO_2 incubator, MTT solution was gently removed and the formazan crystals were dissolved in DMSO. The plates were then shaken for 10 min. The optical density of each well was determined at 595 nm using a Zenyth 3100 multimode microplate detector. Experiments were performed in triplicate to obtain mean values. Results are presented as a ratio to the control value (untreated cells). Also, by use of Microsoft Office Excel 2010, IC_{50} values were calculated.

Detection of Apoptosis. The type of cell death of tumor cells was estimated by an annexin V−fluorescein isothiocyanate (FITC)/7-amino-actinomycin D (7-AAD) test. MDA-MB-231 and 4T1 cells were incubated with the appropriate IC_{50} concentrations (calculated previously by MTT assay results) of **1**, **2**, and cisplatin or with DMEM media alone (control) for 24 h at 37 °C under an atmosphere of 5% CO_2 and at absolute humidity. Afterward, cells were trypsinized, washed in PBS, centrifuged, and resuspended in 100 μL of ice-cold binding buffer. In addition, cells were stained with both 10 μL of Annexin V-FITC and 20 μL of 7-AAD, incubated for 15 min at room temperature in the dark. Afterward, 400 μL of binding buffer was added to each tube. Data were analyzed by flow cytometry (BD FACSCalibur, BD Biosciences, Franklin Lakes, NJ) and FlowJo.

Cell Cycle Analysis by Flow Cytometry. In order to examine the potential effects of tested ruthenium complexes on the cell cycle progression of 4T1 and MDA-MB-231 cells, these cells were incubated with the appropriate IC_{50} concentrations of ruthenium complexes **1** and **2** and cisplatin or with media alone (control) for 24 h at 37 °C under an atmosphere containing 5% CO_2 at the absolute humidity. Cell cycle analysis was performed with Vybrant DyeCycleTM Ruby stain (Thermo Fisher Scientific, Inc. USA) according to the manufacturer's instructions. After treatment, cells were stained with Vybrant DyeCycle Ruby and analyzed by a FACS Calibur flow cytometer (BD Biosciences, San Jose, USA). The cell cycle distribution was analyzed using FlowJo software.

Hydrogen Peroxide Determination. The level of hydrogen peroxide (H_2O_2) in cell cultures of 4T1 and MDA-MB 231 cells treated with complexes **1** and **2**, as well as with cisplatin, was determined by a spectrophotometric method. The protocol for H_2O_2 is based on the oxidation of phenol red in the presence of horseradish peroxidase. A 200 μL sample with 800 μL of PRS (phenol red solution) and 10 μL of POD (horseradish peroxidase) were combined (1/20). The level of H_2O_2 was measured at 610 nm.[78]

Animals. BALBc, 6−8 weeks old female mice, were used. Mice were equalized in weight and randomized in experimental and control groups. All mice were maintained in our animal facilities. Mice were housed in a temperature-controlled environment with a 12 h light−dark cycle and were given standard laboratory chow and water ad libitum. All animals received humane care, and all experiments were approved by, and conducted in accord with, the Guidelines of the Animal Ethics Committee of the Faculty of Medical Sciences of the University of Kragujevac (Kragujevac, Serbia).

Induction of Mouse Breast Cancer and Application of Complexes 1 and 2. Mice were inoculated with 5×10^4 4T1 tumor cells/50 μL phosphate-buffered saline (PBS, Invitrogen, USA) orthotopically into the fourth mammary fat-pad, as described previously.[77] When tumors became palpable (15 days after injection of 4T1 cells), mice (two times per week) received complex **1** or **2** (10 mg/kg), cisplatin (4 mg/kg), or vehicle (PBS) by intraperitoneal injection.[79] Primary 4T1 mammary tumors were measured morphometrically using electronic calipers. Tumor volumes (mm^3) were calculated as $LW^2/2$, where L represents the major axis of the tumor, while W represents the minor axis.[57]

Isolation of Tumor-Infiltrating Leukocytes. Primary 4T1 tumors were minced and placed in 5 mL of DMEM containing 1 mg/mL of collagenase I, 1 mM ethylenediaminetetraacetic acid (EDTA), and 2% FBS (all from Sigma-Aldrich) for enzymatic digestion. After an incubation time of 2 h at 37 °C, 10 mL of 0.25% trypsin was added and the mixture incubated for 3 min followed by DNase I (Sigma-Aldrich) solution for 1 min. The cells were filtered through a 40 μm nylon cell-strainer (BD Biosciences) into a clean 50 mL conical tube. Then, cells were pelleted by centrifuging 10 min at 450*g*, at 4 °C.[57]

Isolation of Splenocytes. The isolation of splenocytes was conducted as previously described.[80] Briefly, the spleens were minced in DMEM and forced gently through a 40 mm cell-strainer nylon mesh using a sterile syringe plunger and centrifuged at 400*g* for 5 min. Pelleted spleen cells were incubated in 2 mL of NH_4Cl/Tris-Cl (pH 7.2) for 5 min, supplemented with 1 mL of FBS, centrifuged at 400*g* for 5 min, and then resuspended in DMEM with 10% FBS. The cells were used for flow cytometry analysis.

Flow Cytometry Analysis. Tumor-infiltrated immune cells and splenocytes were analyzed by flow cytometry.[81] Cells were incubated with antimouse antibodies CD4, CD8, CD49, CD11c, and F4/80 conjugated with fluorescein isothiocyanate (FITC; BD Biosciences, Franklin Lakes, NJ), phycoerythrin (PE; BD Biosciences), peridinin chlorophyll protein (BD Biosciences), or allophycocyanin (APC; BD Biosciences). Flow cytometric analysis was conducted on a BD Biosciences FACS Calibur and analyzed using the Flowing Software program. Immune cells derived from the tumor and spleen were concomitantly stained for the intracellular contents of TNF-α, IL-10, IL-17, IL-12, IFN-γ, and forkhead box P3 (FoxP3) by using the fixation/permeabilization kit and antimouse monoclonal antibodies conjugated with FITC, PE, PerCP, and APC. For intracellular cytokine staining, cells were stimulated with 50 ng/mL of PMA and 500 ng/mL of ionomycin for 5 h, and GolgiStop (BD Biosciences) was added. Cells were fixed in Cytofix/Cytoperm, permeabilized with 0.1% saponin, and stained with fluorescent Abs. Flow cytometric analysis was conducted on a BD Biosciences FACSCalibur and analyzed by using the Flowing Software analysis program.

Statistical Analysis. The results were analyzed using Student's *t* test. All data in this study were expressed as the mean ± standard error of the mean (SEM). Values of $p < 0.05$ were considered as statistically significant.

■ ASSOCIATED CONTENT

Supporting Information

The Supporting Information is available free of charge on the ACS Publications website at DOI: 10.1021/acs.organomet.8b00604.

NMR spectra, FT-IR spectra, ESI-MS and MALDI TOF MS spectra, UV−vis spectra, and molecular docking study (PDF)

■ AUTHOR INFORMATION

Corresponding Authors

*T.K.: tel, +381(0)34306800; e-mail, tatjanakanjevac@yahoo.com.

*A.R.S.: tel, +381(0)34300262; fax, +381(0)34335040; e-mail, anarilak@kg.ac.rs;.

ORCID

Milan M. Milutinović: 0000-0003-4838-3998
Petar P. Čanović: 0000-0002-2119-4954
Dragana Stevanović: 0000-0003-3199-0775
Romana Masnikosa: 0000-0002-5220-4334
Milan Vraneš: 0000-0001-8259-7549
Milan M. Zarić: 0000-0001-7004-2239
Maja Misirkić Marjanović: 0000-0002-0510-826X
Ljubica Vučićević: 0000-0003-2802-2773
Maja Savić: 0000-0001-8013-0662
Vladimir Trajković: 0000-0002-8061-2968
Ana Rilak Simović: 0000-0001-8731-3605

Author Contributions

@M.M.M. and P.P.C. contributed equally to this paper.

DOI: 10.1021/acs.organomet.8b00604
Organometallics 2018, 37, 4250−4266

Notes

The authors declare no competing financial interest.

■ ACKNOWLEDGMENTS

This work is dedicated to the deceased Prof. Dr. Živadin D. Bugarčić, a great scientist in the field of bioinorganic reaction mechanisms, a teacher, and a real friend. The authors wish to thank Dr. Slobodan Nikolić and Vera Lukić from the Institute of Forensic Medicine Milovan Milovanović, Belgrade, Serbia, for their help in acquiring ESI Q-TOF mass spectra. The authors gratefully acknowledge financial support from the Ministry of Education and Science of the Republic of Serbia (Project Nos. 172011, 175069, 175103, and 172034) and Faculty of Medical Sciences, University of Kragujevac (No. MP 01/18).

■ ABBREVIATIONS USED

tpy, 2,2′:6′,2′′-terpyridine; mtefc, (2-(methylthio)ethyl)-ferrocene; mtpfc, (3-(methylthio)propyl)ferrocene; CT DNA, calf thymus DNA; EB, ethidium bromide; BSA, bovine serum albumin; MDA-MB-231, human breast cancer cell; 4T1, murine breast cancer cell; ethyl acetate, EtOAc; PBS, phosphate buffer; 1BNA, dodecamer d(CGCGAATTCGCG)$_2$; M1, M2, macrophages; TNF-α, tumor necrosis factor-α; IL-10, IL-12, IL-17, -nterleukin-10, -12, -17; DCs, tumor-infiltrating dendritic cells; Tregs, regulatory T cells; FITC, fluorescein isothiocyanate; 7-AAD, 7-amino-actinomycin D

■ REFERENCES

(1) Lazarević, T.; Rilak, A.; Bugarčić, Ž. D. Platinum, palladium, gold and ruthenium complexes as anticancer agents: Current clinical uses, cytotoxicity studies and future perspectives. *Eur. J. Med. Chem.* **2017**, *142*, 8−31.

(2) Romero-Canelon, I.; Sadler, P. J. Next-Generation Metal Anticancer Complexes: Multitargeting via Redox Modulation. *Inorg. Chem.* **2013**, *52*, 12276−12291.

(3) Zhang, C. X.; Lippard, S. J. New metal complexes as potential therapeutics. *Curr. Opin. Chem. Biol.* **2003**, *7*, 481−489.

(4) Noffke, A. L.; Habtemariam, A.; Pizarro, A. M.; Sadler, P. J. Designing organometallic compounds for catalysis and therapy. *Chem. Commun.* **2012**, *48*, 5219−5246.

(5) van Rijt, S. H.; Sadler, P. J. Current applications and future potential for bioinorganic chemistry in the development of anticancer drugs. *Drug Discovery Today* **2009**, *14*, 1089−1097.

(6) Alessio, E. *Bioinorganic Medicinal Chemistry*; Wiley-VCH: Weinheim, Germany, 2011.

(7) Chen, H.; Parkinson, J. A.; Parsons, S.; Coxall, R. A.; Gould, R. O.; Sadler, P. J. Organometallic ruthenium(II) diamine anticancer complexes: arene-nucleobase stacking and stereospecific hydrogen-bonding in guanine adducts. *J. Am. Chem. Soc.* **2002**, *124*, 3064−3082.

(8) Trondl, R.; Heffeter, P.; Kowol, C. R.; Jakupec, M. A.; Berger, W.; Keppler, B. K. NKP-1339, the first ruthenium-based anticancer drug on the edge to clinical application. *Chem. Sci.* **2014**, *5*, 2925−2932.

(9) Ang, W. H.; Casini, A.; Sava, G.; Dyson, P. J. Organometallic ruthenium-based antitumor compounds with novel modes of action. *J. Organomet. Chem.* **2011**, *696*, 989−998.

(10) Habtemariam, A.; Melchart, M.; Fernandez, R.; Parsons, S.; Oswald, I. D. H.; Parkin, A.; Fabbiani, F. P. A.; Davidson, J. E.; Dawson, A.; Aird, R. E.; Jodrell, D. I.; Sadler, P. J. Structure-activity relationships for cytotoxic ruthenium(II) arene complexes containing N,N-, N,O-, and O,O-chelating ligands. *J. Med. Chem.* **2006**, *49*, 6858−6868.

(11) Milutinović, M. M.; Bugarčić, Ž. D.; Wilhelm, R. A. Camphor based 1,3-diamine Ru(II) terpyridine complex: synthesis, characterization, kinetic investigation and DNA binding. *New J. Chem.* **2018**, *42*, 7607−7611.

(12) Barry, P. E. N.; Sadler, P. J. Exploration of the medical periodic table: towards new targets. *Chem. Commun.* **2013**, *49*, 5106−5131.

(13) Yan, Y. K.; Melchart, M.; Habtemariam, A.; Sadler, P. J. Organometallic chemistry, biology and medicine: ruthenium arene anticancer complexes. *Chem. Commun.* **2005**, 4764−4776.

(14) Suss-Fink, G. Arene ruthenium complexes as anticancer agents. *Dalt. Trans.* **2010**, *39*, 1673−1688.

(15) Milutinović, M. M.; Rilak, A.; Bratsos, I.; Klisurić, O.; Vraneš, M.; Gligorijević, N.; Radulović, S.; Bugarčić, Ž. D. New 4'-(4-chlorophenyl)-2,2':6',2''-terpyridine ruthenium(II) complexes: Synthesis, characterization, interaction with DNA/BSA and cytotoxicity studies. *J. Inorg. Biochem.* **2017**, *169*, 1−12.

(16) Nišavić, M.; Stoiljković, M.; Crnolatac, I.; Milošević, M.; Rilak, A.; Masnikosa, R. Highly water-soluble ruthenium(II) terpyridine coordination compounds form stable adducts with blood-borne metal transporting proteins. *Arabian J. Chem.* **2018**, *11*, 291−304.

(17) Čanović, P.; Rilak Simović, A.; Radisavljević, S.; Bratsos, I.; Demitri, N.; Mitrović, M.; Zelen, I.; Bugarčić, Ž. D. Impact of aromaticity on anticancer activity of polypyridyl ruthenium(II) complexes: synthesis, structure, DNA/protein binding, lipophilicity and anticancer activity. *JBIC, J. Biol. Inorg. Chem.* **2017**, *22*, 1007−1028.

(18) Woodward, R. B.; Rosenblum, M.; Whiting, M. A new aromatic system. *J. Am. Chem. Soc.* **1952**, *74*, 3458−3459.

(19) Sathyaraj, G.; Kiruthika, M.; Weyhermüller, T.; Unni Nair, B. Oxidative Cleavage of DNA by Ruthenium(II) Complexes Containing a Ferrocene/Non-Ferrocene Conjugated Imidazole Phenol Ligand. *Organometallics* **2012**, *31*, 6980−6987.

(20) Anderson, C. M.; Jaina, S. S.; Silber, K.; Chen, S.; Guha, W.; Zhang, E. C.; McLaughlin, Y.; Hu, J.; Tanski, M. Synthesis and characterization of water-soluble, heteronuclear ruthenium(III)/ferrocene complexes and their interactions with biomolecules. *J. Inorg. Biochem.* **2015**, *145*, 41−50.

(21) Kondapi, A. K.; Satyanarayana, N.; Saikrishna, A. D. A study of the topoisomerase II activity in HIV-1 replication using the ferrocene derivatives as probes. *Arch. Biochem. Biophys.* **2006**, *450*, 123−132.

(22) Paitandi, R. P.; Gupta, R. K.; Singh, R. S.; Sharma, G.; Koch, B.; Pandey, D. S. Interaction of ferrocene appended Ru(II), Rh(III) and Ir(III) dipyrrinato complexes with DNA/protein, molecular docking and antitumor activity. *Eur. J. Med. Chem.* **2014**, *84*, 17−29.

(23) Fouda, M. F. R.; Abd-Elzaher, M. M.; Abdelsamaia, R. A.; Labib, A. A. On the medicinal chemistry of ferrocene. *Appl. Organomet. Chem.* **2007**, *21*, 613−625.

(24) Zhang, J. Preparation, characterization, crystal structure and bioactivity determination of ferrocenyl−thiazoleacylhydrazones. *Appl. Organomet. Chem.* **2008**, *22*, 6−11.

(25) Ornelas, C. Application of ferrocene and its derivatives in cancer research. *New J. Chem.* **2011**, *35*, 1973−1985.

(26) Jaouen, G.; Top, S.; Vessires, A.; Leclercq, M.; McGlinchey, J. The first organometallic selective estrogen receptor modulators (SERMs) and their relevance to breast cancer. *Curr. Med. Chem.* **2004**, *11*, 2505−2517.

(27) Van Staveren, D. R.; Metzler-Nolte, N. Bioorganometallic chemistry of ferrocene. *Chem. Rev.* **2004**, *104*, 5931−5985.

(28) Von Poelhsitz, G.; Bogado, A. L.; de Araujo, M. P.; Selistre-de-Araújo, H. S.; Ellena, J.; Castellano, E. E.; Batista, A. A. Synthesis, characterization, X-ray structure and preliminary in vitro antitumor activity of the nitrosyl complex fac-[$RuCl_3$(NO)(dppf)], dppf = 1,1′-bis(diphenylphosphine)ferrocene. *Polyhedron* **2007**, *26*, 4707.

(29) Tabbi, G.; Cassino, C.; Cavigiolio, G.; Colangelo, D.; Ghiglia, A.; Viano, I.; Osella, D. Water stability and cytotoxic activity relationship of a series of ferrocenium derivatives. ESR insights on the radical production during the degradation process. *J. Med. Chem.* **2002**, *45*, 5786−5796.

(30) Plażuk, D.; Zakrzewski, J.; Salmain, M.; Błauż, A.; Rychlik, B.; Strzelczyk, P.; Bujacz, A.; Bujacz, G. Ferrocene−Biotin Conjugates Targeting Cancer Cells: Synthesis, Interaction with Avidin, Cytotoxic Properties and the Crystal Structure of the Complex of Avidin with a Biotin−Linker−Ferrocene Conjugate. *Organometallics* **2013**, *32*, 5774.

(31) Poynton, F. E.; Bright, S. A.; Blasco, S.; Clive Williams, D.; Kelly, J. M.; Gunnlaugsson, T. The development of ruthenium(II) polypyridyl

DOI: 10.1021/acs.organomet.8b00604
Organometallics 2018, 37, 4250−4266

complexes and conjugates for in vitro cellular and in vivo applications. *Chem. Soc. Rev.* **2017**, *46*, 7706−7756.
(32) Rilak, A.; Bratsos, I.; Zangrando, E.; Kljun, J.; Turel, I.; Bugarčić, Ž. D.; Alessio, E. New water-soluble ruthenium(II) terpyridine complexes for anticancer activity: synthesis, characterization, activation kinetics, and interaction with guanine derivatives. *Inorg. Chem.* **2014**, *53*, 6113−6126.
(33) Lazić, D.; Arsenijević, A.; Puchta, R.; Bugarčić, Ž. D.; Rilak, A. DNA binding properties, histidine interaction and cytotoxicity studies of water soluble ruthenium(II) terpyridine complexes. *Dalton. Trans.* **2016**, *45*, 4633−4646.
(34) Milutinović, M. M.; Elmroth, S. K. C.; Davidović, G.; Rilak, A.; Klisurić, O.; Bratsos, I.; Bugarčić, Ž. D. Kinetic and mechanistic study on the reactions of ruthenium(II) chlorophenyl terpyridine complexes with nucleobases, oligonucleotides and DNA. *Dalton. Trans.* **2017**, *46*, 2360−369.
(35) Ilić, D.; Damljanović, I.; Stevanović, D.; Vukićević, M.; Radulović, N.; Kahlenberg, V.; Laus, G.; Vukićević, R. D. Synthesis, spectral characterization, electrochemical properties and antimicrobial screening of sulfur containing acylferrocenes. *Polyhedron* **2010**, *29*, 1863−1869.
(36) Routaboul, L.; Chiffre, J.; Balavoine, G. G. A.; Daran, J. C.; Manoury, E. Highly efficient reduction of ferrocenyl derivatives by borane. *J. Organomet. Chem.* **2001**, *637-639*, 364−371.
(37) Chatterjee, D.; Sengupta, A.; Mitra, A. Synthesis, characterization and reactivity of a novel ruthenium(II) complex containing polypyridyl ligand. *Polyhedron* **2007**, *26*, 178−183.
(38) Papaefstathiou, G. S.; Sofetis, A.; Raptopoulou, C. P.; Terzis, A.; Spyroulias, G. A.; Zafiropoulos, T. F. 2,2′-Bipyridine, 1,10-phenanthroline and 2,2′:6′,2″-terpyridine in gallium(III) chemistry: Complexes containing the $\{GaIII_2(\mu\text{-}OH)_2\}^{4+}$ core. *J. Mol. Struct.* **2007**, *837*, 5−14.
(39) Patel, M. N.; Gandhi, D. S.; Parmar, P. A.; Joshi, H. N. DNA-binding and cleavage activity of polypyridyl ruthenium(II) complexes. *J. Coord. Chem.* **2012**, *65*, 1926−1936.
(40) Jeitler, J. R.; Turnbull, M. M.; Wikaira, J. L. Synthesis, characterization and structure of transition metal complexes of 4′-methylthio-2,2′:6′,2″-terpyridyl. *Inorg. Chim. Acta* **2003**, *351*, 331−344.
(41) Gupta, N.; Grover, N.; Neyhart, G. A.; Singh, P.; Thorp, H. H. Synthesis and properties of new DNA cleavage agents based on oxoruthenium(IV). *Inorg. Chem.* **1993**, *32*, 310−316.
(42) Takeuchi, K. J.; Thompson, M. S.; Pipes, D. W.; Meyer, T. J. Redox and spectral properties of monooxo polypyridyl complexes of ruthenium and osmium in aqueous media. *Inorg. Chem.* **1984**, *23*, 1845−1851.
(43) Dovletoglou, A.; Adeyemi, S. A.; Meyer, T. J. Coordination and redox chemistry of substituted-polypyridyl complexes of ruthenium. *Inorg. Chem.* **1996**, *35*, 4120−4127.
(44) Jovanović, S.; Obrenčević, K.; Bugarčić, Ž. D.; Popović, I.; Žakula, J.; Petrović, B. New bimetallic palladium(II) and platinum(II) complexes: studies of the nucleophilic substitution reactions, interactions with CT-DNA, bovine serum albumin and cytotoxic activity. *Dalton Trans* **2016**, *45*, 12444−12457.
(45) Nišavić, M.; Masnikosa, R.; Butorac, A.; Perica, K.; Rilak, A.; Korićanac, L.; Hozić, A.; Petković, M.; Cindrić, M. Elucidation of the binding sites of two novel Ru(II) complexes on bovine serum albumin. *J. Inorg. Biochem.* **2016**, *159*, 89−95.
(46) Ćoćić, D.; Jovanović, S.; Nišavić, M.; Baskić, D.; Todorović, D.; Popović, S.; Bugarčić, Ž. D.; Petrović, B. New dinuclear palladium(II) complexes: Studies of the nucleophilic substitution reactions, DNA/BSA interactions and cytotoxic activity. *J. Inorg. Biochem.* **2017**, *175*, 67−79.
(47) Mondal, B.; Walawalkar, M. G.; Lahiri, G. K. Ruthenium terpyridine complexes incorporating azo-imine based ancillary ligands. Synthesis, crystal structure, spectroelectro chemical properties and solution reactivities. *J. Chem. Soc. Dalton. Trans.* **2000**, *22*, 4209−4217.
(48) Tarushi, A.; Polatoglou, E.; Kljun, J.; Turel, I.; Psomas, G.; Kessissoglou, D. P. Interaction of Zn(II) with quinolone drugs: structure and biological evaluation. *Dalton Trans* **2011**, *40*, 9461−9473.
(49) Tarushi, A.; Lafazanis, K.; Kljun, J.; Turel, I.; Pantazaki, A. A.; Psomas, G.; Kessissoglou, D. P. First- and second-generation quinolone antibacterial drugs interacting with zinc(II): structure and biological perspectives. *J. Inorg. Biochem.* **2013**, *121*, 53−65.
(50) Tarushi, A.; Psomas, G.; Raptopoulou, C. P.; Kessissoglou, D. P. Zinc complexes of the antibacterial drug oxolinic acid: structure and DNA-binding properties. *J. Inorg. Biochem.* **2009**, *103*, 898−905.
(51) Koumousi, E. S.; Zampakou, M.; Raptopoulou, C. P.; Psycharis, V.; Beavers, C. M.; Teat, S. J.; Psomas, G.; Stamatatos, T. C. First palladium(II) and platinum(II) complexes from employment of 2,6-diacetylpyridine dioxime: synthesis, structural and spectroscopic characterization, and biological evaluation. *Inorg. Chem.* **2012**, *51*, 7699−7710.
(52) Li, D. D.; Tian, J. L.; Gu, W.; Liu, X.; Yan, S. P. A novel 1,2,4-triazole-based copper(II) complex: synthesis, characterization, magnetic property and nuclease activity. *J. Inorg. Biochem.* **2010**, *104*, 171−179.
(53) Jiang, M.; Li, Y.; Wu, Z.; Liu, Z.; Yan, C. Synthesis, crystal structure, cytotoxic activities and DNA-binding properties of new binuclear copper(II) complexes bridged by N,N′-bis(N-hydroxyethylaminoethyl)oxamide. *J. Inorg. Biochem.* **2009**, *103*, 833−844.
(54) Wang, Y.; Zhang, H.; Zhang, G.; Tao, W.; Tang, S. Interaction of the flavonoid hesperidin with bovine serum albumin: A fluorescence quenching study. *J. Lumin.* **2007**, *126*, 211−218.
(55) Psomas, G.; Kessissoglou, D. P. Quinolones and non-steroidal anti-inflammatory drugs interacting with copper(II), nickel(II), cobalt(II) and zinc(II): structural features, biological evaluation and perspectives. *Dalton Trans* **2013**, *42*, 6252−6276.
(56) Costa, M. S.; Gonçalves, Y. G.; Nunes, D. C. O.; Napolitano, D. R.; Maia, P. I. S.; Rodrigues, R. S.; Rodrigues, V. M.; Von Poelhsitz, G.; Yoneyama, K. A. G. Anti-Leishmania activity of new ruthenium(II) complexes: Effect on parasite-host interaction. *J. Inorg. Biochem.* **2017**, *175*, 225−231.
(57) Fernández, M.; Arce, E. R.; Sarniguet, C.; Morais, T. S.; Tomaz, A. I.; Azar, C. O.; Figueroa, R.; Diego Maya, J.; Medeiros, A.; Comini, M.; Helena Garcia, M.; Otero, L.; Gambino, D. Novel ruthenium(II) cyclopentadienyl thiosemicarbazone compounds with antiproliferative activity on pathogenic trypanosomatid parasites. *J. Inorg. Biochem.* **2015**, *153*, 306−314.
(58) Magán, R.; Marín, C.; Rosales, M. J.; Salas, J. M.; Sánchez-Moreno, M. Therapeutic potential of new Pt(II) and Ru(III) triazolepyrimidine complexes against Leishmania donovani. *Pharmacology* **2005**, *73*, 41−48.
(59) Jovanović, I. P.; Pejnović, N. N.; Radosavljević, G. D.; Pantić, J. M.; Milovanović, M. Z.; Arsenijević, N. N.; Lukić, M. L. Interleukin-33/ST2 axis promotes breast cancer growth and metastases by facilitating intratumoral accumulation of immunosuppressive and innate lymphoid cells. *Int. J. Cancer* **2014**, *134*, 1669−1682.
(60) Meraz, I. M.; Savage, D. J.; Segura-Ibarra, V.; Li, J.; Rhudy, J.; Gu, J.; Serda, R. E. Adjuvant cationic liposomes presenting MPL and IL-12 induce cell death, suppress tumor growth, and alter the cellular phenotype of tumors in a murine model of breast cancer. *Mol. Pharmaceutics* **2014**, *11*, 3484−3491.
(61) Blick, M.; Sherwin, S. A.; Rosenblum, M.; Gutterman, J. Phase I study of recombinant tumor necrosis factor in cancer patients. *Cancer Res.* **1987**, *47*, 2986−2989.
(62) Milosavljević, M.; Jovanović, I. P.; Pejnović, N. N.; Mitrović, S. L.; Arsenijević, N. N.; Simović Marković, B. J.; Lukić, M. L. Deletion of IL-33R attenuates VEGF expression and enhances necrosis in mammary carcinoma. *Oncotarget* **2016**, *7*, 18106−18115.
(63) Ruffell, B.; Chang-Strachan, D.; Chan, V.; Rosenbusch, A.; Ho, C. M.; Pryer, N.; Daniel, D.; Hwang, E. S.; Rugo, H. S.; Coussens, L. M. Macrophage IL-10 blocks CD8+ T cell-dependent responses to chemotherapy by suppressing IL-12 expression in intratumoral dendritic cells. *Cancer Cell* **2014**, *26*, 623−637.
(64) Wu, T. C.; Xu, K.; Banchereau, R.; Marches, F.; Yu, C. I.; Martinek, J.; Anguiano, E.; Pedroza-Gonzalez, A.; Snipes, G. J.; O'Shaughnessy, J.; Nishimura, S.; Liu, Y. J.; Pascual, V.; Banchereau, J.;

DOI: 10.1021/acs.organomet.8b00604
Organometallics 2018, 37, 4250−4266

Oh, S.; Palucka, K. Reprogramming tumor-infiltrating dendritic cells for CD103+ CD8+ mucosal T-cell differentiation and breast cancer rejection. *Cancer Immunol. Res.* **2014**, *2*, 487−500.
(65) Abdellateif, M. S.; Shaarawy, S. M.; Kandeel, E. Z.; El-Habashy, A. H.; Salem, M. L.; El-Houseini, M. E. A novel potential effective strategy for enhancing the antitumor immune response in breast cancer patients using a viable cancer cell-dendritic cell-based vaccine. *Oncol. Lett.* **2018**, *16*, 529−535.
(66) Jadidi-Niaragh, F.; Atyabi, F.; Rastegari, A.; Kheshtchin, N.; Arab, S.; Hassannia, H.; Ajami, M.; Mirsanei, Z.; Habibi, S.; Masoumi, F.; Noorbakhsh, F.; Shokri, F.; Hadjati, J. CD73 specific siRNA loaded chitosan lactate nanoparticles potentiate the antitumor effect of a dendritic cell vaccine in 4T1 breast cancer bearing mice. *J. Controlled Release* **2017**, *246*, 46−59.
(67) Gelao, L.; Criscitiello, C.; Esposito, A.; De Laurentiis, M.; Fumagalli, L.; Locatelli, M. A.; Minchella, I.; Santangelo, M.; De Placido, S.; Goldhirsch, A.; Curigliano, G. Dendritic cell-based vaccines: clinical applications in breast cancer. *Immunotherapy* **2014**, *6*, 349−360.
(68) Yang, L.; Qi, Y.; Hu, J.; Tang, L.; Zhao, S.; Shan, B. Expression of Th17 cells in breast cancer tissue and its association with clinical parameters. *Cell Biochem. Biophys.* **2012**, *62*, 153−159.
(69) Demir, L.; Yigit, S.; Ellidokuz, H.; Erten, C.; Somali, I.; Kucukzeybek, Y.; Alacacioglu, A.; Cokmert, S.; Can, A.; Akyol, M.; Dirican, A.; Bayoglu, V.; Sari, A. A.; Tarhan, M. O. Predictive and prognostic factors in locally advanced breast cancer: effect of intratumoral FOXP3+ Tregs. *Clin. Exp. Metastasis* **2013**, *30*, 1047−1062.
(70) Shou, J.; Zhang, Z.; Lai, Y.; Chen, Z.; Huang, J. Worse outcome in breast cancer with higher tumor-infiltrating FOXP3+ Tregs: a systematic review and meta-analysis. *BMC Cancer* **2016**, *16*, 1−8.
(71) Montani, M.; Pazmay, G. V. B.; Hysi, A.; Lupidi, G.; Pettinari, R.; Gambini, V.; Tilio, M.; Marchetti, F.; Pettinari, C.; Ferraro, S.; Iezzi, M.; Marchini, C.; Amici, A. The water soluble ruthenium(II) organometallic compound [Ru(p-cymene)(bis(3,5-dimethylpyrazol-1-yl)-methane)Cl]Cl suppresses triple negative breast cancer growth by inhibiting tumor infiltration of regulatory T cells. *Pharmacol. Res.* **2016**, *107*, 282−290.
(72) Garg, A. D.; Dudek-Peric, A. M.; Romano, E.; Agostinis, P. Immunogenic cell death. *Int. J. Dev. Biol.* **2015**, *59*, 131−140.
(73) Wasylenko, D. J.; Ganesamoorthy, C.; Kolvisto, B. D.; Henderson, M. A.; Berllnguette, C. P. Insight into water oxidation by mononuclear polypyridyl Ru catalysts. *Inorg. Chem.* **2010**, *49*, 2202−2209.
(74) *Schrödinger Suite 2015, Protein Preparation Wizard*; Schrödinger, LLC, New York, NY.
(75) Rostkowski, M.; Olsson, M.; Sondergaard, C.; Jensen, J. Graphical analysis of pH-dependent properties of proteins predicted using PROPKA. *BMC Struct. Biol.* **2011**, *11*, 6.
(76) Jorgensen, W. L.; Tirado-Rives, J. Potential energy functions for atomic-level simulations of water and organic and biomolecular systems. *Proc. Natl. Acad. Sci. U. S. A.* **2005**, *102*, 6665−6670.
(77) Pick, E.; Keisari, Y. A simple colorimetric method for the measurement of hydrogen peroxide produced by cells in culture. *J. Immunol. Methods* **1980**, *38*, 161−170.
(78) Mosmann, T. Rapid colorimetric assay for cellular growth and survival: application to proliferation and cytotoxicity assays. *J. Immunol. Methods* **1983**, *65*, 55−63.
(79) Jovanović, I.; Radosavljević, G.; Mitrović, M.; Juranić, V. L.; McKenzie, A. N.; Arsenijević, N.; Jonjić, S.; Lukić, M. L. ST2 deletion enhances innate and acquired immunity to murine mammary carcinoma. *Eur. J. Immunol.* **2011**, *41*, 1902−1912.
(80) Wang, J. Q.; Zhang, P. Y.; Ji, L. N.; Chao, H. A. Ruthenium(II) complex inhibits tumor growth in vivo with fewer side-effects compared with cisplatin. *J. Inorg. Biochem.* **2015**, *146*, 89−96.
(81) Volarević, V.; Milovanović, M.; Ljujić, B.; Pejnović, N.; Arsenijević, N.; Nilsson, U.; Leffer, H.; Lukić, M. L. Galectin-3 defciency prevents concanavalin A-induced hepatitis in mice. *Hepatology* **2012**, *55*, 1954−1964.

DOI: 10.1021/acs.organomet.8b00604
Organometallics 2018, 37, 4250−4266

Newly synthesized heteronuclear ruthenium(II)/ferrocene complexes suppress 4T1 mammary carcinoma growth in BALB/c mice by promoting activation of anti-tumor immunity

Milan M. Milutinović,[†‡#] Petar P. Čanović,[§#] Dragana Stevanović,[†] Romana Masnikosa,[‖] Milan Vraneš,[Δ] Aleksandar Tot,[Δ] Milan M. Zarić,[§] Bojana Simović Marković,[◊], Maja Misirkić Marjanović,[¥] Ljubica Vučićevič,[¥], Maja Savić,[ł] Vladimir Jakovljević,[ƒ] Vladimir Trajković,[¥] Vladislav Volarević,[◊] Tatjana Kanjevac[↓] and Ana Rilak Simović*[†]*

#equal contribution as the first authors

[†]University of Kragujevac, Faculty of Science, R. Domanovića 12, P. O. Box 60, 34000 Kragujevac, Serbia.

[‡] University of Paderborn, Department of Organic Chemistry, Warburgerstraße 100, 33098 Paderborn, Germany

[§]University of Kragujevac, Serbia, Faculty of Medical Sciences, Department of Biochemistry, S. Markovića 69, 34000 Kragujevac, Serbia

[‖]University of Belgrade Vinča Institute of Nuclear Sciences, Department of Physical Chemistry, Mike Petrovića Alasa 12-14, 11000 Belgrade, Serbia.

[Δ] University of Novi Sad, Faculty of Sciences, Department of Chemistry, Biochemistry and Environmental Protection, Trg Dositeja Obradovića 3, 21000 Novi Sad, Serbia.

[◊]University of Kragujevac, Serbia, Faculty of Medical Sciences, Department of Microbiology and Immunology, Center for Molecular Medicine and Stem Cell Research, S. Markovića 69, 34000 Kragujevac, Serbia

[¥]University of Belgrade, Serbia, School of Medicine, Institute of Microbiology and Immunology, Dr Subotića 1, 11000 Belgrade, Serbia

[ƒ] University of Kragujevac, Serbia, Faculty of Medical Sciences, Department of Physiology, S. Markovića 69, 34000 Kragujevac, Serbia

[ł]University of Kragujevac, Serbia, Faculty of Medical Sciences, Department of Pharmaceutical Biotechnology, S. Markovića 69, 34000 Kragujevac, Serbia

[↓]University of Kragujevac, Serbia, Faculty of Medical Sciences, Department of Dentistry, S. Markovića 69, 34000 Kragujevac, Serbia

Table of Contents: ^{1}H NMR spectrum of mtefc ligand in $CDCl_3$ at ambient temperature; ^{13}C NMR spectra of A) mtefc ligand and B) complex **1** in $CDCl_3$ at ambient temperature; The 2D heteronuclear ^{1}H-^{13}C HSQC NMR spectrum of complex **1** in $CDCl_3$ at ambient temperature; The 2D heteronuclear ^{1}H-^{13}C HMBC NMR spectrum of complex **1** in $CDCl_3$ at ambient temperature; The 2D homonuclear ^{1}H-^{1}H NOESY NMR spectrum of complex **1** in $CDCl_3$ at ambient temperature; ^{1}H NMR spectra of A) mtpfc ligand and B) complex **2** in $CDCl_3$ at ambient temperature; ^{13}C NMR spectra of A) mtpfc ligand and B) complex **2** in $CDCl_3$ at ambient temperature; MALDI TOF mass spectra of the complexes **1** (A) and **2** (B) in dithranol, The spectra were acquired in the positive reflectron mode. Each spectrum was obtained by averaging at least 300 laser shots. Instrumental settings were: accelerating voltage 9000 V, grid voltage 40%, guide wire 0.05%, extraction delay time 185 ns (**1**) or 120 ns (**2**), acquisition mass range 300 – 800 *m/z*, laser intensity 2825, low mass gate OFF. The arrows show the signals originating from molecular ions (M); UV-Vis spectra of complexes **1** and **2** in water over a 24 h period. [Ru(II)] = 1 x 10^{-4} M, T = 25 ºC; Absorption spectra of the complexes **1** and **2** in PBS (137 mM NaCl, pH 7.4) upon addition of CT DNA. [Ru] = 1.30 x 10^{-5} M, [DNA] = (0.13-1.30) x 10^{-5} M. Arrows show the absorbance changing upon increasing CT DNA concentrations; Plots of $[DNA]/(\varepsilon_A - \varepsilon_f)$ *versus* [DNA] for the complexes **1** and **2**; The relative intensity of fluorescent emission of EB at λ_{em} = 612 nm (λ_{ex} = 527 nm) *vs r* (*r* = [compound]/[CT DNA]) for the complexes **1** and **2** in PBS (137 mM NaCl, pH 7.4); Emission spectra of EB bound to DNA in the presence of complexes **1** and **2**. [EB] = 80 μM, [DNA] = 80 μM; [Ru] = 0–80 μM; λ_{ex} = 527 nm. The arrows show the intensity changes upon increased concentrations of the complexes; Stern-Volmer quenching plot of EB-DNA for complexes **1** and **2**; Relative viscosity $(\eta/\eta_0)^{1/3}$ of CT DNA (0.01 mM) in PBS (137 mM NaCl, pH 7.4) in the presence of the complexes **1** and **2** at increasing amounts (*r*); Plot of % relative fluorescence intensity at λ_{em} = 364 nm (%) *vs* r (r = [complex]/[BSA]) for the complexes **1** and **2** (4.3% of the initial fluorescence intensity for **1** and 2.4% for **2**) in buffer solution (10 mM PBS at pH = 7.4); Emission spectra of BSA in the presence of complexes **1** and **2**. [BSA] = [Ru] = 0–80 μM; λ_{ex} = 295 nm. The arrows show the intensity changes upon increasing concentrations of the complexes; Stern-Volmer quenching plot of BSA for complexes **1** and **2**; Scatchard plot of BSA for complexes **1** and **2**; Assignments of ^{1}H resonances (δ) for the ligands **mtefc**, **mtpfc** and complexes **1** and **2** in $CDCl_3$; The peaks detected in the positive ion mode MALDI TOF mass spectra of the complexes **1** and **2**;

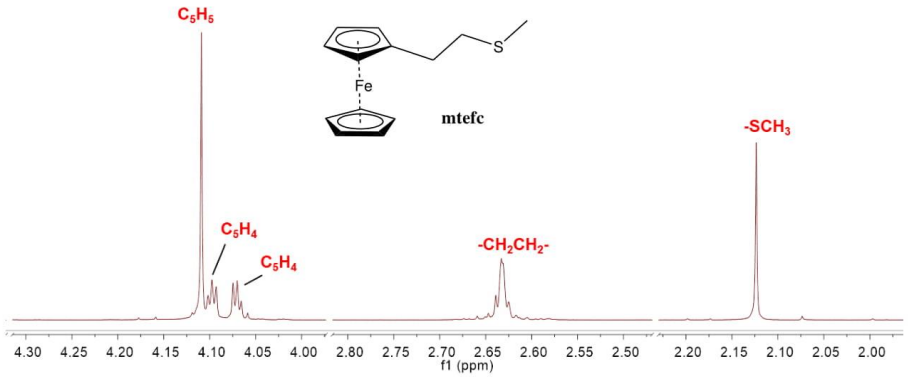

Fig. S1. ^{1}H NMR spectrum of mtefc ligand in $CDCl_3$ at ambient temperature.

A)

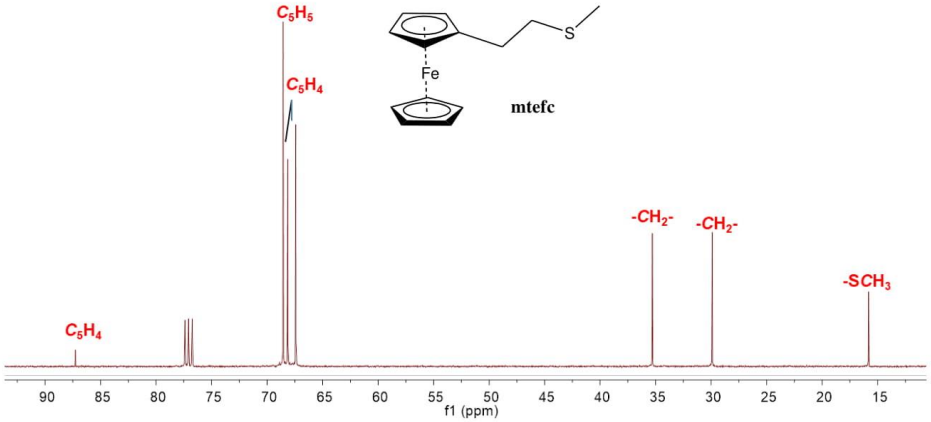

B)

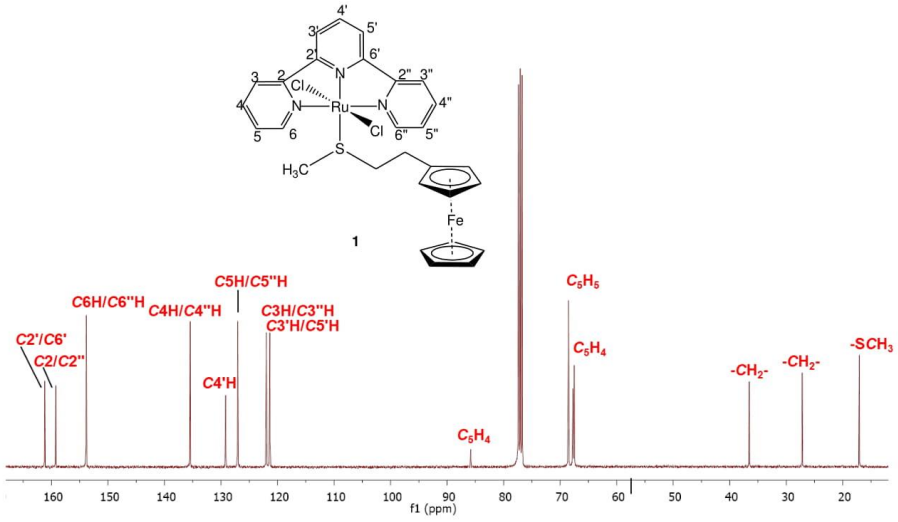

Fig. S2. ^{13}C NMR spectra of A) mtefc ligand and B) complex **1** in $CDCl_3$ at ambient temperature.

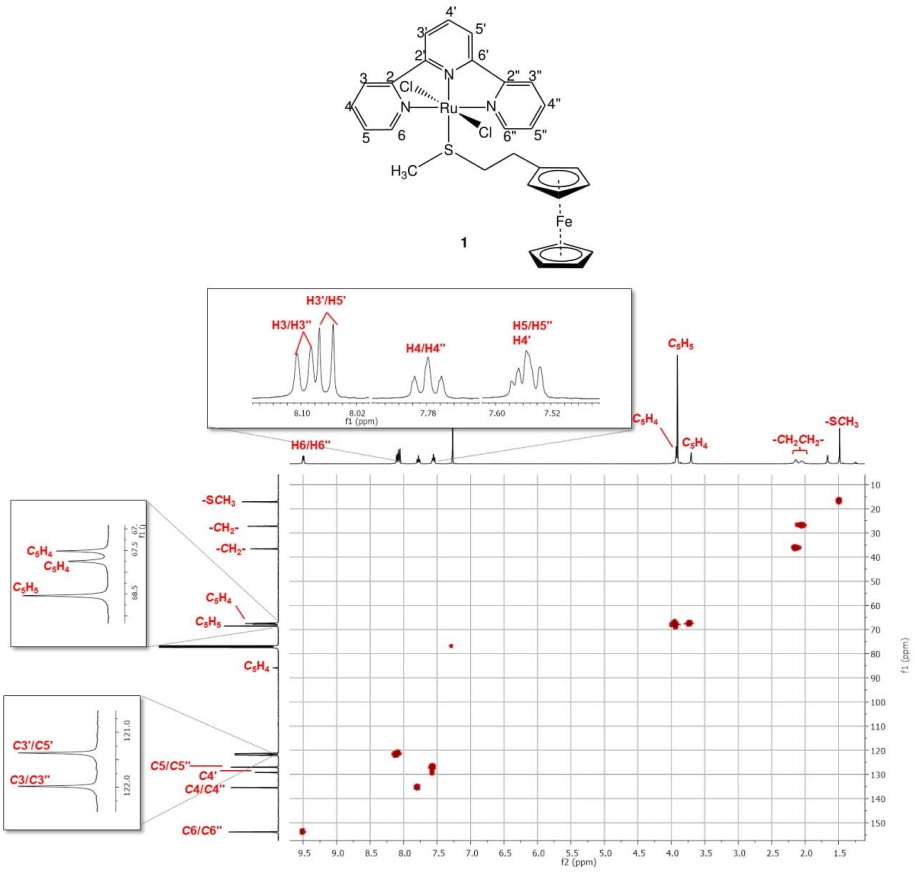

Fig. S3. The 2D heteronuclear ^{1}H-^{13}C HSQC NMR spectrum of complex **1** in $CDCl_3$ at ambient temperature.

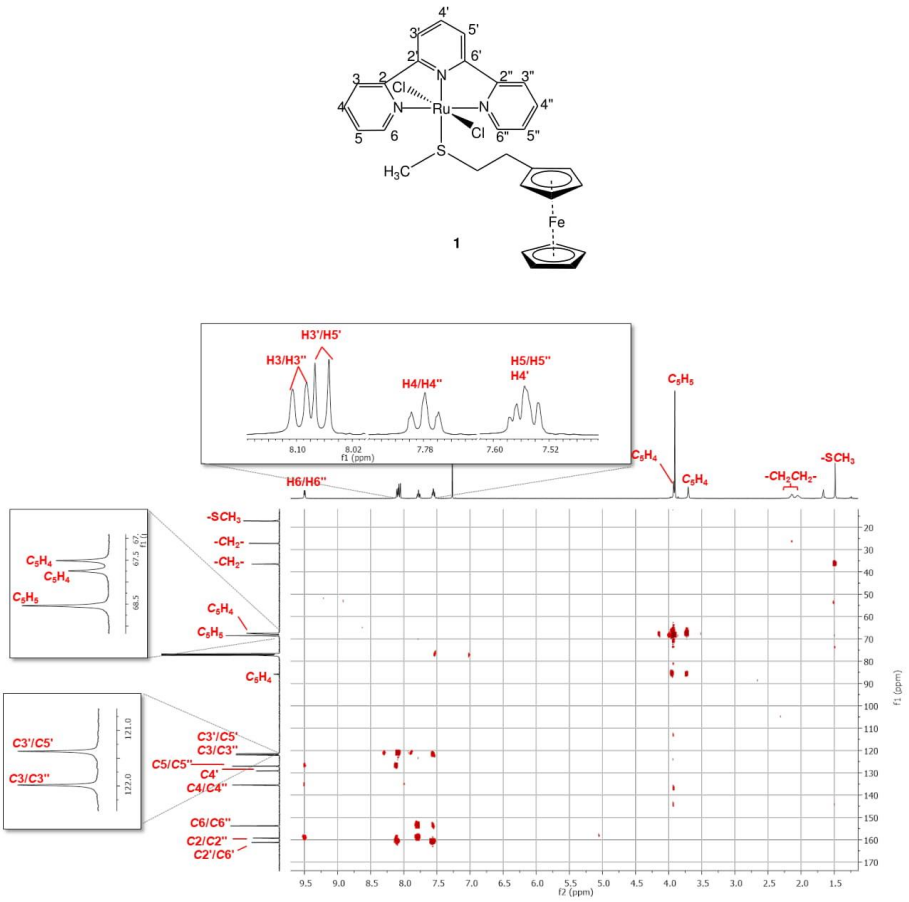

Fig. S4. The 2D heteronuclear ^{1}H-^{13}C HMBC NMR spectrum of complex **1** in $CDCl_3$ at ambient temperature.

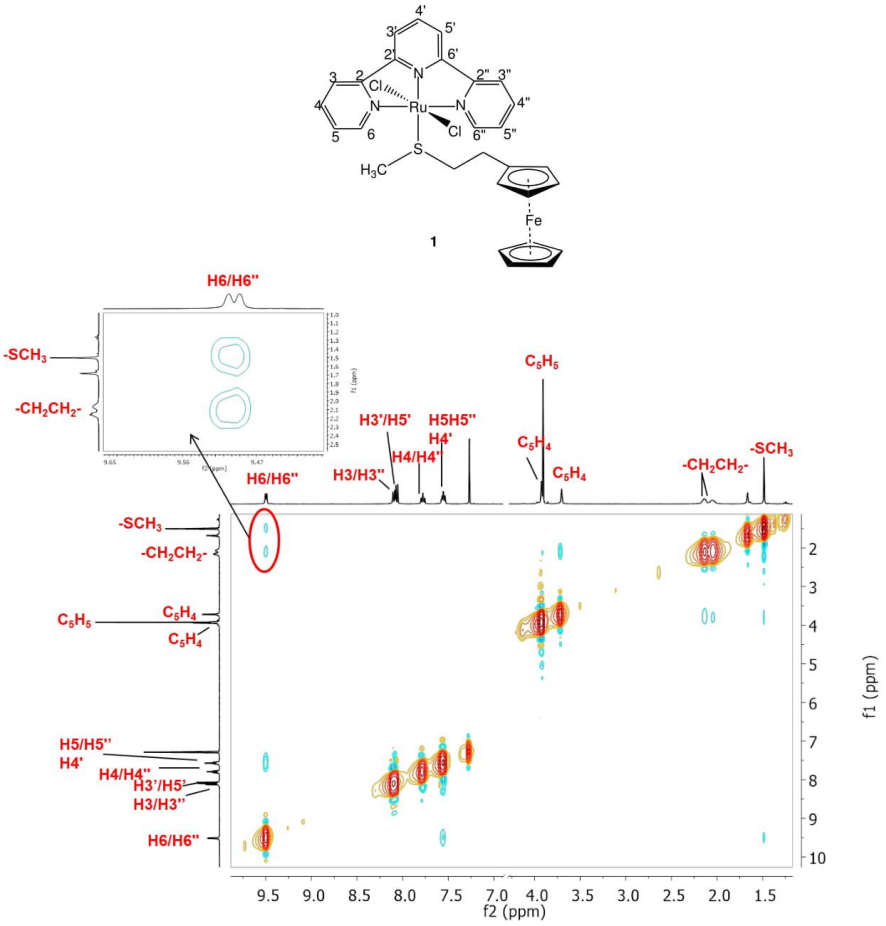

Fig. S5. The 2D homonuclear ^{1}H-^{1}H NOESY NMR spectrum of complex **1** in $CDCl_3$ at ambient temperature.

A)

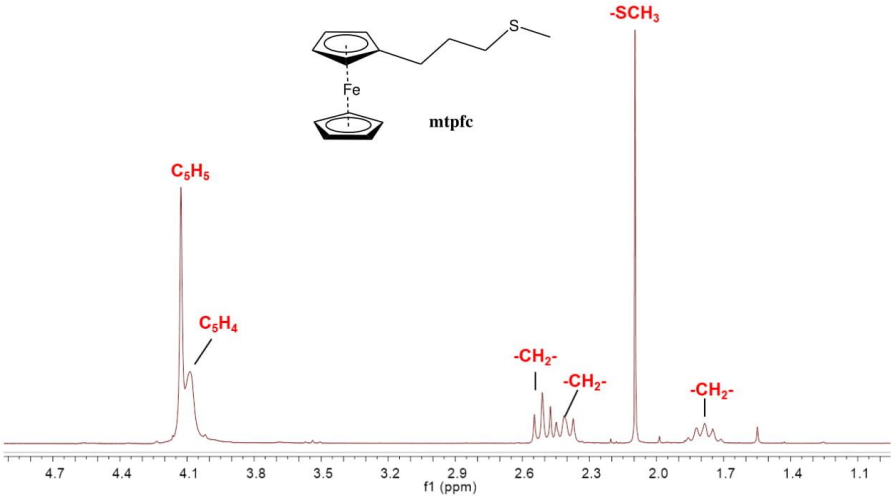

B)

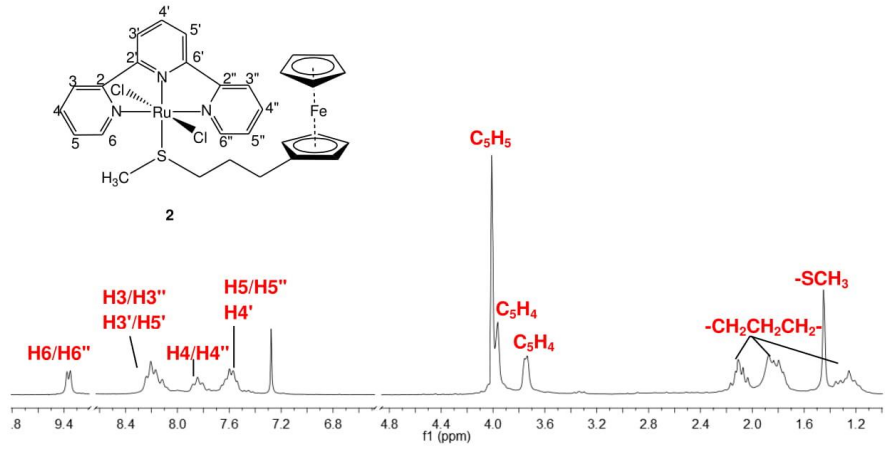

Fig. S6. ^{1}H NMR spectra of A) mtpfc ligand and B) complex **2** in $CDCl_3$ at ambient temperature.

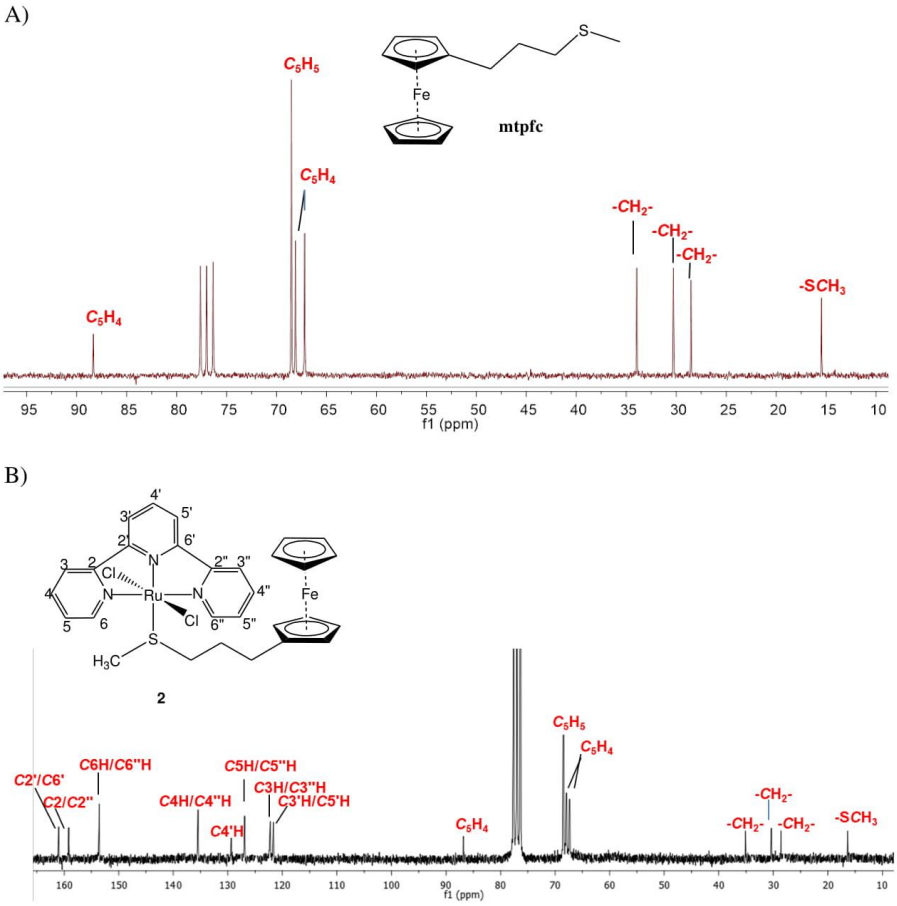

Fig. S7. ^{13}C NMR spectra of A) mtpfc ligand and B) complex **2** in $CDCl_3$ at ambient temperature.

A)

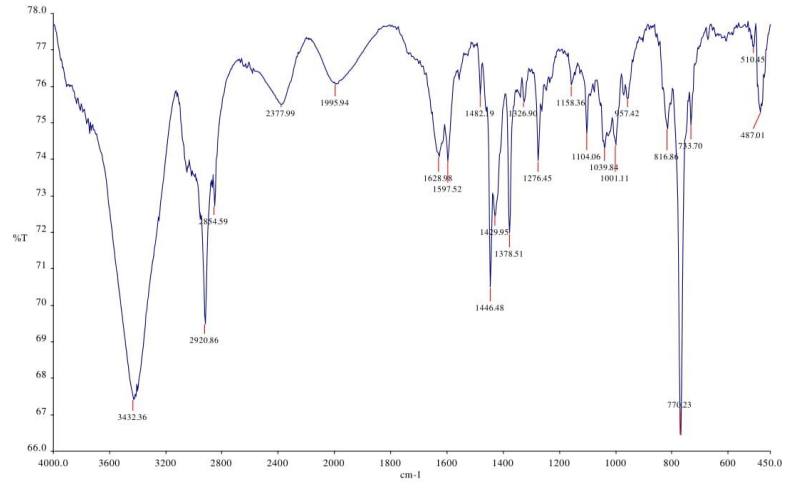

B)

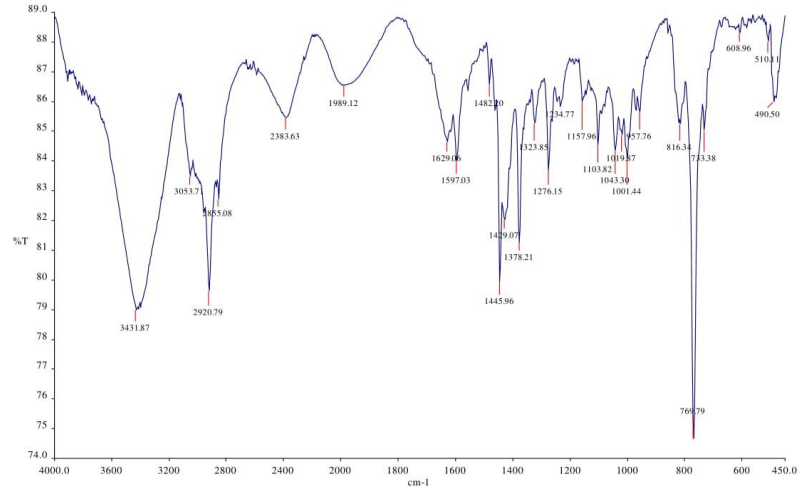

Fig. S8. FT-IR spectra of A) complex **1** and B) complex **2**.

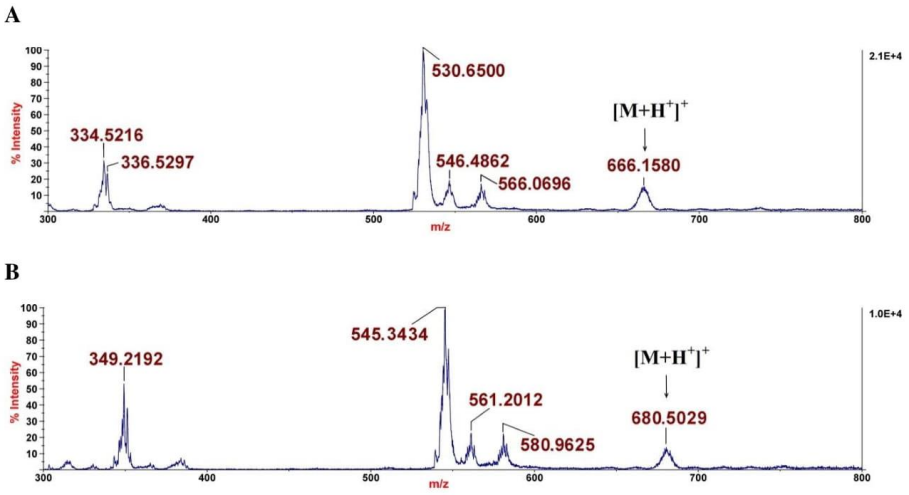

Fig. S9. MALDI TOF mass spectra of the complexes **1** (A) and **2** (B) in dithranol. The spectra were acquired in the positive reflectron mode. Each spectrum was obtained by averaging at least 300 laser shots. Instrumental settings were: accelerating voltage 9000 V, grid voltage 40%, guide wire 0.05%, extraction delay time 185 ns (**1**) or 120 ns (**2**), acquisition mass range 300 – 800 *m/z*, laser intensity 2825, low mass gate OFF. The arrows show the signals originating from molecular ions (M).

A)

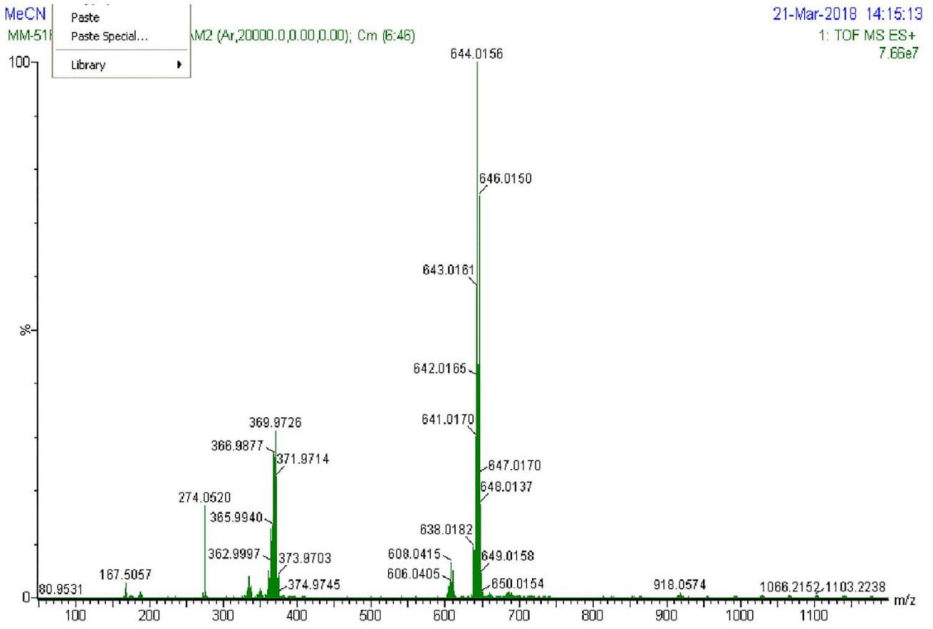
MeCN
Paste
Paste Special...
Library
21-Mar-2018 14:15:13
1: TOF MS ES+
7.66e7
644.0156
646.0150
643.0161
642.0165
641.0170
647.0170
648.0137
638.0182
649.0158
650.0154
369.9726
366.9877
371.9714
274.0520
365.9940
362.9997
373.9703
374.9745
187.5057
80.9531
608.0415
606.0405
918.0574
1066.2152
1103.2238
m/z

B)

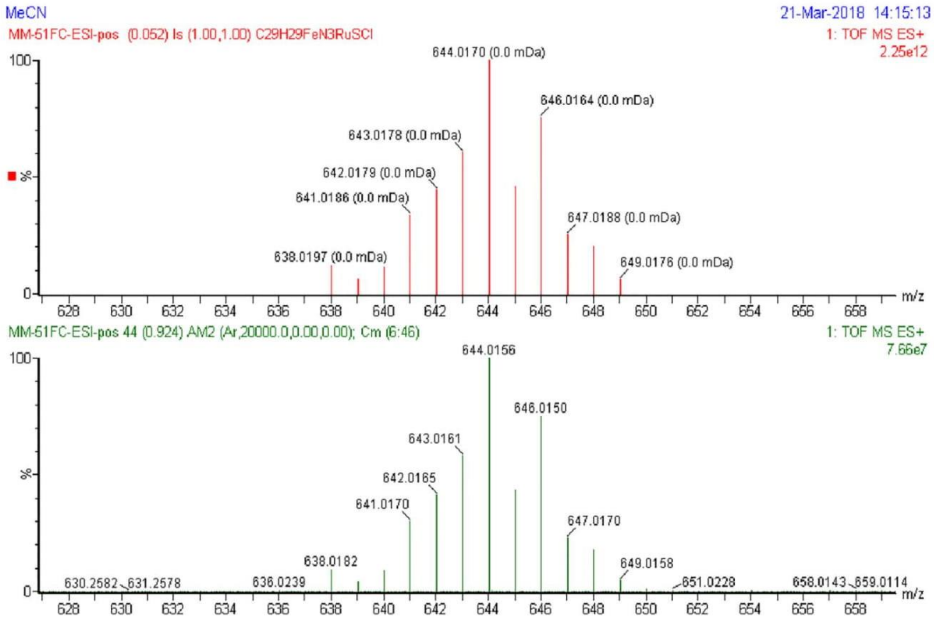
MeCN
21-Mar-2018 14:15:13
MM-51FC-ESI-pos (0.052) Is (1.00,1.00) C29H29FeN3RuSCl
1: TOF MS ES+
2.25e12
644.0170 (0.0 mDa)
646.0164 (0.0 mDa)
643.0178 (0.0 mDa)
642.0179 (0.0 mDa)
641.0186 (0.0 mDa)
647.0188 (0.0 mDa)
638.0197 (0.0 mDa)
649.0176 (0.0 mDa)
m/z
MM-51FC-ESI-pos 44 (0.924) AM2 (Ar,20000.0,0.00,0.00); Cm (6:46)
1: TOF MS ES+
7.66e7
644.0156
646.0150
643.0161
642.0165
641.0170
647.0170
638.0182
649.0158
630.2582
631.2578
636.0239
651.0228
658.0143
659.0114
m/z

C)

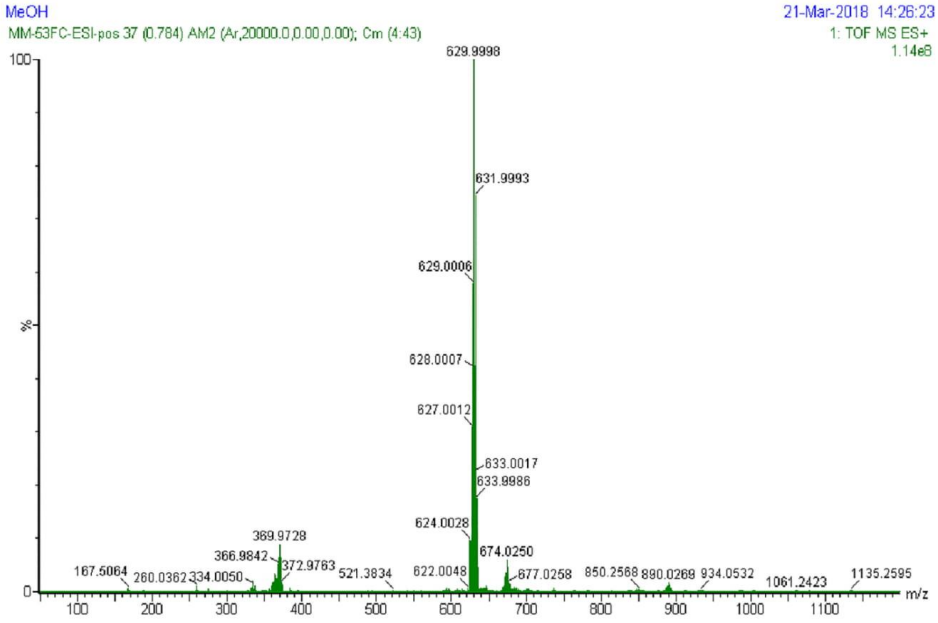
MeOH
21-Mar-2018 14:26:23
MM-53FC-ESI-pos 37 (0.784) AM2 (Ar,20000.0,0.00,0.00); Cm (4:43)
1: TOF MS ES+
1.14e8
629.9998
631.9993
629.0006
628.0007
627.0012
633.0017
633.9986
624.0028
674.0250
369.9728
366.9842
372.9783
167.5064
260.0362
334.0050
521.3834
622.0048
677.0258
850.2568
890.0268
934.0532
1061.2423
1135.2595
m/z

D)

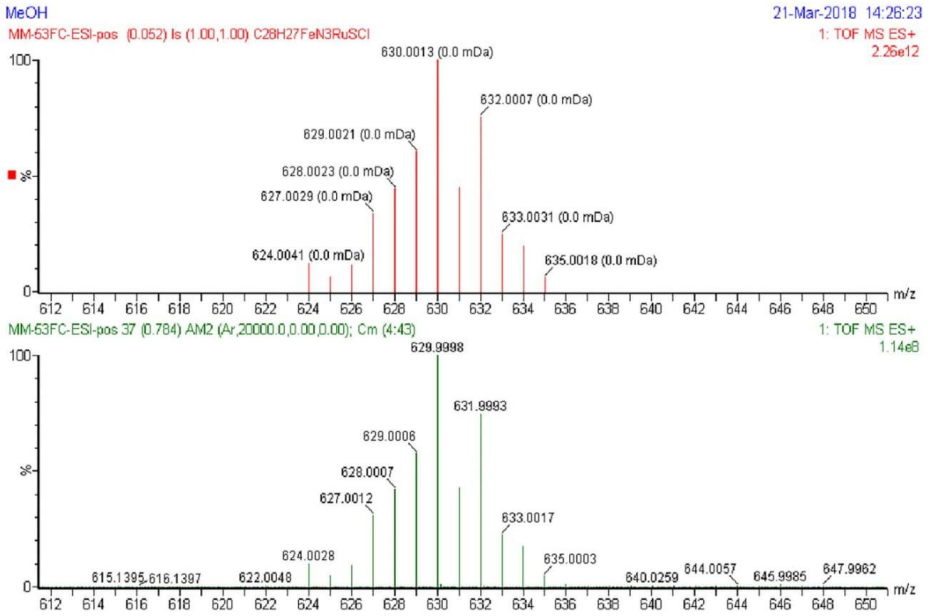
MeOH
21-Mar-2018 14:26:23
MM-53FC-ESI-pos (0.052) Is (1.00,1.00) C28H27FeN3RuSCl
1: TOF MS ES+
2.26e12
630.0013 (0.0 mDa)
632.0007 (0.0 mDa)
629.0021 (0.0 mDa)
628.0023 (0.0 mDa)
627.0029 (0.0 mDa)
633.0031 (0.0 mDa)
624.0041 (0.0 mDa)
635.0018 (0.0 mDa)
m/z
MM-53FC-ESI-pos 37 (0.784) AM2 (Ar,20000.0,0.00,0.00); Cm (4:43)
1: TOF MS ES+
1.14e8
629.9998
631.9993
629.0006
628.0007
627.0012
633.0017
624.0028
635.0003
615.1395
616.1397
622.0048
640.0259
644.0057
645.9985
647.9962
m/z

Fig. S10. ESI Q-TOF mass spectra of the complexes **1** (A) and **2** (C) dissolved in methanol. The spectra were acquired in the positive mode. Instrumental settings were: capillary voltage 2.8 kV, cone voltage 32 V, desolvation gas 650 L/h, desolvation temperature 350 °C and source temperature 120 °C. The isotopic distributions of the major peaks from the spectra (m/z 644.0156 in (A)) and (m/z C)) are shown in Figures (B) and (D), respectively. The theoretical (red signals) and experimentally obtained (green signals) isotopic distributions are shown in parallel.

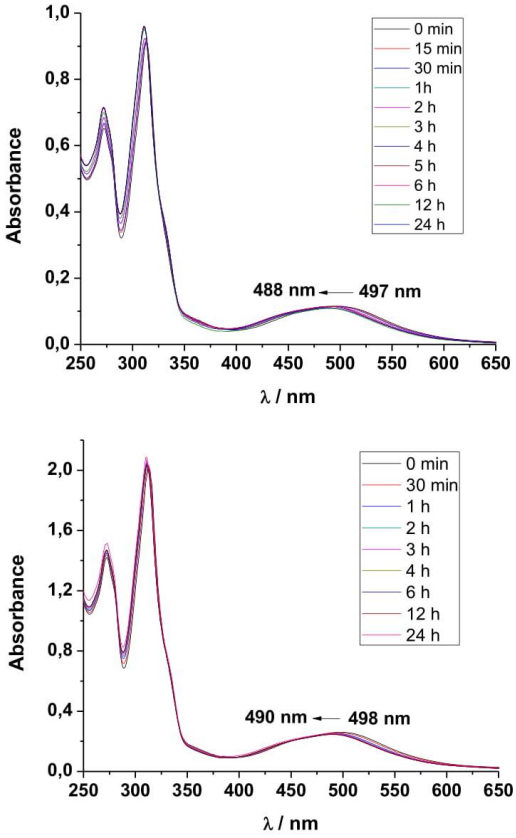

Fig. S11. UV-Vis spectra of complexes **1** and **2** in water over a 24 h period. [Ru(II)] = 1 x 10^{-4} M, T = 25 ºC.

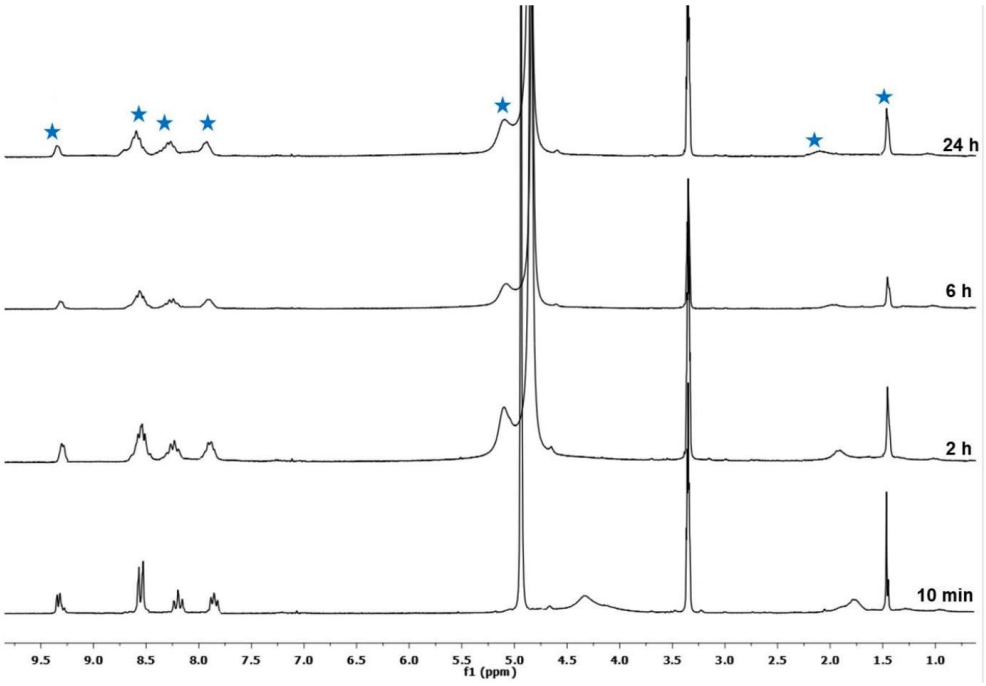

Fig. S12. Time evolution of the ^{1}H NMR spectrum of complex **1** upon dissolution in 70% MeOD-d4/30% D2O (v/v) at ambient temperature. The asterisks indicate the peaks assigned to the hydrolyzed complex formed over time.

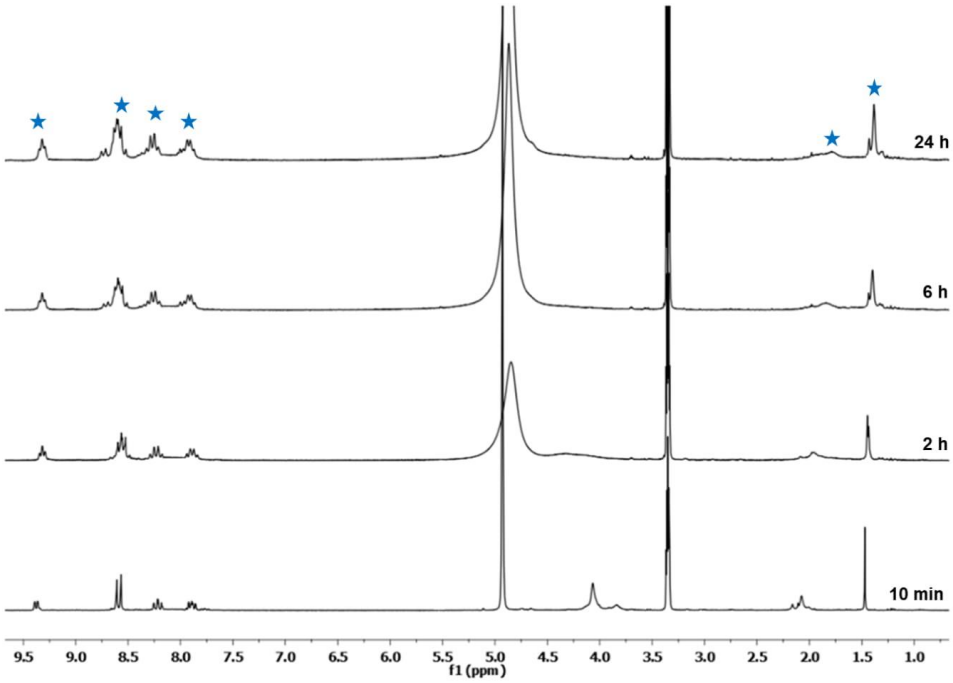

Fig. S13. Time evolution of the ^{1}H NMR spectrum of complex **2** upon dissolution in 70% MeOD-d4/30% D2O (v/v) at ambient temperature. The asterisks indicate the peaks assigned to the hydrolyzed complex formed over time.

DNA-binding studies

Calculation of DNA-binding constants

In order to compare quantitatively the binding strength of the complexes, the intrinsic binding constants K_b were determined by monitoring the changes in absorption at the MLCT band with increasing concentration of CT DNA using the following equation (S1)[S1]

$$[DNA]/(\varepsilon_A - \varepsilon_f) = [DNA]/(\varepsilon_b - \varepsilon_f) + 1/[K_b(\varepsilon_b - \varepsilon_f)] \quad (S1)$$

K_b is given by the ratio of slope to the *y* intercept in plots $[DNA]/(\varepsilon_A - \varepsilon_f)$ *versus* [DNA] (Fig. S15), where [DNA] is the concentration of DNA in base pairs, $\varepsilon_A = A_{obs}/[complex]$, ε_f is the extinction coefficient for the unbound complex and ε_b is the extinction coefficient for the complex in the fully bound form.

Stern-Volmer equation for EB competitive studies

The relative binding of complexes to CT-DNA is described by Stern-Volmer equation (S2)[S2]:

$$I_0/I = 1 + K_{sv}[Q] \quad (S2)$$

where I_0 and I are the emission intensities in the absence and the presence of the quencher (complexes **1, 2** or **3**), respectively, [Q] is the total concentration of quencher, K_{sv} is the Stern-Volmer quenching constant, which can be obtained from the slope of the plot of I_0/I *versus* [Q] (Fig. S16).

Stern-Volmer equation for BSA quenching studies

Fluorescence quenching is described by Stern–Volmer equation:

$$I_0/I = 1 + k_q\tau_0[Q] = 1 + K_{sv}[Q] \quad (S3)$$

where I_0 = the initial tryptophan fluorescence intensity of BSA, I = the tryptophan fluorescence intensity of BSA after the addition of the quencher, k_q = the quenching rate constants of BSA, K_{sv} = the dynamic quenching constant, τ_0 = the average lifetime of BSA without the quencher, [Q] = the concentration of the quencher respectively.

$$K_{sv} = k_q\tau_0 \quad (S4)$$

and, taking as fluorescence lifetime (τ_0) of tryptophan in BSA at around 10^{-8} s, K_{sv} (M^{-1}) can be obtained by the slope of the diagram I_0/I *vs* [Q] (Stern-Volmer plots, Fig. S22), and subsequently the approximate k_q (M^{-1} s^{-1}) may be calculated.[S2]

The simple Stern–Volmer plots were not applicable for complexes **1** and **2** as the plot between I_0/I and [Q] showed/exhibited an upward curvature (Fig. S22). A factor, $\exp^{(V[Q])}$ where *V* is the static quenching constant, can be introduced into Stern–Volmer, equation S4, in order to describe both quenching modes [S4,S5]:

$$I_0/I = (1 + K_{sv}[Q])e^{V[Q]} \quad (S5)$$

The static quenching constant, *V* was obtained from the equation (S6) by plotting $I_0/Ie^{V[Q]}$ versus [Q] by varying *V* until a linear plot was obtained. The highest value of correlation coefficient was used as criterion for linearity of the plot to obtain a precise value of *V*. The (dynamic) collisional quenching constant, K_{sv} was then obtained from the slope of linear plots (inset Fig. S22).

Scatchard equation for BSA quenching studies

From Scatchard equation:

$r/D_f = nK - rK$ (S6)

where r ($r = \Delta I/I_0$) is the moles of drug bound per mole of protein and D_f is the molar concentration of free metal complex. The association binding constant K (M^{-1}) may be calculated from the slope in the Scatchard plots r/D_f *vs* r and the number of binding sites per albumin (n) is given by the ratio of *y* intercept to the slope (Scatchard plots, Fig. S23).[S6]

References

S1. Pyle, A.M.; Rehmann, J.P.; Meshoyrer, R.; Kumar, C.V.; Turro, N.J.; Barton, J.K. Mixed-ligand complexes of ruthenium(II): factors governing binding to DNA. *J. Am. Chem. Soc.* **1989**, *111*, 3051-3058.

S2. Lakowicz, R.; Weber, G. Quenching of fluorescence by oxygen. Probe for structural fluctuations in macromolecules. *Biochemistry* **1973**, *12*, 4161-4170.

S3. Lehrer, S.S. Solute perturbation of protein fluorescence. Quenching of the tryptophyl fluorescence of model compounds and of lysozyme by iodide ion. *Biochemistry* **1971**, *10*, 3254 – 3263.

S4. Lakowicz, J.R. Principles of Fluorescence Spectroscopy, 3rd ed., Springer, New York, **2006**, *8*, 278–327.

S5. Seedher, N.; Agarwal, P. Complexation of fluoroquinolone antibiotics with human serum albumin: A fluorescence quenching study. *J Lumin.* **2010**, *130*, 1841–1848.

S6. Wu, S.; Yuan, W.; Wang, H.; Zhang, Q.; Liu, M.; Yu, K. Synthesis, crystal structure and interaction with DNA and HSA of (*N,N′*-dibenzylethane-1,2-diamine) transition metal complexes. *J. Inorg. Biochem.* **2008**, *102*, 2026-2034.

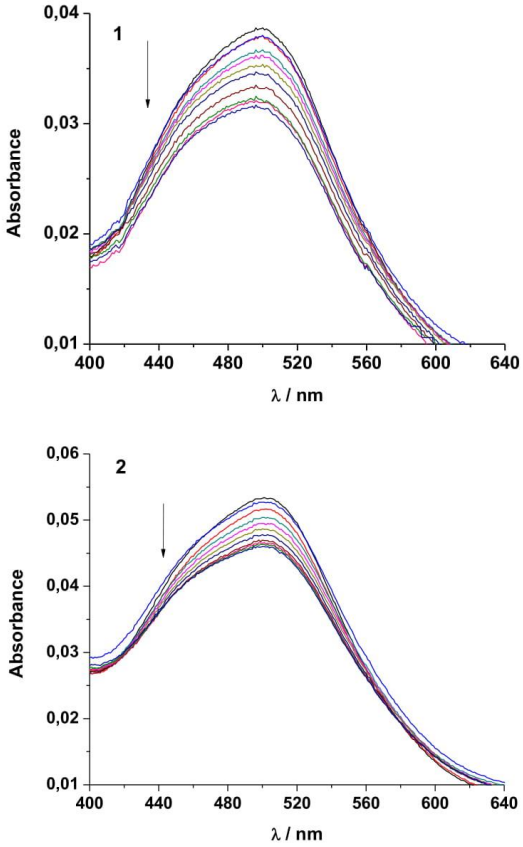

Fig. S14. Absorption spectra of the complexes **1** and **2** in PBS (137 mM NaCl, pH 7.4) upon addition of CT DNA. [Ru] = 1.30 x 10^{-5} M, [DNA] = (0.13-1.30) x 10^{-5} M. Arrows show the absorbance changing upon increasing CT DNA concentrations.

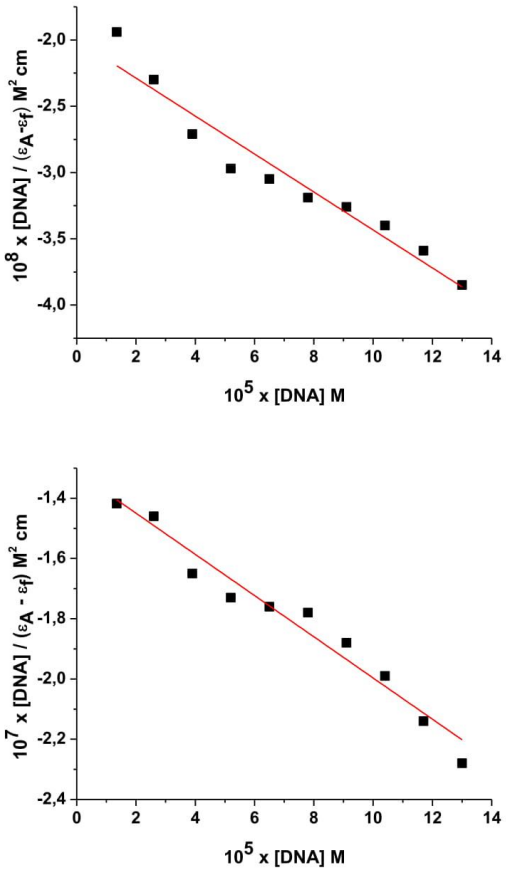

Fig. S15. Plots of [DNA]/($\varepsilon_A - \varepsilon_f$) *versus* [DNA] for the complexes **1** and **2**.

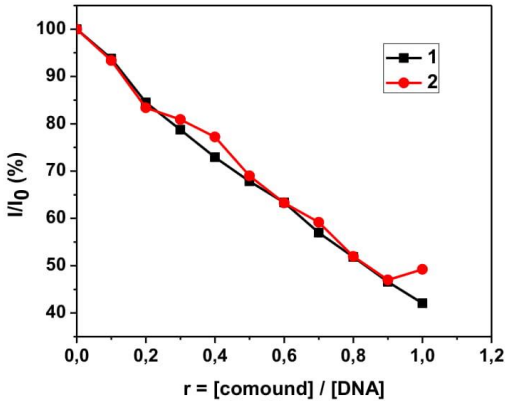

Fig. S16. The relative intensity of fluorescent emission of EB at λ_{em} = 612 nm (λ_{ex} = 527 nm) *vs r* (*r* = [compound]/[CT DNA]) for the complexes **1** and **2** in PBS (137 mM NaCl, pH 7.4).

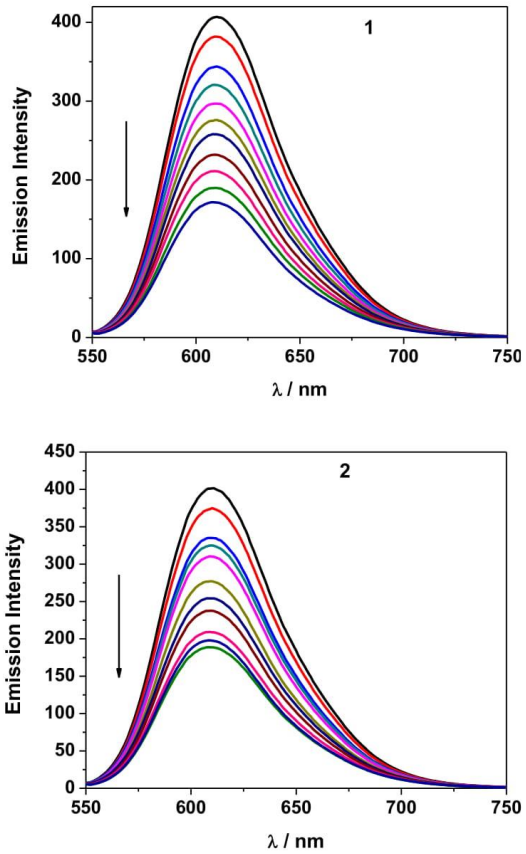

Fig. S17. Emission spectra of EB bound to DNA in the presence of complexes **1** and **2**. [EB] = 80 μM, [DNA] = 80 μM; [Ru] = 0–80 μM; λ_{ex} = 527 nm. The arrows show the intensity changes upon increased concentrations of the complexes.

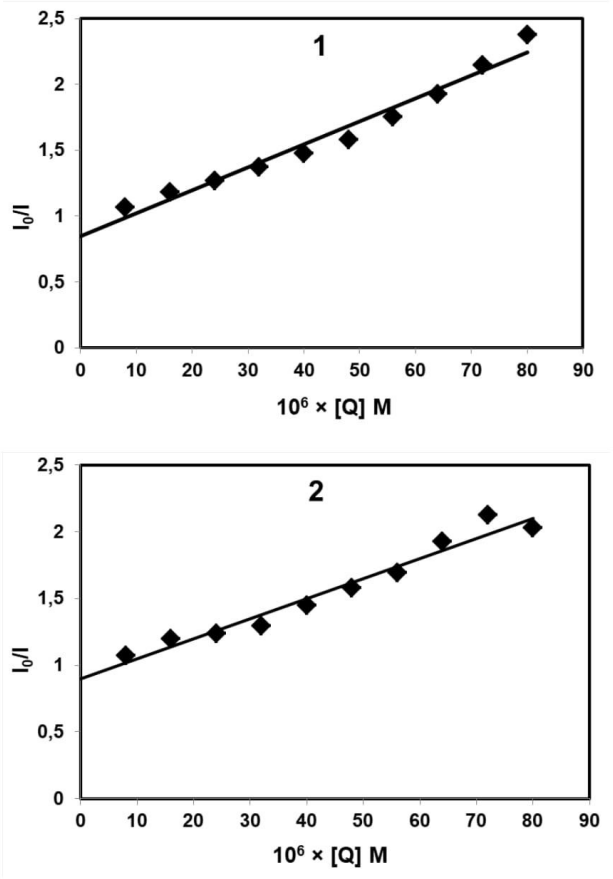

Fig. S18. Stern-Volmer quenching plot of EB-DNA for complexes **1** and **2**.

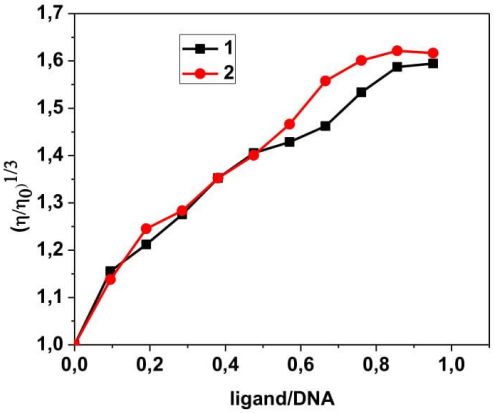

Fig. S19. Relative viscosity $(\eta/\eta_0)^{1/3}$ of CT DNA (0.01 mM) in PBS (137 mM NaCl, pH 7.4) in the presence of the complexes **1** and **2** at increasing amounts (*r*).

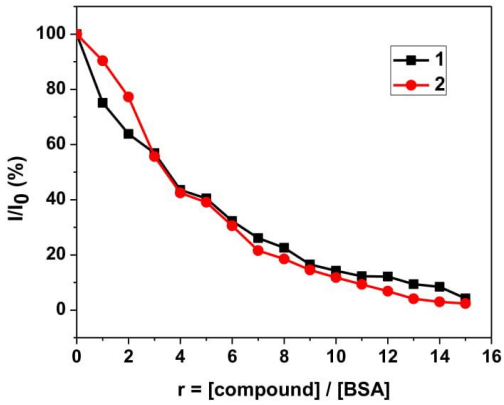

Fig. S20. Plot of % relative fluorescence intensity at λ_{em} = 364 nm (%) *vs* r (r = [complex]/[BSA]) for the complexes **1** and **2** (4.3% of the initial fluorescence intensity for **1** and 2.4% for **2**) in buffer solution (10 mM PBS at pH = 7.4)

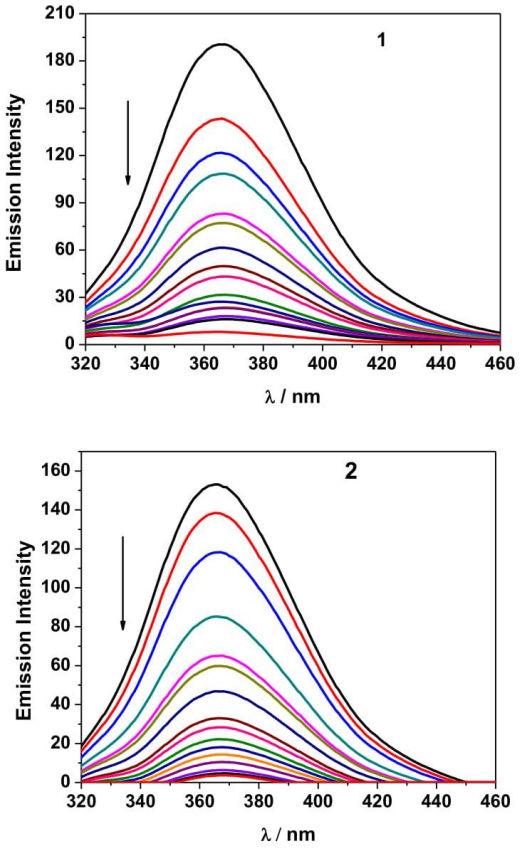

Fig. S21. Emission spectra of BSA in the presence of complexes **1** and **2**. [BSA] = [Ru] = 0–80 μM; λ_{ex} = 295 nm. The arrows show the intensity changes upon increasing concentrations of the complexes.

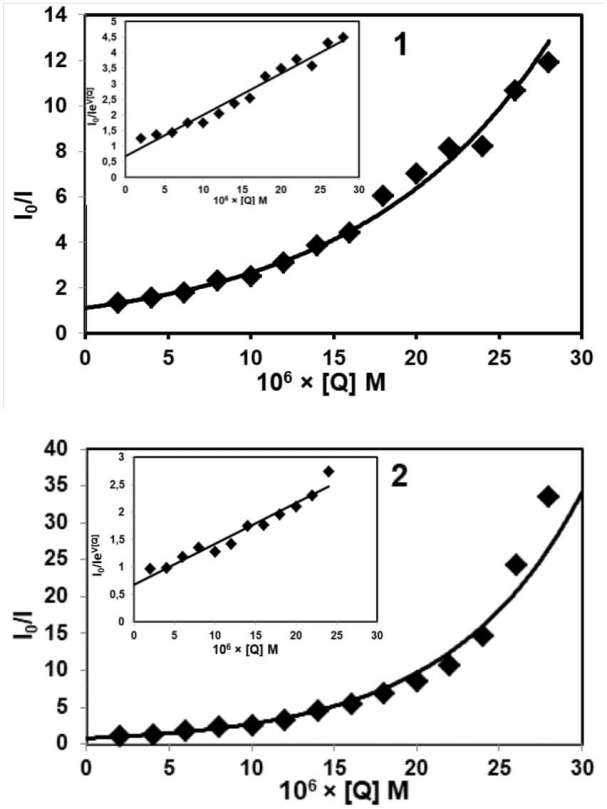

Fig. S22. Stern-Volmer quenching plot of BSA for complexes **1** and **2**.

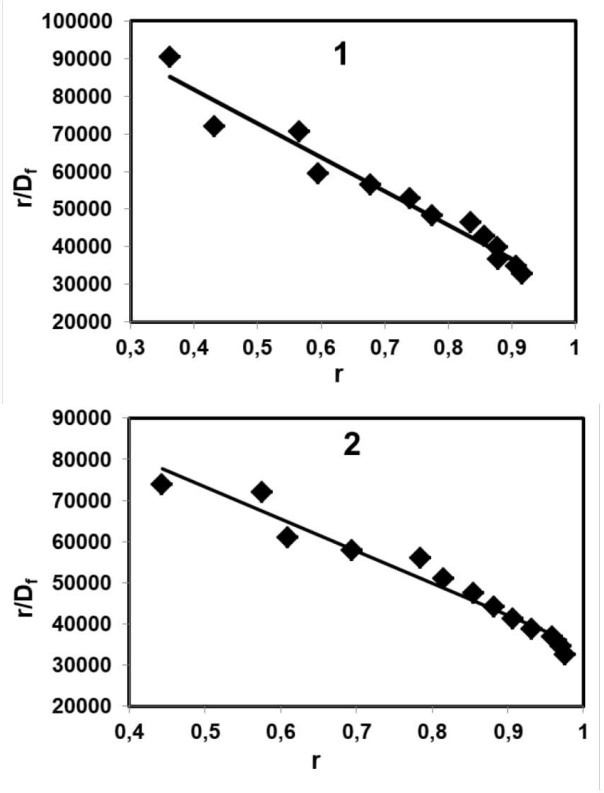

Fig. S23. Scatchard plot of BSA for complexes **1** and **2**.

A)

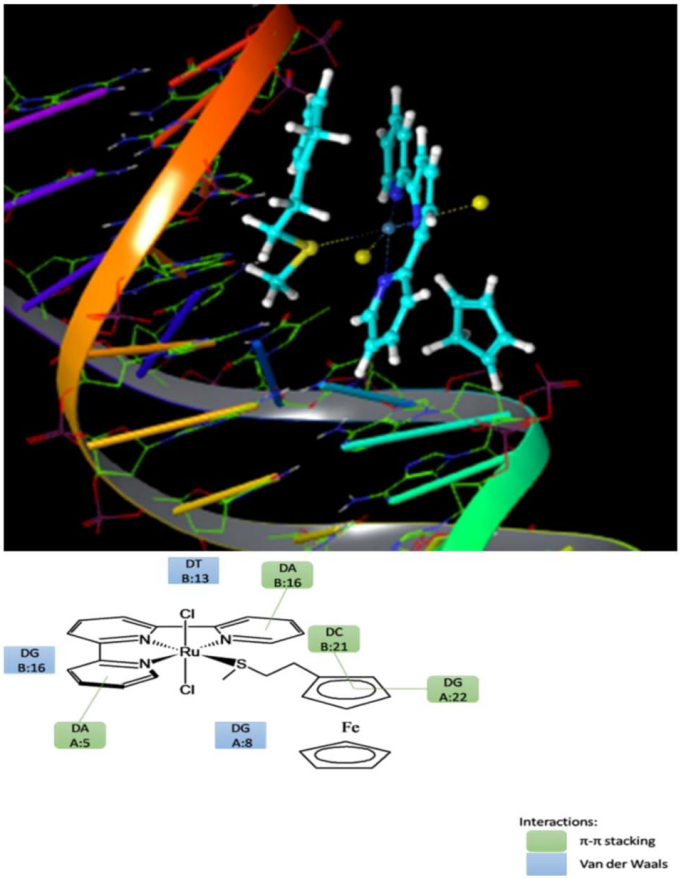
DT
B:13
DA
B:16
DC
B:21
DG
A:22
DG
B:16
DA
A:5
DG
A:8
Cl
Ru
N
N
N
S
Cl
Fe
Interactions:
π-π stacking
Van der Waals

B)

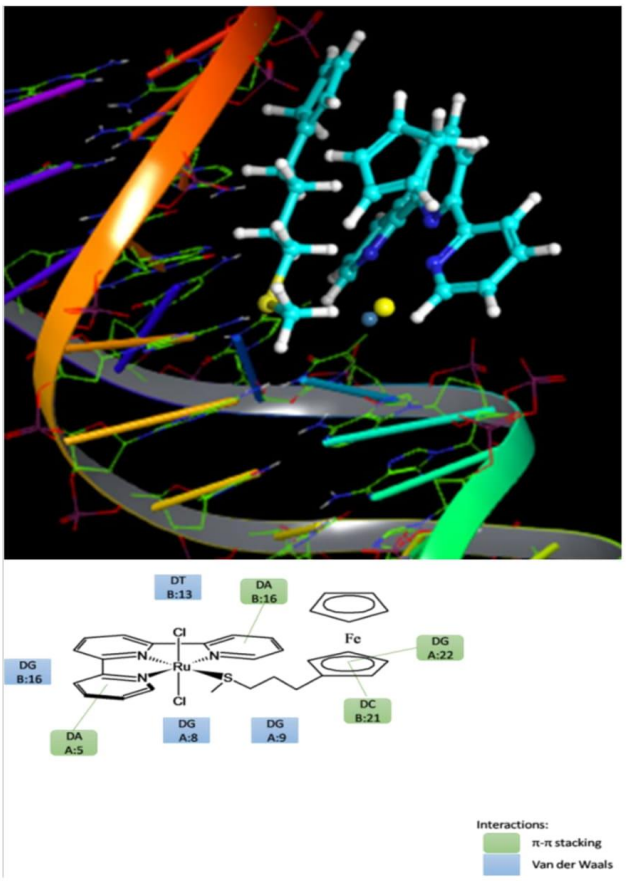

Fig. S24. Visual representation of complexes **1** (A) and **2**(B) bound to 1BNA dodecamer, along with a schematic representation of interactions.

A)

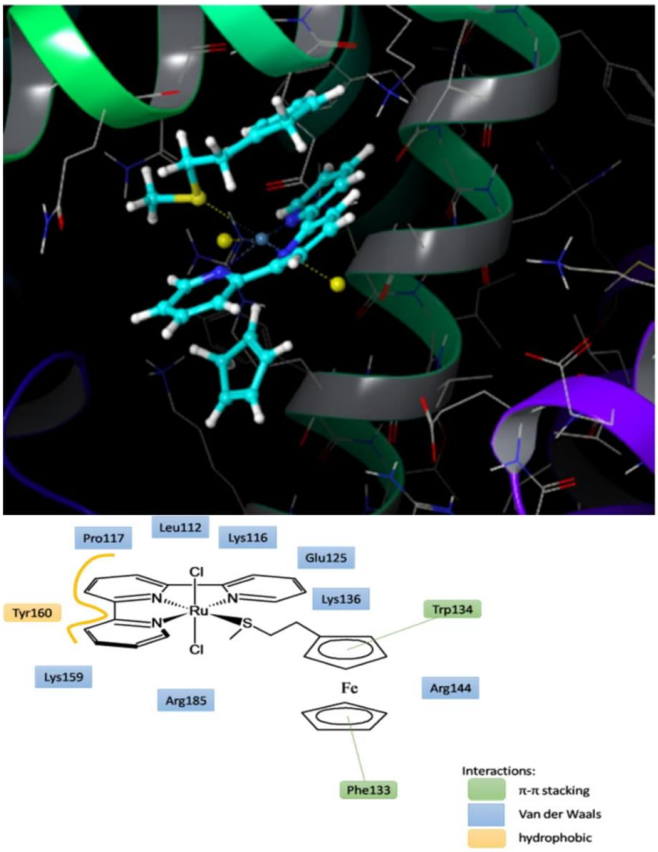
Pro117
Leu112
Lys116
Glu125
Tyr160
Lys136
Trp134
Lys159
Arg185
Arg144
Phe133
Cl
Ru
N
S
Fe
Interactions:
π-π stacking
Van der Waals
hydrophobic

B)

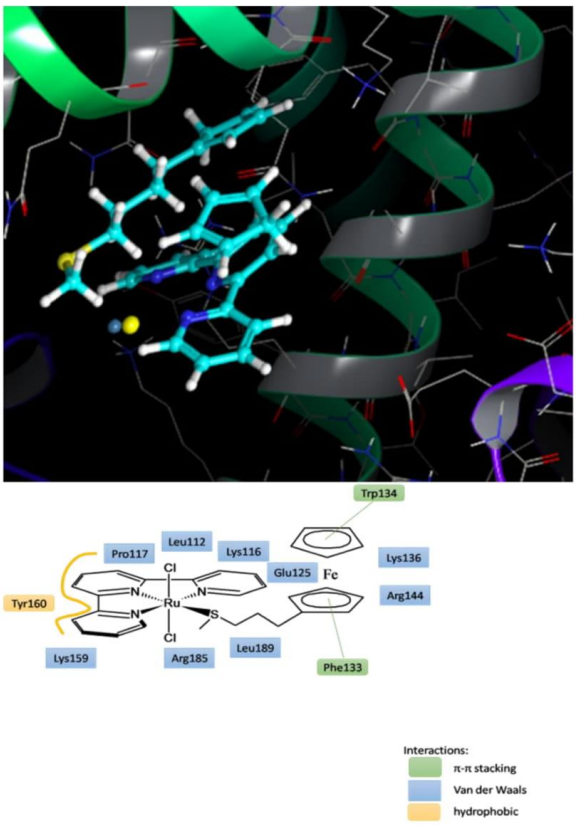

Fig. S25. Visual representation of complexes **1** (A) and **2**(B) bound to BSA, along with a schematic representation of interactions.

Table S1. Assignments of ^{1}H resonances (δ) for the ligands: **mtefc**, **mtpfc** and complexes **1** and **2** in $CDCl_3$.

	mtefc	**1**	**mtpfc**	**2**
C$_5$*H*$_5$	4.11	3.91	4.13	4.00
C$_5$*H*$_4$	4.11 – 4.09 & 4.08 – 4.06	3.92 & 3.70	4.11 – 4.03	3.98 – 3.92 & 3.79 – 3.69
-C*H*$_2$C*H*$_2$-	2.69 – 2.56	2.19 – 2.10 & 2.10 – 1.98		
-C*H*$_2$C*H*$_2$C*H*$_2$-			2.51, 2.46 – 2.35 & 1.87 – 1.69	2.19 – 1.98, 1.98 – 1.70 & 1.35 – 1.10
-SC*H*$_3$	2.12	1.48	2.10	1.45
C3*H*/C3''*H*		8.10		8.30 – 8.06
C4*H*/C4''*H*		7.78		7.84
C5*H*/C5''*H* **C4'*H***		7.54		7.67 – 7.50
C6*H*/C6''*H*		9.49		9.36
C3'*H*/C5'*H*		8.07		8.30 – 8.06

Table S2. Assignments of ^{13}C resonances (δ) for the ligands **mtefc**, **mtpfc** and complexes **1** and **2** in $CDCl_3$.

	mtefc	**1**	**mtpfc**	**2**
C$_5$*H*$_5$	68.6	68.54	68.7	68.5
C$_5$*H*$_4$	87.3, 68.1 & 67.4	85.8, 67.7 & 67.48	88.6, 68.3 & 67.4	86.9, 67.7 & 67.5
-C*H*$_2$C*H*$_2$-	35.0 & 29.9	36.5 & 27.1		
-C*H*$_2$C*H*$_2$C*H*$_2$-			34.0, 30.3 & 28.5	35.1, 30.3 & 28.1
-SC*H*$_3$	15.8	17.1	15.5	16.4
***C*2'/*C*6'**		161.1		161.0
C2/C2''		159.2		159.2
C3*H*/C3''*H*		121.9		122.2
C4*H*/C4''*H*		135.4		135.5
***C*4'H**		129.2		129.3
C5*H*/C5''*H*		127.0		126.9
C6*H*/C6''*H*		153.8		153.6
C3'*H*/C5'*H*		121.3		121.6

Table S3. The peaks detected in the positive ion mode MALDI TOF mass spectra of the complexes **1** and **2**.

Peak position (*m/z*)	*m/z* range	Peak assignment
complex **1**		
334.52	331.43-336.53	$[Ru(tpy)]^{\cdot+}$
530.65	526.55-532.64	$[Ru(tpy)(SCH_3C_2H_4C_pFe)+H]^{\cdot+}$
546.49	543.24-548.40	$[Ru(tpy)(C_2H_4)(ferrocene)-H]^{\cdot+}$
566.07	562.04-568.04	$[Ru(tpy)Cl(CH_3)(SCH_3CH_2C_pFe)]^{+}$
666.16	663.23-671.18	$[M+H^+]^+$
complex **2**		
349.22	343.21-353.21	$[Ru(tpy)(CH_3)-H^+]^+$
545.34	541.30-547.40	$[Ru(tpy)(SCH_3C_3H_6C_pFe)+H]^{\cdot+}$
561.20	555.18-563.13	$[Ru(tpy)(C_3H_6)(ferrocene)-H]^{\cdot+}$
580.96	578.98-584.90	$[Ru(tpy)Cl(CH_3)(SCH_3C_2H_4C_pFe)+ H]^{\cdot+}$
680.50	678.75-684.37	$[M+H^+]^+$

where Cp is cyclopentadienyl moiety (C_5H_4-), M is a molecular ion, tpy is terpyridine

CHAPTER 3

RHODIUM AS POTENTIAL ANTICANCER DRUG

3.1. Synthesis and structures of a pincer-type rhodium(III) complexes: reactivity toward biomolecules

Within the paper a novel rhodium(III) complex contacting pincer-type ligand was synthesized. Single crystal X-ray measurement was performed. The reactivity toward small biomolecules, such as L-methionine, guanosine-5'-monophosphate, L-histidine and glutathione and a series of duplex DNAs and RNA was investigated by UV-Vis spectroscopy. Furthermore, an interaction with DNA/BSA and rhodium(III) complex was monitored by UV-Vis spectroscopy.

Participations in the publication:

M. M. Milutinović, J. V. Bogojeski, S. K. C. Elmroth, Ž. D. Bugarčić – Synthesis, UV-Vis spectroscopy, NMR measurements, kinetic investigation of DNAs, RNA and BSA by UV-Vis spectroscopy, implementing of all results and writing a paper;

A. Scheurer – Synthesis of a pincer-type ligand:

O. Klisurić – X-ray measurements.

DOI: 10.1039/C6DT02772E

Dalton Transactions

PAPER

View Article Online
View Journal | View Issue

Cite this: *Dalton Trans.*, 2016, **45**, 15481

Synthesis and structures of a pincer-type rhodium(III) complex: reactivity toward biomolecules†

Milan M. Milutinović,[a,d] Jovana V. Bogojeski,*[a] Olivera Klisurić,[b] Andreas Scheurer,[c] Sofi K. C. Elmroth[d] and Živadin D. Bugarčić*[a]

Received 13th July 2016,
Accepted 26th August 2016

DOI: 10.1039/c6dt02772e

www.rsc.org/dalton

A novel rhodium(III) complex $[Rh^{III}(H_2L^{tBu})Cl_3]$ (**1**) (H_2L^{tBu} = 2,6-bis(5-*tert*-butyl-1*H*-pyrazol-3-yl)pyridine) containing a pincer type, tridentate nitrogen-donor chelate system was synthesized. Single crystal X-ray structure analysis revealed that **1** crystallizes in the orthorhombic space group *Pbcn* with *a* = 20.7982(6), *b* = 10.8952(4), *c* = 10.9832(4) Å, *V* = 2488.80(15) Å^3, and eight molecules in the unit cell. The rhodium center in the complex $[Rh^{III}(H_2L^{tBu})Cl_3]$ (**1**) is coordinated in a slightly distorted octahedral geometry by the tridentate N,N,N-donor and three chloro ligands, adopting a *mer* arrangement with an essentially planar ligand skeleton. Due to the tridentate coordination of the N,N,N-donor, the central nitrogen atom N1 is located closer to the Rh^{III} center. The reactivity of the synthesized complex toward small biomolecules (L-methionine (L-Met), guanosine-5′-monophosphate (5′-GMP), L-histidine (L-His) and glutathione (GSH)) and to a series of duplex DNAs and RNA was investigated. The order of reactivity of the studied small biomolecules is: 5′-GMP > GSH > L-Met > L-His. Duplex RNA reacts faster with the $[Rh^{III}(H_2L^{tBu})Cl_3]$ complex than duplex DNA, while shorter duplex DNA (15mer GG) reacts faster compared with 22mer GG duplex DNA. In addition, a higher reactivity is achieved with a DNA duplex with a centrally located GG-sequence than with a 22GTG duplex DNA, in which the GG-sequence is separated by a T base. Furthermore, the interaction of this metal complex **1** with calf thymus DNA (CT-DNA) and bovine serum albumin (BSA) was examined by absorption (UV-Vis) and emission spectral studies (EthBr displacement studies). Overall, the studied complex exhibited good DNA and BSA interaction ability.

Introduction

The design of new metal-based therapeutic agents with a unique mechanism of action is facilitated due to the great variety of coordination chemistry. Considering the roles which both the metal and the ligands play in recognition processes, as well as the understanding of thermodynamics and kinetics of metal complex reactions under conditions of biological relevance are the key to such a discovery.[1–3] Despite the evolution of cisplatin analogues, only two other agents of this type, carboplatin and oxaliplatin, are currently in global clinical use. This fact has led to growing interest in the properties of complexes containing metals other than platinum.[1–3] Over two decades ruthenium metallo-drugs were intensively investigated, revealing these types of drugs to exhibit better properties compared to platinum metallo-drugs, but to date none of these metallo-drugs have been approved for clinical use.[1–3] Presently, research in this field is more directed toward metal complexes from the 9th group of the Periodic Table, for example iridium and rhodium.[4–6]

The antitumor activity of the rhodium(III) salt $RhCl_3{\cdot}xH_2O$, was first mentioned in 1953, more than a decade before the antitumor activity of a platinum complex was reported.[7,8] The main drawback of the metal complexes from the 9th group of the Periodic Table is that they have shown inertness and only recently Rh^{III} complexes have received increasing attention. Their reactivities, binding preferences, and cellular uptake are strongly dependent on their ligand combination and coordination geometry.[4] Also, this specific characteristic of the complexes of 9th group metals, inertness, has contributed to the design of complexes which can target specific proteins and enzyme inhibitors as well as DNA.[4] To date, a lot of Rh^{III} complexes such as half-sandwich Rh^{III} complexes and

[a]*University of Kragujevac, Faculty of Science, Radoje Domanovića 12, 34000 Kragujevac, Serbia. E-mail: jrosic@kg.ac.rs, bugarcic@kg.ac.rs; Fax: +381(0)34335040; Tel: +381(0)34300262*
[b]*University of Novi Sad, Faculty of Science, Department of Physics, Trg Dositeja Obradovića 3, 21000 Novi Sad, Serbia*
[c]*Lehrstuhl für Anorganische und Allgemeine Chemie, Department Chemie und Pharmazie, Universität Erlangen-Nürnberg, Egerlandstr. 1, 91058 Erlangen, Germany*
[d]*Lund University, Biochemistry and Structural Biology, KILU, P.O. Box 124, SE-221 00 Lund, Sweden*

†Electronic supplementary information (ESI) available. CCDC 1482787. For ESI and crystallographic data in CIF or other electronic format see DOI: 10.1039/c6dt02772e

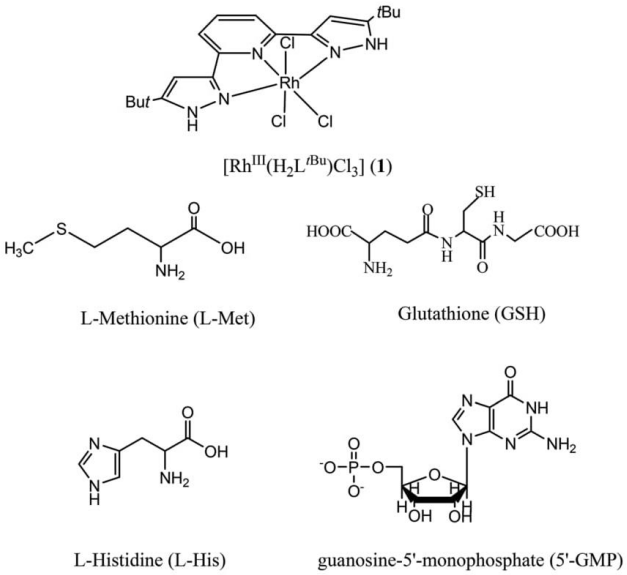

Fig. 1 Structures of the investigated rhodium(III) complex **1** and nucleophiles, along with their abbreviations.

polypyridyl Rh^{III} complexes were investigated.[4] However, our interest was directed towards the pincer-type ligands since these ligands were investigated during the past few decades due to their very specific characteristics (*e.g.* photophysical and biological properties) and diverse applications in catalysis.[9,10] Therefore, the aim of our research was to see if this type of ligand can enhance the reactivity of Rh^{III} complexes toward biomolecules which are characteristic binding targets for cisplatin.

Based on these facts, the focus of this paper was the design of a new Rh^{III} complex with increased activity by the use of a spectator ligand to notably improve the rate of substitution. Also, the studies of the substitution process have been performed with selected biomolecules (Fig. 1), a duplex of DNA and RNA, CT-DNA as well as protein albumin in order to improve the understanding of biological reactivity preferences. These kinds of biomolecules were chosen since these biomolecules are known as targeting molecules for Pt^{II} complexes, thus, enabling a comparison of the properties of the new Rh^{III} complex with Pt^{II} complexes, which have established antitumor features.

Results and discussion

Preparation and structure of $[Rh^{III}(H_2L^{tBu})Cl_3]$ (1)

The complex $[Rh^{III}(H_2L^{tBu})Cl_3]$ (**1**) (Fig. 1) was synthesized by stirring equimolar amounts of $RhCl_3{\cdot}xH_2O$ and 2,6-bis(5-*tert*-butyl-1*H*-pyrazol-3-yl)pyridine (H_2L^{tBu}) in ethanol at 50 °C. The Rh^{III} complex **1** was characterized by means of standard analytical methods and its purity was confirmed by elemental analysis. Single crystals suitable for X-ray structure analysis were also obtained for the determination of the molecular structure.

Crystal structure discussion

The perspective view of the molecular structure of the Rh^{III} complex **1** is shown in Fig. 2. Selected metal–ligand bond lengths and angles of **1** are given in Table 1.

Suitable crystals for X-ray structural analysis were obtained from a DMF/water mixture of **1** upon prolonged standing. The complex $[Rh^{III}(H_2L^{tBu})Cl_3]{\cdot}2H_2O$ (**1**·$2H_2O$) crystallizes in the orthorhombic crystal system and the *Pbcn* space group, with one half of the molecule in the asymmetric unit since the 2-fold axis passes through the special position of Rh1, Cl1, N1, and C10 atoms. In the outer sphere of the complex, there are two H_2O solvent molecules. From a structural point of view, one must emphasize two features of complex **1**, namely, the coordination of the Rh1 atom and the crystal packing. The rhodium center in complex **1** is coordinated in a slightly distorted octahedral geometry with the tridentate N,N,N-donor adopting a *mer* arrangement with the essentially planar ligand skeleton (Fig. 2). Due to the tridentate coordination of the N,N,N-donor, the central nitrogen atom N1 is located closer to the rhodium(III) center (Table 1). It therefore applies a *trans* influence to Cl1, which explains the slightly larger value of the Rh1–Cl1 bond length compared to Rh1–Cl2 (Table 1). The

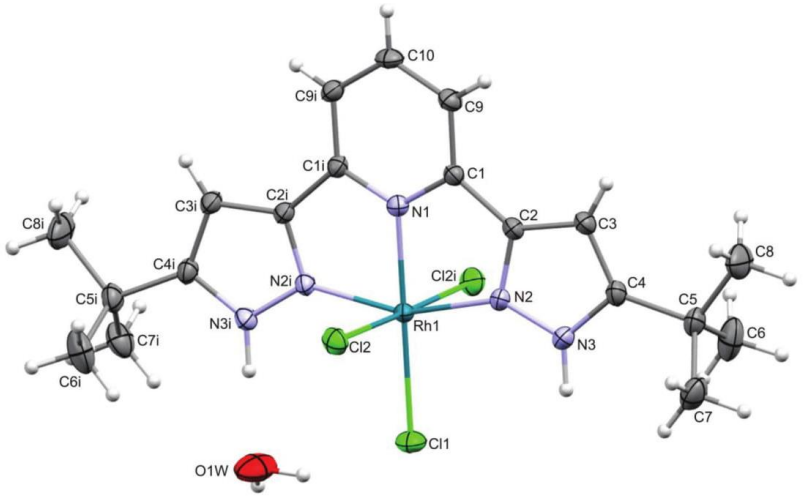

Fig. 2 ORTEP presentation of the molecular structure of the $[Rh^{III}(H_2L^{tBu})Cl_3]$ complex together with one of the cocrystallized water molecules and the non-H atom numbering scheme with thermal ellipsoids at the 30% probability level. Symmetry transformations used to generate equivalent atoms labeled with i is: $-x + 1, y, -z + 3/2$.

Table 1 Selected geometrical parameters for complex $[Rh^{III}(H_2L^{tBu})Cl_3]$ (**1**)

Bond lengths [Å]	
Rh1–N1	1.968(3)
Rh1–N2	2.034(2)
Rh1–Cl1	2.3690(10)
Rh1–Cl2	2.3276(7)
N2–N3	1.346(3)
N1–C1	1.346(3)
N2–C2	1.346(3)
N3–C4	1.354(3)
Bond angles [°]	
N1–Rh1–N2	79.09(6)
$N2^i$–Rh1–N2	158.17(12)
N2–Rh1–$Cl2^i$	87.43(6)
N1–Rh1–Cl2	89.37(2)
N2–Rh1–Cl2	92.34(6)
$Cl2^i$–Rh1–Cl2	178.74(4)
N1–Rh1–Cl1	180.0
N2–Rh1–Cl1	100.91(6)
Cl2–Rh1–Cl1	90.63(2)
Torsion angles [°]	
Rh1–N2–N3–C4	165.4(2)
Rh1–N1–C1–C9	−179.48(19)
Rh1–N1–C1–C2	1.8(2)
Rh1–N2–C2–C3	−170.14(18)
Rh1–N2–C2–C1	5.6(3)

Symmetry code: (i) $-x + 1, y, -z + 3/2$.

bond angles N1–Rh1–Cl2/N2 approach 90°, while the N2–Rh1–Cl1/Cl2 angles are larger than 90°, showing the steric influence of a bulky H_2L^{tBu} chelating ligand. The group Rh1Cl1N1N2 is perfectly planar since there is no displacement from the same weighted least-squares plane. The angle between the N2C2C3C4N3 ring plane and the Rh1Cl1N1N2 plane is 9.64(7)° confirming a slight distortion from the planarity of the ligand skeleton.

The crystal packing of complex **1**·$2H_2O$ (Fig. S1†) is based on hydrogen bonding interactions involving the water molecules, the hydrogen atom attached to the N3 nitrogen atom, and all Cl ligands. The water molecules, as a two-time donor to Cl and one time acceptor to NH, form three hydrogen bonds (Table S1†) leading to an infinite spiral chain along the *c* axis (Fig. S1†).[11]

Kinetic studies

The substitution reactions of complex 1 with L-Met, GSH, 5′-GMP and L-His. Complexes of metal ions from the 9th group of the Periodic Table are characterized by their kinetic inertness and accordingly slow substitution reactions are typical of these complexes. In the last few years, it has been shown that introduction of different spectator ligands in the coordination sphere of Rh^{III} complexes can improve the reactivity of these complexes.[4] To get an idea of the reactivity of the Rh^{III} complex under physiological conditions, the substitution reactions of the Rh^{III} complex, (**1**), with selected nucleophiles (Fig. 1) were investigated. The change in absorbance was followed, at suitable wavelengths, as a function of time at 310 K and pH ≈ 7.2 in 25 mM Hepes buffer and 50 mM NaCl.

The proposed reaction pathways for all observed substitution processes are presented in Scheme 1.

In the present study direct nucleophilic attack proceeds in a reversible manner as mentioned in Scheme 1. All kinetic experiments were performed under pseudo-first-order conditions, for which the concentration of the Rh^{III} complex was always in at least a 10-fold excess. To suppress the solvolytic pathway, a 50 mM NaCl solution was added.

The rate constants for substitution could be determined, under pseudo-first-order conditions, from the plot of the linear dependence of k_{obsd} *vs.* the total complex concentration, according to eqn (1). All kinetic data are summarized in Tables S2–S5 (ESI†).

$$k_{obsd} = k_2[\mathbf{1}] + k_1[Cl^-] \quad (1)$$

The direct nucleophilic attack is characterized by the rate constant k_2, and the reverse reactions are presented by the rate constant k_1. The second-order rate constant k_2, characterizing the formation of the product, can be evaluated from the slope of a plot k_{obsd} *vs.* the Rh^{III} complex concentration. The experimental results for the displacement of a chloride ion from complex **1** are summarized in Table 2. Representative plots are shown in Fig. 3 (others are given in the ESI Fig. S2†).

According to the values of k_2, summarized in Table 2, the used nucleophiles are good entering ligands for the substitution reactions of the Rh^{III} complex. Comparing the reactivity of the nucleophiles we observed that the reactivity decreases in the following order: 5′-GMP > GSH > L-Met > L-His at 310 K. To date, there are not many studies of substitution reactions of

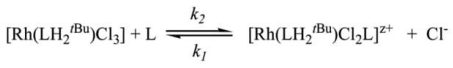

L= L-Met, GSH, 5′-GMP, L-His

Scheme 1 Schematic representation of the substitution reactions of the **1** complex with the nucleophiles: L-Met, GSH, 5′-GMP and L-His.

Table 2 The rate constants for the substitution reactions of the Rh^{III} complex with L-Met, GSH, 5′-GMP, and L-His at pH = 7.2 (25 mM Hepes buffer) in the presence of 50 mM NaCl

		$[Rh^{III}(H_2L^{tBu})Cl_3]$			
	T (K)	$10^1\,k_2$ ($M^{-1}\,s^{-1}$)	$10^4\,k_1[Cl^-]$ ($M^{-1}\,s^{-1}$)	$\Delta H_2^{\neq}$ (kJ mol^{-1})	$\Delta S_2^{\neq}$ (J $K^{-1}\,mol^{-1}$)
L-Met	288.0	1.7 ± 0.1	0.48 ± 0.01		
	298.0	1.9 ± 0.1	0.32 ± 0.01	11 ± 2	−240 ± 5
	310.0	2.4 ± 0.2	0.15 ± 0.03		
5′-GMP	288.0	1.0 ± 0.1	0.14 ± 0.01		
	298.0	2.3 ± 0.2	0.35 ± 0.01	43 ± 5	−130 ± 20
	310.0	4.1 ± 0.1	0.53 ± 0.02		
GSH	310.0	2.9 ± 0.3	0.87 ± 0.05	—	—
L-His	310.0	2.2 ± 0.2	1.01 ± 0.04	—	—

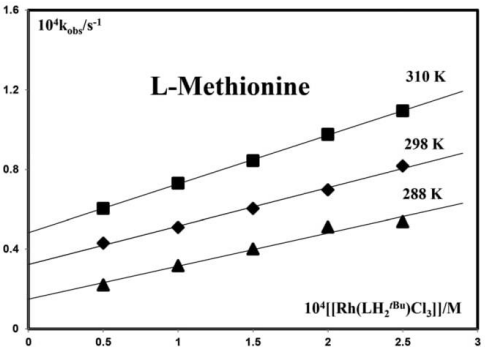

Fig. 3 Pseudo-first-order rate constants plotted as a function of complex **1** concentration for the substitution reactions of complex **1** with L-Met at pH = 7.2 (25 mM Hepes buffer) in the presence of 50 mM NaCl.

different small biomolecules and Rh^{III} complexes, thus the obtained results were compared with the results obtained for substitution reactions of few Pt^{II} complexes.[13] Based on the comparisons, it was observed that the order of reactivity of biomolecules in the substitution reactions with the Rh(III) complex was opposite to the obtained order for Pt(II) complexes (L-Met > GSH > 5′-GMP). In order to explain the fact stated, it is necessary to take a combination of various factors that attribute to the observed scenario. In this context, the other factors such as the type (group, period)[12] and the oxidation state of the metal, ligands, co-ligands, (co)solvents, *etc.* contribute to the different affinities towards biomolecules. But in this context, further detailed theoretical investigations (in solution) are needed, which are beyond the focus of this present study.

The activation parameters $\Delta H^{\neq}$ and $\Delta S^{\neq}$ (Table 2) were calculated using the Eyring equation for the reactions with L-Met and 5′-GMP. The activation parameters support an associative mechanism for each of these reactions, which are supported by the significantly negative activation entropies.

The substitution reactions of $[Rh^{III}(H_2L^{tBu})Cl_3]$ with a series of duplex DNAs and RNA. The interaction of DNA and cisplatin is one of the best-explained interactions of DNA molecules and metal ions. Cisplatin anticancer activity is today known to involve disruption of repair and induction of apoptosis as a consequence of covalent modification of nuclear DNA.[1–3,14] However, the new generation of transition metal complexes, such as Rh^{III} complexes, do not have DNA as a favored target site. Of note is that both proteins and RNA have been experimentally verified as targets of the new generation of metallodrugs.[2–4] In an attempt to prove that DNA is a possible target of rhodium(III) complexes, we have studied the kinetics of reactions of complex **1** with a duplex of DNA-1, DNA-2, and DNA-3 (Scheme 2). Also, the reaction with one of the duplex RNAs was studied for comparison.

DNA-1	(a)	5'-CTT CTT **GG**T TCT CTT-3'
	(b)	3'-GAA GAA CCA AGA GAA-5'
DNA-2	(a)	5'-TCT CCT TCT T**GG** TTC TCT TCT C-3'
	(b)	3'-A GAG AGG AAG AAC CAA GAG AAG-5'
DNA-3	(a)	5'-TCT CCT TCT T**GT** **G**TC TCT TCT C-3'
	(b)	3'-A GAG AGG AAG AAC ACA GAG AAG-5'
RNA-1	(a)	5'-UUC UU**G** **G**UU CUC U-3'
	(b)	3'-A AGA ACC AAG AGA-5'

Scheme 2 Schematic representation of the used duplex of DNA or RNA.

All reactions were studied by the conventional UV-Vis methodology. Investigation of how the overall length and changes of base pairing in the close vicinity of a centrally located GG-site affect the rate of Rh^{III} binding was performed. For this purpose, the reactivity of three different DNA-1, DNA-2, and DNA-3 duplex DNAs was monitored at 310 K. In addition, the reaction between the Rh^{III} complex and 13-mer duplex RNA was also monitored at 310 K.

Metal-induced kinetics were studied after the addition of the rhodium(III) complex **1** to the buffered and temperature equilibrated solutions of duplex DNAs or RNA. Pseudo-first order conditions were applied, at least a 10-fold excess of the Rh^{III} complex, compared with the total DNA or RNA-strand concentration (C_T), was used to allow for quantitative determination of observed reaction rate constants (k_{obsd}) by a fit of a single-exponential function to the experimentally obtained ΔA-values ($\Delta A_t = A_t - A_{t=0}$). The standard expression for the exponential decay according to eqn (2) was used for determination of k_{obsd}, with ΔA_∞ denoting the maximum absorbance difference reached at the end of the studied time interval.

$$\Delta A_t = \Delta A_\infty(1 - \exp(-k_{obsd}t)) \quad (2)$$

The obtained representative kinetic traces, together with the corresponding fitted single-exponential functions, are shown in Fig. S3.†

The observed rate constants were plotted as a function of added concentration of complex **1**; a linear dependence on $C_{(1)}$ (Fig. 4). The obtained linear dependence is in agreement with a reaction mechanism in which the interaction between complex **1** and duplex DNA or duplex RNA constitutes the rate determining step, see eqn (3) and (4), where $k_{2,app}$ presents the apparent second-order rate constant for the studied reaction. For such a reaction model, the second-order rate constant $k_{2,app}$ can thus be directly obtained from the slope of a plot of k_{obsd} *vs.* $C_{(1)}$.[15,16]

$$\text{dsDNA(or dsRNA)} + (\mathbf{1}) \underset{k_{-2}}{\overset{k_{2,app}}{\rightleftharpoons}} \text{dsDNA(or dsRNA)} - \mathbf{1} + Cl^- \quad (3)$$

$$k_{obsd} = k_{2,app}[\mathbf{1}] + k_{-2}[Cl^-] \quad (4)$$

The obtained rate constants for the reaction between Rh^{III} complex **1** and the chosen DNA or RNA duplex are summarized in Table 3. Representative plots are shown in Fig. 4.

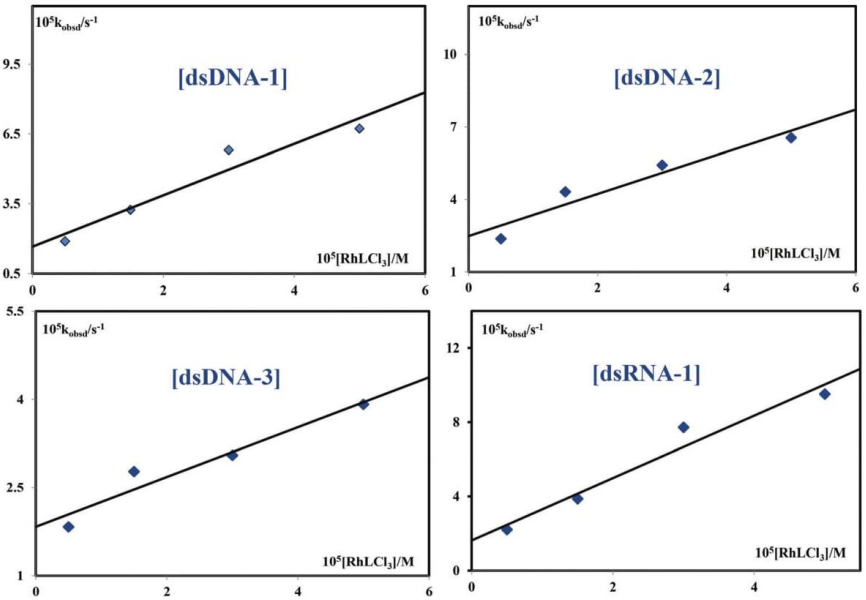

Fig. 4 Pseudo-first-order rate constants plotted as a function of complex **1** concentration for the substitution reactions of the complexes **1** with DNA-1, DNA-2, DNA-3, and RNA-1 in PBS buffer solution at pH = 7.4, T = 310 K.

Table 3 The obtained rate constants, $k_{2,app}$, for the reaction between complex **1** and duplex DNAs and RNA in PBS buffer at 310 K

	$k_{2,app}$ (M^{-1} s^{-1})	$k_{-2}[Cl^-]$ (10^5 M^{-1} s^{-1})
DNA-1	1.11 ± 0.02	2.0 ± 0.2
DNA-2	0.87 ± 0.01	2.5 ± 0.1
DNA-3	0.42 ± 0.01	1.8 ± 0.1
RNA-1	1.68 ± 0.01	1.6 ± 0.1

From the obtained and above presented data it can be seen that the investigated complex **1** interacts with duplex DNAs as well as with RNA. Various length duplexes of DNA, 15GG (DNA-1), and 22GG (DNA-2) were used in this study. The following order of reactivity was obtained: RNA-1 > DNA-1 > DNA-2 > DNA-3. It turned out that the shorter 15GG duplex reacts faster than the longer 22GG duplex, which is consistent with previously published results.[15,16] Furthermore, the duplexes of the same length, but of different sequences, 22GG (DNA-2) and 22GTG (DNA-3) were studied. It was observed that a higher reactivity is achieved with a DNA duplex with a centrally located GG-sequence than with a 22GTG duplex in which the GG-sequence is separated by a T base. In all studied reactions similar intercepts could be evaluated, Fig. 4 and eqn (4).

DNA interactions

UV-Vis absorption studies. UV-Vis CT-DNA titrations were carried out using complex **1**. The intrinsic equilibrium binding constant (K_b) was evaluated. Therefore, the metal complex absorption titration studies were carried out at room temperature using a fixed concentration of complex **1** (12.5 μM) in PBS buffer, and varying the amount of CT-DNA (0–20 μM).[17] A studied systematic addition of CT-DNA to a solution of the Rh^{III} complex resulted in a significant hyperchromic effect with the appearance of a new band at 258 nm, but with only insignificant absorption changes in the 300–500 nm region, see Fig. 5. A significant hyperchromic shift with the appearance of a new signal in UV-Vis spectra clearly suggested a strong interaction between the complex and CT-DNA through external contacts, presumably hydrogen bonding and electrostatic interactions.[18]

Ethidium bromide (EthBr) displacement studies

Interaction of complex **1** with CT-DNA has also been performed by EthBr displacement studies, which provide strong evidence about competitive binding of drugs with CT-DNA. EthBr itself fluorescences weakly,[18] however in the presence of CT-DNA it strongly emits at ~600 nm due to strong intercalation between EthBr and DNA base pairs. Interaction of complex **1** with CT-DNA led to significant quenching of fluorescence intensity due to the displacement of EthBr from the EthBr–DNA complex.[19] The quenching parameters for the Rh^{III} complex **1** have been calculated using the Stern–Volmer equation. Therefore, EthBr displacement studies have been performed by changing the concentration of metal complexes and monitoring the emission intensity of the EthBr–DNA complex.[17] An increase in the concentration of **1** (0–30 μM) exhibited a significant decrease in the fluorescence intensity with a noticeable red shift. It indicated that EthBr is released from the EthBr–DNA complex due to its exchange by the studied complex. Thus, complex **1** is capable of displacing EthBr from the EthBr–DNA complex and could strongly interact with DNA binding sites (Fig. 6).[20]

As indicated above, the fluorescence intensity at 612 nm was used to estimate K_{sv} but the fluorescence quenching data

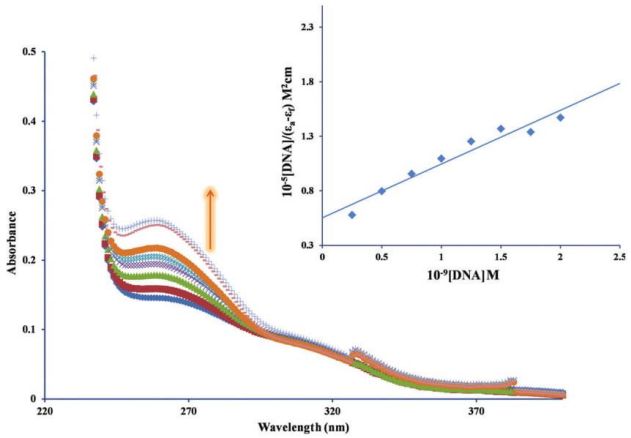

Fig. 5 UV-Vis titration spectra of complex **1** (12.5 μM) in PBS buffer (phosphate buffer solution = 0.01 M, C_{NaCl} = 0.137, C_{KCl} = 0.0027 M, pH 7.4) with the increasing concentration of CT-DNA (0–20 μM). The arrow shows hyperchromism in the spectral band. Insert graph: plots of [DNA]/($\varepsilon_A - \varepsilon_f$) *vs.* [DNA].

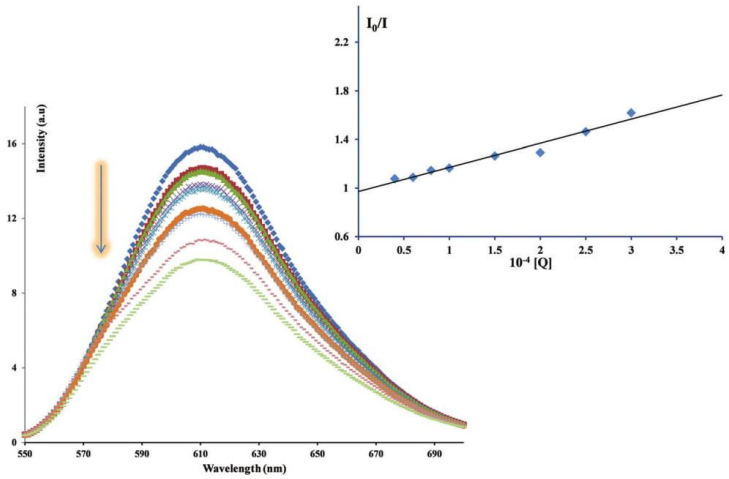

Fig. 6 Fluorescence titration spectra of EthBr–DNA and of EthBr (10 μM) bound to DNA (10 μM) in the presence of varying amounts of complexes **1**. [The arrow shows changes in the fluorescence intensity upon increasing concentration of **1** (4–30 μM).] Insert graph: Stern–Volmer plots for EthBr–DNA fluorescence titration with **1**.

Table 4 The obtained constants for the interaction between complex **1** and CT-DNA

	$[Rh^{III}(H_2L^{tBu})Cl_3]$		
	K_b $[M^{-1}]$	K_{sv} $[M^{-1}]$	K_{bin} $[M^{-1}]$
CT-DNA	$(9.7 \pm 0.1) \times 10^4$	$(1.9 \pm 0.1) \times 10^4$	$(2.4 \pm 0.1) \times 10^4$
BSA	—	$(3.0 \pm 0.1) \times 10^4$	$(7.4 \pm 0.1) \times 10^3$

could be used to determine the binding sites (n) and the equilibrium-binding constant by using the Scatchard equation:

$$\log(I_0/I) = \log K_{bin} + n \log[Q]$$

K_{bin} is the binding constant of complex **1** with CT-DNA and n is the number of binding sites. The number of binding sites (n) and the binding constant (K_{bin}) have been calculated from

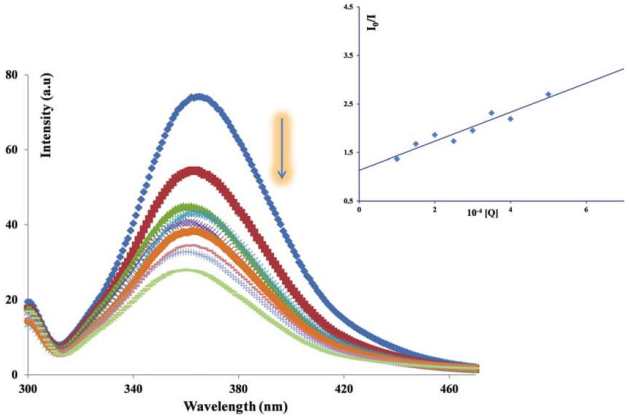

Fig. 7 Emission spectrum of BSA (2 μM; λ_{ex}, 295 nm; λ_{em} 363 nm) in the presence of increasing amounts of **1** (0–60 μM). The arrow shows that the emission intensity changes upon increasing the concentration of the complex. Insert graph: plots of I_0/I *vs.* [*Q*].

the plot of $\log(I_0/I)$ *vs.* log[Q] (see Fig. S4†). The calculated value of the number of binding sites (n) is 1.03. The value of (n) is approximately equal to 1, and it indicates the existence of one binding site in DNA for the rhodium(III) complex **1**.

According to the values of constants presented in Table 4 a good interaction of the studied complex with CT-DNA is evident. Also, the results obtained by fluorescence spectroscopy are in excellent agreement with the UV-Vis spectral data, demonstrating that the studied complex interacts with CT-DNA.

Protein binding studies

To gain a better insight into the interaction between the studied complex **1** and BSA, BSA fluorescence quenching experiments in the presence of the Rh^{III} complex **1** were performed. Fluorescence spectroscopy can provide useful information about the structure, dynamics, and protein folding.[21–23] Changes in the fluorescence spectrum of BSA upon addition of different concentrations of complex **1** (0–60 μM) in the range of 300–500 nm (λ_{ex} = 295 nm) are presented in Fig. 7. As illustrated here, a decrease in the fluorescence intensity at 363 nm and some interactions between the complexes and BSA protein are observed. Fluorescence quenching data have been analyzed using the Stern–Volmer equation and the quenching constant (K_{sv}) was calculated by using the plot of I_0/I *vs.* [Q], Fig. 7. The equilibrium binding constant K_{bin} and n, the number of binding sites, can be analyzed by the Scatchard equation (see Fig. S5, ESI†). The value of n for the studied complex is 0.85 which is approximate to 1 and strongly suggests the existence of a single binding site in BSA for the Rh^{III} complex **1**.

According to the obtained constants, complex **1** interacts satisfactorily with BSA protein (Table 4). By comparing the obtained quenching constant (K_{sv}) for the interaction of the rhodium(III) complex with CT-DNA and BSA it can be seen that they are almost similar (Table 4).

Conclusion

In this study, a novel rhodium(III) complex $[Rh^{III}(H_2L^{tBu})Cl_3]$ (**1**) with pincer-type tridentate nitrogen donor ligands and three vacant coordination sites was synthesized. X-ray structure analysis on single crystals of complex **1**·$2H_2O$ was carried out, indicating that the rhodium center in complex **1** is coordinated in a slightly distorted octahedral geometry with the tridentate N,N,N-donor adopting a *mer* arrangement and an essentially planar ligand skeleton. Kinetic experiments were performed with selected small bio-molecules (*i.e.* L-methionine, L-histidine, glutathione, and guanosine-5′-monophosphate) under pseudo-first-order conditions as a function of complex concentration and temperature using UV-Vis spectrophotometry. These measurements showed that the synthesized complex has good affinity toward studied ligands and the obtained order of reactivity is: 5′-GMP > GSH > L-Met > L-His with small differences in the values of obtained second-order rate constants. Thus, this implies that rhodium(III) ions have almost the same affinity to bound to sulfur-donor biomolecules and nitrogen-donor biomolecules, which is in accordance with the fact that Rh^{III} belongs to the borderline group, *i.e.* this metal ion is soft–hard acid. Also the kinetic measurements between complex **1** and a duplex DNA and RNA were performed. These results show a higher reactivity of the Rh^{III} complex toward a duplex RNA than DNA, and with the shorter 15mer DNA reacting faster compared with the 22mer DNA. Furthermore, it was observed that a better reactivity is achieved with a DNA duplex with a centrally located GG-sequence than with a 22GTG duplex in which the GG-sequence is separated by a T base. The interaction between complex **1** and calf thymus DNA (CT-DNA) and bovine serum albumin (BSA) was also examined by absorption (UV-Vis) and emission spectral studies (EthBr displacement studies). Overall, this examination shows that the Rh^{III} complex **1** has almost the same affinity to interact with calf thymus DNA (CT-DNA) and bovine serum albumin (BSA).

All the obtained results in this study indicate that the introduction of a pincer-type spectator ligand can improve the reactivity of rhodium(III) complexes. Furthermore, the kinetic measurements reveal a similar affinity of the complex **1** toward sulfur-donor and nitrogen-donor biomolecules, combined with good affinity toward both duplex DNA and RNA. Lastly, the Rh^{III} complex was found to interact with both CT-DNA and BSA. Together, these observations show the reactivity characteristics needed for a potential anti-tumor agent, with the ability to target both DNA and proteins. Every new contribution in this field is highly warranted due to the current lack of clinically used metallo-based alternatives to cisplatin.

Experimental

Material and methods

L-Methionine (L-Met), glutathione (GSH), guanosine-5′-monophosphate sodium salt (5′-GMP), L-histidine (L-His), and $RhCl_3{\cdot}xH_2O$ were obtained from Acros Organics or Sigma Aldrich and used without further purification. Hepes buffer (*N*-2-hydroxyethylpiperazine-*N*′-2-ethanesulfonic acid) was obtained from Sigma Aldrich. All oligonucleotides (5′-CTT CTT GGT TCT CTT-3′ and 5′-AAG AGA ACC AAG AAG-3′ (DNA-1), 5′-TCT CCT TCT TGG TTC TCT TCT C-3′ and 5′-GAA GAG AAC CAA GAA GGA GAG A-3′ (DNA-2), 5′-TCT CCT TCT TGT GTC TCT TCT C-3′ and 5′-GAA GAG ACA CAA GAA GGA GAG A-3′ (DNA-3), 5′-UUC UUG GUU CUC U-3′ and 5′-AGA GAA CCA AGA A-3′ (RNA-1)) were purchased from IBA GmbH (IBA Nucleic Acids Synthesis, Göttingen, Germany) of HPLC grade quality. Disodium hydrogen phosphate dihydrate ($Na_2HPO_4{\cdot}2H_2O$), sodium chloride (NaCl), and potassium chloride (KCl) were obtained from Merck. Potassium dihydrogen phosphate monohydrate ($KH_2PO_4{\cdot}H_2O$) was obtained from Sigma. Phosphate buffers were prepared according to the literature procedure.[24] The serum protein albumin and CT-DNA were used as received without further purification and the solutions were prepared with deionized water. All water used

was of Millipore quality and autoclaved before use. All the other chemicals were of the highest purity commercially available and were used without further purification. Ultra-pure water was used in all experiments. Nucleophile stock solutions were prepared shortly before use by dissolving the chemicals. Preparation of the ligand H_2L^{tBu} was accomplished according to the literature procedures.[25]

Synthesis and characterization of the Rh^{III} complex $[Rh^{III}(H_2L^{tBu})Cl_3]$ (1)

To a solution of 100 mg (0.380 mmol) $RhCl_3{\cdot}xH_2O$ in 60 ml of ethanol was added 122.75 mg (0.380 mmol; 1 eq.) of ligand H_2L^{tBu} in 20 mL of ethanol. The reaction mixture was stirred overnight at 50 °C affording a yellow precipitate. The precipitate was filtered and dried in a vacuum. The product was obtained as a yellow solid, which was further purified by recrystallization from a mixture of DMF and water yielding yellow crystals (162.26 mg, 78%). ^{1}H NMR (d_6-DMSO): δ = 8.19 (d, 2H, $^3J_{HH}$ = 7.6 Hz, pyridine), 7.30 (t, 1H, $^3J_{HH}$ = 7.6 Hz, pyridine), 7.22 (s, 2H, pyrazole), 2.47 (s, 18H, CMe_3) ppm. Anal. Calcd for ($C_{19}H_{25}Cl_3N_5Rh{\cdot}1.25H_2O$) C: 41.10; H: 4.99; N: 12.61. Found: C: 40.95; H: 4.85; N: 12.96. IR (KBr, 4000–300 cm^{-1}): 3466 (N–H stretch); 2924 (C–H stretch) 1623, 1574, 1442 (C=C and C=N stretch); 635 (Rh–N stretch).

The synthesized complex is poorly soluble in water, thus in all experiments an aqueous solution of complex **1** with additional 5% of DMF (v/v) was used in order to improve the solubility.

Instrumentation

NMR spectra were recorded on a 200 MHz Varian Gemini-2000 device. Chemicals shifts (δ) are reported in ppm and referenced to tetramethylsilane. Coupling constants (J) are reported in hertz (Hz) and splitting patterns are indicated as s (singlet) and d (doublet). Elemental analyses (C, H, N) were performed by combustion and gas chromatographic analysis with an Elementar Vario MICRO elemental analyzer. pH measurements were carried out using a Mettler Delta 350 digital pH meter with a resolution ±0.01 mV, with a combination glass electrode. This electrode was calibrated using standard buffer solutions of pH 4, 7, and 9 obtained from Sigma. Kinetic measurements of the rhodium(III) complex **1** were carried out on a Perkin-Elmer Lambda 25 or 35 double-beam spectrophotometer in thermostated 1.00 cm quartz Suprasil cells. The temperature was controlled to ±0.1 °C. Varian Cary 100 spectrophotometers equipped with a thermal control unit were also used in kinetic experiments. All kinetic measurements were performed under pseudo-first-order conditions, *i.e.*, at least a 10-fold excess of the complex was used. Fluorescence measurements were performed on a RF-1501 PC spectrofluorometer (Shimadzu, Japan).

Kinetic measurements with small biomolecules

The kinetics of the substitution of the coordinated chloride can be omitted spectrophotometrically by following the change in absorbance at suitable wavelengths as a function of time. The working wavelengths were determined by recording the spectra of the reaction mixture over the wavelength range of 220 to 450 nm. All kinetic experiments were performed under pseudo-first-order conditions, for which the concentration of the Rh^{III} complex **1** was always in at least a 10-fold excess. The reactions were initiated by mixing 0.50 mL of the nucleophile complex solution with 2.50 mL of the thermally equilibrated complex solution in the UV-Vis cuvette, and reactions were followed for at least 8 half-lives. The observed pseudo-first-order rate constants, k_{obsd}, represent an average value of two to four independent kinetic runs for each experimental condition. Some of the reactions were studied at three temperatures (288, 298, and 310 K). The experimental data are summarized in the ESI (Tables S1–S4†). The values of the constants and other thermodynamic parameters were determined using the computer programs Microsoft Excel 2007 and OriginPro 8.

Kinetic measurements with a series of duplex DNAs and RNA

Kinetic studies were performed on a Varian Cary 100 spectrophotometer, equipped with a thermal control unit. Each duplex of DNA-1, DNA-2, DNA-3 and RNA-1 (Scheme 2) with equal concentrations of the (a) and (b) strands, was separately mixed in a buffer solution where the total strand concentration (C_T; $C_T = C_{Xa} + C_{Xb}$) was 3.0 μM and the measurements were conducted. The complementary duplexes were first heated to 90 °C, after being hybridized by slow cooling (0.5 °C min^{-1}) to 20 °C and then heated to 37 °C (0.5 °C min^{-1}) with the added complex **1**. The absorbance change was measured at λ = 260 nm after addition of **1**, where the final concentrations of **1** were: 5, 15, 30, and 50 μM for up to *ca.* 19 h.

UV-Vis DNA interactions

A stock solution of CT-DNA was prepared in PBS buffer, which gave a ratio of UV absorbances at 260 nm and 280 nm (A_{260}/A_{280}) of *ca.* 1.8–1.9, indicating that the DNA was sufficiently free of protein and the concentration was determined by the UV absorbance at 260 nm (ε = 6600 M^{-1} cm^{-1}).[26] The UV-Vis spectra were obtained on a Perkin-Elmer Lambda 35 or 25 double beam spectrophotometer, using 1.0 cm path-length quartz cuvettes (3.0 mL). Fluorescence measurements were performed on a RF-1501 PC spectrofluorometer (Shimadzu, Japan). The fluorescence spectra were recorded in the range of 550–750 nm upon excitation at 527 nm in all cases. The excitation and emission bandwidths were both 10 nm.

UV-Vis absorption studies

In order to compare quantitatively the binding strength of the complexes, the intrinsic binding constant K_b was determined by monitoring the changes in absorption at the MLCT band with an increasing concentration of CT-DNA using the following eqn (5).

$$[DNA]/(\varepsilon_A - \varepsilon_f) = [DNA]/(\varepsilon_b - \varepsilon_f) + 1/[K_b(\varepsilon_b - \varepsilon_f)] \quad (5)$$

K_b is given by the ratio of the slope to the y intercept in plots $[DNA]/(\varepsilon_A - \varepsilon_f)$ *vs.* [DNA], where [DNA] is the concentration

of DNA in base pairs, $\varepsilon_A = A_{obsd}/[complex]$, ε_f is the extinction coefficient for the unbound complex and ε_b is the extinction coefficient for the complex in the fully bound form.

Ethidium bromide (EthBr) displacement studies

The relative binding of complexes to CT-DNA was determined by calculating the quenching constant (K_{sv}) from the slopes of straight lines obtained from the Stern–Volmer equation (eqn (6)).

$$I_0/I = 1 + K_{sv}[Q] \quad (6)$$

I_0 and I are the emission intensities in the absence and the presence of the quencher (complex **1**), respectively, [Q] is the total concentration of the quencher, and K_{sv} is the Stern–Volmer quenching constant which can be obtained from the slope of the plot of I_0/I *vs.* [Q].

Protein binding studies

Fluorescence spectroscopy is an efficient tool for protein-binding studies, such as interaction of metal complexes with BSA. The fluorescence of the BSA arises due to the presence of fluorophores like tryptophan, tyrosine and phenylalanine. Accordingly, tryptophan fluorescence quenching experiments were carried out using bovine serum albumin (BSA 2.0 μM) in PBS buffer. The quenching of the emission intensity of the tryptophan residue of BSA at 363 nm was monitored in the presence of the increasing concentration of the Rh^{III} complex **1** (10.0–60.0 μM) as a quencher. Fluorescence measurements were performed on a RF-1501 PC spectrofluorometer (Shimadzu, Japan). Fluorescence spectra were recorded from 300 to 500 nm at an excitation wavelength of 295 nm. The excitation and emission bandwidths were both 10 nm.

X-ray diffraction studies

A single crystal of complex $[Rh^{III}(H_2L^{tBu})Cl_3]\cdot 2H_2O$ (**1**·$2H_2O$) was selected and mounted on a glass fiber. Diffraction data were collected using the Oxford Diffraction Gemini S four-circle goniometer equipped with a Sapphire CCD detector. The crystal to detector distance was 45.0 mm and graphite monochromated MoKα (λ = 0.7107 Å) radiation was used for the experiment at 293 K. The collected data set consisted of 2 runs of 155 frames of intensity (1° in ω). The collected frames were integrated by using an orientation matrix determined from the frame scans. CrysAlisPro and CrysAlis RED software packages[27] were used for data collection and data integration. Analysis of the integrated data did not reveal any decay. Final cell parameters were determined by a global refinement of 1975 reflections ($4.3 < \theta < 28.8°$). Collected data were corrected for absorption effects by multi-scan absorption correction using spherical harmonics as implemented in the SCALE3 ABSPACK[28] scaling algorithm.

Structure solution and refinement were carried out with the programs SHELXT and SHELXL-2014/6 respectively.[29] ORTEP-3 for Windows[30] was employed for molecular graphics and WinGx software was used to prepare material for publication.[31] Full-matrix least-squares refinement was carried out by minimizing ($F_o^2 - F_c^2$). All non-hydrogen atoms were refined anisotropically and refinement was carried out without geometric or ADP restraints. Hydrogen atoms attached to carbon atoms in methyl groups were placed in geometrically idealized positions and refined as riding on their parent atoms with $U_{iso}(H) = 1.5U_{eq}(C)$. The positions of all other hydrogens were found from the inspection of the difference Fourier maps. Crystal data and experimental details of the structure determination are listed in Table 5. Crystallographic data have been deposited with the Cambridge Crystallographic Data Centre as supplementary publications no. CCDC 1482787.

Table 5 Crystallographic data and refinement parameters for complex $[Rh^{III}(H_2L^{tBu})Cl_3]\cdot 2H_2O$ (**1**·$2H_2O$)

	1·$2H_2O$
Chemical formula	$C_{9.50}H_{14.50}Cl_{1.50}N_{2.50}ORh_{0.50}$
M_r	284.37
Crystal system, space group	Orthorhombic, *Pbcn*
a, b, c (Å)	20.7982(6), 10.8952(4), 10.9832(4)
V (Å^3)	2488.80(15)
Z	8
$F(000)$	1160
μ (mm^{-1})	1.03
Crystal shape	Prism
Colour	Yellow
Crystal size (mm)	0.46 × 0.18 × 0.15
Absorption correction	Multi-scan CrysAlis PRO, Agilent Technologies, empirical absorption correction using spherical harmonics, implemented in SCALE3 ABSPACK scaling algorithm.
T_{min}, T_{max}	0.978, 1.000
No. of measured, independent and observed [$I > 2\sigma(I)$] reflections	7072, 2867, 2220
R_{int}	0.020
θ values (°)	θ_{max} = 29.1, θ_{min} = 3.3
Range of h, k, l	$h = -15 \rightarrow 26$, $k = -7 \rightarrow 14$, $l = -14 \rightarrow 12$
$R[F^2 > 2\sigma(F^2)]$, $wR(F^2)$, S	0.033, 0.073, 1.10
No. of reflections	2867
No. of parameters	161
No. of restraints	2
H-atom treatment	H atoms treated by a mixture of independent and constrained refinement
ρ_{max}, ρ_{min} (e Å^{-3})	0.31, −0.45

Computer programs: CrysAlis PRO, Agilent Technologies, Version 1.171.37.35 (release 13-08-2014 CrysAlis171 .NET) (compiled August 13, 2014, 18:06:01), SHELXL2014/6 (Sheldrick, 2014).

Acknowledgements

The authors gratefully acknowledge financial support from the Ministry of Science and Technological Development of the Republic of Serbia, project No. 172011 and the Swedish Cancer foundation (Grant to S.K.C.E No. 13 0317). M. M. would like to thank Prof. Dr. Sofi K. C. Elmroth for hosting this work and continuously support at Kemicentrum, Lund University, Sweden and Dr Alak Alchikh for her support.

Notes and references

1 *Bioinorganic Medicinal Chemistry*, ed. E. Alessio, Wiley-VCH, Weinheim, 2011, ch. 1–4.
2 (*a*) P. E. N. Barry and J. P. Sadler, *Chem. Commun.*, 2013, **49**, 5106; (*b*) L. Ronconi and J. P. Sadler, *Coord. Chem. Rev.*, 2007, **251**, 1633.
3 S. Dilruba and G. V. Kalayda, *Cancer Chemother. Pharmacol.*, 2016, **77**, 1103.
4 C.-H. Leung, H.-J. Zhong, D. S.-H. Chan and D.-L. Ma, *Coord. Chem. Rev.*, 2013, **257**, 1764; Y. Geldmacher, M. Oleszak and W. S. Sheldrick, *Inorg. Chim. Acta*, 2012, **393**, 84.
5 Z. Liu, I. Romero-Canelón, B. Qamar, J. M. Hearn, A. Habtemariam, N. P. E. Barry, A. M. Pizarro, G. J. Clarkson and P. J. Sadler, *Angew. Chem., Int. Ed.*, 2014, **53**, 3941.
6 S. H. van Rijt, I. Romero-Canelón, Y. Fu, S. D. Shnyder and P. J. Sadler, *Metallomics*, 2014, **6**, 1014.
7 N. Cutillas, G. S. Yellol, C. Haro, C. Vicente, V. Rodriguez and J. Ruil, *Coord. Chem. Rev.*, 2013, **257**, 2784.
8 J. L. Bear, R. A. Howard and J. E. Korn, *Inorg. Chim. Acta*, 1979, **32**, 123.
9 (*a*) D. Morales-Morales and C. M. Jensen, *The Chemistry of Pincer Compounds*, Elsevier, Amsterdam, 2007; (*b*) J. T. Singleton, *Tetrahedron*, 2003, **59**, 1837; (*c*) L. C. Liang, *Coord. Chem. Rev.*, 2006, **250**, 1152; (*d*) V. C. Gibson, C. Redshaw and G. A. Solan, *Chem. Rev.*, 2007, **107**, 1745; (*e*) D. Pugh and A. A. Danopoulos, *Coord. Chem. Rev.*, 2007, **251**, 610; (*f*) D. Benito-Garagorri and K. Kirchner, *Acc. Chem. Res.*, 2008, **41**, 201; (*g*) W. Leis, H. A. Mayer and W. C. Kaska, *Coord. Chem. Rev.*, 2008, **252**, 1787; (*h*) M. T. Whited and R. H. Grubbs, *Acc. Chem. Res.*, 2009, **42**, 1607; (*i*) J. I. van der Vlugt and J. N. H. Reek, *Angew. Chem.*, 2009, **121**, 8990, (*Angew. Chem., Int. Ed.*, 2009, **48**, 8832); (*j*) H. Nishiyama and J. Ito, *Chem. Commun.*, 2010, **46**, 203; (*k*) J. Choi, A. H. R. MacArthur, M. Brookhart and A. S. Goldman, *Chem. Rev.*, 2011, **111**, 1761; (*l*) N. Selander and K. J. Szab, *Chem. Rev.*, 2011, **111**, 2048; (*m*) J. L. Niu, X. Q. Hao, J. F. Gong and M. P. Song, *Dalton Trans.*, 2011, **40**, 5135; (*n*) H. Zhang and A. Lei, *Dalton Trans.*, 2011, **40**, 8745; (*o*) J. I. van der Vlugt, *Eur. J. Inorg. Chem.*, 2012, 363.
10 (*a*) J. A. G. Williams, *Chem. Soc. Rev.*, 2009, **38**, 1783; (*b*) Y. Chi and P. T. Chou, *Chem. Soc. Rev.*, 2010, **39**, 638.
11 C. F. Macrae, P. R. Edgington, P. McCabe, E. Pidcock, G. P. Shields, R. Taylor, M. Towler and J. van de Streek, *J. Appl. Crystallogr.*, 2006, **39**, 453.
12 Z. E. Housecroft and A. G. Sharp, *Inorganic Chemistry*, Essex, England, 2005, ch. 6, p. 188.
13 Ž. D. Bugarčić, J. Bogojeski, B. Petrović, S. Hochreuther and R. van Eldik, *Dalton Trans.*, 2012, **41**, 12329.
14 *Cisplatin, Chemistry and Biochemistry of Leading Antitumor Drugs*, ed. B. Lippert, Wiley-VCH, Zürich, 1999.
15 C. Polonyi and S. K. C. Elmroth, *Dalton Trans.*, 2013, **42**, 14959.
16 C. Polonyi, A. Alshiekh, L. A. Sarsam, M. Clausén and S. K. C. Elmroth, *Dalton Trans.*, 2014, **43**, 11941.
17 (*a*) E. C. Long and J. K. Barton, *Acc. Chem. Res.*, 1990, **23**, 271; (*b*) R. F. Pasternack, E. J. Gibbs and J. Villafranca, *J. Biochem.*, 1983, **22**, 251.
18 (*a*) E. S. Koumousi, M. Zampakou, C. P. Raptopoulou, V. Psycharis, C. M. Beavers, S. J. Teat, G. Psomas and T. C. Stamatatos, *Inorg. Chem.*, 2012, **51**, 7699; (*b*) M. A. Rizvi, M. Zaki, M. Afzal, M. Mane, M. Kumar, B. A. Shah, S. Srivastav, S. Srikrishna, G. M. Peerzada and S. Tabassum, *Eur. J. Med. Chem.*, 2015, **90**, 876.
19 R. F. Pasternack, E. J. Gibbs and J. Villafranca, *Biochemistry*, 1983, **22**, 2406.
20 (*a*) F. J. Meyer-Almes and D. Porschke, *Biochemistry*, 1993, **32**, 4246; (*b*) Z. C. Liu, B. D. Wang, Z. Y. Yang, Y. Li, D. D. Qin and T. R. Li, *Eur. J. Med. Chem.*, 2009, **44**, 4477; (*c*) G. M. Howe, K. C. Wu and W. R. Bauer, *Biochemistry*, 1976, **19**, 339.
21 E. Ramachandran, S. P. Thomas, P. Poornima, P. Kalaivani, R. Prabhakaran, V. V. Padma and K. Natarajan, *Eur. J. Med. Chem.*, 2012, **50**, 405.
22 R. P. Paitandi, R. K. Gupta, R. S. Singh, G. Sharma, B. Koch and D. S. Pandey, *Eur. J. Med. Chem.*, 2014, **84**, 17.
23 J. N. Miller, *Proc. Anal. Div. Chem. Soc.*, 1979, **16**, 203.
24 D. D. Moore, *Curr. Protoc. Mol. Biol.*, 2001, **35**, A.2.1.
25 (*a*) R. W. Saalfrank, A. Scheurer, R. Puchta, F. Hampel, H. Maid and F. W. Heinemann, *Angew. Chem., Int. Ed.*, 2007, **46**, 265; (*b*) S. Begel, A. Scheurer and R. Puchta, *J. Coord. Chem.*, 2015, **68**, 3374; (*c*) J. Korzekwa, A. Scheurer, F. W. Heinemann and K. Meyer, unpublished results.
26 K. A. Meadows, F. Liu, J. Sou, B. P. Hudson and D. R. McMillin, *Inorg. Chem.*, 1993, **32**, 2919.
27 Oxford Diffraction, *CrysAlis CCD and CrysAlis Red*, Oxford Diffraction, Abingdon, 2009.
28 *SCALE3 ABSPACK CrysAlisPro, Agilent Technologies, Version 1.171.35.19*.
29 G. M. Sheldrick, *Acta Crystallogr., Sect. A: Fundam. Crystallogr*, 2015, **71**, 3.
30 L. J. Farrugia, *J. Appl. Crystallogr.*, 1997, **30**, 565.
31 L. J. Farrugia, *J. Appl. Crystallogr.*, 1999, **32**, 837.

Supplementary Material

Synthesis and Structures of Pincer-Type Rhodium(III) complex; Reactivity Toward Biomolecules

Milan M. Milutinović,[a] Jovana V. Bogojeski,[a*] Olivera Klisurić,[b] Andreas Scheurer,[c] Sofi K.C. Elmroth,[d] Živadin D. Bugarčić[a*]

[a]*University of Kragujevac, Faculty of Science, Radoje Domanovića 12, 34000 Kragujevac, Serbia*

[b]*University of Novi Sad, Faculty of Science, Department of Physics, Trg Dositeja Obradovića 3, 21000 Novi Sad, Serbia*

[c]*University of Erlangen-Nürnberg, Department Chemie und Pharmazie, Lehrstuhl für Anorganische und Allgemeine Chemie, Egerlandstr. 1, 91058 Erlangen, Germany*

[d]*Lund University, Biochemistry and Structural Biology, KILU, POBox 124, SE-221 00 Lund, Sweden*

[*] **Corresponding authors:** Prof. Dr. Živadin D. Bugarčić
Faculty of Science, University of Kragujevac
Radoje Domanovića 12, 34000 Kragujevac, Serbia
Tel: +381(0)34300262
Fax: +381(0)34335040
e-mail: bugarcic@kg.ac.rs

Dr. Jovana Bogojeski
Faculty of Science, University of Kragujevac
Radoje Domanovića 12, 34000 Kragujevac, Serbia
Tel: +381(0)34300262
Fax: +381(0)34335040
e-mail: jrosic@kg.ac.rs

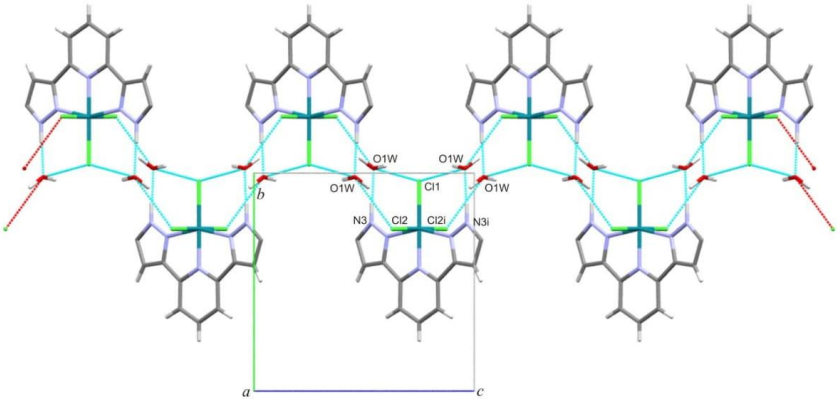

Figure S1. MERCURY[11] drawing showing the crystal packing of [Rh($LH_2{}^{t}Bu$)Cl_3] complex along the *a* axis. Hydrogen bonds are shown as light blue dashed lines.

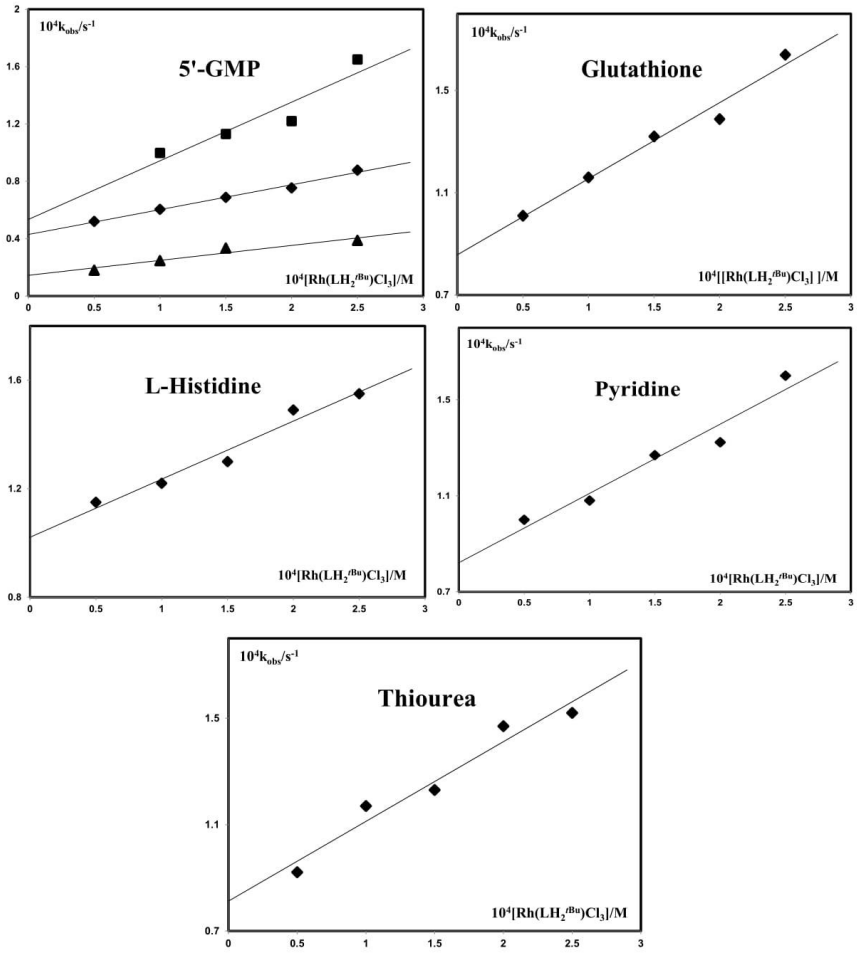

Figure S2. *Pseudo*-first order rate constants, k_{obsd}, as a function of complex concentration and temperature for the substitution reactions between complex (**1**) and 5′-GMP (310, 298 and 288 K), GSH, Py and L-His at pH = 7.2 (25 mM Hepes buffer) in the presence of 50 mM NaCl at 310, 298 and 288 K.

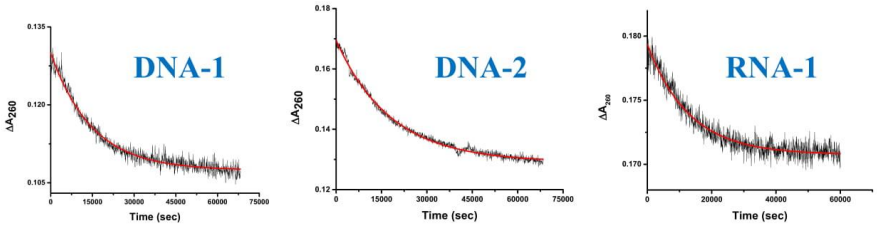

Figure S3. Absorbance change as a function of time after the addition of Rh^{III} complex to DNA-1, DNA-2 and RNA-1. All measurements were conducted with (**1**) = 50.0 μM, C_T = 3.0 μM and T = 37 °C in PBS buffered solution; Phosphate buffer solution = 0.01 M, C_{NaCl} = 0.137, C_{KCl} = 0.0027 M, pH 7.4). Fits of a single-exponential function to the experimental data are indicated with a solid line (red).

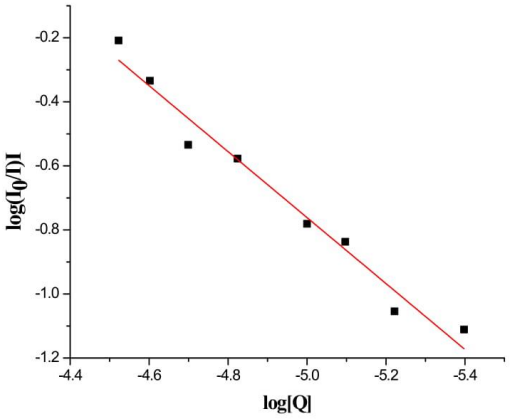

Figure S4. The linear plot shows log[(Io/I)/I] vs. log[Q] for the interaction between (**1**) complex and CT-DNA; Q = (**1**)

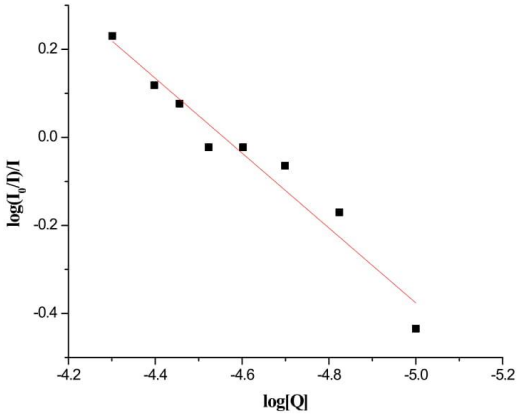

Figure S5. The linear plot shows log[(Io/I)/I] vs. log[Q] for the interaction between (**1**) complex and BSA; Q = (**1**).

Table S1. Hydrogen bond parameters for $[Rh^{III}(H_2L^{tBu})Cl_3]$ complex (Å, °)

D–H…A	***D–H***	***H…A***	***D…A***	***D–H…A***
O1W-H1W…Cl1[1]	0.89(4)	2.35(4)	3.153(4)	151(4)
O1W-H2W…Cl2[2]	0.88(4)	2.43(4)	3.215(3)	149(4)
N3-H3…O1W[3]	0.95(3)	1.76(3)	2.712(4)	177(3)

Symmetry codes: **1**: -x,1-y,-z; **2**: -x,y,1/2-z; **3**: x,1-y,-1/2+z

Table S2. Observed *pseudo*-first order rate constants as a function of complex concentration and temperature for the reaction between complex (**1**) and L-Met at pH = 7.2 (25 mM Hepes buffer) in the presence of 50 mM NaCl at 310, 298 and 288 K.

T(K)	$10^4 C_{(1)}$/M	$10^4 k_{obsd}$/s^{-1}
288.0	2.5	0.54(3)[a]
	2.0	0.51(3)
	1.5	0.40(3)
	1.0	0.32(3)
	0.5	0.22(3)
298.0	2.5	0.82(2)
	2.0	0.70(3)
	1.5	0.60(3)
	1.0	0.51(3)
	0.5	0.48(3)
310.0	2.5	1.10(4)
	2.0	0.98(3)
	1.5	0.84(3)
	1.0	0.73(3)
	0.5	0.64(4)

[a]Number of runs in parenthesis

Table S3. Observed *pseudo*-first order rate constants as a function of complex concentration and temperature for the reaction between complex (**1**) and 5'-GMP at pH = 7.2 (25 mM Hepes buffer) in the presence of 50 mM NaCl at 310, 298 and 288 K.

T(K)	$10^4C_{(1)}$/M	$10^4k_{obsd}/s^{-1}$
288.0	2.5	0.39(3)
	2.0	/
	1.5	0.33(3)
	1.0	0.25(3)
	0.5	0.18(3)
298.0	2.5	0.88(2)
	2.0	0.75(3)
	1.5	0.69(3)
	1.0	0.60(3)
	0.5	0.52(3)
310.0	2.5	1.65(4)
	2.0	1.22(3)
	1.5	1.13(3)
	1.0	1.00(3)
	0.5	/

Table S4. Observed *pseudo*-first order rate constants as a function of complex concentration and temperature for the reaction between complex (**1**) and GSH at pH = 7.2 (25 mM Hepes buffer) in the presence of 50 mM NaCl at 310, 298 and 288 K.

T(K)	$10^4C_{(1)}$/M	10^4k_{obsd}/s^{-1}
310.0	2.5	1.64(3)
	2.0	1.39(3)
	1.5	1.32(3)
	1.0	1.16(3)
	0.5	1.01(3)

Table S5. Observed *pseudo*-first order rate constants as a function of complex concentration and temperature for the reaction between complex (**1**) and L-His at pH = 7.2 (25 mM Hepes buffer) in the presence of 50 mM NaCl at 310, 298 and 288 K.

T(K)	$10^4C_{(1)}$/M	10^4k_{obsd}/s^{-1}
310.0	2.5	1.55(3)

	2.0	1.49(3)
	1.5	1.30(3)
	1.0	1.22(3)
	0.5	1.15(3)

Table S6. Observed *pseudo*-first order rate constants as a function of complex concentration for the reaction between (**1**) and DNA-1 in PBS buffer.

T(K)	10^5 $C_{(1)}$/M	10^5 k_{obsd}/s^{-1}
310.0	0.5	1.88(3)[a]
	1.5	3.24(3)
	3.0	5.81(3)
	5.0	6.73(3)

[a]Number of runs in parenthesis

Table S7. Observed *pseudo*-first order rate constants as a function of complex concentration for the reaction between (**1**) and DNA-2 in PBS buffer.

T(K)	10^5 $C_{(1)}$/M	10^5 k_{obsd}/s^{-1}
310	0.5	2.36(3)
	1.5	4.32(3)

	3.0	5.42(3)
	5.0	6.55(3)

Table S8. Observed *pseudo*-first order rate constants as a function of complex concentration for the reaction between (**1**) and DNA-3 in PBS buffer.

T(K)	10^5 $C_{(1)}$/M	10^5 k_{obsd}/s^{-1}
310	0.5	1.83(3)
	1.5	2.77(3)
	3.0	3.05(3)
	5.0	3.92(3)

Table S9. Observed *pseudo*-first order rate constants as a function of complex concentration for the reaction between (**1**) and RNA-1 in PBS buffer.

T(K)	10^5 $C_{(1)}$/M	10^5 k_{obsd}/s^{-1}
310	0.5	2.21(3)
	1.5	3.87(3)
	3.0	7.72(3)
	5.0	9.52(3)

3.2. Synthesis of Camphor-Derived Bis(pyrazolylpyridine) Rhodium(III) Complexes: Structure−Reactivity Relationships and Biological Activity

Within the paper two novel rhodium(III) complexes were synthesized with camphor-derivatives. Single crystal X-ray measurements were performed. The reactivity of the synthesized rhodium(III) complexes was studied with small biomolecules such as L-methionine, guanosine-5'-monophosphate and glutathione. DNA/BSA interactions with rhodium(III) complexes were monitored by UV-Vis spectroscopy. Also DFT and molecular docking studies were performed, as well as the cytotoxic studies on human epithelial colorectal carcinoma HCT-116 cell line.

Participations in the publication:

A. Petrović, **M. M. Milutinović,** J. V. Bogojeski – Synthesis, characterization, UV-Vis spectroscopy, NMR measurements, kinetic investigation of small biomolecule and DNA/BSA studies by UV-Vis spectroscopy, implementation of all results and writing a paper;

M. Živanović, N. Milivojević – cytotoxic studies;

R. Puchta – DFT calculations;

A. Scheurer, J. Korzekwa – Synthesis of ligands;

O. Klisurić – X-ray measurements.

DOI: https://pubs.acs.org/doi/10.1021/acs.inorgchem.8b02390

Inorganic Chemistry
Cite This: Inorg. Chem. 2019, 58, 307−319
Article
pubs.acs.org/IC

Synthesis of Camphor-Derived Bis(pyrazolylpyridine) Rhodium(III) Complexes: Structure−Reactivity Relationships and Biological Activity

Angelina Petrović,[†] Milan M. Milutinović,[†,▽] Edward T. Petri,[#] Marko Živanović,[†] Nevena Milivojević,[†] Ralph Puchta,[‡,§,∥] Andreas Scheurer,[‡] Jana Korzekwa,[‡] Olivera R. Klisurić,[⊥] and Jovana Bogojeski*[,†]

[†]Faculty of Science, University of Kragujevac, Radoja Domanovića 12, 34000 Kragujevac, Serbia

[‡]Inorganic Chemistry, Department of Chemistry and Pharmacy, [§]Computer Chemistry Center, Department of Chemistry and Pharmacy, and [∥]Zentralinstitut für Scientific Computing, University of Erlangen-Nürnberg, 91058 Erlangen, Germany

[⊥]Faculty of Science, Department of Physics and [#]Faculty of Science, Department of Biology and Ecology, University of Novi Sad, Trg Dositeja Obradovića 4, 21000 Novi Sad, Serbia

[▽]Department of Organic Chemistry, University of Paderborn, Warburgerstraße 100, 33098 Paderborn, Germany

Supporting Information

ABSTRACT: Two novel rhodium(III) complexes, namely, $[Rh^{III}(X)Cl_3]$ (X = 2 2,6-bis((4*S*,7*R*)-7,8,8-trimethyl-4,5,6,7-tetrahydro-1*H*-4,7-methanoindazol-3-yl)pyridine or 2,6-bis((4*S*,7*R*)-1,7,8,8-tetramethyl-4,5,6,7-tetrahydro-1*H*-4,7-methanoindazol-3-yl)pyridine), were synthesized from camphor derivatives of a bis(pyrazolylpyridine), tridentate nitrogen-donor chelate system, giving $[Rh^{III}(H_2L^*)Cl_3]$ (**1a**) and $[Rh^{III}(Me_2L^*)Cl_3]$ (**1b**). A rhodium(III) terpyridine (terpy) ligand complex, $[Rh^{III}(terpy)Cl_3]$ (**1c**), was also synthesized. By single-crystal X-ray analysis, **1b** crystallizes in an orthorhombic $P2_12_12_1$ system, with two molecules in the asymmetric unit. Tridentate coordination by the N,N,N-donor localizes the central nitrogen atom close to the rhodium(III) center. Compounds **1a** and **1b** were reactive toward L-methionine (L-Met), guanosine-5′-monophosphate (5′-GMP), and glutathione (GSH), with an order of reactivity of 5′-GMP > GSH > L-Met. The order of reactivity of the Rh^{III} complexes was: **1b**> **1a** > **1c**. The Rh^{III} complexes showed affinity for calf thymus DNA and bovine serum albumin by UV−vis and emission spectral studies. Furthermore, **1b** showed significant in vitro cytotoxicity against human epithelial colorectal carcinoma cells. Since the Rh^{III} complexes have similar coordination modes, stability differences were evaluated by density functional theory (DFT) calculations (B3LYP(CPCM)/LANL2DZp). With (H_2L^*) and (terpy) as model ligands, DFT calculations suggest that both tridentate ligand systems have similar stability. In addition, molecular docking suggests that all test compounds have affinity for the minor groove of DNA, while **1b** and **1c** have potential for DNA intercalation.

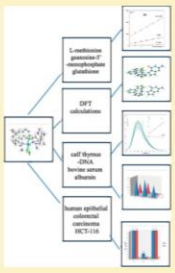

INTRODUCTION

Transition-metal complexes have a range of applications in supramolecular chemistry,[1] catalytic chemistry,[2] and as medicinal agents.[3] In chemical biology, transition-metal complexes were investigated as inhibitors,[4−9] imaging agents,[10−12] biological probes,[13,14] or catalysts with unique properties. Over the last century, platinum-based complexes have been used as anticancer drugs.[15,16] However, side effects, such as cell-acquired resistance and high toxicity,[17] have prompted investigation of other metal complexes.[18,19] Despite their variable oxidation states, the anticancer properties of rhodium complexes have not been extensively explored.[20,21] However, kinetically inert transition-metal complexes could serve as scaffolds for pharmacological agents due to their inertness, stability, unique geometries, and structural diversity.[22] Recently, such metal complexes were shown to have affinity both for DNA, their primary target, as well as various proteins,[23−27] suggesting potential use in the design of anticancer agents.

Transition-metal complexes have been synthesized with pyridine-containing tridentate triamine ligands, for use in catalytic reactions or as potential antitumor agents, etc. Tridentate triamine ligands have advantages, including ready availability, relatively low cost, and low toxicity.[28] Various metal complexes with camphor-based pyridine ligands have also been used for asymmetric catalytsis[29] and tested for biomolecular interactions or antitumor activity.[30−33]

Previously, we synthesized a Rh^{III} complex with a tridentate nitrogen-donor pincer-type ligand that displayed promising properties and biomolecular reactivity.[20] Thus, we sought to expand our investigation of Rh^{III} complexes to pincer-type ligands with diverse substituent patterns on the pyrazolyl moiety, creating differences in space configuration and electron density distribution that could influence biomolecular interaction potential or cytotoxicity.

Received: August 24, 2018
Published: December 19, 2018

DOI: 10.1021/acs.inorgchem.8b02390
Inorg. Chem. 2019, 58, 307−319

Therefore, in the present study we designed two new Rh^{III} complexes ($[Rh^{III}(H_2L^*)Cl_3]$ and $[Rh^{III}(Me_2L^*)Cl_3]$), where H_2L^* and Me_2L^* are camphor derivatives of a previously introduced bis(pyrazolylpyridine) ligand (Figure 1). For

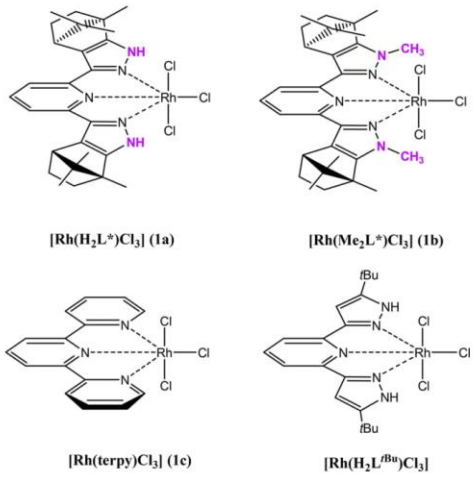

Figure 1. Structures of the investigated Rh^{III} complexes.

comparison, a Rh^{III} terpyridine (terpy) complex was also synthesized and examined. Substitution reactions with biomolecules were studied, and biomolecular interaction potential with calf thymus DNA (CT-DNA) and bovine serum albumin (BSA) were measured. New compounds were tested for in vitro cytotoxicity using a 3-(4,5-dimethylthiazol-2-yl)-2,5-diphenyltetrazolium bromide (MTT) assay and human epithelial colorectal carcinoma cells (HCT-116). density functional theory (DFT) calculations were conducted to explore the similarity between our basic bis(pyrazolylpyridine) ligand system and the well-known terpyridine complex analogue.

EXPERIMENTAL SECTION

Chemicals and Solutions. Commercial chemicals were used without purification. L-Methionine (L-Met), glutathione (GSH), guanosine-5′-monophosphate sodium salt (5′-GMP), 2,2′:6′,2″-terpyridine (terpy), $RhCl_3{\cdot}xH_2O$, *N*-2-hydroxyethylpiperazine-*N*′-2-ethanesulfonic acid (HEPES), phosphate-buffered saline (PBS), CT-DNA, ethidium bromide (EB), and BSA were from Sigma-Aldrich. CT-DNA was dissolved in triple-distilled deionized water and stored at 4 °C for less than one week. The UV absorbance ratio (260_{nm}/280_{nm}) of CT-DNA solutions in PBS (phosphate = 0.01 M, c(NaCl) = 0.137, c(KCl) = 0.0027 M, pH 7.4) was 1.8−1.9, indicating a lack of protein contamination.[34] Nucleophile stock solutions were freshy prepared before use. Dulbecco's Modified Eagle Medium (DMEM) and PBS were obtained from GIBCO, Invitrogen. Fetal bovine serum (FBS) and trypsin−ethylenediaminetetraacetic acid (EDTA) were from PAA (The Cell Culture Company). Dimethyl sulfoxide (DMSO) and MTT were from SERVA. Doubly distilled deionized water was used for all experiments. Preparations of H_2L^* and Me_2L^* ligands were according to published procedures.[35] $[Rh(terpy)Cl_3]$ (**1c**) was prepared as published and characterized by standard analytical methods.[36]

Synthesis and Characterization of $[Rh^{III}(H_2L^*)Cl_3]$ (1a) and $[Rh^{III}(Me_2L^*)Cl_3]$ (1b). In general, a solution of H_2L^* or Me_2L^* (0.380 mmol; 1 equiv) in 20 mL of ethanol was slowly added to a solution of 100 mg (0.380 mmol) of $RhCl_3{\cdot}xH_2O$ in 60 mL of ethanol. The mixture was stirred and refluxed overnight, affording a yellow precipitate that was filtered and dried under vacuum. The resulting yellow solid was purified by recrystallization. Crystallization of **1b** was induced by slow diffusion of *n*-hexane into a dichloromethane solution of the **1b** complex.

Synthesis of $[Rh^{III}(H_2L^*)Cl_3]$ (1a). H_2L^* (162.5 mg) yielded **1a** as a yellow solid (196 mg; 0.31 mmol; 81%).

^{1}H NMR (500 MHz, CD_3CN): δ = 8.1 (t, J_{HH} = 7.8 Hz, para-Ar−CH, 1H), 7.82 (d, J_{HH} = 7.8 Hz, meta-Ar−CH, 2H), 6.94 (br s, NH, 2H), 3.35 (d, J_{HH} = 3.9 Hz, $HCCH_2CH_2$, 2H), 2.41−2.37 (m, $HCCH_2CH_2$, 2H), 2.10−2.04 (m, $HCCH_2CH_2$, 2H), 1.65−1.48 (m, $HCCH_2CH_2$ and $HCCH_2CH_2$, 4H), 1.38 (s, CCH_3, 6H), 1.08 (s, $C(CH_3)_2$, 6H), 0.89 (s, $C(CH_3)_2$,6H) ppm.

^{13}C NMR (126 MHz, CD_3CN): δ = 158.9 (ortho-Ar-C, 2C), 146.0 (HN−CCC, 2C), 139.2 (para-Ar−CH, 1C), 135.4 (HN−CCC, 2C), 127.0 (meta-Ar−CH, 2C), 121.0 (HN−CCC, 2C), 63.2 (CCH_3, 2C), 52.1 ($C(CH_3)_2$, 2C), 50.5 ($HCCH_2CH_2$, 2C), 36.3 ($HCCH_2CH_2$, 2C), 29.8 ($HCCH_2CH_2$, 2C), 25.0 ($C(CH_3)_2$, 2C), 21.6 ($C(CH_3)_2$, 2C), 11.2 (CCH_3, 2C) ppm.

Anal. Calcd for ($C_{27}H_{33}Cl_3N_5Rh$) C: 50.92; H: 5.22; N: 11.00. Found: C: 51.26; H: 5.93; N: 11.14%.

ESI-MS: $[M\text{-}Cl]^+$: Calcd: 599.64.09; Found: 599.18.

Synthesis of $[Rh^{III}(Me_2L^*)Cl_3]$ (1b). Me_2L^* (173.1 mg) yielded **1b** as a yellow solid (189.5 mg; 0.28 mmol, 75%).

^{1}H NMR (500 MHz, CD_3CN): δ = 8.14 (dd, J_{HH} = 8.5 Hz, meta-Ar−CH, 2H), 7.82 (t, J_{HH} = 8.5 Hz, para-Ar−CH, 1H), 4.38 (s, NCH_3, 6H), 3.33 (d, J_{HH} = 3.8 Hz, $HCCH_2CH_2$, 2H), 2.31−2.05 (m, $HCCH_2CH_2$, 2H), 2.05−1.91 (m, $HCCH_2CH_2$, 2H), 1.52−1.33 (m, $HCCH_2CH_2$ and $HCCH_2CH_2$, 4H), 1.41 (s, CCH_3, 6H), 1.08 (s, $C(CH_3)_2$, 6H), 0.78 (s, $C(CH_3)_2$, 6H) ppm.

^{13}C NMR (126 MHz, CD_3CN): δ = 159.9 (CH_3N−CCC, 2C), 151.9 (ortho-Ar-C, 2C), 143.8 (CH_3N−CCC, 2C), 140.1 (para-Ar−CH, 1C), 128.9 (CH_3N−CCC, 2C), 119.5 (meta-Ar−CH, 2C), 63.6 (CCH_3, 2C), 53.7 ($C(CH_3)_2$, 2C), 47.8 ($HCCH_2CH_2$, 2C), 38.5 (NCH_3, 2C), 32.6 ($HCCH_2CH_2$, 2C), 26.7 ($HCCH_2CH_2$, 2C), 19.6 ($C(CH_3)_2$, 2C), 18.3 ($C(CH_3)_2$, 2C), 10.0 (CCH_3, 2C) ppm.

Anal. Calcd for ($C_{29}H_{37}Cl_3N_5Rh$) C: 52.39; H: 5.61; N: 10.53. Found: C: 52.26; H: 5.53; N: 10.01%.

ESI-MS: $[M\text{-}Cl]^+$: Calcd: 628.12; Found: 628.14.

Instrumentation. NMR spectra were recorded on a 200 MHz Varian Gemini-2000 and 500 MHz Bruker Avance spectrometer. NMR signals were referenced to residual proton or carbon signals of the deuterated solvent (^{1}H and ^{13}C NMR) and are reported in parts per million relative to tetramethylsilane (TMS). Elemental analyses (C, H, N) were performed by combustion and gas chromatographic analysis with an Elementar Vario MICRO elemental analyzer. pH measurements were done using a Mettler Delta 350 digital pH meter with resolution of ±0.01 mV and a combination glass electrode calibrated using standard buffer solutions (Sigma) at pH 4, 7, and 9. UV−Vis and kinetic measurements were conducted on a PerkinElmer Lamda 25 and 35 double-beam spectrophotometer with thermostated 1.00 cm quartz Suprasil cells. Temperature was controlled to ±0.1 °C. Fluorescence was measured on an RF-1501 PC spectrofluorometer (Shimadzu). Mass spectrometry was measured on a Waters Quadrupole TOF Synapt 2G using electrospray ionization (ESI).

Solubility Measurements. The concentrations of saturated solutions of the studied Rh^{III} complexes were determined by UV−vis spectrometry. Therefore, the specific absorptivity of the compounds in the water was determined first. This was measured using five dilution series (5, 10, 30, 40, 50 mM) of the studied complexes, and then the calibration curve was calculated using Lambert−Beer law. The slope of the curve gave specific absorptivity. The required quantity of water solution was added to the 5 mL volumetric flask. The solution was heated to 298 K. A previously weighed quantity of Rh^{III} complex was added to the volumetric flask, until the saturation point occurred. Stirring was continued up to 7 h at

DOI: 10.1021/acs.inorgchem.8b02390
Inorg. Chem. 2019, 58, 307−319

298 K. The sample was filtered through 0.20 μm membrane filter. A measured quantity of filtered sample was transferred into another volumetric flask and made further dilutions. The absorbance was measured using UV−vis spectrophotometry. The same process was repeated two times.

Kinetic Measurements. The hydrolysis of complexes **1a**, **1b**, and **1c** was studied by UV−vis spectrometry at 298 K. The samples (0.10 mM) were prepared in a buffer solution (25 mM HEPES buffer, pH = 7.2) or PBS. The working wavelength of each reaction corresponded to that of a maximum change in absorption derived from the difference spectra. The absorbance at the selected wavelength was recorded at 30 s intervals, and the absorption/time data for each complex were fitted to the first-order rate equation, which gave the k_{H2O} value for each aquation process.

The kinetics of the substitution of coordinated chloride was measured spectrophotometrically by following the change in absorbance at suitable wavelengths as a function of time. Working wavelengths were determined by recording spectra of the reaction mixture from 220 to 450 nm. Kinetic measurements were performed under pseudo-first-order conditions, with nucleophile concentrations at least 10-fold in excess. Reactions were initiated by mixing 0.50 mL of a nucleophile complex solution with 2.50 mL of thermally equilibrated complex solution in a UV−vis cuvette, and reactions were followed for at least eight half-lives. The observed pseudo-first-order rate constant k_{obs} represents an average value of three to four independent kinetic runs for each experimental condition. Some reactions were studied at three temperatures (288, 298, and 310 K). Experimental data are summarized in the Supporting Information (Tables S1−S9). Values for constants and other thermodynamic parameters were determined using Microsoft Excel 2007 and OriginPro 8.

UV−Vis DNA Interactions. CT-DNA stock solutions were prepared in PBS, resulting in a UV absorbance ratio A_{260}/A_{280} of ca. 1.8−1.9, indicating negligible protein contamination. CT-DNA concentrations were determined using A_{260} with ε = 6600 M^{-1} cm^{-1}.[37]

Fluorescence spectra were recorded in the range of 550−750 nm with excitation at 527 nm. Excitation and emission bandwidths were both 10 nm.

UV−Vis Absorption Studies. To quantitatively compare the binding strength of the complexes, the intrinsic binding constant K_b was determined by monitoring changes in absorption at the metal-to-ligand charge transfer (MLCT) band with increasing concentration of CT-DNA using the following eq 1.

$$[DNA]/(\varepsilon_A - \varepsilon_f) = [DNA]/(\varepsilon_b - \varepsilon_f) + 1/[K_b(\varepsilon_b - \varepsilon_f)] \quad (1)$$

K_b is given by the ratio of the slope to the y intercept in plots of $[DNA]/(\varepsilon_A - \varepsilon_f)$ versus [DNA], where [DNA] is the concentration of DNA in base pairs, $\varepsilon_A = A_{obsd}/[complex]$, ε_f is the extinction coefficient for the unbound complex, and ε_b is the extinction coefficient for the complex in the fully bound form.

Ethidium Bromide Displacement Studies. The relative binding of complexes to CT-DNA was determined by calculating the quenching constant (K_{sv}) from the slopes of straight lines obtained from the Stern−Volmer equation (eq 2)

$$I_0/I = 1 + K_{sv}[Q] \quad (2)$$

where I_0 and I are emission intensities in the absence and presence of quencher (complexes **1a**, **1b**, and **1c**), respectively, [Q] is the total concentration of quencher, and K_{sv} is the Stern−Volmer quenching constant, which was obtained from the slope of the plot of I_0/I versus [Q].

Viscosity Measurements. Changes in DNA viscosity were measured in the presence of increasing amounts of complexes **1a**, **1b**, and **1c**. Flow time was measured with a digital stopwatch. Each sample was measured in triplicate, and the average flow time was calculated. Data are presented as $(\eta/\eta_0)^{1/3}$ against r, where η is the DNA viscosity in the presence of complex, and η_0 is the viscosity of DNA in buffer alone. Viscosity values were calculated from the observed flow time of DNA-containing solutions (t) corrected for the flow time of buffer alone (t_0), $\eta = (t - t_0)/t_0$.

Protein Binding Studies. Protein fluorescence is due to natural fluorophores such as tryptophan, tyrosine, and phenylalanine. Changes in BSA fluorescence were used to monitor interaction with metal complexes. Tryptophan fluorescence quenching experiments were conducted using 2.0 μM BSA in PBS. Quenching of the emission intensity of BSA tryptophan residues at 363 nm in the presence of increasing concentrations of Rh^{III} complexes **1a**, **1b**, and **1c** (0−10.0 μM) was monitored. Fluorescence spectra were recorded in the range of 300−500 nm with excitation at 295 nm. Excitation and emission bandwidths were both 10 nm.

Cell Preparation and Culturing. HCT-116 cells were purchased from the American Tissue Culture Collection. Cells were maintained in controlled physiological conditions and grown in DMEM supplemented with 10% fetal bovine serum, 100 IU/mL penicillin, and 100 μg/mL streptomycin in a humidified atmosphere with 5% CO_2 at 37 °C.

Viability Effects. A standardized MTT colored reaction (Mosmann, 1983)[38] was measured on an ELISA microplate reader (Rayto-2100C) as described in our previous work.[39−41]

X-ray Diffraction Studies. X-ray diffraction data for $[Rh^{III}(Me_2L^*)Cl_3]$ (**1b**) were collected at room temperature on an Oxford Diffraction Gemini S diffractometer. Graphite-monochromated Mo Kα radiation (λ = 0.7107 Å) was used to measure diffraction from suitable single crystals of complex **1b**. CrysAlisPro and CrysAlis RED software packages[42] were used for data collection and data integration. Space group determinations were based on analysis of the Laue class and systematically absent reflections. Collected data were corrected for absorption effects using the Multiscan method, applying an empirical absorption correction using spherical harmonics as implemented in SCALE3 ABSPACK.[42] Structure solution and refinement were performed with the programs SHELXT and SHELXL-2014/6, respectively.[43] MERCURY[44] was employed for molecular graphics, and WinGX[45] software was used to prepare material for publication. Non-hydrogen atoms were refined anisotropically; C−H hydrogen atoms were included at calculated positions riding on their attached atoms with fixed distances of CH = 0.93 Å and CH_2 = 0.96 Å with $U_{iso}(H)$ = 1.2 $U_{eq}(C)$ for methylene and methyne groups, and CH_3 = 0.97 Å with $U_{iso}(H)$ = 1.5 $U_{eq}(C)$ for methyl groups. $[Rh^{III}(Me_2L^*)Cl_3]$ complex had contributions from disordered solvent molecules that were removed by the SQUEEZE routine implemented in PLATON,[46] and the output from SQUEEZE calculations is attached in the CIF file. Crystal data and refinement parameters are summarized in Table 1.

Quantum Chemical Methods. To enable comparison with earlier studies,[47] we performed B3LYP/LANL2DZp hybrid DFT calculations, with pseudopotentials on the heavy elements and the valence basis set augmented with polarization functions.[48,49] During structure optimization, only symmetry constraints were applied. In addition, resulting structures were characterized as minima, by computation of vibrational frequencies. Relative energies were corrected for zero-point vibrational energies (ZPE). The influence of bulk solvent water was evaluated via single-point calculations using CPCM formalism,[50] that is, B3LYP(CPCM)/LANL2DZp//B3LYP/LANL2DZp. The Gaussian suite of programs was used.[51]

Molecular Docking Simulations. Structural coordinates representing a fragment of (1) canonical B-DNA (PDB: 1BNA) or (2) DNA with an intercalation gap (PDB: 1Z3F) were obtained from the protein data bank (http://www.rcsb.org). Water molecules, ligands, and heteroatoms were removed if present. Hydrogen atoms and Gasteiger partial charges were added; nonpolar hydrogen atoms were merged in AutoDockTools[52] (http://autodock.scripps.edu), and coordinates were converted to PDBQT format. For ligands (**1a**, **1b**, **1c**, or $[Rh^{III}(H_2L^{tBu})Cl_3]$), nonpolar hydrogen atoms were merged, and Gasteiger partial charges were added in AutoDockTools.[52] Natual population analysis (NPA) partial charges for Rh and Cl atoms were calculated in Gaussian16 with B3LYP/LANL2DZp and merged into final ligand PDBQT files. Grid maps were calculated in AutoGrid4 using coordinates for 1BNA or 1Z3F. Grid maps were centered, and a

DOI: 10.1021/acs.inorgchem.8b02390
Inorg. Chem. 2019, 58, 307−319

Table 1. Experimental Details: Crystalographic Data and Refinement Parameters for $[Rh^{III}(Me_2L^*)Cl_3]$ Complex 1b

crystal data	
chemical formula	$C_{29}H_{37}Cl_3N_5Rh$
M_r	664.89
crystal system, space group	orthorhombic, $P2_12_12_1$
a, b, c (Å)	13.4941 (3), 19.4283 (4), 28.9799 (13)
V (Å^3)	7597.6 (4)
Z	8
radiation type	Mo $K\alpha$
No. of reflections for cell measurement	9233
θ range (deg) for cell measurement	2.8−28.4
μ (mm^{-1})	0.68
crystal shape	prism
crystal size (mm)	0.51 × 0.42 × 0.14
data collection	
diffractometer	Xcalibur, Sapphire3, Gemini
absorption correction	multiscan
Tmin, Tmax	0.882, 1.000
No. of measured, independent and observed [$I > 2\sigma(I)$] reflections	27 626, 13 398, 10 655
R_{int}	0.052
θ values (deg)	θ_{max} = 25.0, θ_{min} = 2.5
$(\sin\theta/\lambda)_{max}$ (Å^{-1})	0.595
range of h, k, l	h = −16→11, k = −23→15, l = −34→29
refinement	
$R[F^2 > 2\sigma(F^2)]$, $wR(F^2)$, S	0.084, 0.228, 1.04
No. of reflections	13 398
No. of parameters	701
No. of restraints	13
H-atom treatment	H-atom parameters constrained
ρ_{max}, ρ_{min} (e Å^{-3})	0.96, −2.41
absolute structure parameter	0.05 (3)

maximum grid box size was chosen to cover the entire DNA molecule. For 1BNA a grid box of 54 × 56 × 106 was centered at x,y,z = 14.72, 20.99, 8.82. For 1ZF3 a grid box of 62 × 50 × 68 was centered at x,y,z = 2.27, 15.76, 37.63. Default grid spacing of 0.375 Å was used. Maps were calculated for all ligand atom types along with electrostatic and desolvation maps using a dielectric value of −0.1465. Initial ligand position, orientation, and dihedral offset were set as random. The number of torsional degrees of freedom for each ligand was fixed to 0 to ensure rigid docking. Docking simulations were conducted in AutoDock4 using the Larmarckian genetic algorithm and default parameters: the maximum number of energy evaluations was 2 500 000, the genetic algorithm (GA) population size was 150, and a total of 10 hybrid genetic algorithm with a local dearch (GA-LS) runs were performed. Parameters for Rh atoms were added to AutoDock as follows: R-eqm = 2.93 Å, weighted epsilon = 0.008, At.frag.vol. = 12.000, At.solv.par. = −0.001, Hb R-eqm = 0.000, weighted Hb epsilon = 0.000, Hb type = 0, bond index = 1. Results were analyzed in AutoDockTools (http://autodock.scripps.edu).[52]

RESULTS AND DISCUSSION

Preparation and Structure of $[Rh^{III}(H_2L^*)Cl_3]$ (1a) and $[Rh^{III}(Me_2L^*)Cl_3]$ (1b). Complexes $[Rh^{III}(H_2L^*)Cl_3]$ (**1a**) and $[Rh^{III}(Me_2L^*)Cl_3]$ (**1b**) (Figure 1) were synthesized by stirring equimolar amounts of $RhCl_3{\cdot}xH_2O$ and H_2L^* or Me_2L^* ligands in ethanol and by refluxing overnight. The synthesized Rh^{III} complexes **1a** and **1b** were characterized by ^1H and ^{13}C NMR spectroscopy, elemental analysis, and ESI mass spectrometry (MS). For the complex **1b** single crystals suitable for the X-ray analysis were also obtained.

Elemental analyses on these complexes were in very good agreement with a complex composition of $[Rh^{III}(H_2L^*)Cl_3]$ or $[Rh^{III}(Me_2L^*)Cl_3]$. The ^1H NMR as well as the ^{13}C NMR spectra of the **1a** and **1b** complexes indicated that only this distinct species is formed. The obtained spectra display a set of signals for the pyrazole moieties, pyridine moiety, and a camphor moiety, significantly shifted, compared to the free ligand. Further, the complexes are characterized by ESI-MS mass spectrometry, in the m/z range of 400−700 that includes main peaks at m/z = 599.18 (1+) and 628.14 (1+), which represents fragments of the **1a** and **1b** complexes, which came about by losing one chloride.

Crystal Structure Discussion. A perspective view of the molecular structure of **1b** with adopted atom-numbering scheme is shown in Figure 2. Selected metal−ligand bond

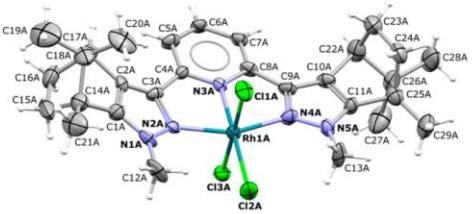

Figure 2. MERCURY[44] drawing of the molecular structure of complex **1b** with labeled non-H atoms (only molecule A is shown for clarity). Displacement ellipsoids are shown at 30% probability, and H atoms are drawn as spheres of arbitrary radii.

lengths, bond angles, and torsion angles are listed in Table 2. $[Rh^{III}(Me_2L^*)Cl_3]$ complex crystallizes in an orthorhombic crystal system and $P2_12_12_1$ space group, where each asymmetric unit consists of two **1b** complex molecules (molecule A and molecule B). From a structural point of view, the coordination of the Rh1A and Rh1B atoms in the **1b** complex is noteworthy. The rhodium centers in the $[Rh^{III}(Me_2L^*)Cl_3]$ complex are coordinated in a slightly distorted octahedral geometry.

Because of the tridentate coordination of the N,N,N-donor, the central nitrogen atom is pushed closer toward the rhodium(III) center, applying a *trans* influence on Cl2 that explains the slightly larger value of the Rh1—Cl2 bond length, which is the same in both A and B molecules (Table 2). Bond angles N3—Rh1—Cl1 (in both molecule A and B) are slightly larger that 90°, while N3—Rh1—Cl3 angles (in both molecule A and B) are smaller than 90°, showing the steric influence of the bulky Me_2L^* chelating ligand. The group Rh1Cl2N2N3N4 is almost perfectly planar, since the largest displacement from the same weighted least-squares plane in both A and B molecules is 0.111(9) Å for atom N3A. Comparing the angles between Rh1Cl2N2N3N4 plane and N1N2C3C2C1 and N4N5C11C10C9 planes in molecule A (21.0 (7)° and 10.7 (7)°, respectively) and the same planes in molecule B (5.2 (7)° and 17.4 (7)°, respectively), one can observe that the molecule A is more disordered from planarity. This leads to the conclusion that molecules A and B of **1b** complex have slightly different conformations, which is confirmed by comparison of the values for torsion angles (Table 2). Visually, this result is

DOI: 10.1021/acs.inorgchem.8b02390
Inorg. Chem. 2019, 58, 307−319

Table 2. Selected Geometric Parameters for $[Rh^{III}(Me_2L^*)Cl_3]$ Complex 1b

	molecule A	molecule B
bond length [deg]		
Rh1−N3	2.027 (9)	1.975 (9)
Rh1−N4	2.063 (14)	2.051 (14)
Rh1−N2	2.080 (12)	2.051 (12)
Rh1−Cl1	2.332 (4)	2.319 (5)
Rh1−Cl3	2.337 (4)	2.341 (4)
Rh1−Cl2	2.351 (3)	2.362 (3)
bond angles [deg]		
N3−Rh1−N4	78.7 (4)	78.4 (5)
N3−Rh1−N2	80.4 (4)	79.6 (4)
N4−Rh1−N2	158.3 (4)	157.8 (4)
N3−Rh1−Cl1	91.8 (3)	90.9 (3)
N4−Rh1−Cl1	89.1 (4)	85.4 (4)
N2−Rh1−Cl1	86.0 (3)	92.1 (4)
N3−Rh1−Cl3	87.0 (3)	86.7 (3)
N4−Rh1−Cl3	91.2 (4)	93.1 (4)
N2−Rh1−Cl3	93.2 (3)	88.5 (4)
Cl1−Rh1−Cl3	178.73 (15)	177.38 (17)
N3−Rh1−Cl2	176.3 (3)	176.5 (3)
N4−Rh1−Cl2	100.9 (3)	101.1 (4)
N2−Rh1−Cl2	100.3 (3)	101.1 (3)
Cl1−Rh1−Cl2	91.82 (17)	92.51 (19)
Cl3−Rh1−Cl2	89.33 (16)	89.87 (17)
torsion angles [deg]		
Rh1−N2−N1−C1	154.1 (11)	−178.1 (12)
Rh1−N2−N1−C12	−19 (2)	6 (2)
Rh1−N2−C3−C4	7.3 (15)	−3.8 (15)
Rh1−N3−C4−C5	−175.6 (10)	−175.0 (10)
Rh1−N3−C8−C7	173.5 (10)	172.1 (11)
Rh1−N3−C8−C9	−1.7 (16)	−6.1 (16)
Rh1−N4−C9−C10	179.5 (10)	166.9 (11)
Rh1−N4−C9−C8	11.6 (17)	−5.5 (16)

depicted in Figure 3, which displays an overlay of A and B molecules of **1b** complex.

Figure 3. MERCURY[44] drawing showing an overlay of two independent molecules in $[Rh^{III}(Me_2L^*)Cl_3]$ **1b** complex: A (yellow) and B (red). Hydrogen atoms were omitted for clarity.

The crystal packing of $[Rh^{III}(Me_2L^*)Cl_3]$ complex is dominantly arranged by van der Waals forces, since classic hydrogen bonds were not found in intra- or intermolecular space.

Solubility of the Studied Rh^{III} Complexes. The prepared Rh^{III} complexes are neutral; UV−vis spectrophotometric measurements showed that they have moderate solubility in water (Table S10). The solubility of the complexes is in line with oxaliplatin and a bit greater of cisplatin.

Kinetics of Aquation. The kinetics of aquation of complexes **1a**, **1b**, and **1c** were quantitatively studied by UV−vis spectroscopy of 0.1 mM solutions in HEPES buffer and PBS at 298 K. The UV−vis spectra of **1a** and **1b** complexes show no significant time-dependent changes in the region of 200−800 nm (Figure S2), which indicates that complexes **1a** and **1b** do not undergo hydrolysis in the observed time period in either 25 mM HEPES buffer or PBS. Complex **1c** hydrolyzes with a constant $k_{H2O} = 3.5 \times 10^{-5}$ s^{-1} ($t_{1/2}$ = 330 min) in PBS and $k_{H2O} = 1.1 \times 10^{-3}$ s^{-1} ($t_{1/2}$ = 9.68 min) in 25 mM HEPES buffer (Figures S3). The results obtained suggest that complex **1c** underwent slow hydrolysis in PBS and significantly hydrolyzed in HEPES buffer, but all kinetic measurements for this study were performed in HEPES buffer in the presence of 50 mM NaCl to prevent hydrolysis.

Kinetic Studies. To measure the reactivity of the Rh^{III} complex under physiological conditions, substitution reactions of Rh^{III} complex (**1a**, **1b**, and **1c**) (Figure 1) with selected nucleophiles L-Met, GSH, and 5′-GMP were investigated. The kinetics of the substitution of coordinated chloride were investigated by UV−vis spectroscopy, by following the change in absorbance as a function of time. Nucleophiles L-Met, GSH, and 5′-GMP were chosen because of their different nucleophilicity, steric hindrance, binding properties, and biological relevance. Since our overal goal is to investigate the anticancer potential of Rh^{III} complexes, kinetic experiments were designed to mimic physiological conditions: measurments were conducted at pH 7.2 (maintained with 25 mM HEPES buffer) in 50 mM NaCl (to suppress the solvolytic pathway) at 310 K. Kinetic experiments were performed under pseudo-first-order conditions, with nucleophile concentrations at least 10-fold in excess. Proposed reaction pathways for all observed substitution processes are shown in Scheme 1.

Scheme 1. Schematic Representation of Substitution Reactions of Complexes 1a, 1b, and 1c with Nucleophiles: L-Met, GSH, and 5′-GMP

$$[Rh(X)Cl_3] + L \underset{k_1}{\overset{k_2}{\rightleftharpoons}} [Rh(X)Cl_2L]^{z+} + Cl^-$$

L= L-Met, GSH, 5′-GMP
X = H_2L^*, Me_2L^*, terpy

Direct nucleophilic attack proceeds in a reversible manner as in Scheme 1. Substitution rate constants were determined under pseudo-first-order conditions by plotting the linear dependence of k_{obs} versus total nucleophile concentration (see eq 3). All kinetic data are summarized in Tables S1−S9 (see Supporting Information).

$$k_{obs} = k_2[\text{nucleophile}] + k_1[Cl^-] \quad (3)$$

Direct nucleophilic attack is characterized by rate constant k_2, and the reverse reactions are represented by rate constant k_1. The second-order rate constant k_2 characterizes product formation and was evaluated from the slope of a plot k_{obs} versus nucleophile concentration. Experimental results for the displacement of a chloride ion from **1a**, **1b**, and **1c** are shown in Table 3. Representative plots are shown in Figure 4.

As can be seen, **1a**, **1b**, and **1c** are reactive toward all of the tested nucleophiles, with order of reactivity 5′-GMP > GSH > L-Met. Rh^{III} complexes are expected to have the highest affinity

DOI: 10.1021/acs.inorgchem.8b02390
Inorg. Chem. 2019, 58, 307−319

Table 3. Rate Constants for the Substitution Reactions of the Rh^{III} Complex with L-Met, 5′-GMP, and GSH at pH = 7.2 (25 mM HEPES Buffer) in the Presence of 50 mM NaCl

		$[Rh^{III}(H_2L^*)Cl_3]$ (1a)			
	T (K)	$1 \times 10^1\ k_2$, $M^{-1}\ s^{-1}$	$1 \times 10^4\ k_1[Cl^-]$, $M^{-1}\ s^{-1}$	$\Delta H_2^{\ddagger}$, kJ mol^{-1}	$\Delta S_2^{\ddagger}$, J K^{-1} mol^{-1}
L-Met	310	2.4 ± 0.1	0.20 ± 0.01		
5′-GMP	288	7.6 ± 0.1	0.27 ± 0.01	40 ± 2	−120 ± 8
	298	13 ± 0.1	0.35 ± 0.01		
	310	27 ± 0.1	0.80 ± 0.02		
GSH	288	1.7 ± 0.1		26 ± 1	−183 ± 2
	298	2.5 ± 0.1			
	310	4.0 ± 0.1			
		$[Rh^{III}(Me_2L^*)Cl_3]$ (1b)			
	T, K	$1 \times 10^1\ k_2$, $M^{-1}\ s^{-1}$	$1 \times 10^4\ k_1[Cl^-]$, $M^{-1}\ s^{-1}$	$\Delta H_2^{\ddagger}$, kJ mol^{-1}	$\Delta S_2^{\ddagger}$, J K^{-1} mol^{-1}
L-Met	288	2.1 ± 0.1	0.10 ± 0.01	17 ± 6	−212 ± 22
	298	3.3 ± 0.1	0.15 ± 0.01		
	310	3.8 ± 0.2	0.20 ± 0.01		
5′-GMP	288	38 ± 0.1	0.50 ± 0.01	10 ± 2	−212 ± 8
	298	43 ± 0.1	2.0 ± 0.1		
	310	56 ± 0.1	7.8 ± 0.2		
GSH	310	19 ± 0.1	0.16 ± 0.01		
		$[Rh^{III}(terpy)Cl_3]$ (1c)			
	T, K	$1 \times 10^1\ k_2$, $M^{-1}\ s^{-1}$	$1 \times 10^5\ k_1[Cl^-]$, $M^{-1}\ s^{-1}$	$\Delta H_2^{\ddagger}$, kJ mol^{-1}	$\Delta S_2^{\ddagger}$, J K^{-1} mol^{-1}
L-Met	310	0.34 ± 0.01	0.01 ± 0.01		
5′-GMP	288	1.3 ± 0.1		35 ± 5	−154 ± 16
	298	2.5 ± 0.1			
	310	4.0 ± 0.1			
GSH	310	0.72 ± 0.01			

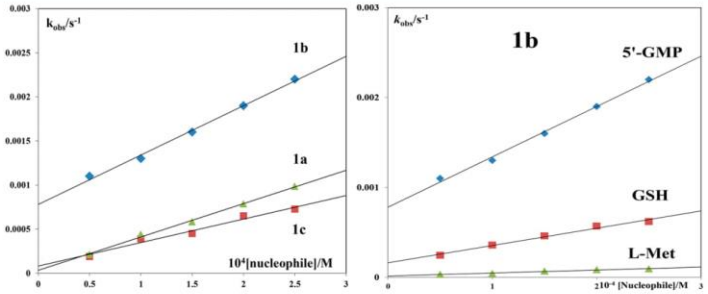

Figure 4. Pseudo-first-order rate constants as a function of nucleophile concentration. (right) k_{obs} vs nucleophile concentation for reaction of **1a**, **1b**, and **1c** complexes and 5′-GMP. (left) k_{obs} vs nucleophile concentation for reaction of **1b** complex and 5′-GMP, L-Met, and GSH; pH = 7.2 and 310 K in 25 mM HEPES and 50 mM NaCl.

for N-bonding nucleophiles, because in addition to the presence of the nitrogen donor atom Rh^{III} ions are borderline hard−soft acids. The lower reactivity of L-Met over GSH could be due to the bulky methyl group in L-Met, making access to the Rh^{III} complexes difficult. Furthermore, the N-donor nucleophile 5′-GMP is able to compete with S-donor nucleophiles L-Met and GSH, and display greater affinity toward the Rh^{III} complexes. These observations are of special interest, since under biological conditions within the cell, these S-donor biomolecules are present in relatively high concentrations and therefore compete with the DNA; suggesting the possibility that the investigated complexes could be bound to DNA and that DNA could be considered a potential target. The order of reactivity of the investigated Rh^{III} complexes is (Table 3):

$$[Rh^{III}(Me_2L^*)Cl_3]\ (\mathbf{1b}) > [Rh^{III}(H_2L^*)Cl_3]\ (\mathbf{1a}) > [Rh^{III}(terpy)Cl_3]\ (\mathbf{1c})$$

The camphor-derived bis(pyrazolylpyridine) Rh^{III} complexes react ∼10 times faster than $[Rh^{III}(terpy)Cl_3]$. Although complexes **1a** and **1b** have similar structure, **1b** is more reactive. Considering steric effects, **1b** is the most bulky Rh^{III} complex, suggesting that electronic effects have a greater impact on reactivity than steric effects. The obtained rate constants are in agreement with an earlier studied complex $[Rh^{III}(H_2L^{tBu})Cl_3]$.[20]

The thermodynamic properties and relative stability of the Rh^{III} complexes were examined comparing 2,6-di(1*H*-pyrazol-3-yl)pyridine (H_2L^H) (representing the smallest possible

DOI: 10.1021/acs.inorgchem.8b02390
Inorg. Chem. 2019, 58, 307−319

Scheme 2. Model Equation to Evaluate (B3LYP/LANL2DZp) the Relative Stability of $[Rh(H_2L^H)(Cl)_2L]^+$ Versus $[Rh(terpy)(Cl)_2L]^+$ [a]

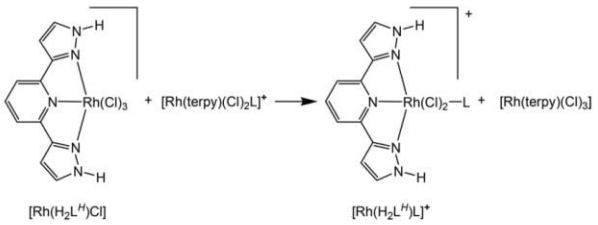

[a]L: Gua, $S(CH_3)_2$, $HSCH_3$.

ligand without hampering substituents) and terpy. Therefore, the following model was calculated as presented in Scheme 2.

As can be seen in Table 4, in gas phase, regardless of whether the trans or cis complexes are investigated, the general trend favors the terpy complexes, with two exceptions, L: dimethyl sulfide in the cis complex and Gua in the trans complex. In the case of trans-coordinated Gua a hydrogen bond of 1.7 Å between the CO group in Gua and the NH group in H_2L^H is formed (see Figure 5). This moderate preference for the terpy complexes likely originates from the slightly smaller size of H_2L^H versus terpy, leading to weaker charge stabilization. Incorporating solvent effects in our calculations supports this, resulting in all Rh^{III}–H_2L^H complexes being favored: the *cis*-$[Rh(H_2L^H)(Cl)_2Gua]^+$ by more than 5 kcal/mol. Generally, the complexes are best addressed as equally stable.

Table 4. Calculated Relative Stabilities for the Model Equation from Figure 5[a]

[kcal mol^{-1}]	cis		trans	
ligand (L)	B3LYP	B3LYP(CPCM)	B3LYP	B3LYP(CPCM)
HS–CH_3	1.51	−0.72	2.78	−1.40
CH_3–S–CH_3	−0.98	−0.98	2.40	−2.11
TU	1.37	−0.41	1.88	−0.95
Gua	1.23	−2.40	−3.94	−5.53
Imi	0.96	−0.09	3.70	−0.13

[a]B3LYP: RB3LYP/LANL2DZp + ZPE(B3LYP/LANL2DZp) B3LYP(CPCM): RB3LYP(CPCM)/LANL2DZp // RB3LYP/LANL2DZp + ZPE(B3LYP/LANL2DZp).

In all investigated terpy complexes, the distance between the central pyridine moiety nitrogen atom and the Rh^{III} center is ∼1.5% smaller than in H_2L^H systems. The N–Rh bonds in the equatorial plane cis to the central pyridine ring is in the case of the terpy-ligand ∼2% longer, whereas the Rh–L distance does not seem affected by the type of tridentate ligand (see Tables S11 and S12). Rh–L coordination is much more affected by the trans influence of pyridine or Cl^- depending on the investigated isomer, indicating that average Rh–N coordination in all test complexes is similar and the H_2L^H ligand is a good alternative to terpy (see Figure S1).

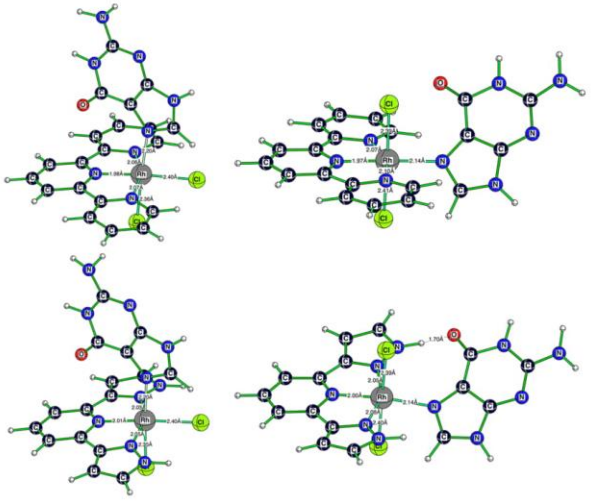

Figure 5. Calculated (B3LYP/LANL2DZp) structure of *cis*- and *trans*-$[Rh(terpy)(Cl)_3Gua]^+$ and of *cis*- and *trans*-$[Rh(H_2L^H)(Cl)_2Gua]^+$.

DOI: 10.1021/acs.inorgchem.8b02390
Inorg. Chem. 2019, 58, 307−319

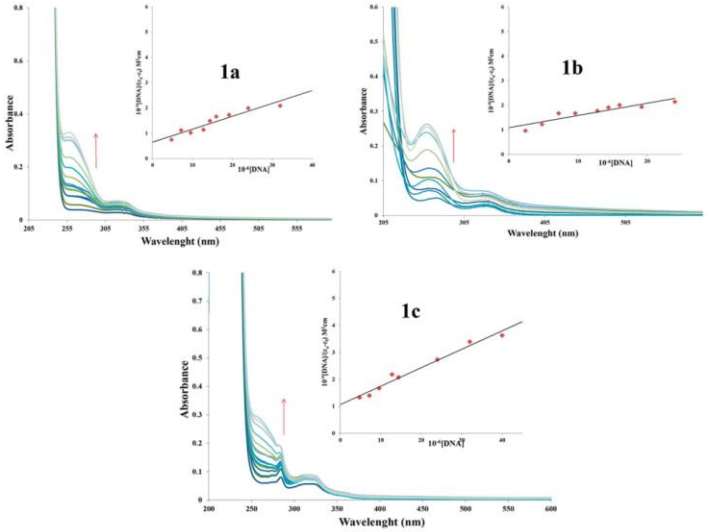

Figure 6. UV−Vis titration spectra of **1a**, **1b**, and **1c** complexes (8 μM) in PBS pH 7.4 with increasing concentration of CT-DNA (0−40 μM). The arrow shows hyperchromism in the spectral band. (inset) Plots of $[DNA]/(\varepsilon_a - \varepsilon_f)$ vs [DNA].

Table 5. Interaction Constants for Rh^{III} Complexes with CT-DNA and BSA

	CT-DNA		BSA
	K_b, M^{-1}	K_{sv}, M^{-1}	K_{sv}, M^{-1}
$[Rh^{III}(H_2L^*)Cl_3]$ (**1a**)	$(5.0 \pm 0.1) \times 10^4$	$(5.0 \pm 0.1) \times 10^4$	$(3.5 \pm 0.1) \times 10^4$
[RhIII(Me2L*)Cl3] (**1b**)	$(8.3 \pm 0.1) \times 10^4$	$(5.5 \pm 0.1) \times 10^4$	$(3.9 \pm 0.1) \times 10^4$
$[Rh^{III}(terpy)Cl_3]$ (**1c**)	$(7.0 \pm 0.1) \times 10^4$	$(3.8 \pm 0.1) \times 10^4$	$(3.4 \pm 0.1) \times 10^3$
$[Rh^{III}(H_2L^{tBu})Cl_3]$[20]	$(9.7 \pm 0.1) \times 10^4$	$(1.9 \pm 0.1) \times 10^4$	$(3.0 \pm 0.1) \times 10^4$

While tridentate complexes allow only one ligand to be substituted due to the chelate effects in square-planar complexes, octahedral complexes offer three possibilities: in our case, two equivalent cis to the central pyridine moiety and one trans. To examine the overall thermodynamic equilibrium, we compared the stability of cis and trans isomers of calculated model complexes $[Rh(H_2L^H)(Cl)_2L]^{n+}$ and $[Rh(terpy)(Cl)_2L]^{n+}$, where in all cases the cis isomer was considered to be the 0 value (Table S13).

As shown in Figure 5, application of the CPCM solvent model reduces the calculated energy gap equalizing the cis and trans isomer. However, the overall trend in the gas phase and especially after application of a solvent model favors the trans isomers. This is likely because, as shown in Figure 5, L has more free space in front of the chelating ligand trans to the central pyridine ring compared to the cis position, where L is above or below the chelating ring.

■ DNA BINDING STUDIES

Electronic Absorption Method. Electronic absorption spectrometry was used to investigate the interactions of metal ion complexes and CT-DNA molecules. In the present study, metal complex absorption titration studies were conducted at room temperature using fixed concentration of complexes (8 μM) in PBS and varying amounts of CT-DNA (0−40 μM).[53] Absorption spectra of **1a**, **1b**, and **1c** complexes in the absence and presence of CT-DNA at varying concentrations are given in Figure 6.

Results show that the Rh^{III} complexes have a strong absorption at ca. 258 nm. The absorption spectra of all three complexes showed hyperchromism and red shift, ∼2 or 3 nm, at the maximum peak with increasing CT-DNA concentrations. This observed hyperchromism and shift at the maximum peak could indicate an intercalative binding mode, possibly involving stacking interactions between the planar aromatic chromophore of the complex and nucleotide base pairs in CT-DNA.[54] However, the exact mode of binding cannot be proposed based on UV−vis spectroscopic methods.[55−57] Intrinsic equilibrium binding constants (K_b) of the Rh^{III} complexes with CT-DNA were evaluated using eq 1. The intrinsic binding constant K_b (Table 5) obtained for these complexes with CT-DNA follows the order: **1b** > **1c** > **1a**, with **1b** displaying the strongest interaction with DNA. However, both camphor-based ligand and terpiridine ligand complexes have nearly the same binding affinity; the intrinsic binding constants, K_b, do not differ considerably among the studied complexes. Kinetic data show that 5′-GMP reacts much more slowly with the Rh^{III} terpy complex than with the camphor-based Rh^{III} complexes. Considering that DNA is a relatively "crowded" molecule, it is possible that steric effects play a significant role in binding Rh^{III} complexes, and steric

DOI: 10.1021/acs.inorgchem.8b02390
Inorg. Chem. 2019, 58, 307−319

effects are thus more pronounced in the case of camphor-based Rh^{III} complexes.

Fluorescence Spectroscopic Methods. Fluorescence spectroscopic studies were used to confirm DNA interactions with rhodium complexes. Because our Rh^{III} complexes interact with DNA by UV−vis, competitive binding experiments were also conducted by adding ethidium bromide (EB) as a known DNA intercalator. While EB itself fluorescences weakly,[54] in the presence of CT-DNA, EB intercalates its planar phenanthridinium ring between adjacent base pairs of the DNA double helix, resulting in strong fluorescence emission at ~600 nm.[58] Addition of complexes **1a**, **1b**, and **1c** to EB-DNA resulted in fluorescence quenching due to displacement of EB from the DNA. Quenching parameters for Rh^{III} complexes were calculated using the Stern−Volmer equation (eq 2). EB displacement studies were performed by changing the concentration of metal complexes and monitoring the emission intensity of the EB-DNA complex.[53] Increasing concentrations of complexes **1a**, **1b**, and **1c** (0−10 μM) resulted in a significant decrease in fluorescence intensity with a noticeable red shift (Figure 7; see also Supporting Information Figures S4 and S5).

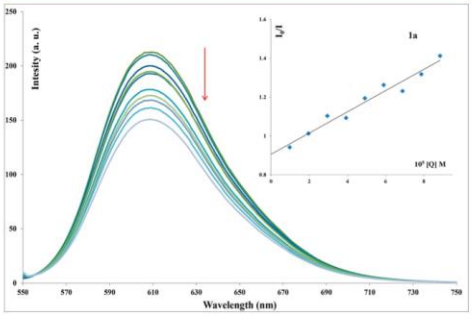

Figure 7. Fluorescence titration spectra of EB-DNA and of EB (10 μM) bound to DNA (10 μM) in the presence of varying amounts of complexes **1a**. [Arrow shows changes in fluorescence intensity upon increasing concentration of **1a** (0−10 μM)]. (inset) Stern−Volmer plots for EB-DNA fluorescence titration with **1a**.

These results suggest that EB is released from the EB-DNA complex due to displacement by the Rh^{III} complexes, indicating that complexes **1a**, **1b**, and **1c** have moderate DNA intercalative ability, with **1b** somewhat stronger than **1a** and **1c**.

As seen in Table 5, the studied Rh^{III} complexes interact moderately with CT-DNA. UV−Vis and fluorescence spectroscopic studies both show that the **1b** complex interacts more strongly than **1a** or **1c**. A previously studied complex, $[Rh^{III}(H_2L^tBu)Cl_3]$, was shown to have very similar affinity toward CT-DNA as the **1a**, **1b**, and **1c** complexes.[20] All three complexes show somewhat higher affinity for CT-DNA than BSA, in agreement with obtained result from kinetic studies, where all complexes reacted faster with 5′-GMP than with sulfur-donor molecules.

Viscosity. Viscosity measurements were conducted to further confirm interactions between **1a**, **1b**, and **1c** with CT-DNA. In classical intercalation, complex formation results in lengthening and stiffening of the DNA double helix, leading to increased DNA viscosity.[59,60]

Addition of increasing amounts (up to r = 1.0) of Rh^{III} complexes to a CT-DNA solution (0.01 mM) resulted in an increase in the relative viscosity of CT-DNA (Figure S6), which was most pronounced upon addition of **1b**, in accordance with UV−vis and fluorescence measurements. In the case of classic intercalation, DNA base pairs must separate to host the bound compound, resulting in increased DNA viscosity as a function of interaction strength. Thus, our results are in agreement with an increase in overall DNA length, possibly caused by compound intercalation between DNA base pairs via aromatic chromophores such as pyridine or pyrazole ligands in the complexes.

PROTEIN BINDING STUDIES

Fluorescence Spectroscopy of BSA. Metal ion complexes with antitumor activity often interact with specific proteins, both as part of their mechanism of action as well as transport and metabolism. In the present study we examined the affinity of **1a**, **1b**, and **1c** for BSA, using tryptophan fluorescence quenching experiments. Fluorescence spectroscopy can monitor changes in protein structure, dynamics, and folding.[61−63] The change in BSA fluorescence upon addition of increasing concentrations of **1a**, **1b**, and **1c** (0−30 μM) over the range of 300−500 nm (λ_{ex} = 295 nm) is presented in Figures S7−S9, Suporting Information. As shown, a decrease in fluorescence intensity at 363 nm was observed. Fluorescence quenching data were analyzed using the Stern−Volmer equation (eq 2), and a quenching constant (K_{sv}) was calculated from I_0/I versus [Q], Figures S7−S9, Supporting Information.

On the basis of these results, **1a** and **1b** have reasonable affinity for BSA, while **1c** displayed slightly lower affinity (Table 5). Quenching constants (K_{sv}) for camphor-derived Rh^{III} complex interactions with CT-DNA and BSA are approximately the same (Table 5 and Figure 8), although

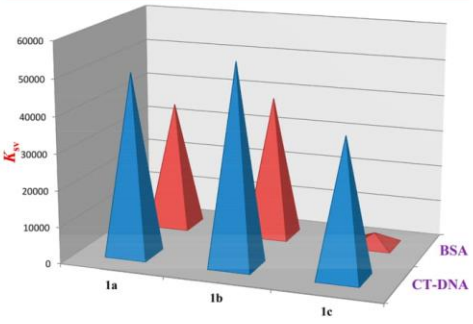

Figure 8. Obtained K_{sv} values for complexes **1a**, **1b**, and **1c** with BSA or CT-DNA.

somewhat higher for **1b**, whereas the terpiridine−Rh^{III} complex **1c** appears to interact stronger with CT-DNA. Values for these constants for **1a**, **1b**, and **1c** are in agreement with those obtained for a previously investigated complex $[Rh^{III}(H_2L^{tBu})Cl_3]$, Table 5.

UV−Vis Spectroscopy of BSA. UV spectroscopy was used to investigate the mode of binding between Rh^{III} complexes

DOI: 10.1021/acs.inorgchem.8b02390
Inorg. Chem. 2019, 58, 307−319

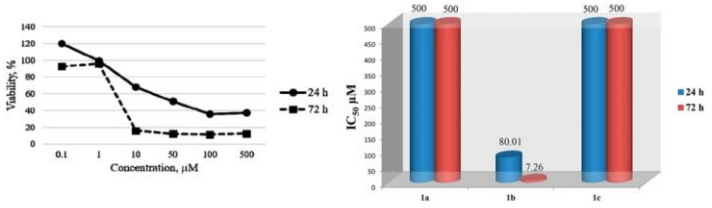

Figure 9. (left) Dose−response curves for the effect of **1b** on HCT-116 cell growth after 24 and 72 h of exposure. The antiproliferative effect was measured by MTT assay. All values are mean ± standard error, $n = 3$, $^*P < 0.05$ as compared with controls. (right) IC_{50} values for studied complexes **1a**, **1b**, and **1c** after incubation with HCT-116 cancer cell lines for 24 and 72 h.

and BSA, which can be considered to be either dynamic quenching or static quenching. In dynamic quenching, upon addition of a quencher, only the excited-state fluorescence molecule is affected, resulting in no change in the UV absorption spectra for BSA, whereas in static quenching, a new compound is formed between BSA and the quencher, considerably affecting the UV−vis spectra. UV spectra for BSA were recorded following addition of equal concentrations of **1a**, **1b**, or **1c**. Figure S10 shows a peak at ∼280 nm due to aromatic residues (Trp, Tyr, and Phe).[64] As shown, the absorption spectra of a mixture of BSA + Rh^{III} complexes descreases in intesity, indicating that the microenvironment of these aromatic side chains is changed, possibly due to interaction with one of the Rh^{III} complexes and consistent with a static quenching mechanism for **1a**, **1b**, and **1c**.

Cell Viability. Transition-metal compounds have been used to inhibit cancer proliferation,[65] and we have previously shown that Rh^{III} complexes display cytotoxicity against HCT-116 cells.[40] Thus, in the present study we investigated the antiproliferative potential of **1a**, **1b**, and **1c** as well as corresponding ligands on human colorectal cancer HCT-116 cells using an MTT assay. Compound **1b** showed the most significant effects with an IC_{50} of 80.01 and 7.26 μM after 24 and 72 h treatment, respectively; see Figure 9, Figure S11, and Table S14.

This antiproliferative effect by **1b** was concentration- and time-dependent. In contrast, **1a** and **1c** were not cytotoxic against HCT-116 cells under our laboratory conditions.

Molecular Docking. Molecular docking simulations were used to test if DNA intercalation or minor groove binding is possible between the studied compounds and DNA. Using Autodock4, ligands (**1a**, **1b**, **1c**, or $[Rh^{III}(H_2L^{tBu})Cl_3]$) were docked into DNA fragments representing either (1) canonical B-DNA (PDB 1BNA) or (2) DNA with an intercalation gap (PDB 1Z3F). 1BNA is the crystal structure of a synthetic DNA dodecamer, while 1Z3F is the crystal structure of a 6 bp DNA fragment in complex with an intercalating anticancer drug, ellipticine. All test compounds were predicted to interact with the minor groove of the B-DNA fragment, with estimated affinities in the micromolar range. In addition **1b**, **1c**, and $[Rh^{III}(H_2L^{tBu})Cl_3]$ showed similar potential for DNA intercalation in the gap created by ellipticine, with estimated binding affinities also in the micromolar range (Figure 10). These results are in agreement with our experimental UV−vis and fluorescence studies and further support the anticancer potential of these Rh^{III} complexes.

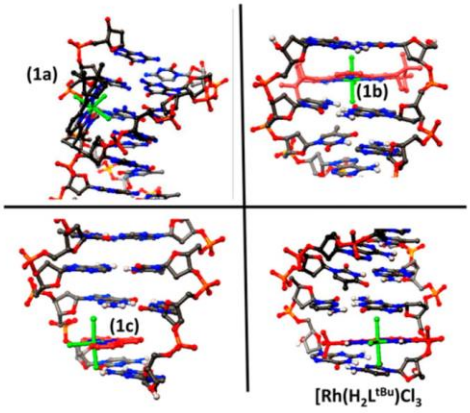

Figure 10. Molecular docking suggests that compounds **1b**, **1c**, and $[Rh^{III}(H_2L^{tBu})Cl_3]$ have potential for DNA intercalation, while all of the tested compounds have affinity for the minor groove of DNA. Minor groove binding by **1a** to B-DNA is shown (upper left).

CONCLUSIONS

We used a camphor-derived bis(pyrazolylpyridine), tridentate nitrogen-donor chelate system for the synthesis of two new Rh^{III} complexes. The crystal structure of **1b** complex was determined. Kinetic experiments were performed with small biomolecules (L-methionine, L-histidine, and glutathione) under pseudo-first-order conditions as a function of complex concentration and temperature by UV−vis spectroscopy. These results show that the synthesized complexes have affinity for the studied ligands, with order of reactivity 5′-GMP > GSH > L-Met. The interaction between the synthesized complexes and CT-DNA and BSA were also examined by absorption (UV−vis) and emission spectral studies (EB displacement studies). Overall, results show that our Rh^{III} complexes have good affinity to interact with CT-DNA and BSA, with somewhat higher affinity toward CT-DNA, with **1b** having the highest affinity toward CT-DNA and BSA. A Rh^{III} complex with terpiridine ligand, **1c**, was also synthesized, and the same type of interactions were examined. In all studied interactions the Rh^{III}−terpy complex reacted slower than the camphor-derived bis(pyrazolylpyridine) complexes, indicating that introduction of a camphor-derived spectator ligand can improve the reactivity of rhodium(III) complexes over use of a terpy spectator ligand. In vitro viability effects against human

DOI: 10.1021/acs.inorgchem.8b02390
Inorg. Chem. 2019, 58, 307−319

epithelial colorectal carcinoma HCT-116 show that **1b** has significant cytotoxic activity, while **1a** and **1c** showed no cytotoxic effects. Molecular docking suggests that all test compounds have affinity for the minor groove of DNA, while **1b** and **1c** have potential for DNA intercalation.

■ ASSOCIATED CONTENT

Supporting Information

The Supporting Information is available free of charge on the ACS Publications website at DOI: 10.1021/acs.inorgchem.8b02390.

Illustrated superposition of calculated structures, UV−vis absorption spectra, plot of absorbance versus time, fluorescence titration spectra, plot of relative viscosity of CT-DNA in PBS with varying amounts of complexes, emission spectra of BSA in presence of increasing amounts of **1a**, **1b**, and **1c**, dose-response curves, tabulated observed pseudo-first-order rate constants, water solubility of Rh^{III} complexes at 298 K, tabulated selected calculated distances, tabulated calculated relative stabilities, tabulated IC_{50} values (PDF)

Accession Codes

CCDC 1847938 contains the supplementary crystallographic data for this paper. These data can be obtained free of charge via www.ccdc.cam.ac.uk/data_request/cif, or by emailing data_request@ccdc.cam.ac.uk, or by contacting The Cambridge Crystallographic Data Centre, 12 Union Road, Cambridge CB2 1EZ, UK; fax: +44 1223 336033.

■ AUTHOR INFORMATION

Corresponding Author

*Phone: +381(0)34336223. Fax: +381(0)34335040. E-mail: jrosic@kg.ac.rs.

ORCID

Milan M. Milutinović: 0000-0003-4838-3998

Andreas Scheurer: 0000-0002-2858-9406

Jovana Bogojeski: 0000-0002-3433-7774

Author Contributions

The manuscript was written with contributions from all authors.

Notes

The authors declare no competing financial interest.

■ ACKNOWLEDGMENTS

The authors gratefully acknowledge financial support from the Ministry of Education, Science and Technological Development Serbia, Project Nos. 172011, 172057, and III41010. We also thank Prof. T. Clark for hosting this work at the Computer Chemistry Center and the Regionales Rechenzentrum Erlangen for a generous allotment of computer time.

■ DEDICATION

This article is dedicated to the memory of Professor Dr. Živadin D. Bugarčić (1954−2017), a great mentor and excellent chemist.

■ REFERENCES

(1) (a) Lindoy, L. Metallosupramolecular Chemistry. *Coord. Chem. Rev.* **2008**, *252*, 811−1050. (b) Saalfrank, R. W.; Maid, H.; Scheurer, A. Supramolecular Coordination Chemistry: The Synergistic Effect of Serendipity and Rational Design. *Angew. Chem.* **2008**, *120*, 8924−8956; *Angew. Chem., Int. Ed.* **2008**, *47*, 8794−8824.

(2) Beller, M.; Bolm, C. *Transition Metals for Organic Synthesis: Building Blocks and Fine Chemicals*; Wiley-VCH: Weinheim, Germany, 2004.

(3) Alessio, E. *Bioinorganic Medicinal Chemistry*; Wiley-VCH: Weinheim, Germany, 2011.

(4) Kastl, A.; Wilbuer, A.; Merkel, A. L.; Feng, L.; Meggers, E.; et al. Dual anticancer activity in a single compound: visible-light-induced apoptosis by an antiangiogenic iridium complex. *Chem. Commun.* **2012**, *48*, 1863−1865.

(5) Peña, B.; David, A.; Pavani, C.; Baptista, M. S.; Pellois, J.-P.; Turro, C.; Dunbar, K. R. Cytotoxicity Studies of Cyclometallated Ruthenium(II) Compounds: New Applications for Ruthenium Dyes. *Organometallics* **2014**, *33*, 1100−1103.

(6) Noor, F.; Wüstholz, A.; Kinscherf, R.; Metzler-Nolte, N. A Cobaltocenium−Peptide Bioconjugate Shows Enhanced Cellular Uptake and Directed Nuclear Delivery. *Angew. Chem., Int. Ed.* **2005**, *44*, 2429−2432.

(7) Pongratz, M.; Schluga, P.; Jakupec, M. A.; Arion, V. B.; Hartinger, C. G.; Allmaier, G.; Keppler, B. K. Transferrin binding and transferrin-mediated cellular uptake of the ruthenium coordination compound KP1019, studied by means of AAS, ESI-MS and CD spectroscopy. *J. Anal. At. Spectrom.* **2004**, *19*, 46−51.

(8) Ernst, R. J.; Komor, A. C.; Barton, J. K. Selective Cytotoxicity of Rhodium Metalloinsertors in Mismatch Repair-Deficient Cells. *Biochemistry* **2011**, *50*, 10919−10928.

(9) Harris, A. L.; Yang, X.; Hegmans, A.; Povirk, L.; Ryan, J. J.; Kelland, L.; Farrell, N. P. Synthesis, Characterization, and Cytotoxicity of a Novel Highly Charged Trinuclear Platinum Compound. Enhancement of Cellular Uptake with Charge. *Inorg. Chem.* **2005**, *44*, 9598−9600.

(10) Lauffer, R. B. Paramagnetic metal complexes as water proton relaxation agents for NMR imaging: theory and design. *Chem. Rev.* **1987**, *87*, 901−927.

(11) Della Rocca, J.; Liu, D.; Lin, W. Nanoscale Metal−Organic Frameworks for Biomedical Imaging and Drug Delivery. *Acc. Chem. Res.* **2011**, *44*, 957−968.

(12) Anderson, C. J.; Welch, M. J. Radiometal-Labeled Agents (Non-Technetium) for Diagnostic Imaging. *Chem. Rev.* **1999**, *99*, 2219−2234.

(13) Domaille, D. W.; Que, E. L.; Chang, C. J. Synthetic fluorescent sensors for studying the cell biology of metals. *Nat. Chem. Biol.* **2008**, *4*, 168−175.

(14) Minus, M. B.; Kang, M. K.; Knudsen, S. E.; Liu, W.; Krüger, M. J.; Smith, M. L.; Redell, M. S.; Ball, Z. T. Assessing the intracellular fate of rhodium(II) complexes. *Chem. Commun.* **2016**, *52*, 11685−11688.

(15) Sliwinska, U.; Pruchnik, F. P.; Pelinska, I.; Ulaszewski, S.; Wilczok, A.; Zajdel, A. Synthesis, structure and antitumor activity of [RhCl3(N−N)(DMSO)] polypyridyl complexes. *J. Inorg. Biochem.* **2008**, *102*, 1947−1951.

(16) Cwikowska, M.; Pruchnik, F. P.; Starosta, R.; Chojnacki, H.; Wilczok, A.; Ulaszewski, S. Dinuclear Rh(II) complexes with one polypyridyl ligand, structure, properties and antitumor activity. *Inorg. Chim. Acta* **2010**, *363*, 2401−2408.

(17) Frade, R. F. M.; Candeias, N. R.; Duarte, C. M. M.; Andre, V.; Duarte, M. T.; Gois, P. M. P.; Afonso, C. A. M. New dirhodium complex with activity towards colorectal cancer. *Bioorg. Med. Chem. Lett.* **2010**, *20*, 3413−3415.

(18) Morrison, D. E.; Aitken, J. B.; de Jonge, M. D.; Issa, F.; Harris, H. H.; Rendina, L. M. Synthesis and Biological Evaluation of a Class of Mitochondrially-Targeted Gadolinium(III) Agents. *Chem. - Eur. J.* **2014**, *20*, 16602−16612.

(19) Huang, H.; Zhang, P.; Chen, H.; Ji, L.; Chao, H. Comparison Between Polypyridyl and Cyclometalated Ruthenium(II) Complexes: Anticancer Activities Against 2D and 3D Cancer Models. *Chem. - Eur. J.* **2015**, *21*, 715−725.

(20) Milutinović, M. M.; Bogojeski, J. V.; Klisurić, O.; Scheurer, A.; Elmroth, S. K. C.; Bugarčić, Ž. D. Synthesis and structures of a pincer-type rhodium(III) complex: reactivity toward biomolecules. *Dalton Trans.* **2016**, *45*, 15481−15491.
(21) Mukhopadhyay, S.; Gupta, R. K.; Paitandi, R. P.; Rana, N. K.; Sharma, G.; Koch, B.; Rana, L. K.; Hundal, M. S.; Pandey, D. S. Synthesis, Structure, DNA/Protein Binding, and Anticancer Activity of Some Half-Sandwich Cyclometalated Rh(III) and Ir(III) Complexes. *Organometallics* **2015**, *34*, 4491−4506.
(22) (a) Mayer, I. A.; Abramson, V. G.; Lehmann, B. D.; Pietenpol, J. A. New Strategies for Triple-Negative Breast Cancer—Deciphering the Heterogeneity. *Clin. Cancer Res.* **2014**, *20*, 782−790. (b) Schatzschneider, U.; Metzler-Nolte, N. New Principles in Medicinal Organometallic Chemistry. *Angew. Chem., Int. Ed.* **2006**, *45*, 1504−1507. (c) Ott, I.; Kircher, B.; Bagowski, C. P.; Vlecken, D. H.; Ott, E. B.; Will, J.; Bensdorf, K.; Sheldrick, W. S.; Gust, R. Modulation of the Biological Properties of Aspirin by Formation of a Bioorganometallic Derivative. *Angew. Chem., Int. Ed.* **2009**, *48*, 1160−1163. (d) Zhong, H.-J.; Wang, W.; Kang, T.-S.; Yan, H.; Yang, Y.; Xu, L.; Wang, Y.; Ma, D.-L.; Leung, C.-H. Pan Assay Interference Compounds (PAINS) and Other Promiscuous Compounds in Antifungal Research. *J. Med. Chem.* **2017**, *60*, 497−503. (e) Chen, F.; Huang, X.; Wu, M.; Gou, S.; Hu, W. A CK2-targeted Pt(IV) prodrug to disrupt DNA damage response. *Cancer Lett.* **2017**, *385*, 168−178. (f) Yang, G.-J.; Zhong, H.-J.; Ko, C.-N.; Wong, S.-Y.; Vellaisamy, K.; Ye, M.; Ma, D.-L.; Leung, C.-H. Identification of a rhodium(III) complex as a Wee1 inhibitor against TP53-mutated triple-negative breast cancer cells. *Chem. Commun.* **2018**, *54*, 2463.
(23) Gupta, R. K.; Pandey, R.; Sharma, G.; Prasad, R.; Koch, B.; Srikrishna, S.; Li, P. Z.; Xu, Q.; Pandey, D. S. DNA Binding and Anti-Cancer Activity of Redox-Active Heteroleptic Piano-Stool Ru(II), Rh(III), and Ir(III) Complexes Containing 4-(2-Methoxypyridyl)-phenyldipyrromethene. *Inorg. Chem.* **2013**, *52*, 3687−3698.
(24) Ganeshpandian, M.; Loganathan, R.; Suresh, E.; Riyasdeen, A.; Akbarsha, M. A.; Palaniandavar, M. Guest to framework photo-induced electron transfer in a cobalt substituted RWLC-2 metal organic framework. *Dalton Trans.* **2014**, *43*, 1203−1219.
(25) Dorcier, A.; Dyson, P. J.; Goessens, C.; Rothlisberger, U.; Scopelliti, R.; Tavernelli, I. Binding of Organometallic Ruthenium(II) and Osmium(II) Complexes to an Oligonucleotide: A Combined Mass Spectrometric and Theoretical Study. *Organometallics* **2005**, *24*, 2114−2123.
(26) Chatterjee, S.; Kundu, S.; Bhattacharyya, A.; Hartinger, C. G.; Dyson, P. J. The ruthenium(II)−arene compound RAPTA-C induces apoptosis in EAC cells through mitochondrial and p53−JNK pathways. *JBIC, J. Biol. Inorg. Chem.* **2008**, *13*, 1149−1155.
(27) Suss-Fink, G. Arene ruthenium complexes as anticancer agents. *Dalton Trans.* **2010**, *39*, 1673−1688.
(28) Dayan, O.; Dayan, S.; Kani, I.; Çetinkaya, B. Ruthenium(II) complexes bearing pyridine-based tridentate and bidentate ligands: catalytic activity for transfer hydrogenation of aryl ketones. *Appl. Organomet. Chem.* **2012**, *26*, 663−670.
(29) Chelucci, G. Synthesis and application in asymmetric catalysis of camphor-based pyridine ligands. *Chem. Soc. Rev.* **2006**, *35*, 1230−1243.
(30) Milutinovic, M.; Bugarčić, Ž. D.; Wilhelm, R. A camphor based 1,3-diamine Ru(II) terpyridine complex: synthesis, characterization, kinetic investigation and DNA binding. *New J. Chem.* **2018**, *42*, 7607−7611.
(31) (a) Sravanthi, N.; Renuka, S.; Rama krishna, K. Pharmacophore Docking based combined In silico study of Kappa Opioid Receptor Agonists. *Int. J. ChemTech Res.* **2011**, *3*, 1897−1902. (b) Murtinho, D.; da Rocha, Z. N.; Pires, A. S.; Jimenez, R. P.; Abrantes, A. M.; Laranjo, M.; Mamede, A. C.; Casalta-Lopes, J. E.; Botelho, M. F.; Pais, A. A. C. C.; Nunes, S. C. C.; Burrows, H. D.; Costa, T.; Silva Serra, M. E. Synthesis, characterization and assessment of the cytotoxic activity of Cu(II), Fe(III) and Mn(III) complexes of camphoric acid-derived salen ligands. *Appl. Organomet. Chem.* **2015**, *29*, 425−432.
(32) (a) Rais, E.; Flörke, U.; Wilhelm, R. Reactivity of Grubbs−Hoveyda II Complexes Including Extended N-Heterocyclic Carbenes with a Bicyclic Camphor-Based Framework. *Synthesis* **2017**, *49*, 2852−2864. (b) Newman, P. D.; Cavell, K. J.; Kariuki, B. M. Metal Complexes of Chiral NHCs Containing a Fused Six- and Seven-Membered Central Ring. *Organometallics* **2010**, *29*, 2724−2734. (c) Newman, P. D.; Cavell, K. J.; Kariuki, B. M. Variable coordination of a chiral diphosphine containing an amidinium/NHC group within its backbone: μ-P,P′, κ2-P,P′ and κ3-P,C,P′ coordination modes. *Dalton Trans.* **2012**, *41*, 12395−12407.
(33) (a) Silva Serra, M. E.; Murtinho, D.; da Rocha, Z. N.; Pires, A. S.; Baptista, J. G.; Abrantes, A. M.; Laranjo, M.; Casalta-Lopes, J. E.; Botelho, M. F.; Pais, A. A. C. C.; Nunes, S. C. C.; Burrows, H. D.; Costa, T. Dibrominated camphoric acid derived salen complexes: Synthesis, characterization and cytotoxic activity. *Polyhedron* **2017**, *137*, 147−156. (b) Jaramillo, D.; Buck, D. P.; Collins, J. G.; Fenton, R. R.; Stootman, F. H.; Wheate, N. J.; Aldrich-Wright, J. R. Synthesis, Characterisation and Biological Activity of Chiral Platinum(II) Complexes. *Eur. J. Inorg. Chem.* **2006**, *2006*, 839−849.
(34) Xu, H.; Zheng, K.-C.; Chen, Y.; Li, Y.-Z.; Lin, L.-J.; Li, H.; Zhang, P.-X.; Ji, L.-N. Effects of ligand planarity on the interaction of polypyridyl Ru(II) complexes with DNA. *Dalton Trans.* **2003**, 2260−2268.
(35) Korzekwa, J.; Scheurer, A.; Heinemann, F. W.; Meyer, K. Synthesis and characterization of uranium(IV) tetrachloro complexes in bis-pyrazolylpyridine ligand environments. *Dalton Trans.* **2017**, *46*, 13811−13823.
(36) Pruchnik, F. P.; Jakimowicz, P.; Ciunik, Z.; Zakrzewska-Czerwinska, J.; Opolski, A.; Wietrzyk, J.; Wojdat, E. Rhodium(III) complexes with polypyridyls and pyrazole and their antitumor activity. *Inorg. Chim. Acta* **2002**, *334*, 59−66.
(37) Meadows, K. A.; Liu, F.; Sou, J.; Hudson, B. P.; McMillin, D. R. Spectroscopic and photophysical studies of the binding interactions between copper phenanthroline complexes and RNA. *Inorg. Chem.* **1993**, *32*, 2919−2923.
(38) Mosmann, T. Rapid colorimetric assay for cellular growth and survival: Application to proliferation and cytotoxicity assays. *J. Immunol. Methods* **1983**, *65*, 55−63.
(39) Petrović, V. P.; Živanović, M. N.; Simijonović, D.; Đorović, J.; Petrović, Z. D.; Marković, S. D. Chelate N,O-palladium(II) complexes: synthesis, characterization and biological activity. *RSC Adv.* **2015**, *5*, 86274−86281.
(40) Čanović, P.; Bogojeski, J.; Košarić, J. V.; Marković, S. D.; Živanović, M. N. Pt(IV), Pd(II), and Rh(III) complexes induced oxidative stress and cytotoxicity in the HCT-116 colon cancer cell line. *Turk. J. Biol.* **2017**, *41*, 141−147.
(41) Živanović, M. N.; Košarić, J. V.; Šmit, B.; Šeklić, D. S.; Pavlović, R. Z.; Marković, S. D. Gen. Novel seleno-hydantoin palladium(II) complex - antimigratory, cytotoxic and prooxidative potential on human colon HCT-116 and breast MDA-MB-231 cancer cells. *Physiol. Biophys.* **2017**, *36*, 187−196.
(42) Oxford Diffraction. *CrysAlis PRO*, CrysAlis CCD, and CrysAlis RED; Oxford Diffraction Ltd.: Abingdon, England, 2015.
(43) Sheldrick, G. M. SHELXT−Integrated space-group and crystal-structure determination. *Acta Crystallogr., Sect. A: Found. Adv.* **2015**, *71*, 3−8.
(44) Bruno, I. J.; Cole, J. C.; Edgington, P. R.; Kessler, M. K.; Macrae, C. F.; McCabe, P.; Pearson, J.; Taylor, R. New software for searching the Cambridge Structural Database and visualizing crystal structures. *Acta Crystallogr., Sect. B: Struct. Sci.* **2002**, *58*, 389−397.
(45) Farrugia, L. J. WinGX suite for small-molecule single-crystal crystallography. *J. Appl. Crystallogr.* **1999**, *32*, 837−838.
(46) Spek, A. L. Structure validation in chemical crystallography. *Acta Crystallogr., Sect. D: Biol. Crystallogr.* **2009**, *65*, 148−155.
(47) Djeković, A.; Petrović, B.; Bugarčić, Ž. D.; Puchta, R.; van Eldik, R. Kinetics and mechanism of the reactions of Au(III) complexes with some biologically relevant molecules. *Dalton Trans.* **2012**, *41*, 3633−3641.

DOI: 10.1021/acs.inorgchem.8b02390
Inorg. Chem. 2019, 58, 307−319

(48) (a) Becke, A. D. Densityfunctional thermochemistry. III. The role of exact exchange. *J. Chem. Phys.* **1993**, *98*, 5648−5652. (b) Lee, C.; Yang, W.; Parr, R. G. Development of the Colle-Salvetti correlation-energy formula into a functional of the electron density. *Phys. Rev. B: Condens. Matter Mater. Phys.* **1988**, *37*, 785−789. (c) Stephens, P. J.; Devlin, F. J.; Chabalowski, C. F.; Frisch, M. J. Ab Initio Calculation of Vibrational Absorption and Circular Dichroism Spectra Using Density Functional Force Fields. *J. Phys. Chem.* **1994**, *98*, 11623−11627. (d) Dunning, T. H., Jr; Hay, P. J. In *Modern Theoretical Chemistry;* Schaefer, H. F., III, Ed.; Plenum Press: New York, 1976; pp 1−28. (e) Hay, P. J.; Wadt, W. R. Ab initio effective core potentials for molecular calculations. Potentials for the transition metal atoms Sc to Hg. *J. Chem. Phys.* **1985**, *82*, 270−283. (f) Wadt, W. R.; Hay, P. J. Ab initio effective core potentials for molecular calculations. Potentials for main group elements Na to Bi. *J. Chem. Phys.* **1985**, *82*, 284−298. (g) Hay, P. J.; Wadt, W. R. Ab initio effective core potentials for molecular calculations. Potentials for K to Au including the outermost core orbitals. *J. Chem. Phys.* **1985**, *82*, 299−310. (h) Huzinaga, S. *Gaussian Basis Sets for Molecular Calculations;* Elsevier: Amsterdam, Netherlands, 1984.

(49) (a) Shyshov, O.; Brachvogel, R.-Ch.; Bachmann, T.; Srikantharajah, R.; Segets, D.; Hampel, F.; Puchta, R.; von Delius, M. Adaptive Behavior of Dynamic Orthoester Cryptands. *Angew. Chem., Int. Ed.* **2017**, *56*, 776−781. (b) Begel, S.; Scheurer, A.; Puchta, R.; van Eldik, R. Host-Guest Complexes of [TriPip222], the Piperazine Analogue of [2.2.2]: Prediction of Ion Selectivity by Quantum Chemical Calculations VIII. *Z. Anorg. Allg. Chem.* **2016**, *642*, 395−402. (c) Begel, S.; Scheurer, A.; Puchta, R. Saalfrank-type {Fe2L3} host−guest complexes − prediction of ion selectivity by quantum chemical calculations VII. *J. Coord. Chem.* **2015**, *68*, 3374−3387. (d) Begel, S.; Puchta, R.; van Eldik, R. Host-guest complexes of calix[4]tubes−prediction of ion selectivity by quantum chemical calculations VI. *J. Mol. Model.* **2014**, *20*, 2200. (e) Begel, S.; Puchta, R.; van Eldik, R. Host−guest complexes of mixed glycol-bipyridine cryptands: prediction of ion selectivity by quantum chemical calculations, part V. *Beilstein J. Org. Chem.* **2013**, *9*, 1252−1268. (f) Schmeisser, M.; Illner, P.; Puchta, R.; Zahl, A.; van Eldik, R. Gutmann Donor and Acceptor Numbers for Ionic Liquids. *Chem. - Eur. J.* **2012**, *18*, 10969−10982. (g) Puchta, R.; Meier, R.; van Eikema Hommes, N. J. R.; van Eldik, R. Quantum Chemical Analysis of the Enantiomerisation Mechanism of Complexes of the Type [MII(XU)-4]F+ (M = Pt, Pd, Ni; X = S, Se, Te;U = urea). *Eur. J. Inorg. Chem.* **2006**, *2006*, 4063−4067. (h) Scheurer, A.; Maid, H.; Hampel, F.; Saalfrank, R. W.; Toupet, L.; Mosset, P.; Puchta, R.; van Eikema Hommes, N. J. R. Influence of the Conformation of Salen Complexes on the Stereochemistry of the Asymmetric Epoxidation of Olefins. *Eur. J. Org. Chem.* **2005**, *2005*, 2566−2574. (i) Illner, P.; Zahl, A.; Puchta, R.; van Eikema Hommes, N. J. R.; Wasserscheid, P.; van Eldik, R. Mechanistic studies on the formation of Pt(II) hydroformylation catalysts in imidazolium-based ionic liquids. *J. Organomet. Chem.* **2005**, *690*, 3567−3576. (j) Weber, C. F.; Puchta, R.; van Eikema Hommes, N. J. R.; Wasserscheid, P.; van Eldik, R. Transition-State Effects of Ionic Liquids in Substitution Reactions of PtII Complexes. *Angew. Chem., Int. Ed.* **2005**, *44*, 6033−6038.

(50) (a) Barone, V.; Cossi, M. Quantum calculation of molecular energies and energy gradients in solution by a conductor solvent model. *J. Phys. Chem. A* **1998**, *102*, 1995−2001. (b) Cossi, M.; Rega, N.; Scalmani, G.; Barone, V. Energies, structures, and electronic properties of molecules in solution with the C-PCM solvation model. *J. Comput. Chem.* **2003**, *24*, 669−681.

(51) Frisch, M. J.; Trucks, G. W.; Schlegel, H. B.; Scuseria, G. E.; Robb, M. A.; Cheeseman, J. R.; Scalmani, G.; Barone, V.; Mennucci, B.; Petersson, G. A.; Nakatsuji, H.; Caricato, M.; Li, X.; Hratchian, H. P.; Izmaylov, A. F.; Bloino, J.; Zheng, G.; Sonnenberg, J. L.; Hada, M.; Ehara, M.; Toyota, K.; Fukuda, R.; Hasegawa, J.; Ishida, M.; Nakajima, T.; Honda, Y.; Kitao, O.; Nakai, H.; Vreven, T.; Montgomery, J. A.; Peralta, J. E.; Ogliaro, F.; Bearpark, M.; Heyd, J. J.; Brothers, E.; Kudin, K. N.; Staroverov, V. N.; Keith, T.; Kobayashi, R.; Normand, J.; Raghavachari, K.; Rendell, A.; Burant, J. C.; Iyengar, S. S.; Tomasi, J.; Cossi, M.; Rega, N.; Millam, J. M.; Klene, M.; Knox, J. E.; Cross, J. B.; Bakken, V.; Adamo, C.; Jaramillo, J.; Gomperts, R.; Stratmann, R. E.; Yazyev, O.; Austin, A. J.; Cammi, R.; Pomelli, C.; Ochterski, J. W.; Martin, R. L.; Morokuma, K.; Zakrzewski, V. G.; Voth, G. A.; Salvador, P.; Dannenberg, J. J.; Dapprich, S.; Daniels, A. D.; Farkas, O.; Foresman, J. B.; Ortiz, J. V.; Cioslowski, J.; Fox, D. J. *Gaussian 09,* Revision C.01; Gaussian, Inc.: Wallingford, CT, 2010.

(52) Morris, G. M.; Huey, R.; Lindstrom, W.; Sanner, M. F.; Belew, R. K.; Goodsell, D. S.; Olson, A. J. AutoDock4 and AutoDockTools4: Automated docking with selective receptor flexibility. *J. Comput. Chem.* **2009**, *30*, 2785−2791.

(53) (a) Long, E. C.; Barton, J. K. On demonstrating DNA intercalation. *Acc. Chem. Res.* **1990**, *23*, 271−273. (b) Pasternack, R. F.; Gibbs, E. J.; Villafranca, J. Interactions of porphyrins with nucleic acids. *Biochemistry* **1983**, *22*, 2406−2414.

(54) (a) Koumousi, E. S.; Zampakou, M.; Raptopoulou, C. P.; Psycharis, V.; Beavers, C. M.; Teat, S. J.; Psomas, G.; Stamatatos, T. C. First Palladium(II) and Platinum(II) Complexes from Employment of 2,6-Diacetylpyridine Dioxime: Synthesis, Structural and Spectroscopic Characterization, and Biological Evaluation. *Inorg. Chem.* **2012**, *51*, 7699−7710. (b) Rizvi, M. A.; Zaki, M.; Afzal, M.; Mane, M.; Kumar, M.; Shah, B. A.; Srivastav, S.; Srikrishna, S.; Peerzada, G. M.; Tabassum, S. Nuclear blebbing of biologically active organoselenium compound towards human cervical cancer cell (HeLa): In vitro DNA/HSA binding, cleavage and cell imaging studies. *Eur. J. Med. Chem.* **2015**, *90*, 876−888.

(55) Tarushi, A.; Polatoglou, E.; Kljun, J.; Turel, I.; Psomas, G.; Kessissoglou, D. P. Interaction of Zn(II) with quinolone drugs: Structure and biological evaluation. *Dalton Trans.* **2011**, *40*, 9461−9473.

(56) Tarushi, A.; Lafazanis, K.; Kljun, J.; Turel, I.; Pantazaki, A. A.; Psomas, G.; Kessissoglou, D. P. First- and second-generation quinolone antibacterial drugs interacting with zinc(II): Structure and biological perspectives. *J. Inorg. Biochem.* **2013**, *121*, 53−65.

(57) Dhar, S.; Nethaji, M.; Chakravarty, A. R. Effect of charge transfer bands on the photo-induced DNA cleavage activity of [1-(2-thiazolylazo)-2-naphtholato]copper(II) complexes. *J. Inorg. Biochem.* **2005**, *99*, 805−812.

(58) Meyer-Almes, F. J.; Porschke, D. Mechanism of intercalation into the DNA double helix by ethidium. *Biochemistry* **1993**, *32*, 4246−4253.

(59) Li, D. D.; Tian, J. L.; Gu, W.; Liu, X.; Yan, S. P. A novel 1,2,4-triazole-based copper(II) complex: Synthesis, characterization, magnetic property and nuclease activity. *J. Inorg. Biochem.* **2010**, *104*, 171−179.

(60) Jiang, M.; Li, Y.; Wu, Z.; Liu, Z.; Yan, C. Synthesis, crystal structure, cytotoxic activities and DNA-binding properties of new binuclear copper(II) complexes bridged by N,N′-bis(N-hydroxyethylaminoethyl)oxamide. *J. Inorg. Biochem.* **2009**, *103*, 833−844.

(61) Ramachandran, E.; Thomas, S. P.; Poornima, P.; Kalaivani, P.; Prabhakaran, R.; Padma, V. V.; Natarajan, K. Evaluation of DNA binding, antioxidant and cytotoxic activity of mononuclear Co(III) complexes of 2-oxo-1,2-dihydrobenzo[h]quinoline-3-carbaldehyde thiosemicarbazones. *Eur. J. Med. Chem.* **2012**, *50*, 405−415.

(62) Paitandi, R. P.; Gupta, R. K.; Singh, R. S.; Sharma, G.; Koch, B.; Pandey, D. S. Interaction of ferrocene appended Ru(II), Rh(III) and Ir(III) dipyrrinato complexes with DNA/protein, molecular docking and antitumor activity. *Eur. J. Med. Chem.* **2014**, *84*, 17−29.

(63) Miller, J. N. Recent advances in molecular luminescence analysis. *Proc. Anal. Div. Chem. Soc.* **1979**, *16*, 203−208.

(64) Wang, F.; Huang, W.; Dai, Z. X. Spectroscopic investigation of the interaction between riboflavin and bovine serum albumin. *J. Mol. Struct.* **2008**, *875*, 509−514.

(65) Ndagi, U.; Mhlongo, N.; Soliman, M. E. Metal complexes in cancer therapy − an update from drug design perspective. *Drug Des., Dev. Ther.* **2017**, *11*, 599−616.

DOI: 10.1021/acs.inorgchem.8b02390
Inorg. Chem. 2019, 58, 307−319

Supporting Information

Synthesis of Camphor-derived Bis-pyrazolylpyridine Rhodium(III) Complexes: Structure–Reactivity Relationships and Biological Activity

Angelina Petrović,[a] *Milan M. Milutinović,*[a,f] *Edward T. Petri,*[g] *Marko Živanović,*[a] *Nevena Milivojević,*[a] *Ralph Puchta,*[b,c,d] *Andreas Scheurer,*[b] Jana Korzekwa,[b] *Olivera R. Klisurić,*[e] *Jovana Bogojeski*[a*]

[a] University of Kragujevac, Faculty of Science, Radoja Domanovića 12, 34000 Kragujevac, Serbia

[b] Inorganic Chemistry, Department of Chemistry and Pharmacy, University of Erlangen-Nürnberg, 91058 Erlangen, Germany

[c] Computer Chemistry Center, Department of Chemistry and Pharmacy, University of Erlangen-Nürnberg, 91058 Erlangen, Germany

[d] ZISC (Zentralinstitut für Scientific Computing), Universität Erlangen-Nürnberg,Martensstrasse 5a,91058 Erlangen, Germany

[e] University of Novi Sad, Faculty of Science, Department of Physics, Trg Dositeja Obradovića 4, 21000 Novi Sad, Serbia

[f] Department of Organic Chemistry, University of Paderborn, Warburgerstraße 100, 33098 Paderborn, Germany

[g] University of Novi Sad, Faculty of Science, Department of Biology and Ecology, Trg Dositeja Obradovića 4, 21000 Novi Sad, Serbia

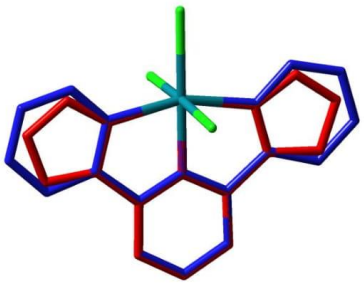

Figure S1. Superposition of the calculated (B3LYP7LANL2DZp) structures of $[Rh(H_2L^H)Cl_3]$ (red) and $[M(terpy)Cl_3]$ (blue).

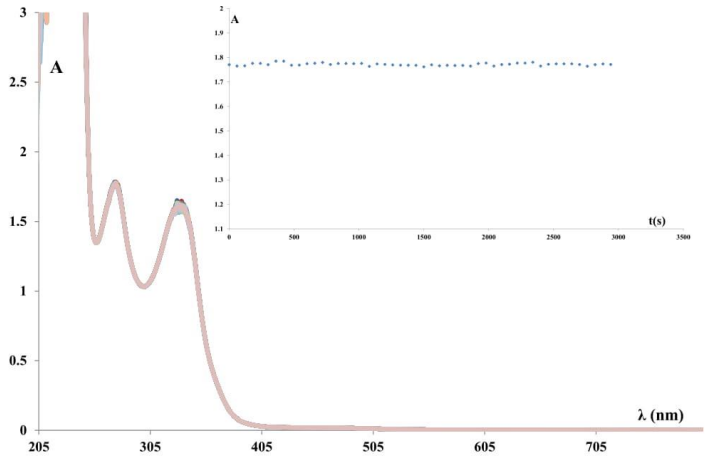

Figure S2. UV-Vis absorption spectra of complex **1b**, recorded for a time period of 3000 s. Insert graph**:** Absorbance as a function of time at maximum wavelength

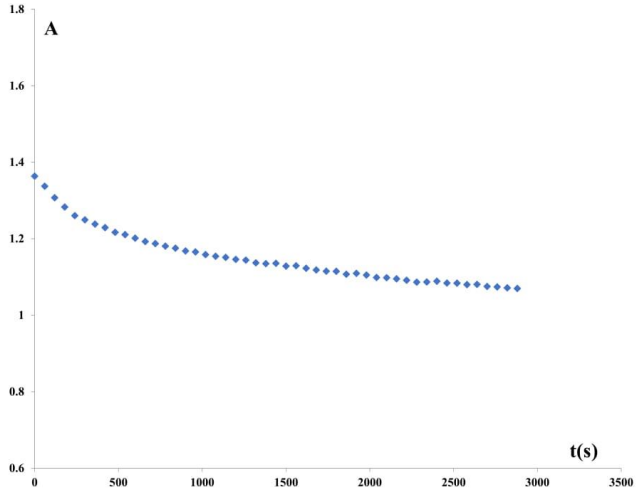

Figure S3. Absorbance as a function of time for complex **1c** (0.1 mM).

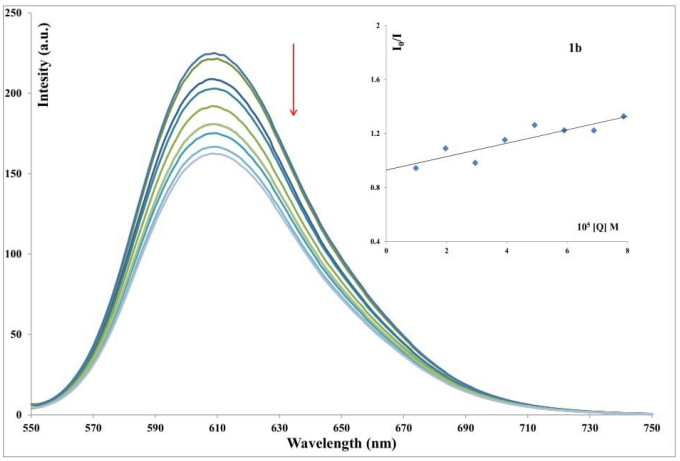

Figure S4. Fluorescence titration spectra of EB-DNA and of EB (10 μM) bound to DNA (10 μM) in the presence of varying amounts of complexes **1b**. [Arrow shows changes in fluorescence intensity upon increasing concentration of **1b** (0–10 μM)]. Insert graph: Stern-Volmer plots for EB-DNA fluorescence titration with **1b**.

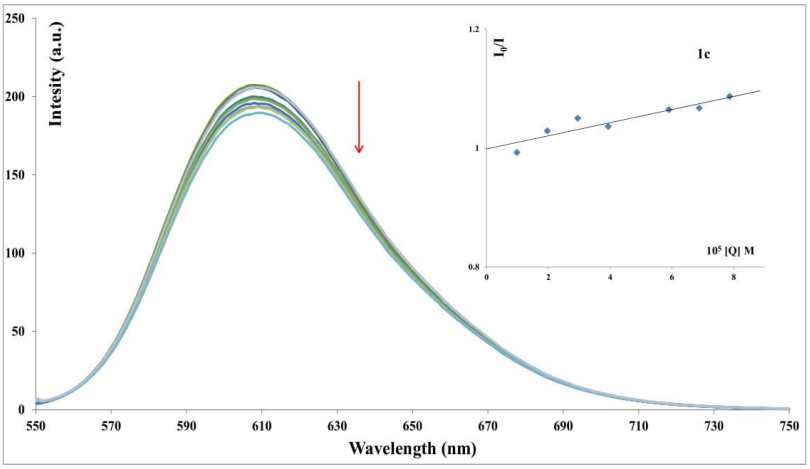

Figure S5. Fluorescence titration spectra of EB-DNA and of EB (10 μM) bound to DNA (10μM) in the presence of varying amounts of complexes **1c**. [Arrow shows changes in fluorescence intensity upon increasing concentration of **1c** (0–10 μM)]. Insert graph: Stern-Volmer plots for EB-DNA fluorescence titration with **1c.**

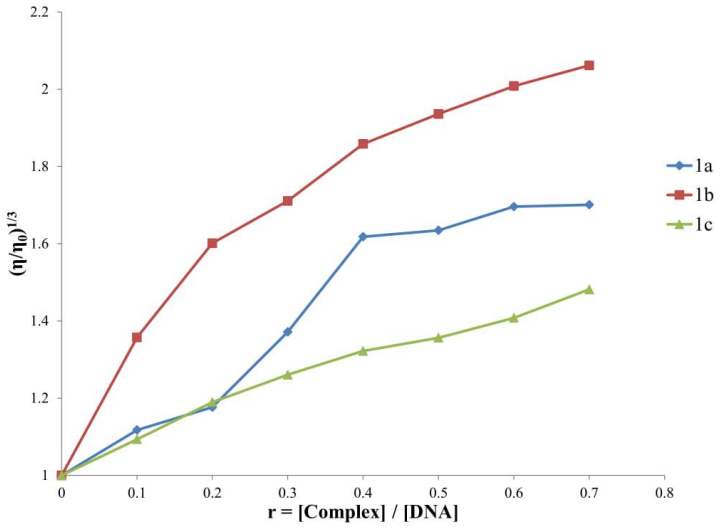

Figure S6. Relative viskosity $(\eta/\eta_0)^{1/3}$ of CT-DNA (0.01 mM) in PBS solution (Phosphate buffer solution = 0.01 M, cNaCl = 0.137, cKCl = 0.0027 M, pH 7.4) in the presence of the complexes **1a, 1b** and **1c** at increasing amounts (*r*).

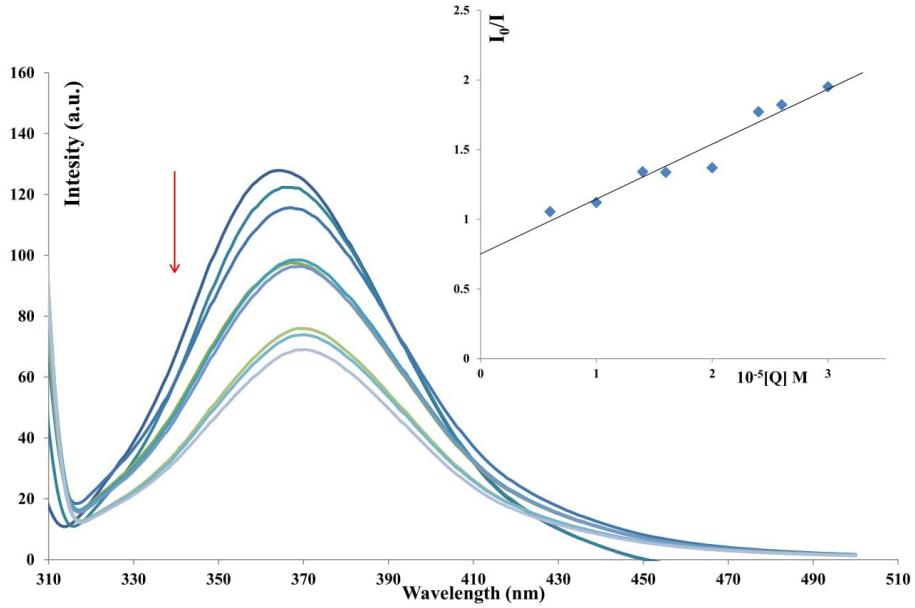

Figure S7. Emission spectrum of BSA (10 μM; λ_{ex} ,= 295 nm; λ_{em} = 365 nm) in the presence of increasing amounts of 1a (0–10 μM), λ_{max} = 365 nm. The arrow shows that emission intensity changes upon increasing the concentration of the complex. Insert graph: Plots of I_0/I vs. [Q].

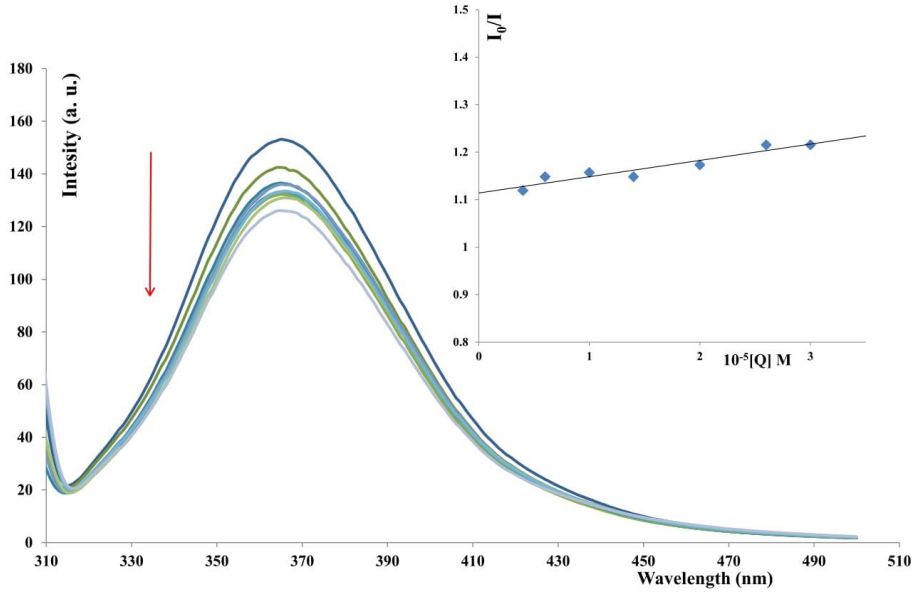

Figure S8. Emission spectrum of BSA (10 μM; λ_{ex}, = 295nm; λ_{em} = 365nm) in the presence of increasing amounts of **1c** (0–10μM), λ_{max} = 363nm. The arrow shows that emission intensity changes upon increasing the concentration of the complex. Insert graph: Plots of I_0/I *vs.* [Q].

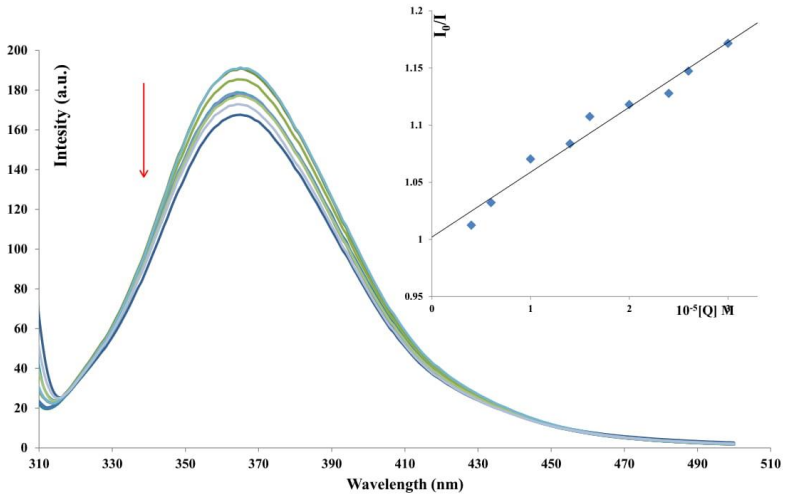

Figure S9. Emission spectrum of BSA (10 μM; λ_{ex},= 295 nm; λ_{em} = 365 nm) in the presence of increasing amounts of **1b** (0–10 μM), λ_{max} = 365 nm. The arrow shows that emission intensity changes upon increasing the concentration of the complex. Insert graph: Plots of I_0/I *vs.* [Q].

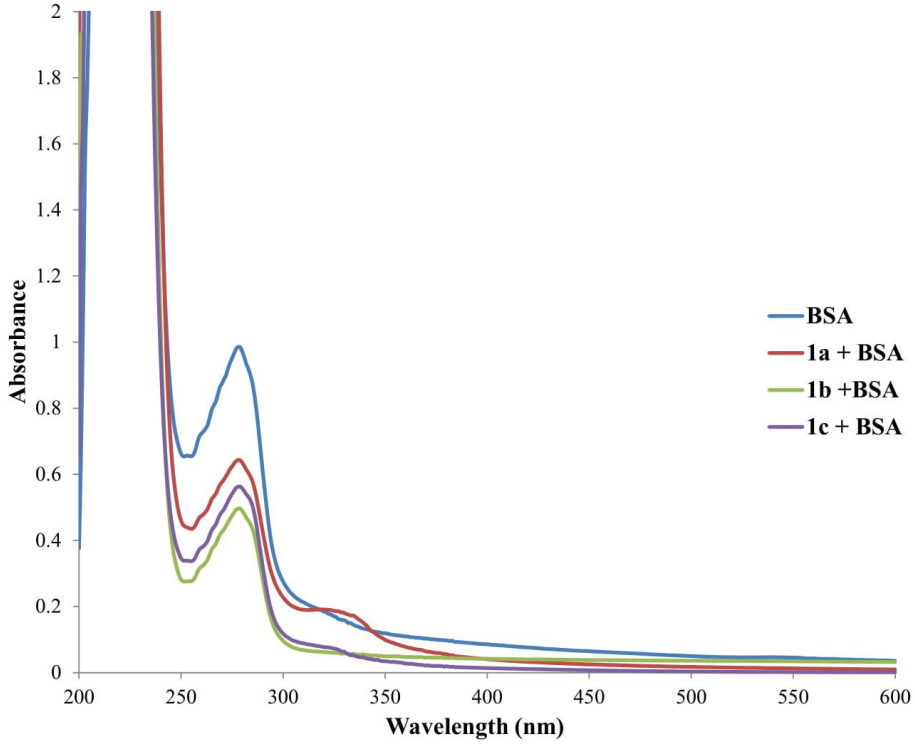

Figure S10. UV-Vis absorption spectra of BSA in the absence and presence of Rh^{III} complexes. c(BSA) = c (**1a**, **1b** or **1c**) = $5x10^{-5}$ M.

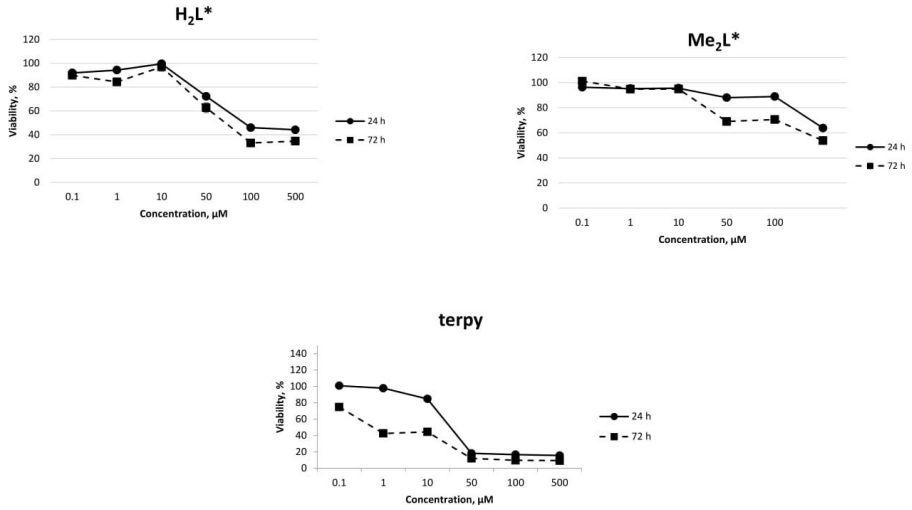

Figure S11. Dose-response curves for the effect of studied ligands on HCT-116 cell growth after 24 and 72 h of exposure. The antiproliferative effect was measured by MTT assay. All values are mean ± standard error, n = 3, *P < 0.05 as compared with controls.

Table S1. Observed *pseudo*-first order rate constants as a function of complex concentration and temperature for the reaction between complex (**1a**) and 5'-GMP at pH = 7.2 (25 mM Hepes buffer) in the presence of 50 mM NaCl at 310, 298 and 288 K.

T(K)	$10^4C_{5'\text{-GMP}}$/M	k_{obs}/s^{-1}
310.0	2.5	0.00073
	2.0	0.00065
	1.5	0.00045
	1.0	0.00039
	0.5	0.00019
298.0	2.5	0.00035
	2.0	0.00030
	1.5	0.00021
	1.0	
	0.5	0.00010
288.0	2.5	0.00022
	2.0	0.00018
	1.5	0.00013
	1.0	0.00011
	0.5	/

Table S2. Observed *pseudo*-first order rate constants as a function of complex concentration and temperature for the reaction between complex (**1a**) and GSH at pH = 7.2 (25 mM Hepes buffer) in the presence of 50 mM NaCl at 310, 298 and 288 K.

T(K)	$10^4C_{(GSH)}$/M	k_{obs}/s^{-1}
310.0	2.5	0.000097
	2.0	0.000083
	1.5	
	1.0	0.000041
	0.5	0.000019
298.0	2.5	0.000064
	2.0	0.000048
	1.5	0.000037
	1.0	0.000024
	0.5	0.000013
288.0	2.5	0.000044
	2.0	0.000032
	1.5	0.000025
	1.0	0.000017
	0.5	/

Table S3. Observed *pseudo*-first order rate constants as a function of complex concentration and temperature for the reaction between complex (**1a**) and L-Met at pH = 7.2 (25 mM Hepes buffer) in the presence of 50 mM NaCl at 310, 298 and 288 K.

T(K)	$10^4 C_{(\mathbf{L\text{-}Met})}$/M	k_{obs}/s^{-1}
310.0	2.5	0.000078
	2.0	0.000063
	1.5	0.000054
	1.0	0.000040
	0.5	0.000029

Table S4. Observed *pseudo*-first order rate constants as a function of complex concentration and temperature for the reaction between complex (**1b**) and 5'-GMP at pH = 7.2 (25 mM Hepes buffer) in the presence of 50 mM NaCl at 310, 298 and 288 K.

T(K)	$10^4 C_{5'\text{-GMP}}$/M	k_{obs}/s^{-1}
310.0	2.5	0.0022
	2.0	0.0019
	1.5	0.0016
	1.0	0.0013
	0.5	0.0011
298.0	2.5	0.0013
	2.0	0.0011
	1.5	0.00085
	1.0	0.00060
	0.5	0.00045
288.0	2.5	0.001
	2.0	0.00078
	1.5	0.00066
	1.0	0.00041
	0.5	/

Table S5. Observed *pseudo*-first order rate constants as a function of complex concentration and temperature for the reaction between complex (**1b**) and L-Met at pH = 7.2 (25 mM Hepes buffer) in the presence of 50 mM NaCl at 310, 298 and 288 K.

T(K)	$10^4C_{(\mathbf{L\text{-}Met})}$/M	k_{obs}/s^{-1}
310.0	2.5	0.00012
	2.0	0.000088
	1.5	0.000080
	1.0	0.000055
	0.5	0.000041
298.0	2.5	0.000094
	2.0	0.000085
	1.5	0.000070
	1.0	0.000043
	0.5	0.000033
288.0	2.5	0.000067
	2.0	0.000050
	1.5	0.000043
	1.0	0.000034
	0.5	/

Table S6. Observed *pseudo*-first order rate constants as a function of complex concentration and temperature for the reaction between complex (**1b**) and GSH at pH = 7.2 (25 mM Hepes buffer) in the presence of 50 mM NaCl at 310, 298 and 288 K.

T(K)	$10^4C_{(\mathbf{GSH})}$/M	k_{obs}/s^{-1}
310.0	2.5	0.00062
	2.0	0.00057
	1.5	0.00046
	1.0	0.00036
	0.5	0.00024

Table S7. Observed *pseudo*-first order rate constants as a function of complex concentration and temperature for the reaction between complex (**1c**) and 5'-GMP at pH = 7.2 (25 mM Hepes buffer) in the presence of 50 mM NaCl at 310, 298 and 288 K.

T(K)	$10^4C_{5'\text{-GMP}}$/M	k_{obs}/s^{-1}
310.0	2.5	0.00098
	2.0	0.00078
	1.5	0.00058
	1.0	0.00044
	0.5	0.00021
298.0	2.5	0.00067
	2.0	0.00047
	1.5	0.00037
	1.0	0.00020
	0.5	
288.0	2.5	0.00032
	2.0	0.00027
	1.5	0.00021
	1.0	0.00012
	0.5	/

Table S8. Observed *pseudo*-first order rate constants as a function of complex concentration and temperature for the reaction between complex (**1c**) and GSH at pH = 7.2 (25 mM Hepes buffer) in the presence of 50 mM NaCl at 310, 298 and 288 K.

T(K)	$10^4C_{(GSH)}$/M	k_{obs}/s^{-1}
310.0	2.5	0.000018
	2.0	0.000016
	1.5	0.000095
	1.0	0.0000062
	0.5	0.0000031

Table S9. Observed *pseudo*-first order rate constants as a function of complex concentration and temperature for the reaction between complex (**1c**) and L-Met at pH = 7.2 (25 mM Hepes buffer) in the presence of 50 mM NaCl at 310, 298 and 288 K.

T(K)	$10^4C_{(GSH)}$/M	k_{obs}/s^{-1}
310.0	2.5	0.0000094
	2.0	0.0000078
	1.5	0.0000067
	1.0	0.0000050
	0.5	0.0000023

Table S10. The water solubility of the studied Rh^{III} complexes at 298 K.

Complex	Solubility in water at 298 K mg/ml
1a	5.5
1b	5.2
1c	4.8
Cisplatin[A]	2.5
Oxaliplatin[B]	5.0

[A] The Merck Index, 12th ed., Entry# 2378; [B] According to Sigma-Aldrich

Table S11. Selected calculated (B3LYP/LANL2DZp) distances in the systems $[Rh(terpy)(Cl)_2L]^{n+}$.

cis-$[Rh(terpy)(Cl)_2L]^{n+}$	**Cl^-** [Å]	**$HS-CH_3$** [Å]	**$H_3C-S-CH_3$** [Å]	**TU** [Å]	**Gua** [Å]	**Imi** [Å]
$Rh-N_{trans}$	1.97	1.98	1.98	1.98	1.98	1.98
$Rh-N_{cis}$	2.05	2.07	2.07	2.07	2.06/2.07	2.07
$Rh-Cl_{cis}$	2.41	2.36	2.37	2.37	2.36	2.36
$Rh-Cl_{trans}$	**2.39**	**2.39**	**2.39**	**2.41**	**2.40**	**2.39**
Rh-L	**-.--**	**2.49**	**2.47**	**2.50**	**2.20**	**2.14**
trans-$[Rh(terpy)(Cl)_2L]^{n+}$	**Cl^-** [Å]	**$HS-CH_3$** [Å]	**$H_3C-S-CH_3$** [Å]	**TU** [Å]	**Gua** [Å]	**Imi** [Å]
$Rh-N_{trans}$	1.97	1.97	1.98	1.98	1.97	1.97
$Rh-N_{cis}$	2.05	2.08//2.09	2.09	2.08	2.07/2.10	2.07
$Rh-Cl_{cis}$	2.41	2.39	2.39	2.38/2.43	2.39/2.41	2.39/2.40
Rh-L	**2.39**	2.44	2.46	2.47	2.14	2.12

Table S12. Selected calculated (B3LYP/LANL2DZp) distances in the systems $[Rh(H_2L^H)(Cl)_2L]^{n+}$.

cis-$[Rh(H_2L^H)(Cl)_2L]^{n+}$	**Cl^-** [Å]	**HS-CH_3** [Å]	**H_3C-S-CH_3** [Å]	**TU** [Å]	**Gua** [Å]	**Imi** [Å]
Rh-N_{trans}	2.00	2.02	2.02	2.01	2.01	2.01
Rh-N_{cis}	2.02	2.04	2.04	2.04/2.05	2.03/2.05	2.04
Rh-Cl_{cis}	2.41	2.36	2.37	2.38	2.35	2.36
Rh-Cl_{trans}	**2.38**	**2.38**	2.38	**2.41**	**2.40**	**2.39**
Rh-L	**-.--**	**2.48**	2.49	**2.50**	**2.20**	**2.14**
trans-$[Rh(H_2L^H)(Cl)_2L]^{n+}$	**Cl^-** [Å]	**HS-CH_3** [Å]	**H_3C-S-CH_3** [Å]	**TU** [Å]	**Gua** [Å]	**Imi** [Å]
Rh-N_{trans}	2.00	2.01	2.01	2.01	2.00	2.00
Rh-N_{cis}	2.02	2.08	2.05/2.08	2.05	2.05/2.08	2.06
Rh-Cl_{cis}	2.41	2.39/2.40	2.40	2.38/.243	2.39	2.40
Rh-L	**2.38**	2.43	2.45	2.46	2.14	2.12
cis-$[Rh(H_2L^H)(Cl)_2L]^{n+}$	**Cl^-** [Å]	**HS-CH_3** [Å]	**H_3C-S-CH_3** [Å]	**TU** [Å]	**Gua** [Å]	**Imi** [Å]
Rh-N_{trans}	2.00	2.02	2.02	2.01	2.01	2.01
Rh-N_{cis}	2.02	2.04	2.04	2.04/2.05	2.03/2.05	2.04
Rh-Cl_{cis}	2.41	2.36	2.37	2.38	2.35	2.36

Rh-Cl_{trans}	**2.38**	**2.38**	2.38	**2.41**	**2.40**	**2.39**
Rh-L	**-.--**	**2.48**	2.49	**2.50**	**2.20**	**2.14**
trans-$[Rh(H_2L^H)(Cl)_2L]^{n+}$	**Cl^-** [Å]	**HS-CH_3** [Å]	**H_3C-S-CH_3** [Å]	**TU** [Å]	**Gua** [Å]	**Imi** [Å]
Rh-N_{trans}	2.00	2.01	2.01	2.01	2.00	2.00
Rh-N_{cis}	2.02	2.08	2.05/2.08	2.05	2.05/2.08	2.06
Rh-Cl_{cis}	2.41	2.39/2.40	2.40	2.38/.243	2.39	2.40
Rh-L	**2.38**	2.43	2.45	2.46	2.14	2.12

Table S13. Calculated relative stabilities for the cis- and trans isomers B3LYP: RB3LYP/LANL2DZp + ZPE(B3LYP/LANL2DZp)

B3LYP(CPCM): RB3LYP(CPCM)/LANL2DZp // RB3LYP/LANL2DZp + ZPE(B3LYP/LANL2DZp)

	$[Rh(terpy)(Cl)_2L]^+$		$[Rh(H_2L^H)(Cl)_2L]^+$	
[kcal mol^{-1}]	B3LYP	B3LYP(CPCM)	B3LYP	B3LYP(CPCM)
HS-CH_3	-3.12	-0.06	-1.85	-0.73
CH_3-S-CH_3	-4.26	+1.28	-0.88	+0.15
TU	-3.59	-1.13	-3.08	-1.67
Gua	+0.22	+0.10	-4.95	-3.02
Imi	-7.34	-2.69	-4.60	-2.72

Table S14. IC50 values (μM) of the investigated complexes and ligands.

Inhibitory activity was expressed as the mean of 50% inhibitory concentration of triplicate experiments

	HCT-116, IC_{50} μM	
Complex	**24 h**	**72 h**
1b	80.01	7.26
1a	>500	>500
1c	>500	>500
H_2L*	267.28	224.81
Me_2L*	>500	215.83
terpy	16.32	0.09

CHAPTER 4

FINAL CONCLUSION & OUTLOOK

Ruthenium(II) and rhodium(III) complexes proved to be suitable for anticancer and biomedical applications. Changing the environment, in coordination sense, in ruthenium and rhodium complexes, and tuning these compounds with respect to their reactivity, ruthenium(II) and rhodium(III) complexes offer a rich chemistry and many possible future applications. The aim of this dissertation was to synthesize, characterize and study the reactivity of these complexes with small biomolecules, as well as to study the interaction with oligonucleotides of small fragments of DNAs and RNA and also to monitor the interactions with different types of DNA and proteins. One of the parts of this dissertation was focused on cytotoxic studies on the synthesized complexes of ruthenium and rhodium.

The crystal structures of the ruthenium(II) complexes [Ru(Cl-Ph-tpy)(bpy)Cl]Cl and low quality resolution of complex [Ru(Cl-Ph-tpy)(en)Cl]Cl were determined. The Ru ion displays the typical distorted octahedral geometry with the tridentate Cl-Ph-tpy ligand coordinated with the expected meridional geometry, the bpy and en as the *N*-*N* bidentate chelating ligand, and the sixth coordination site occupied by a chloride ion. Single crystal X-ray structure analysis for the rhodium complexes $[Rh^{III}(H_2L^{tBu})Cl_3]$ and $[Rh^{III}(Me_2L^*)Cl_3]$ revealed that both complexes crystallizes in the orthorhombic space group, where for complex $[Rh^{III}(H_2L^{tBu})Cl_3]$ the orthorhombic space group *P*bcn and for complex $[Rh^{III}(Me_2L^*)Cl_3]$ the orthorhombic space group $P2_12_12_1$ are favored.

In view of the potential anticancer activity of all the new ruthenium(II) and rhodium(III) complexes, their chemical behavior in aqueous solution was studied by UV-Vis and NMR spectroscopy. For the ruthenium(II) terpyridine complexes studies showed that complexes [Ru(Cl-Ph-tpy)(en)Cl]Cl, [Ru(Cl-Ph-tpy)(dach)Cl]Cl, [Ru(Cl-Ph-tpy)(bpy)Cl]Cl, [Ru(tpy)(κ^2(*1S,3R*)-$NH_2 \cap NH_2$)Cl]Cl, [Ru(tpy)(mtefc)Cl]Cl and [Ru(tpy)(mtpfc)Cl]Cl release the Cl^- ligand to form the corresponding aqua species. The rate of hydrolysis for the complexes [Ru(Cl-Ph-tpy)(en)Cl]Cl, [Ru(Cl-Ph-tpy)(dach)Cl]Cl, [Ru(Cl-Ph-tpy)(bpy)Cl]Cl and [Ru(tpy)(κ^2(*1S,3R*)-$NH_2 \cap NH_2$)Cl]Cl was found to depend markedly on the nature of the

chelating ligand (minutes for en, dach and κ^2(*1S,3R*)-$NH_2 \cap NH_2$, hours for bpy), but its extent, as similar in all cases, with a *ca*. 1:9 ratio between intact and aquated species at equilibrium in NMR measurements for ruthenium(II) terpyridine complexes containing en, dach and bpy as bidentate ligands.

Complexes containing both ruthenium and rhodium as a metal center are stable in biological solutions, such as phosphate buffer solution or HEPES buffer. Electronic absorption spectra for all complexes remained unchanged for 24h after dissolution, suggesting a good stability of the complexes.

It was of particular interest to elucidate the similarities and differences in the behavior of the ruthenium(II) and rhodium(III) complexes towards mononucleotides, oligonucleotides and DNA, and to relate these properties to biological effect. This thesis provides information on the mechanism of substitution of ruthenium(II) and rhodium(III) complexes with the guanine model compounds such as guanosine-5'-monophosphate, L-histidine, 9-methylguanine, as well as the interaction with sulfur donor biomolecules such as L-cysteine and L-methionine. The kinetic data for the reactions of ruthenium(II) terpyridine derivatives with guanosine-5'-monophosphate clearly showed that the rate of the reactions depends on the nature of the chelating ligand where ruthenium(II) complexes which contain en, dach and κ^2(*1S,3R*)-$NH_2 \cap NH_2$ react *ca.* 2 times faster than ruthenium(II) complex containing bpy as bidentate ligand. The reactivity of the synthesized rhodium(III) complexes toward small biomolecules, such as L-methionine, guanosine-5'-monophosphate, L-histidine and glutathione is: 5'-GMP > GSH > L-Met > L-His. The order of reactivity of the investigated rhodium(III) complexes follow the order: $[Rh^{III}(Me_2L^*)Cl_3]$ > $[Rh^{III}(H_2L^{tBu})Cl_3]$ = $[Rh^{III}(H_2L^*)Cl_3]$ > $[Rh^{III}(tpy)Cl_3]$. This implies that rhodium(III) complexes have almost the same affinity to bind to sulfur-donor biomolecules and nitrogen-donor biomolecules, which is in accordance with the fact that rhodium(III) belongs to the borderline group, *i.e.* this metal ion is a soft-hard acid.

Quantitative kinetic investigations on ruthenium(II) chlorophenyl-terpyridine complexes and rhodium(III) pincer-type complex were also performed with oligonucleotides such as small fragments of DNAs and RNA with centrally located GG-binding sites. Concerning the length of the fragments of DNAs and RNA, it can be seen that shorter 13GG duplex RNA reacts faster than the longer 15GG duplex DNA-1 and 22GG duplex DNA-2. For the rhodium(III) complex $[Rh^{III}(H_2L^{tBu})Cl_3]$ an additional measurement with one more DNA fragment which contains 22GTG duplex was added. It was observed that a better reactivity is

achieved with DNA duplex with a centrally located GG- sequence than with a 22GTG duplex in which the GG-sequence is separated by a T base.

The interactions of ruthenium(II) and rhodium(III) complexes with calf thymus DNA were examined by absorption using UV-Vis spectroscopy and fluorescence emission spectral studies by ethidium bromide displacement studies, but also by viscosity measurements and for some of the complexes molecular docking studies. The results revealed the ability of the complexes to bind to calf thymus DNA covalently and non-covalently through intercalation. All complexes show good binding to protein bovine serum albumin, with relatively high binding constants. The high K values observed for the all complexes suggest that these complexes can be efficiently stored and transported in the body by protein bovine serum albumin.

Furthermore, the interactions with calf thymus DNA and herring testes DNA were studied by "stopped-flow" UV-Vis spectroscopy with [Ru(Cl-Ph-tpy)(en)Cl]Cl, [Ru(Cl-Ph-tpy)(dach)Cl]Cl and [Ru(Cl-Ph-tpy)(bpy)Cl]Cl complexes and also a gel mobility shift assay. According to the obtained rate constants, the complexes with bidentate aliphatic diamines proved to be superior to those with bpy in terms of reactivity and capability to bind oligonucleotides and DNA. In addition, the reactions with herring testes DNA were faster compared to those with calf thymus DNA probably due to the higher percentage of guanine in herring testes DNA. The reactivity of the complexes and their efficiency to unwind closed, negatively supercoiled DNA are not in line with their biological activity. These differences may play a very important role in their antitumor activity and could contribute to a different mechanism for cytotoxic compared to cisplatin.

In vitro studies of ruthenium(II) complexes [Ru(Cl-Ph-tpy)(en)Cl]Cl, [Ru(Cl-Ph-tpy)(dach)Cl]Cl and [Ru(Cl-Ph-tpy)(bpy)Cl]Cl was evaluated against two different cancer cell lines, HeLa and A549, and one normal cell line, MRC-5, in comparison with their analogues and cisplatin. Ruthenium(II) complexes which contained bpy as a bidentate ligand displayed the highest cytotoxicity, and it roughly correlates with the ability to hydrolyze the monodentate ligand at a reasonable rate. *In vitro* studies have also been performed on MDA-MB-231 and 4T1 cancer cell lines with complexes [Ru(tpy)(mtefc)Cl]Cl and [Ru(tpy)(mtpfc)Cl]Cl, with apoptosis being the main mechanism of complex-induced death. It is worth noting that both complexes promoted activation of innate and acquired anti-tumor immunity, which contributed to the reduced growth and progression of mammary carcinoma *in vivo*.

In vitro viability effects against human epithelial colorectal carcinoma HCT-116 of $[Rh^{III}(H_2L^*)Cl_3]$, $[Rh^{III}(Me_2L^*)Cl_3]$ and $[Rh^{III}(tpy)Cl_3]$ complexes were also determined. Rhodium complex $[Rh^{III}(Me_2L^*)Cl_3]$ showed significant cytotoxic effects, while the other two rhodium(III) complexes showed no cytotoxic effect.

In summary, the presented study of ruthenium(II) and rhodium(III) complexes indicates that ruthenium or rhodium as a metal center in complexes are promising anticancer candidates. Every new contribution in this field is highly warranted due to the current lack of clinically used metallo-based alternatives to cisplatin. The results in this thesis represent a further improvement in the structure-pharmacological relationship needed for the design of new anticancer ruthenium or rhodium drugs and chemotherapeutic strategies.

REFERENCES

1. A. Levina, A. Mitra and P. A. Lay, *Metallomics*, 2009, **1**, 458-470.
2. S. Filipović, *Osnovi kliničke onkologije*, Naša knjiga, Beograd, 2009.
3. a)G. Sava and A. Bergamo, *Int. J. Can.*, 2000, **17**, 353-365; b)B. K. Keppler, M. R. Bergamo, M. H. Heim, *Can. Treat. Rev.*, 1990, **17**, 261-277.
4. L. Fass, *Mol. Oncol.*, 2008, **2**, 115-152.
5. S. Valastyan, R. A. Weinberg, *Cell*, 2011, **147**, 275-292.
6. J. Ferlay, I. Soerjomataram, R. Dikshit, S. Eser, C. Mathers, M. Rebelo, D. F. Parkin, D. Forman, F. Bray, *Int. J. Cancer*, 2015, **136**, E359-E386.
7. S. Thota, D. A. Rodrigues, D. C. Crans, E. J. Barreiro, *J. Med. Chem*., 2018, **61**, 5805–5821.
8. F. Muggia, *Gynecol. Oncol.*, 2009, **112**, 275-281.
9. L. Kelland, *Nat. Rev.Cancer*, 2007, **7**, 573-584.
10. S. Nikolić, L. Rangasamy, N. Gligorijević, S. Aranđelović, S. Radulović, G. Gasser, S. Grgurić-Šipka, *J. Inorg. Biochem.*, 2016, **160**, 156-165.
11. A. Mihajlović, *Doctoral Dissertation*, University of Kragujevac, 2016.
12. A. Rilak, *Doctoral Dissertation*, University of Kragujevac, 2015.
13. A. Taylor, N. Carmichael, *Cancer Studies*, 1953, **2**, 36-79.
14. a)B. Rosenberg, L. VanCamp, T. Krigas, *Nature*, 1965, **205**, 698-699; b)B. Rosenberg, L. VanCamp, J. E. Trosko, V. H. Mansour, *Nature*, 1965, **222**, 385-386.
15. Y. Geldmacher, M. Oleszak, W. S. Sheldrick, *Inorg, Chim. Acta*, 2012, **393**, 84-102.
16. J. Reedijk, *Platinum Met. Rev.*, 2008, **52**, 2-11.
17. M. A. Jakupec, M. Galanski, V. B. Arion, C. G. Hartinger, B. K. Keppler, *Dalton Trans.*, 2008, 183-194.
18. M. J. Clarke, *Coord. Chem. Rev.*, 2002, **232**, 69-93.
19. Y. K. Yan, M. Melchart, A. Habtemariam, P. J. Sadler, *Chem. Commun*., 2005, 4764-4776.
20. A. Levina, A. Mitra, P. A. Lay, *Metallomics*, 2009, **1**, 458-470.
21. G. Süss-Fink, *Dalton Trans*., 2010, **39**, 1673-1688.
22. a)H. Taube, *Surv. Prog. Chem.*, 1973, **6**, 1-46; b)H. Taube, *Coord. Chem. Rev.*, 1978, **26**, 1-5.

23. I. Haiduc, C. Silvestru, *"Cobalt, Rhodium and Iridium" in Organometallics in Cancer Chemotherapy*, CRC Press, Boca Raton, Florida, 1990, 169-207.
24. N. Katsaros, A. Anagnostopoulou, *Crit. Rev. Oncol.*, 2002, **42**, 297-308.
25. P. Qu, H. He, X. Liu, *Prog. Chem.*, 2006, **18**, 1646-1651.
26. R. G. Hughes, J. L. Bear, A. P. Kimball, *Proc. Am. Assoc. Cancer Res.*, 1972, **13**, 120-123.
27. F. Bottyomley, *Can. J. Chem.*, 1977, **55**, 2788-2791.
28. D. Frasca, J. Ciampa, J. Emerson, R. S. Umans and M. J. Clarke, *Met.-Based Drugs*, 1996, **3**, 197-209.
29. J. R. Durig, J. Danneman, W. D. Behnke and E. E. Mercer, *Chem. Biol. Interact*, 1976, **13**, 287-294.
30. M. J. Clarke, *Coord. Chem. Rev.*, 2003, **236**, 209-233.
31. M. J. Clarke, F. Zhu, D. R. Frasca, *Chem. Rev.*, 1999, **99**, 2511-2534.
32. M. J. Clarke, *Coord. Chem. Rev.*, 2002, **232**, 69-93.
33. M. J. Clarke, *Biochim. Biophys. Acta. Gen. Subj*., 1980, **627**, 332-333.
34. G. Mestroni, E. Alessio, G. Sava, S. Pacor, M. Coluccia, A. Boccarelli, *Metal-Based Drugs*, 1994, **1**, 41-63.
35. E. Alessio, *Chem. Rev.*, 2004, **104**, 4203-4242.
36. I. Bratsos, S. Jedner, T. Gianferrara, E. Alessio, *Chimia*, 2007, **61**, 692-697.
37. E. Alessio, G. Mestroni, A. Bergamo, G. Sava, *Met. Ions Biol. Syst.*, 2004, **42**, 323-351.
38. A. Bergamo, G. Sava, *Dalton. Trans.*, 2007, 1267-1272.
39. E. Reisner, V. B. Arion, B. K. Keppler, A. J. L. Pombeiro, *Inorg. Chim. Acta*, 2008, **361**, 1569-1583.
40. C. G. Hartinger, M. A. Jakupec, S. Zorbas-Seifried, M. Groessl, A. Egger, W. Berger, H. Zorbas, P. J. Dyson, B. K. Keppler, *Chem. Biodiversity*, 2008, **5**, 2140-2155.
41. C. G. Hartinger, S. Zorbas-Seifried, M. A. Jakupec, B. Kynast, H. Zorbas, B. K. Keppler, *J. Inorg. Biochem.*, 2006, **100**, 891-904.
42. M. J. Clarke, F. Zhu, D. R. Frasca, *Chem. Rev.*, 1999, **99**, 2511-2533.
43. N. J. Wheate, C. R. Brodie, J. G. Collins, S. Kemp, J. R. Aldrich-Wright, *Mini-Rev. Med. Chem.*, 2007, **7**, 627–648.
44. E. Corral, A. C. G. Hotze, H. den Dulk, A. Leczkowska, A. Rodger, M. J. Hannon, J. Reedijk, *J. Biol. Inorg. Chem.*, 2009, **14**, 439–448.
45. D. Chatterjee, A. Mitra, G. S. De, *Platinum Met. Rev.*, 2006, **50**, 2–12.

46. W. H. Ang, P. J. Dyson, *Eur. J. Inorg. Chem.*, 2006, 4003–4018.
47. a)S. J. Dougan, P. J. Sadler, *Chimia*, 2007, **61**, 704–715; b)M. Koppenwallner, E. Rais, M. Uzarewicz-Baig, S. Tabassum, M. A. Gilani, R. Wilhelm, *Synthesis*, 2015, **47**, 789-800; c)E. Rais, U. Flörke, R. Wilhelm, *Synthesis*, 2017, **49**, 2852-2864.
48. P. J. Dyson, *Chimia*, 2007, **61**, 698–703.
49. Y. K. Yan, M. Melchart, A. Habtemariam, P. J. Sadler, *Chem. Commun.*, 2005, 4764–4776.
50. M. Melchart, P. J. Sadler, *Bioorganometallics*, Ed. G. Jaouen, Wiley-VCH, Weinheim, Germany, 2006, 39–64.
51. A. Bergamo, A. Masi, P. J. Dyson, G. Sava, *Int. J. Oncol.*, 2008, **33**, 1281–1289.
52. V. Brabec, *Prog. Nucleic Acid Res. Mol. Biol.*, 2002, **71**, 1–68.
53. V. Brabec, O. Novakova, *Drug Resist. Updates*, 2006, **9**, 111–122.
54. A. R. Timerbaev, C. G. Hartinger, S. S. Aleksenko, B. Keppler, *Chem. Rev.*, 2006, **106**, 2224–2248.
55. D. Kalinowski, D. R. Richardson, *Pharmacol. Rev.*, 2005, **57**, 547–583.
56. B. Gava, S. Zorzet, P. Spessotto, M. Cocchietto, G. Sava, *J. Pharmacol. Exp. Ther.*, 2006, **317**, 284–291.
57. G. Sava, F. Frausin, M. Cocchietto, F. Vita, E. Podda, P. Spessotto, A. Furlani, V. Scarcia, G. Zabucchi, *Eur. J. Cancer*, 2004, **40**, 1383–1396.
58. G. Sava, S. Zorzet, C. Turrin, F. Vita, M. Soranzo, G. Zabucchi, M. Cocchietto, A. Bergamo, S. DiGiovine, G. Pezzoni, L. Sartor, S. Garbisa, *Clin. Cancer Res.*, 2003, **9**, 1898–1905.
59. A. Casini, C. Gabbiani, F. Sorrentino, M. P. Rigobello, A. Bindoli, T. J. Geldbach, A. Marrone, N. Re, C. G. Hartinger, P. J. Dyson, L. Messori, *J. Med. Chem.*, 2008, **51**, 6773–6781.
60. W. H. Ang, A. De Luca, C. Chapuis-Bernasconi, L. Juillerat-Jeanneret, M. Lo Bello, P. J. Dyson, *ChemMedChem*, 2007, **2**, 1799–1806.
61. D. Chatterjee, A. Mitra, A. Levina, P. A. Lay, *Chem. Commun.*, 2008, 2864–2866.
62. E. Meggers, *Curr. Opin. Chem. Biol.*, 2007, **11**, 287–292.
63. P. C. A. Bruijnincx, P. J. Sadler, *Curr. Opin. Chem. Biol.*, 2008, **12**, 197–206.
64. G. I. Pascu, A. C. G. Hotze, C. Sanchez-Cano, B. M. Kariuki, M. J. Hannon, *Angew. Chem., Int. Ed.*, 2007, **46**, 4374–4378.

65. G. Sava, E. Alessio, A. Bergamo, G. Mestroni, *Topics in Biological Inorganic Chemistry Eds.*, and M. J. Clarke, P. J. Sadler, Springer, Berlin, 1999, 143-169.
66. E. Alessio, G. Mestroni, A. Bergamo, G. Sava, *Curr. Topics Med. Chem.*, 2004, **4**, 1525-1535.
67. M. Groessl, E. Reisner, C. G. Hartinger, R. Eichinger, O. Semenova, A. R. Timerbaev, M. A. Jakupec, V. B. Arion, B. K. Keppler, *J. Med. Chem.*, 2007, **50**, 2185-2193.
68. M. Brindell, I. Stawoska, J. Supel, A. Skoczowski, G. Stochel, R. Eldik, *J. Biol. Inorg. Chem.*, 2008, **13**, 909-918.
69. G. Sava, I. Capozzi, K. Clerici, G. Gagliardi, E. Alessio, G. Mestroni, *Clin. Exp. Metastasis*, 1998, **16**, 371–379.
70. E. S. Antonarakis, A. Emadi, *Cancer Chemother. Pharmacol.*, 2010, **66**, 1-9.
71. H. Chen, J. A. Parkinson, S. Parsons, R. A. Coxall, R. O. Gould, P. J. Sadler, *J. Am. Chem. Soc.*, 2002, **124**, 3064-3082.
72. R. E. Aird, J. Cummings, A. A. Ritchie, M. Muir, R. E. Morris, H. Chen, P. J. Sadler, D. I. Jodrell, *Br. J. Cancer*, 2002, **86**, 1652-1657.
73. A. F. A. Peacock, P. J. Sadler, *Chem Asian J.*, 2008, **3**, 1890-1899.
74. S. Grgurić-Šipka, I. Ivanović, G. Rakić, N. Todorović, N. Gligorijević, S. Radulović, V. B. Arion, B. K. Keppler, Ž. Lj. Tešić, *Eur. J. Med. Chem.*, 2010, **45**, 1051-1058.
75. F. Wang, A. Habtemariam, E. P. L. Van der Geer, R. Fernandez, M. Melchart, R. J. Deeth, R. Aird, S. Guichard, F. P. A. Fabbiani, P. Lozano-Casal, I. D. H. Oswald, D. I. Jodrell, S. Parsons, P. J. Sadler, *P. Natl. Acad. Sci.*, USA, 2005, **112**, 18269-18274.
76. W. Kandioller, *Doctoral dissertation*, University of Vienna. Fakultät für Chemie, 2009.
77. F. Wang, H. Chen, S. Parsons, I. D. H. Oswald, J. E. Davidson, P. J. Sadler, *Chem. Eur. J.*, 2003, **9**, 5810-5820.
78. C. S. Allardyce, P. J. Dyson, D. J. Ellis, S. L. Heath, *Chem. Comm.*, 2001, **15**, 1396-1397.
79. C. Scolaro, A. Bergamo, L. Brescacin, R. Delfino, M. Cocchietto, G. Laurenczy, T. J. Geldbach, G. Sava, P. J. Dyson, *J. Med. Chem.*, 2005, **48**, 4161-4171.
80. A. Kurzwernhart, W. Kandioller, C. Bartel, S. Bächler, R. Trondl, G. Mühlgassner, M. A. Jakupec, V. B. Arion, D. Marko, B. K. Keppler, C. G. Hartinger, *Chem. Commun.*, 2012, **48**, 4839-4841.
81. M. Kubanik, J. K. Y. Tu, T. Söhnel, M. Hejl, M. A. Jakupec, W. Kandioller, B. K. Keppler, C. G. Hartinger, *Metallodrugs*, 2015, **1**, 24-35.

82. A. Kurzwernhart, W. Kandioller, S. Bächler, C. Bartel, S. Martic, M. Buczkowska, G. Mühlgassner, M. A. Jakupec, H. B. Kraatz, P. J. Bednarski, V. B. Arion, D. Marko, B. K. Keppler, C G. Hartinger, *J. Med. Chem.*, 2012, **55**, 10512-10522.
83. A. Kurzwernhart, W. Kandioller, E. A. Enyedy, M. Novak, M. A. Jakupec, B. K. Keppler, C. G. Hartinger, *Dalton Trans.*, 2013, **42**, 6193-6202.
84. A. Kurzwernhart, S. Mokesch, E. Klapproth, M. S. Adib-Ravazi, M. A. Jakupec, C. G. Hartinger, W. Kandioller, B. K. Keppler, *Eur. J. Inorg. Chem.*, 2016, 240-246.
85. S. Movassaghi, E. Leung, M. Hanif, B. Y. T. Lee, H. U. Holtkamp, J. K. Y. Tu, T. Söhnel, S. M. F. Jamieson, C. G. Hartinger, *Inorg. Chem.*, 2018, **57**, 8521-8529.
86. S. Movassaghi, M. Hanif, H. U. Holtkamp, T. Söhnel, S. M. Jamieson, C. G. Hartinger, *Dalton Trans.*, 2018, **47**, 2192-2201.
87. H. Chen, J. A. Parkinson, R. E. Morris, P. J. Sadler, *J. Am. Chem. Soc.*, 2003, **125**, 173-186.
88. a)H. Chen, J. A. Parkinson, R. E. Morris, P. J. Sadler, *J. Am. Chem. Soc.*, 2003, **125**, 173-186. b)H.-K. Liu, S. J. Berners-Price, F. Wang, J. A. Parkinson, J. Xu, J. Bella, P. J. Sadler, *Angew. Chem*., 2006, **45**, 8153-8156. c)R. E. Morris, R. E. Aird, P. del S. Murdoch, H. Chen, J. Cummings, N. D. Hughes, S. Parsons, A. Parkin, G. Boyd, D. I. Jodrell, P. J. Sadler, *J. Med. Chem.*, 2001, 44, 3616-3621.
89. J. Reedijk, *Proc. Natl. Acad. Sci.*, U.S.A, 2003, **100**, 3611-3616.
90. L. Messori, P. Orioli, D. Vullo, E. Alessio, E. Iengo, *Eur. J. Biochem.*, 2000, **267**, 1206-1213.
91. L. Messori, F. Gonzales Vilchez, R. Vilaplana, F. Piccioli, E. Alessio, B. Keppler, *Met. Based Drugs*, 2000, **7**, 335-342.
92. W. Hu, Q. Luo, X. Ma, K. Wu, J. Liu, Y. Chen, S. Xiong, J. Wang, P. J. Sadler, F. Wang, *Chem. Eur. J.*, 2009, **15**, 6586-6594.
93. O. Novakova, J. Kasparkova, O. Vrana, P. M. van Vliet, J. Reedijk, V. Brabec, *Biochemistry*, 1995, **34**, 12369-12378.
94. P. M. van Vliet, S. M. S. Toekim, J. G. Haasnoot, J. Reedijk, O. Novakova, O. Vrana, V. Brabec, *Inorg. Chim. Acta*, 1995, **231**, 57-64.
95. P. M. van Vliet, J. G. Haasnoot, J. Reedijk, *Inorg. Chem.*, 1994, **33**, 1934-1939.
96. F. Zobi, M. Hohi, I. Zimmermann, R. Alberto, *Inorg. Chem.*, 2004, **43**, 2771-2772.
97. C. C. Cheng, W. L. Lee, J. G. Su, C. L. Liu, *J. Chin. Chem. Soc.*, 2000, **47**, 213-220.

98. E. Corral, A. C. G. Hotze, D. M. Tooke, A. L. Spek, J. Reedijk, *Inorg. Chim. Acta*, 2006, **359**, 830-838.
99. K. Karidi, A. Garoufis, N. Hadjiliadis, M. Lutz, A. L. Spek, J. Reedijk, *Inorg. Chem.*, 2006, **45**, 10282-10292.
100. E. Corral, A. C. G. Hotze, A. Magistrato, J. Reedijk, *Inorg. Chem.*, 2007, **46**, 6715-6722.
101. A. H. Velders, H. Kooijman, A. L. Spek, J. G. Haasnoot, D. de Vos, J. Reedijk, *Inorg. Chem.*, 2000, **39**, 2966-2967.
102. A. C. G. Hotze, S. E. Caspers, D. de Vos, H. Kooijman, A. L. Spek, A. Flamigni, M. Bacac, G. Sava, J. G. Haasnoot, J. Reedijk, *J. Biol. Inorg. Chem.*, 2004, **9**, 354-364.
103. A. C. G. Hotze, M. Bacac, A. H. Velders, B. A. J. Jansen, H. Kooijman, A. L. Spek, J. G. Haasnoot, J. Reedijk, *J. Med. Chem.*, 2003, **46**, 1743-1750.
104. R. E. Morris, R. E. Aird, P. del S. Murdoch, H. Chen, J. Cummings, N. D. Hughes, S. Parsons, A. Parkin, G. Boyd, D. I. Jodrell, P. J. Sadler, *J. Med. Chem.*, 2001, **44**, 3616-3621.
105. A. C. G. Hotze, E. P. L. van der Geer, H. Kooijman, A. L. Spek, J. G. Haasnoot, J. Reedijk, *Eur. J. Inorg. Chem.*, 2005, **13**, 2648-2657.
106. A. Rilak, I. Bratsos, E. Zangrando, J. Kljun, I. Turel, Ž. D. Bugarčić, E. Alessio, *Inorg. Chem.*, 2014, **53**, 6113-6126.
107. D. Lazić, A. Arsenijević, R. Puchta, Ž. D. Bugarčić, A. Rilak, *Dalton Trans.*, 2016, **45**, 4633-4646.
108. M. Nišavić, M. Stoiljković, I. Crnolatac, M. Milošević, A. Rilak, R. Masnikosa, *Arab. J. Chem.*, 2016, **11**, 291-304.
109. T. Lazarević, A. Rilak, Ž. D. Bugarčić, *Eur. J. Med. Chem.*, 2017, **142**, 8-31.
110. P.J. Loferski, *Platinum-Group Metals*, 2016, 57.0-57.12.
111. Z. Wu, K. L. Hull, *Chem. Sci.*, 2016, **7**, 969-975.
112. J. Hansen, H. M. L. Davies, *Coord. Chem. Rev.*, 2008, **252**, 545-555.
113. S. Kim, S. Han, J. Park, S. Sharma, N. K. Mishra, H. Oh, J. H. Kwak, I. S. Kim, *Chem. Commun.*, 2017, **53**, 3006-3009.
114. J. Ohata, Z. T. Ball, *Dalton Trans.*, 2018, doi: 10.1039/C8DT03032D .
115. M. J. Cleare, P. C. Hydes, *Met. Ions Biol. Syst.*, 1980, **11**, 1-62.
116. G. Mestroni, E. Alessio, A. Sessanti o Santi, S. Geremia, A. Bergamo, G. Sava, A. Boccarelli, A. Schettino, M. Coluccia, *Inorg. Chim. Acta*, 1998, **273**, 62-71.

117. M. Harlos, I. Ott, R. Gust, H. Alborzinia, S. Wölfl, A. Kromm, W. S. Sheldrick, *J. Med. Chem.*, 2008, **51**, 3024-3033.
118. Y. Geldmacher, K. Splith, I. Kitanović, H. Alborzinia, S. Can, R. Rubbiani, Mhd. A. Nazif, P. Wefelmeier, A. Prokop, I. Otto, S. Wölfl, I. Neundorf, W. S. Sheldrick, *J. Biol. Inorg. Chem.*, 2012, **17**, 631-646.
119. Y. Geldmacher, I. Kitanović, H. Alborzinia, K. Bergerhoff, R. Rubbiani, P. Wefelmeier, A. Prokop, R. Gust, I. Otto, S. Wölfl, I. Neundorf, W. S. Sheldrick, *ChemMedChem*, 2011, **6**, 429-439.
120. M. Oleszak, *Doctoral Dissertation*, Ruhr-Universität Bochum, 2009.
121. E. L. Menon, R. Perera, M. Navarro, R. J. Kuhn, H. Morrison, *Inorg. Chem.*, 2004, **43**, 5373-5381.
122. D. Loganathan, H. Morrison, *Photochem. Photobiol.*, 2006, **82**, 237-247.
123. M. R. Kim, H. Morrison, S. I. Mohammed, *Anti-Cancer Drugs*, 2011, **22**, 896-904.
124. L. Dadci, H. Elias, U. Frey, A. Hörnig, U. Koelle, A. F. Merbach, H. Paulus, J. S. Schneider, *Inorg. Chem.*, 1995, **34**, 306-315.
125. Z. Liu, A. Habtemariam, A. M. Pizarro, S. A. Fletcher, A. Kisova, O. Vrana, L. Salassa, P. C. A. Bruijnincx, G. J. Clarkson, V. Brabec, P. J. Sadler, *J. Med. Chem.*, 2011, **54**, 3011-3026.
126. M. A. Scharwitz, I. Otto, Y. Geldmacher, G. Rust, W. S. Sheldrick, *J. Organomet. Chem.*, 2008, **693**, 2299-2309.
127. S. Writh, C. J. Rohbogner, M. Cieslack, J. Kazmierczak-Baranska, S. Donevski, B. Nawrot, I. P. Lorenz, *J. Biol. Inorg. Chem.*, 2010, **15**, 429-440.
128. U. Sliwinska, F. P. Pruchnik, S. Ulaszewski, M. Latocha, D. Nawrocka-Musial, *Polyhedron*, 2010, **29**, 1653-1659.
129. F.-M. Siu, I. W.-S. Lin, K. Yan, C.-N. Lok, K.-H. Low, T. Y.-C. Leung, T.-L. Lam, C.-M. Che, *Chem. Sci.*, 2012, **3**, 1785-1793.
130. D.-L. Ma, M. Wang, Z. Mao, C. Yang, C.-T. Ng, C.-H. Leung, *Dalton Trans.*, 2016, **45**, 2762-2771.
131. M. E. Moragues, R. Brines, M. Terencio, F. Sancenon, R. Martinez-Manez, M. Alcaraz, *Inorg. Chem.*, 2013, **52**, 13806-13808.
132. J. Ohata, M. K. Miller, C. M. Mountain, F. Vohidov, Z. T. Ball, *Angew. Chem. Int. Ed.*, 2018, **57**, 2827-2830.

133. J. R. Rubin, T. P. Haromy, M. Sundaralingam, *Acta Crystallogr., Sect. C: Cryst. Struct. Commun.*, 1991, **47**, 1712-1714
134. K. R. Dunbar, J. H. Matonic, V. P. Saharan, C. A. Crawford, G. Christou, *J. Am. Chem. Soc.*, 1994, **116**, 2201-2202.
135. J. D. Aguirre, A. M. Angeles-Boza, A. Chouai, J.-P. Pellois, C. Turro, K. R. Dunbar, *J. Am. Chem. Soc.*, 2009, **131**, 11353-11360.
136. R. van Eldik, *Coord. Chem. Rev.*, 2007, **251**, 1649.
137. C. H. Langford, H. B. Gray, *in Ligand Substitution Processes, Benjamin*, New York, 1974, ch. 2.
138. M. L. Tobe, J. Burgess, *in Inorganic Reaction Mechanism*, Longman, England, 1999, p. 70, 74, 364 ch. 2,4.
139. Ž. D. Bugarčić, *Kinetika i Mehanizam Supstitucionih Reakcija*, PMF Kragujevac, 1996, p. 12.
140. I. Gal, *Mehanizmi Neorganskih Reakcija*, Naučna knjiga, 1979, ch. 2, 3.
141. K. J. Laidler, *in Chemical Kinetics, Harper and Row*, New York, 1987, ch. 4, 6.
142. M. Kotowski, R. van Eldik, *in Inorganic High Pressure Chemistry, Kinetics and Mechanism, Ed.*, R. van Eldik, Elsevier, Amsterdam, 1986, ch. 1, 3, 4.
143. T. Asano, W. J. Le Noble, *Chem. Rev.*, 1978, **78**, 407-489.
144. J. H. Espenson, *in Chemical Kinetics and Reaction Mechanism*, 2nd Ed, McGrow Hill, New York, 1995, ch. 2, 6.
145. F. Basolo, R. C. Johnson, *in Coordination Chemistry*, 2nd Ed., *Science Reviews*, London, 1987, ch. 6.
146. Z. E. Housecroft, A. G. Sharp, *Inorg. Chem.*, Essex, England, 2001, ch. 6, 19, 20, 25.
147. D. T. Richens, *in The Chemistry of Aqua Ions*, John Wiley & Sons, NY, 1997, ch 1.
148. A. M. Pyle, J. P. Rehmann, R. Meshoyrer, C. V. Kumar, N. J. Turro, J. K. Barton, *J. Am. Chem. Soc.*, 1989, **111**, 3051-3058.
149. R. Lakowicz, G. Weber, *Biochemistry*, 1973, **12**, 4161-4170.
150. Lakowicz J.R., *Principles of Fluorescence Spectroscopy*, 3rd ed., Springer, New York, 2006, **8**, 278–327.
151. N. Seedher, P. Agarwal, *J. Lumin.*,2010, **130**, 1841–1848.
152. S. Wu, W. Yuan, H. Wang, Q. Zhang, M. Liu, K. Yu, *J. Inorg. Biochem.* 2008, **102**, 2026-2034.

153. a)H. C. Kolb, M. S. Van Nieuwenhze, K. B. Sharpless, *Chem. Rev.*, 2002, **94**, 2483-2547. b)T. J. Colacot, *Platinum Met. Rev.*, 2001, **46**, 82-83.
154. J. M. Rademaker-Lakhai, D. Van den Bongard, D. Pluim, J. H. Beijnen, J. H. M. Schellens, *Cin. Cancer Res.*, 2004, **10**, 3717-3727.
155. C. C. Konkankit, S. C. Marker, K. M. Knopf, J. J. Wilson, *Dalton Trans.*, 2018, **47**, 9934-9974.
156. S. M. Meier-Menches, C. Gerner, W. Berger, C. G. Hartinger, B. K. Keppler, *Chem. Soc. Rev.*, 2018, **47**, 909-928.
157. G. E. Buchel, I. N. Stepanenko, M. Hejl, M. A. Jakupec, B. K. Keppler, V. B. Arion, *Inorg. Chem.*, 2011, **50**, 7690-7697.
158. M. Groessl, E. Reisner, C. G. Hartinger, R. Eichinger, O. Semenova, A. R. Timerbaev, M. A. Jakupec, V. B. Arion, B. K. Keppler, *J. Med. Chem.*, 2007, **50**, 2185-2193.
159. B. Cebrian-Losantos, A. A. Krokhin, I. N. Stepanenko, R. Eichinger, M. A. Jakupec, V. B. Arion, B. K. Keppler, *Inorg. Chem.*, 2007, **46**, 5023-5033.
160. A. Dorcier, P. J. Dyson, C. Gossens, U. Rothlisberger, R. Scopelliti, I. Tavernelli, *Organometallics*, 2005, **24**, 2114-2123.
161. A. Dorcier, W. H. Ang, S. Bolano, L. Gonsalvi, L. Juillerat-Jeannerat, G. Laurenczy, M. Peruzzini, A. D. Phillips, F. Zanobini, P. J. Dyson, *Organometallics*, 2006, **25**, 4090-4096.
162. Y. Hung, W. J. Kung, H. Taube, *Inorg. Chem.*, 1981, **20**, 457-463.
163. M. Steblerrothlisberger, W. Hummel, P. A. Pittet, H. B. Burgi, A. Ludi, A. E. Merbach, *Inorg. Chem.*, 1988, **27**, 1358-1363.
164. C. A. Riedl, L. S. Flocke, M. Hejl, A. Roller, M. H. Klose, M. A. Jakupec, W. Kandioller, B. K. Keppler, *Inorg. Chem.*, 2017, **56**, 528-541.